

Aus dem Bereich Innere Medizin II – Gastroenterologie, Hepatologie & Endokrinologie
Theoretische Medizin und Biowissenschaften
der Medizinischen Fakultät
der Universität des Saarlandes, Homburg/Saar

Microparticles – A novel liquid biopsy tool to identify and classify primary hepatic cancer

Dissertation zur Erlangung des Grades eines Doktors der Naturwissenschaften
der Medizinischen Fakultät
der UNIVERSITÄT DES SAARLANDES
(2018)

vorgelegt von: Henrike Julich-Haertel geb. Julich
geb. am: 28.10.1988 in Erfurt

Tag der Promotion

Dekan

Prof. Dr. Michael D. Menger

Erstberichterstatter

Jun. Prof. Dr. Dr. Veronika Lukacs-Kornek

Zweitberichterstatter

The experimental work depicted in this thesis has been carried out at the Department of Internal Medicine II – Gastroenterology, Hepatology & Endocrinology at Saarland University Medical Center in Homburg/Saar, Germany.

Dissertation advisor: Jun. Prof. Dr. Dr. Veronika Lukacs-Kornek

FÜR OSKAR & LUTZ

ONE COULD NOT BE DEDICATED TO ANYTHING
UNLESS ONE BELIVED IN IT PASSIONATELY.

FRANCIS CRICK

FÜR MAMA & HARRY

FOLLOW YOUR INTEREST, YOUR AMBITION,
YOUR PASSION.

CHRISTIANE NÜSSLEIN-VOLHARD

ABSTRACT

The liver is the fifth most frequent tumor site worldwide, and importantly liver tumors are accompanied by a poor prognosis and short life expectancy. Primary hepatic cancer is divided into several types depending on their origin, including hepatocellular carcinoma, originates from hepatocytes and cholangiocarcinoma, which starts in intrahepatic bile ducts. In diagnosis of hepatocellular carcinoma and cholangiocarcinoma, serum markers and various imaging modalities play a crucial role. However, diagnostic potential is limited, particularly in monitoring of patients at risk to develop a tumor.

Liquid biopsies examine tumor-derived cells, DNA, microRNA or extracellular vesicles circulating in the vasculature, what could possibly be used to detect cancer at an early stage to improve the prognosis. Microparticles, a subtype of extracellular vesicles, are shed by membrane budding and thereby contain surface markers from the cell of origin. Thus, examining these vesicles using specific marker combination may allow identifying the origin of circulating microparticles. Due to different surface markers profiles, previous studies showed disease-specific expansion of various microparticle populations in patients with chronic hepatitis C and non-alcoholic fatty liver disease as well as in tumor-bearing patients.

This study addresses the hypothesis that microparticles carry origin-dependent individual surface marker profiles and therefore could serve as novel liquid biopsy tool. Thus, the aim of this study was to examine the diagnostic potential of liver- and liver tumor-derived microparticles, isolated from human sera, in diagnosis of hepatic cancer, particularly hepatocellular- and cholangiocarcinoma.

A surface marker panel suitable for flow cytometry analysis, included AnnexinV, EpCAM, CD133, ASGPR1 and gp38, was first explored in human cancer cell lines and within the murine hepatic progenitor compartment and finally was evaluated by microparticle profiling in healthy controls and patients bearing cirrhosis, hepatocellular carcinoma, cholangiocarcinoma, colorectal-, non-small cell lung- and pancreatic cancer. AnnexinV⁺EpCAM⁺ microparticles were increased in sera of patients with cirrhosis and various cancer entities, albeit with moderate diagnostic potential (over 50 % in sensitivity, specificity, positive- and negative prediction value). Despite, this data suggest this microparticle population as a pan-cancer marker. Furthermore, the marker combination of AnnexinV⁺EpCAM⁺CD133⁺ and

AnnexinV⁺EpCAM⁺CD133⁺ASGPR1⁺ corresponds to liver disorder-associated microparticles and only expand in patients with cirrhosis, hepatocellular- and cholangiocarcinoma, resulting in 73 to 83 % sensitivity, 50 % specificity and 81 to 83 % positive prediction value. Additionally, AnnexinV⁺EpCAM⁺ASGPR1⁺ microparticles discriminate patients with liver disorders in malignancies (hepatic cancer) and non-malignancies (cirrhosis) with solid diagnostic potential (75 % sensitivity and 78 % positive prediction value.). Notably, this subpopulation does not only correlate with the liver tumor load, but values drop after tumor resection and thus suggest a strong dependency on tumor presence. Importantly, with this approach, 64 % of patients with liver disorders and 54 % of patients with primary hepatic cancers were identified correctly.

Moreover, AnnexinV⁺gp38⁺CD133⁺ and AnnexinV⁺EpCAM⁺gp38⁺CD133⁺ microparticles expand in patients with cholangiocarcinoma and therefore classification of primary hepatic cancer between hepatocellular carcinoma and cholangiocarcinoma is feasible and results in moderate diagnostic potential (68 to 82 % sensitivity, 55 to 67 % specificity and 55 to 58 % positive prediction value). Nonetheless, using these marker combinations, 59 % of patients with cholangiocarcinoma and 52 % of patients with hepatocellular carcinoma could be correctly identified.

Taken together, microparticle profiling enables the detection of primary hepatic cancer and thus distinguishing hepatocellular- and cholangiocarcinoma. However, this method needs further exploration and likely be used in addition to conventional methods of liver cancer diagnosis, particularly in patients at risk to develop primary hepatic cancer to improve cancer detection at an early stage.

ZUSAMMENFASSUNG

Die Leber gehört weltweit zu den fünfthäufigsten Tumorentitäten und ist gezeichnet von einer schlechten Prognose und geringer Lebenserwartung. Es gibt je nach Ursprung verschiedene Typen des primären Leberkarzinoms. Hierzu gehören zum einen das Leberzellkarzinom, mit seinem Ursprung in Hepatozyten und zum anderen das Cholangiokarzinom, welches in intrahepatischen Gallengängen beginnt. Bei der Diagnose des Leberzell- und Cholangiokarzinoms spielen Tumormarker und verschiedene bildgebende Verfahren eine entscheidende Rolle. Jedoch ist das diagnostische Potential limitiert, vor allem bei Risikopatienten.

„Liquid Biopsies“ untersuchen tumorabstammende Zellen, DNA, microRNA oder extrazelluläre Vesikel, die im Gefäßsystem zirkulieren. Diese könnte möglicherweise verwendet werden, um ein Karzinom im frühen Stadium zu erkennen und so eine bessere Prognose zu ermöglichen.

Mikropartikel gehören zu der Klasse der extrazellulären Vesikel und werden durch Membranknospung freigesetzt, wodurch sie die Oberflächenmarkern ihrer Ursprungszelle erhalten. Dies könnte genutzt werden um mittels spezifischer Markerkombinationen den Ursprung der zirkulierenden Mikropartikel zu identifizieren. Basierend auf verschiedenen Oberflächenmarkern haben Studien gezeigt, dass verschiedene Mikropartikelpopulationen krankheitsspezifisch in Patienten mit chronischer Hepatitis C und nicht-alkoholischer Fettleber, sowie auch bei Tumorpatienten mit unterschiedlichen Tumorentitäten vermehrt vorkommen.

Darauf basierend befasst sich diese Studie mit der Hypothese, dass Mikropartikel herkunftsabhängig individuelle Oberflächenmarker tragen und somit als neue „Liquid Biopsy“-Methode genutzt werden können. Ziel dieser Studie war daher die Untersuchung des diagnostischen Potentials von leber- und lebertumorabstammenden zirkulierenden Mikropartikeln, isoliert aus humanen Seren, bei der Diagnose des primären Leberkarzinoms bzw. von Leberzell- und Cholangiokarzinom.

Eine für die Durchflusszytometrie geeignete Auswahl an Oberflächenmarkern, einschließlich AnnexinV, EpCAM, CD133, ASGPR1 und gp38, wurde zunächst an humanen Zelllinien und Subpopulationen muriner hepatischer Vorläuferzellen untersucht und anschließend bei der Untersuchung von Mikropartikelprofilen in gesunden Probanden und Patienten mit Zirrhose, Leberzell-, Cholangio-, Kolon-, nicht-kleinzelligem Bronchial- und Pankreaskarzinom evaluiert.

AnnexinV⁺EpCAM⁺ Mikropartikel scheinen generell ein Marker für die Tumorerkennung zu sein, da diese hauptsächlich vermehrt in Patienten mit Zirrhose oder Tumoren vorkommen. Jedoch zeigt diese Population nur ein mäßiges diagnostisches Potential mit jeweils über 50 % im Bezug auf Sensitivität, Spezifität, positiven und negativen Prädiktivem Wert.

Des Weiteren scheinen Annexin⁺EpCAM⁺CD133⁺ und Annexin⁺EpCAM⁺CD133⁺ASGPR1⁺ Mikropartikel spezifisch Lebererkrankungen zu detektieren, da sie speziell in Patienten mit Zirrhose und primären Leberkarzinom vermehrt vorkommen und in 73 bis 83 % Sensitivität, 50 % Spezifität, und 81 bis 83% positiven Prädiktivem Wert resultierten. Zusätzlich ermöglichen Annexin⁺EpCAM⁺ASGPR1⁺ Mikropartikel die Unterscheidung in nicht-maligne (Zirrhose) und maligne (primärer Leberkrebs) Lebererkrankungen mit einem guten diagnostischen Potential (75 % Sensitivität und 78 % positiven Prädiktivem Wert). Bemerkenswerterweise besteht eine Korrelation zwischen Annexin⁺EpCAM⁺ASGPR1⁺ Mikropartikeln und der Tumorlast, sowie auch mit der Tumorpräsenz, aufgrund abnehmenden Mikropartikelwerte nach Tumorresektion. Mit Hilfe dieser Mikropartikelpopulationen konnten 64 % der Patienten mit Lebererkrankungen und 54 % der Patienten mit primären Leberkarzinom richtig identifiziert werden.

Darüber hinaus zeigen Annexin⁺gp38⁺CD133⁺ und Annexin⁺EpCAM⁺gp38⁺CD133⁺ Mikropartikel hauptsächlich ein gehäuftes vorkommen in Patienten mit Cholangiokarzinom, wodurch mutmaßlich eine Klassifizierung des primären Leberkarzinoms in Leberzell- und Cholangiokarzinom, mit einem guten diagnostischen Potential, möglich ist (68 bis 82 % Sensitivität, 55 bis 67 % Spezifität, und 55 bis 58% positiven Prädiktivem Wert). Schließlich konnten 59 % der Patienten mit einem Cholangiokarzinom und 52 % der Patienten mit Leberzellkarzinom als diese identifiziert werden.

Daraus resultiert, dass mittels verschiedener Mikropartikelprofile die Detektion des primären Leberkarzinoms und insbesondere eine Klassifizierung in Leberzell- und Cholangiokarzinom ermöglicht wird. Jedoch bedarf diese Methode weiterer Untersuchungen und könnte zusätzlich zu den konventionellen Methoden der Leberkrebsdiagnostik Anwendung finden, besonders bei Risikopatienten um die Krebsdetektion in einem früheren Stadium zu verbessern.

INDEX

ABSTRACT	I
ZUSAMMENFASSUNG	III
LIST OF FIGURES	IX
LIST OF TABLES	XII
INDEX OF ABBREVIATIONS	XIV
1 INTRODUCTION	1
1.1 CONTEMPORARY ESTIMATES OF CANCER INCIDENCE AND MORTALITY	1
1.2 PRIMARY HEPATIC CANCER: MALIGNANT NEOPLASMS OF THE LIVER	3
1.2.1 TYPES AND STAGING OF PRIMARY HEPATIC CANCER	4
1.2.2 CONVENTIONAL METHODS IN DIAGNOSIS OF PRIMARY HEPATIC CANCER	6
1.2.2.1 Serum tumor markers in the diagnosis of primary hepatic cancer	7
1.2.2.2 Imaging modalities to assess primary hepatic cancer	8
1.3 MICROPARTICLES AS A POSSIBLY LIQUID BIOPSY TOOL	10
1.3.1 MICROPARTICLES – A SUBTYPE OF EXTRACELLULAR VESICLES	10
1.3.2 MICROPARTICLE POPULATIONS EXPAND INJURY-SPECIFIC	12
1.4 AIM OF THE CURRENT STUDY	13
2 MATERIAL & METHODS	15
2.1 MATERIAL	15
2.1.1 CELL CULTURE MEDIA AND BUFFER	15
2.1.2 BUFFER FOR GENERATING LIVER SINGLE-CELL SUSPENSION	16
2.1.3 FLOW CYTOMETRY BUFFER & REAGENTS USED FOR CELL STAINING	17
2.1.4 BUFFER FOR MAGNETIC MICROBEAD-BASED ENRICHMENT OF PROGENITOR CELLS	18
2.2 METHODS	20
2.2.1 TISSUE CULTURE WORK OF HUMAN CANCER CELL LINES	20
2.2.1.1 Thawing cryopreserved cells	20
2.2.1.2 Subcultivation for maintaining adherent cell lines	21
2.2.1.3 Cryopreservation of cell lines	22
2.2.1.4 Harvesting of cell lines to generate cell line single-cell suspension	22
2.2.2 ISOLATION AND ANALYSIS OF MURINE HEPATIC PROGENITOR CELLS	23
2.2.2.1 Hepatotoxicant thioacetamide to induce acute liver injury	23
2.2.2.2 CDE-diet for activation of the hepatic progenitor cell compartment	24

2.2.2.3	DDC-diet for activation of the hepatic progenitor cell compartment	24
2.2.2.4	Preparation of liver single-cell suspension	25
2.2.3	SURFACE STAINING OF HUMAN CANCER CELL LINES AND LIVER SINGLE-CELL SUSPENSION	27
2.2.3.1	Determining of the cell count by flow cytometry-based cell quantification	28
2.2.3.2	Staining of human cancer cell lines and murine liver cells.....	28
2.2.4	GENE EXPRESSION ANALYSIS OF HEPATIC PROGENITOR SUBSETS COMBINED FROM MULTIPLE LIVERS.....	35
2.2.4.1	Magnetic MicroBead-based enrichment and automated cell purification of CD133 ⁺ progenitor cells	35
2.2.4.2	RNA extraction using RNeasy® Plus Mini Kit	37
2.2.4.3	Synthesis of cDNA using QuantiNova™ Reverse Transcription Kit.....	38
2.2.4.4	Gene expression analysis of CD133 ⁺ oval cells using QuantiNova™ SYBR® PCR Kit.....	38
2.2.5	ISOLATION AND DETECTION OF HUMAN CELL-DERIVED MICROPARTICLES.....	40
2.2.5.1	Isolation of human serum	41
2.2.5.2	Isolation of cell-derived microparticles from human serum by sequential centrifugation	42
2.2.5.3	Staining of human cell-derived microparticles for flow cytometry analysis	43
2.2.6	FLOW CYTOMETRY ANALYSIS USING MACSQUANT® ANALYZER 10	46
2.2.7	DATA ANALYSIS SOFTWARE USED WITHIN THE CURRENT STUDY	46
2.2.7.1	Flow cytometry analysis using FlowJo®	46
2.2.7.2	Determining calculations using Excel®	47
2.2.7.3	Analysis and preparation of scientific data using GraphPad Prism®	47
2.2.7.4	Statistical power analysis using G*Power	48
3	RESULTS	49
3.1	SURFACE MARKER TO DISTINGUISH CANCER ENTITIES AND HEPATIC PROGENITOR CELLS	49
3.1.1	CANCER AND HEPATIC PROGENITOR CELLS-RELATED SURFACE MARKER.....	49
3.1.2	SURFACE MARKER PROFILES DIFFER LIVER CANCER CELL LINES FROM PANCREATIC CANCER CELL LINES	51
3.2	THE MURINE HEPATIC PROGENITOR CELL COMPARTMENT	55
3.2.1	CLASSIFICATION OF THE HEPATIC PROGENITOR CELL COMPARTMENT IN HEALTHY LIVER.....	55
3.2.2	THE HEPATIC PROGENITOR CELL COMPARTMENT DURING TAA-INDUCED LIVER FIBROSIS.....	59
3.2.3	CDE-INDUCED ACTIVATION OF THE HEPATIC PROGENITOR CELL COMPARTMENT	61
3.2.4	DDC-INDUCED ACTIVATION OF THE HEPATIC PROGENITOR CELL COMPARTMENT.....	64
3.2.5	SUMMARY – THE MURINE HEPATIC PROGENITOR CELL COMPARTMENT	69

3.3	MICROPARTICLES DETECTABLE IN HUMAN BLOOD SAMPLES	72
3.3.1	HUMAN STUDY COHORT - TUMOR-RELATED MICROPARTICLES TO IDENTIFY PRIMARY HEPATIC CANCER	72
3.3.2	HUMAN STUDY COHORT - OVAL CELL-RELATED MICROPARTICLES TO CLASSIFY PRIMARY HEPATIC CANCER	75
3.3.3	TITRATION OF ANTIBODY CONCENTRATION USED FOR MICROPARTICLE DETECTION	78
3.3.4	ANNEXIN ^V + MICROPARTICLES DETECTABLE IN EACH STUDY COHORT	80
3.4	TUMOR-RELATED MICROPARTICLES TO IDENTIFY PRIMARY HEPATIC CANCER	83
3.4.1	ANNEXIN ^V +EP ^{CAM} + MICROPARTICLES INDICATE MODERATE DIAGNOSTIC POTENTIAL	83
3.4.1.1	Tumor-bearing patients indicate elevated levels of Annexin ^V +Ep ^{CAM} + tumor- associated microparticles.....	85
3.4.1.2	Annexin ^V +Ep ^{CAM} + microparticles during cirrhosis	91
3.4.1.3	Liver tumor load affect levels of Annexin ^V +Ep ^{CAM} + microparticles.....	93
3.4.2	ANNEXIN ^V +EP ^{CAM} +CD133+ AND ANNEXIN ^V +EP ^{CAM} +CD133+ASGPR1+ MICROPARTICLES ALLOW DETECTION OF LIVER DISORDERS.....	95
3.4.2.1	Annexin ^V +Ep ^{CAM} +CD133+ and Annexin ^V +Ep ^{CAM} +CD133+ASGPR1+ microparticles expand in patients bearing liver disorders	97
3.4.2.2	Patients with cirrhosis indicate elevated levels of Annexin ^V +Ep ^{CAM} +CD133+ and Annexin ^V +Ep ^{CAM} +CD133+ASGPR1+ microparticles	107
3.4.2.3	Annexin ^V +Ep ^{CAM} +CD133+ and Annexin ^V +Ep ^{CAM} +CD133+ASGPR1+ microparticles correlate with liver tumor load	108
3.4.3	ANNEXIN ^V +EP ^{CAM} +ASGPR1+ MICROPARTICLES DIFFER BETWEEN CIRRHOSIS AND LIVER MALIGNANCIES.....	111
3.4.3.1	Annexin ^V +Ep ^{CAM} +ASGPR1+ taMPs differ between patients with cirrhosis and patients bearing liver tumors	112
3.4.3.2	Annexin ^V +Ep ^{CAM} +ASGPR1+ taMPs and liver tumor load	117
3.4.4	SURGICAL RESECTION LEADS TO DECREASE IN LIVER TUMOR-SPECIFIC TAMP VALUES	118
3.4.5	SUMMARY – TUMOR-RELATED MICROPARTICLES TO IDENTIFY PRIMARY HEPATIC CANCER.....	120
3.5	OVAL CELL-RELATED MICROPARTICLES TO CLASSIFY PRIMARY HEPATIC CANCER.....	124
3.5.1	LIVER DISORDERS DETECTABLE BY GP38/CD133 TUMOR-ASSOCIATED MICROPARTICLES	124
3.5.2	ANNEXIN ^V + AND ANNEXIN ^V +EP ^{CAM} + OVAL CELL-ASSOCIATED MICROPARTICLE SUBPOPULATIONS DIFFER IN HEPATOCELLULAR CARCINOMA AND CHOLANGIOCARCINOMA	131
3.5.3	SUMMARY - OVAL CELL-RELATED MICROPARTICLES TO CLASSIFY PRIMARY HEPATIC CANCER.....	143
4	DISCUSSION	146
4.1	EXPLORATION OF SURFACE MARKER PROFILES.....	146
4.1.1	SURFACE MARKER PROFILES DIFFER LIVER CANCER FROM PANCREATIC CANCER CELL LINES.....	147
4.1.2	THE MURINE HEPATIC PROGENITOR CELL COMPARTMENT	148

4.1.2.1	Revising of the hepatic progenitor compartment in murine liver under steady state conditions.....	149
4.1.2.2	Populations of the hepatic progenitor cell compartment change liver injury-specific.....	151
4.2	VALIDATION OF SURFACE MARKER PROFILES BY MICROPARTICLE PROFILING	154
4.2.1	LIVER DISORDER-ASSOCIATED MICROPARTICLES DIFFER IN NON-MALIGNANCIES AND HEPATIC CANCER.....	155
4.2.2	OVAL CELL-RELATED MICROPARTICLES ALLOW DISCRIMINATION IN HEPATOCELLULAR CARCINOMA AND CHOLANGIOCARCINOMA.....	157
4.3	PERSPECTIVES.....	158
5	BIBLIOGRAPHY	160
6	SUPPLEMENTARY DATA	174
6.1	SUPPLEMENTARY TABLES.....	174
6.2	SUPPLEMENTARY FIGURES	177
7	APPENDIX	184
7.1	EUROPEAN ASSOCIATION OF THE STUDY OF THE LIVER (EASL)	184
7.2	PUBLICATIONS.....	187
8	ACKNOWLEDGEMENTS.....	198
9	INFORMED CONSENT BY SABINE KATHARINA URBAN.....	199

LIST OF FIGURES

Figure 1: Most common tumor incidences and mortalities worldwide.	1
Figure 2: Tumor incidence and survival rates of the most common tumor localizations in Germany.	2
Figure 3: Liver cancer statistics and its development in the last few years.	3
Figure 4: Formation and release of extracellular vesicles.	10
Figure 5: Membrane characteristics of extracellular vesicles.	11
Figure 6: Workflow for preparation of liver single-cell suspension.	27
Figure 7: Cell count determination of human cancer cell lines and isolated murine liver cells by flow cytometry analysis.	28
Figure 8: Schematic view of the magnetic MicroBead-based enrichment and automated cell purification of CD133 ⁺ hepatic progenitor cells.	36
Figure 9: Schematic view of the isolation of cell-derived microparticles from human serum by sequential centrifugation.	42
Figure 10: Surface marker profiles in human liver cancer cell lines and pancreatic cancer cell lines.	52
Figure 11: Surface marker profiles differ liver cancer cell lines from pancreatic cancer cell lines.	54
Figure 12: Classification of the murine hepatic progenitor cell compartment in healthy liver.	56
Figure 13: Progenitor cell-associated surface marker expression in murine hepatic progenitor cell (HPC) subsets.	57
Figure 14: Gene expression analysis of enriched and purified CD133 ⁺ oval cells in healthy murine liver.	59
Figure 15: Classification of the murine hepatic progenitor cell compartment (HPCC) in TAA-induced injured liver.	60
Figure 16: Classification of the murine hepatic progenitor cell compartment (HPCC) in CDE-induced injured liver.	62
Figure 17: CDE-induced changes within the surface marker expression in progenitor subsets of murine liver.	63
Figure 18: Classification of the murine hepatic progenitor cell compartment (HPCC) in DDC-induced injured liver.	66
Figure 19: DDC-induced changes within the surface marker and gene expression by progenitor subsets.	68
Figure 20: Abstract of the murine hepatic progenitor cell compartment (HPCC) and its expression pattern in healthy and injured liver.	69
Figure 21: Age distribution of each entity participated in the ‘Tumor-related microparticles to identify primary hepatic cancer’ study.	73
Figure 22: Age distribution of each entity participated in the ‘Oval cell-related microparticles to classify primary hepatic cancer’ study.	76
Figure 23: Antibody titration used for microparticle (MP) detection by flow cytometry analysis.	79
Figure 24: Detection of AnnexinV ⁺ microparticles (MPs) using flow cytometry analysis.	80

Figure 25: AnnexinV ⁺ microparticles (MPs) detected in each cohort of the human cell-derived MPs study.....	82
Figure 26: Detection of AnnexinV ⁺ EpCAM ⁺ tumor-associated microparticles (taMPs) using flow cytometry analysis.....	84
Figure 27: Detection of AnnexinV ⁺ EpCAM ⁺ tumor-associated microparticles (taMPs) in human serum.....	85
Figure 28: AnnexinV ⁺ EpCAM ⁺ tumor-associated microparticles (taMPs) detect tumor-bearing patients.	88
Figure 29: Connection between serum markers and AnnexinV ⁺ EpCAM ⁺ tumor-associated microparticles (taMPs) of patients bearing liver disorders.	90
Figure 30: MELD-score and Child-Pugh score to assess the prognosis of chronic liver disease in relation to AnnexinV ⁺ EpCAM ⁺ tumor-associated microparticles (taMPs).	92
Figure 31: AnnexinV ⁺ EpCAM ⁺ tumor-associated microparticles (taMPs) correlate with liver tumor load.	94
Figure 32: Detection of AnnexinV ⁺ EpCAM ⁺ CD133 ⁺ and AnnexinV ⁺ EpCAM ⁺ CD133 ⁺ ASGPR1 ⁺ liver disorder-associated microparticles (MPs) using flow cytometry analysis.....	95
Figure 33: Detection of AnnexinV ⁺ EpCAM ⁺ CD133 ⁺ and AnnexinV ⁺ EpCAM ⁺ CD133 ⁺ ASGPR1 ⁺ tumor-associated microparticles (taMPs) in human serum.....	96
Figure 34: AnnexinV ⁺ EpCAM ⁺ CD133 ⁺ and AnnexinV ⁺ EpCAM ⁺ CD133 ⁺ ASGPR1 ⁺ tumor-associated microparticles (taMPs) detect patients bearing liver disorders.....	100
Figure 35: Diagnostic performance of liver disorder-associated AnnexinV ⁺ EpCAM ⁺ CD133 ⁺ and AnnexinV ⁺ EpCAM ⁺ CD133 ⁺ ASGPR1 ⁺ tumor-associated microparticles (taMPs).	101
Figure 36: Almost absent association between tumor markers and AnnexinV ⁺ EpCAM ⁺ CD133 ⁺ and AnnexinV ⁺ EpCAM ⁺ CD133 ⁺ ASGPR1 ⁺ tumor-associated microparticles (taMPs) in patients bearing liver disorders.	105
Figure 37: Almost no correlation of blood chemistry with AnnexinV ⁺ EpCAM ⁺ CD133 ⁺ and AnnexinV ⁺ EpCAM ⁺ CD133 ⁺ ASGPR1 ⁺ tumor-associated microparticles (taMPs) in patients bearing liver disorders.....	106
Figure 38: MELD-score and Child-Pugh score to assess the prognosis of cirrhosis in relation to AnnexinV ⁺ EpCAM ⁺ CD133 ⁺ and AnnexinV ⁺ EpCAM ⁺ CD133 ⁺ ASGPR1 ⁺ tumor-associated microparticles (taMPs).	107
Figure 39: Liver disorder-associated AnnexinV ⁺ EpCAM ⁺ CD133 ⁺ and AnnexinV ⁺ EpCAM ⁺ CD133 ⁺ ASGPR1 ⁺ tumor-associated microparticles (taMPs) correlate with liver tumor load.....	110
Figure 40: Detection of AnnexinV ⁺ EpCAM ⁺ ASGPR1 ⁺ liver tumor-associated microparticles (taMPs) using flow cytometry analysis.....	111
Figure 41: Detection of AnnexinV ⁺ EpCAM ⁺ ASGPR1 ⁺ tumor-associated microparticles (taMPs) in human serum.	112
Figure 42: AnnexinV ⁺ EpCAM ⁺ ASGPR1 ⁺ tumor-associated microparticles (taMPs) detect liver tumor-bearing patients.	116

Figure 43: Values of AnnexinV ⁺ EpCAM ⁺ ASGPR1 ⁺ tumor-associated microparticles (taMPs) correlate with liver tumor load.	117
Figure 44: Liver tumor-specific taMPs decrease after surgical R0 resection in liver tumor patients.	119
Figure 45: Tumor-associated microparticles (taMPs) and their diagnostic potential.	122
Figure 46: Proposal of a possibly screening method to identify primary hepatic cancer using several tumor-associated microparticle (taMP) populations.	123
Figure 47: Detection of gp38/CD133 tumor-associated microparticles (taMPs) subpopulations by flow cytometry.	125
Figure 48: Detection of gp38/CD133 tumor-associated microparticle (taMP) subpopulations in human serum.	126
Figure 49: AnnexinV ⁺ EpCAM ⁺ gp38 ⁻ CD133 ⁺ tumor-associated microparticles (taMPs) detect patients bearing liver disorders.	128
Figure 50: Diagnostic performance of AnnexinV ⁺ EpCAM ⁺ gp38 ⁻ CD133 ⁺ tumor-associated microparticles (taMPs) for patients bearing liver disorders.	131
Figure 51: Detection of AnnexinV ⁺ and AnnexinV ⁺ EpCAM ⁺ oval cell-associated microparticles (ocMP) using flow cytometry analysis.	132
Figure 52: Detection of AnnexinV ⁺ and AnnexinV ⁺ EpCAM ⁺ oval cell-associated microparticles (ocMP) in human serum.	133
Figure 53: Oval cell-associated microparticles (ocMPs) differ patients bearing cholangiocarcinoma from patients bearing hepatocellular carcinoma.	134
Figure 54: Diagnostic performance of AnnexinV ⁺ and AnnexinV ⁺ EpCAM ⁺ oval cell-associated microparticles (ocMPs) for patients bearing cholangiocarcinoma.	138
Figure 55: Serum tumor markers correlate moderately with AnnexinV ⁺ and AnnexinV ⁺ EpCAM ⁺ oval cell-associated microparticles (ocMPs) of patients bearing primary hepatic cancers.	141
Figure 56: Blood chemistry values correlate almost not with AnnexinV ⁺ and AnnexinV ⁺ EpCAM ⁺ oval cell-associated microparticles (ocMPs) of patients bearing primary hepatic cancers.	142
Figure 57: Oval cell-associated microparticles (ocMPs) an their diagnostic potential.	144
Figure 58: Proposal of a possible screening method to classify primary hepatic cancer in hepatocellular carcinoma and cholangiocarcinoma using several tumor- and oval cell-associated microparticle populations.	145
Figure 59: Summary of exploration and validation of surface marker profiles to examine microparticles (MPs) as novel minimal invasive liquid biopsy tool to identify and classify primary hepatic cancer.	146

LIST OF TABLES

Table 1: Classification of primary malignant neoplasms in liver.	5
Table 2: TNM classification of hepatocellular carcinoma and cholangiocarcinoma.....	6
Table 3: Human cancer cell lines used during the current study.	20
Table 4: Staining procedure for the analysis of single-cell suspensions.....	30
Table 5: Overview of antibodies and MicroBeads used for the analysis of human cancer cell lines and murine liver cells.	32
Table 6: Composition of the qRT-PCR reaction mix used for gene expression analysis of CD133 ⁺ oval cells.....	39
Table 7: Overview of QuantiTect Primer Assays used for the SYBR® Green-based gene expression analysis of CD133 ⁺ oval cells.	39
Table 8: Conditions of qRT-PCR for gene expression analysis of CD133 ⁺ oval cells.	40
Table 9: Summary of the various departments involved in collection of human blood samples.	41
Table 10: Staining procedure to analyze human cell-derived microparticles.	43
Table 11: Overview of antibodies used for the analysis of human cell-derived microparticles.	45
Table 12: Optical configuration of the MACSQuant® Analyzer 10.	46
Table 13: Statistical power analysis to determine need for sera.	48
Table 14: Assortment of cancer- and hepatic progenitor cells-related surface markers.	50
Table 15: Demographics of each entity participated in the ‘Tumor-related microparticles to identify primary hepatic cancer’ study.....	74
Table 16: Demographics of each entity participated in the ‘Oval cell-related microparticles to classify primary hepatic cancer’ study.	77
Table 17: Values of AnnexinV ⁺ microparticles (MPs) from human serum of each cohort participated in the human cell-derived MPs study.	81
Table 18: Values of AnnexinV ⁺ EpCAM ⁺ tumor-associated microparticles (taMPs) from human serum of each cohort participated in the human cell-derived MPs study.	87
Table 19: Diagnostic performance of AnnexinV ⁺ EpCAM ⁺ tumor-associated microparticles (taMPs) of each cohort.	89
Table 20: Values of AnnexinV ⁺ EpCAM ⁺ CD133 ⁺ and AnnexinV ⁺ EpCAM ⁺ CD133 ⁺ ASGPR1 ⁺ liver disorder-associated microparticles (MPs) from human serum of each cohort participated in the human cell-derived MPs study.	102
Table 21: Diagnostic performance of AnnexinV ⁺ EpCAM ⁺ CD133 ⁺ and AnnexinV ⁺ EpCAM ⁺ CD133 ⁺ ASGPR1 ⁺ liver disorder-associated microparticles (MPs) of each cohort.....	103
Table 22: Values of AnnexinV ⁺ EpCAM ⁺ ASGPR1 ⁺ tumor-associated microparticles (taMPs) from human serum of each cohort participated in the human cell-derived MPs study.	113
Table 23: Diagnostic performance of AnnexinV ⁺ EpCAM ⁺ ASGPR1 ⁺ values of patients bearing liver disorders.....	115

Table 24: Values of AnnexinV ⁺ EpCAM ⁺ gp38/CD133 tumor-associated microparticle (taMP) subpopulations from human serum of each cohort participated in the human cell-derived MPs study.	129
Table 25: Diagnostic performance of AnnexinV ⁺ EpCAM ⁺ gp38 ⁺ CD133 ⁺ tumor-associated microparticles (taMPs) for patients bearing liver disorders.	130
Table 26: Values of oval cell-associated microparticles (ocMPs) from human serum of each cohort participated in the human cell-derived MPs study.	135
Table 27: Diagnostic performance of AnnexinV ⁺ and AnnexinV ⁺ EpCAM ⁺ oval cell-associated microparticles (ocMPs) for patients bearing cholangiocarcinoma.	139

INDEX OF ABBREVIATIONS

#	Number
%	Percent
°C	Degrees Celsius
ΔCt	Delta cycle threshold
ACC	Acceleration
AFP	Alpha-1 fetoprotein
AJCC	American Joint Committee on Cancer
ALT	Alanine transaminase
AnnexinV ⁺ ocMPs	AnnexinV ⁺ gp38 ⁺ CD133 ⁺ oval cell-associated microparticles
AnnexinV ⁺ EpCAM ⁺ ocMPs	AnnexinV ⁺ EpCAM ⁺ gp38 ⁺ CD133 ⁺ oval cell-associated microparticles
ANOVA	Analysis of variance
ASGPR/ASGPR1	Asialoglycoprotein receptor 1
AUC	Area under curve
B2M	Beta-2-microglobulin
BMI	Body mass index
BSA	Bovine serum albumin
CA 19-9	Carbohydrate-antigen 19-9
Ca ²⁺	unbound, ionized calcium
CCA	Cholangiocarcinoma
CCL2	C-C motif chemokine ligand 2
CCL ₄	Carbon tetrachloride
CDE	Choline-deficient, ethionine-supplemented
CDH1	Cadherin 1
cDNA	Complementary DNA
CEA	Carcinoembryonic antigen
cm ³	Cubic centimeter
CO ₂	Carbon dioxide
CrC	Colorectal cancer
CT	Computed tomography
Ctrl	Healthy and Athletes
DDC	3,5-diethoxycarbonyl-1,4-dihydrocollidine
DEC	Deceleration
DMSO	Dimethyl sulfoxide
DNA	Deoxyribonucleic acid
EDTA	Ethylenediaminetetraacetic acid
EMT	Epithelial-mesenchymal transition
EpCAM	Epithelial cell adhesion molecule (CD326)
EVs	Extracellular vesicles

INDEX OF ABBREVIATIONS

FAS	Fas cell surface death receptor
FBS	Fetal bovine serum
FMO	Fluorescence minus one
g / mg / µg / ng	Gram / Milligram / Microgram / Nanogram
H ₂ O	Water
HBSS	Hanks' balanced salt solution
HBV	Hepatitis B virus
HCC	Hepatocellular carcinoma
HCV	Hepatitis C Virus
HNF1A	Hepatocyte nuclear factor 1-alpha
HNF1B	Hepatocyte nuclear factor 1-beta
HNF4A	Hepatic nuclear factor 4-alpha
HNF6	Hepatocyte nuclear factor 6
HPC / HPCs	Hepatic progenitor cell(s)
HPCC	Hepatic progenitor cell compartment
IARC	International Agency for Research on Cancer
ICAM-1	Intercellular adhesion molecule-1 (CD54)
ICD-10-GM-2017	International classification of diseases, 10 th revision, German modification, version 2017
iNKT cells	invariant natural killer T cells
INR	International normalized ratio
IP	Intraperitoneally
KRT19	Keratin 19
L / dL / mL / µL	Liter / Deciliter / Milliliter / Microliter
MCD	Methionine, choline-deficient
MDR2-KO	Multidrug resistance protein 2-knockout
MELD	Model of end-stage liver disease
MFI	Mean fluorescence intensity
MIC1-1C3	Macrophage inhibitory cytokine-1-1C3
min	Minutes
mm	Millimeter
MP / MPs	Microparticle(s)
MRI	Magnetic resonance imaging
N	Sample size
N/A	Not available
NAFLD	Non-alcoholic fatty liver disease
NASH	Non-alcoholic steatohepatitis
Non-biliary CA	Non-biliary cancer
NPV	Negative prediction value
Ns	Not significant
NSCLC	Non-small-cell lung cancer

INDEX OF ABBREVIATIONS

ocMP / ocMPs	Oval cell-associated microparticle(s)
<i>P</i>	<i>p</i> value
P/S	Penicillin-Streptomycin
PaCa	Pancreatic cancer
PBS	Dulbecco's phosphate buffered saline
PDPN	Podoplanin (gp38)
PI	Propidium iodide
Post-OP	Postoperative
PPV	Positive prediction value
Pre-OP	Preoperative
PROM1	Prominin 1 (CD133)
qRT-PCR	Real-time quantitative polymerase chain reaction
<i>r</i>	Pearson's correlation coefficient
R0 resection	No residual tumor after surgical resection
R^2	Coefficient of determination
RNA	Ribonucleic acid
ROC	Receiver-operating characteristic
RPMI	Roswell Park Memorial Institute
RT	Room temperature
Sca-1	Stem cell antigen-1 (Ly-6A/E)
SD	Standard deviation
SE	Standard error
SEM	Standard error of the mean
TAA	Thioacetamide
taMP / taMPs	Tumor-associated microparticle(s)
TNM	Tumor, Nodes, Metastases
U	Enzyme unit
UICC	Union for International Cancer Control
US	Ultrasound, ultrasonography, sonography
v/v	Volume per volume
w/v	Weight per volume
WHO	World Health Organization
x g	Units of gravity
y	Years
YAP1	Yes-associated protein 1
ZfKD	German Center for Cancer Registry Data (<i>ger: Zentrum für Krebsregisterdaten</i>)

1 Introduction

1.1 Contemporary estimates of cancer incidence and mortality

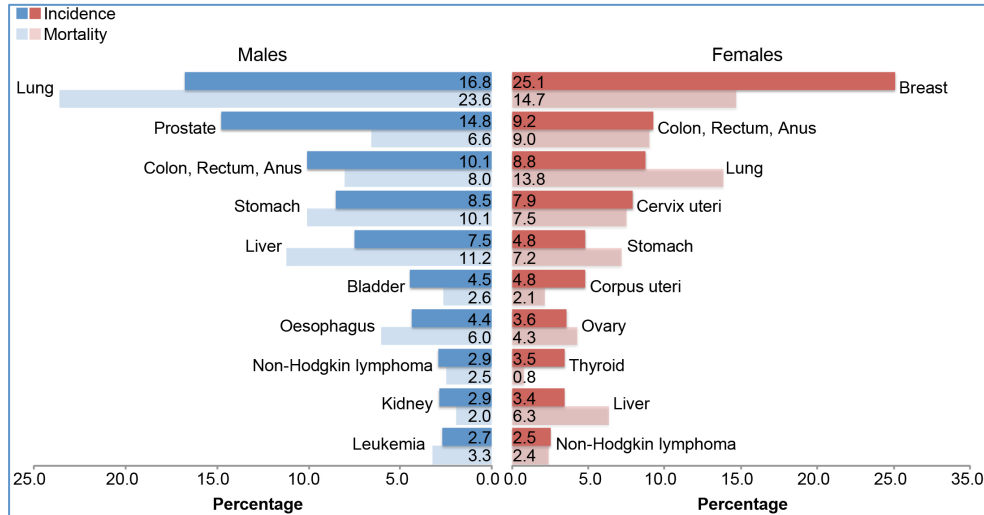


Figure 1: Most common tumor incidences and mortalities worldwide.

Estimates numbers of the most common tumor localizations and cancer death cases worldwide in 2012 for females and males are displayed in percentages (Data according to estimates of GLOBOCAN 2012 project of the International Agency for Research on Cancer (Ferlay *et al.*, 2015)).

According to World Health Organization (WHO) estimates for 2015, with 8.8 million deaths cancer is the second leading cause of death globally (World Health Organisation, 2017). The GLOBOCAN 2012 project of the International Agency for Research on Cancer (IARC) estimates incidence, mortality and prevalence from major cancer types for 184 countries worldwide in 2012 (Ferlay *et al.*, 2015). About 14.07 million cancer incidences (females: 6.66 million; males: 7.41 million) and 8.20 million deaths caused by cancer (females: 3.55 million; males: 4.65 million) were estimated. The most common tumor localizations for both sexes worldwide in 2012 are the lung (1.82 million, 13.0 %), female breast (1.67 million, 11.9 %) and colon (1.36 million, 9.7 %). In comparison, the liver is the fifth most frequent tumor site with 0.78 million (5.6 %; females: 0.23 million, 3.4 %; males: 0.55 million, 7.5 %). The most common mortality for both sexes worldwide was estimated for lung cancer (1.59 million, 19.4 %), liver cancer (0.75 million, 9.1 %) and stomach cancer (0.72 million, 8.8 %) (Figure 1) (Ferlay *et al.*, 2015).

Altogether 0.48 million cancer diseases including all malignant neoplasm together with lymphomas and leukemia, were diagnosed for the first time in Germany, 2013 according to estimates of the German Center for Cancer Registry Data (*ger.*: *Zentrum für Krebsregisterdaten*, ZfKD). A total of 0.23 million females and 0.25 million males

were affected by cancer in Germany, 2013. Most common tumor localizations are the breast (72 thousand, 15 %; females: 31,2 %; males: 0.3 %), colon (62 thousand, 12.9 %; females: 12.3 %; males: 13.5 %), prostate (60 thousand; males: 23.6 %) and lung (54 thousand, 11.1 %; females: 8.2 %, males: 13.7 %). In Germany, the liver belongs to the less frequent tumor sites with 9 thousand incidences in 2013 (1.8 %; females: 1.1 %; males: 2.4 %) (Figure 2A) (Robert Koch Institut - Zentrum für Krebsregistrierdaten, 2017).

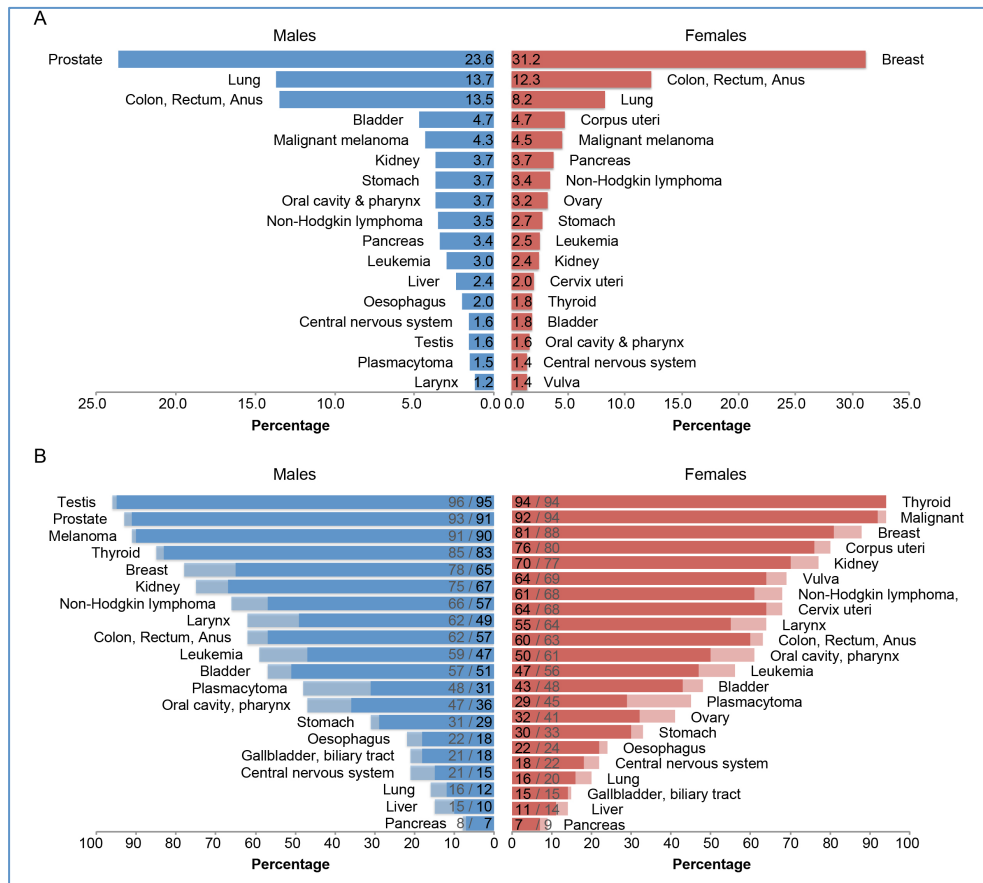


Figure 2: Tumor incidence and survival rates of the most common tumor localizations in Germany.

A) Percentage distribution of the most common tumor localizations of all tumor incidences in Germany, 2013 for females and males are displayed. B) Five-year (light blue/ light red/ grey) and ten-year (blue/ red/ black) relative survival for females and males according to tumor localization in Germany, 2011-2012 are depicted (period analysis). Survival rates are given as percentages for each tumor localization (Data according to estimates of German Center for Cancer Registry Data (Robert Koch Institut - Zentrum für Krebsregistrierdaten, 2017)).

The relative survival rate indicates how many people with cancer are still alive in comparison to the general population after five or ten years after cancer diagnosis. The relative survival rates differ depending on the tumor localization. Tumor localizations in testis, prostate, thyroid (females) or malignant melanoma show five-year relative survival rates over 90 %. However, short life expectancy with below 20 % five-year relative survival is present in tumor diagnoses in the lung, liver, pancreas and

gallbladder (females). Figure 2B compares the five-year and ten-year relative survival rates of the most common tumor localizations in Germany 2011-2012 (Robert Koch Institut - Zentrum für Krebsregistrierdaten, 2017).

1.2 Primary hepatic cancer: malignant neoplasms of the liver

The liver is the fifth most frequent tumor site worldwide, albeit one of the less frequent tumor sites in Germany, importantly liver tumors are accompanied by a poor prognosis. The incidence of hepatic cancer has increased in the past twenty years. According to estimates of the ZfKD, about 2 females and 5.4 males per 100,000 inhabitants were diagnosed for the first time with hepatic cancer in Germany, 1995, whereas the incidence per 100,000 inhabitants increased to 2.4 females and 7 males in Germany, 2013 (Figure 3A). The incidence rate increases with advancing age in Germany, 1995-2013 (Figure 3B). At an age of 40-44, the incidence rate is 0.9 females and 1.5 males per 100,000 inhabitants. Compared

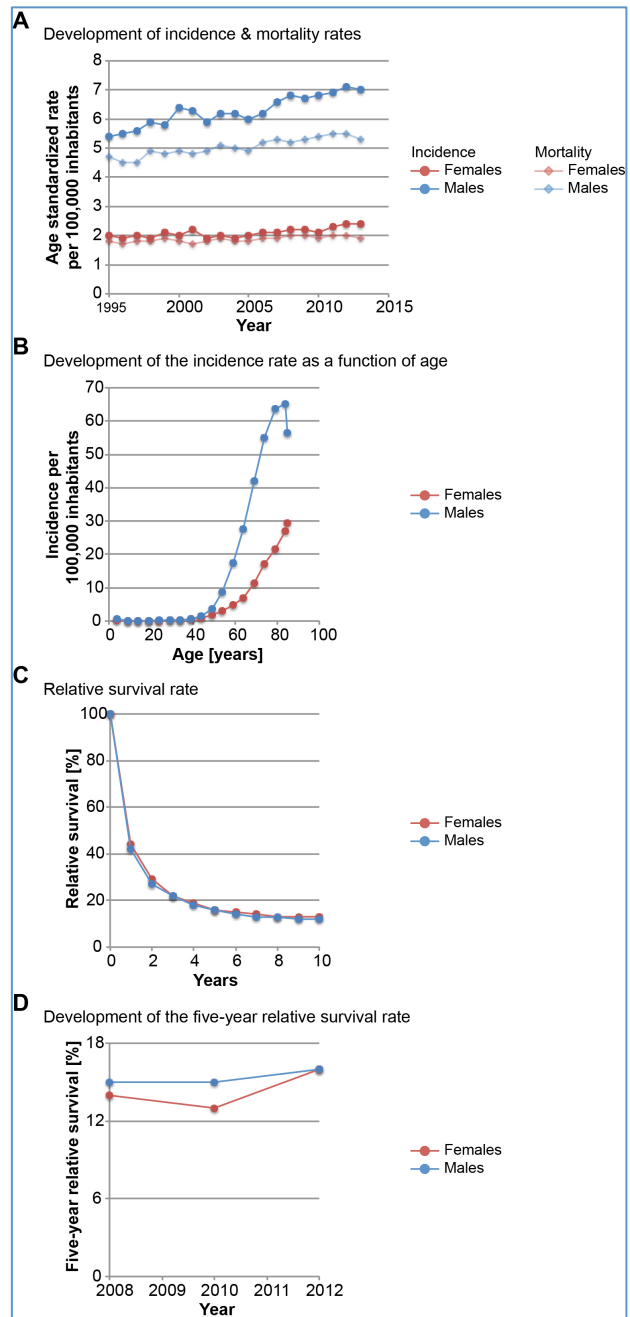


Figure 3: Liver cancer statistics and its development in the last few years.

A) Progress of incidence (red/ blue) and mortality (light red/ light blue) rates of liver cancer through the years are indicated as age standardized rate (Segi World Standard) per 100,000 inhabitants in Germany, 1995-2013 for females (red) and males (blue). B) Incidence of liver cancer and its dependency on age are displayed. Data are given per 100,000 inhabitants in Germany, 1995-2013 for females and males. C) Relative survival rate till 10 years after diagnosis for females and males is depicted. Data are age standardized and given as percentage for Germany, 2012 (period analysis). D) Development of the five-year relative survival rates over the years is indicated. Data are age standardized and given as percentage for females and males in Germany, 2008, 2010 and 2012 (period analysis) (Data according to estimates of German Center for Cancer Registry Data (Robert Koch Institut - Zentrum für Krebsregistrierdaten, 2017)).

thereto, the incidence rate increases by about 8 times for females and even 18 times for males at an age of 60-64. At an age of 80-84, the incidence rate increases to 27.1 females and 65.1 males per 100,000 inhabitants.

The mortality rate of hepatic cancer also indicates an increase through the years (Figure 3A). The poor prognosis in hepatic cancer is reflected in age standardized five-year and ten-year relative survival rates below 20 %, in Germany 2011-2012. Only 16 % of females and males are still alive five years after first diagnosis. Ten years after first diagnosis, survival rate decreases further to 13 % and 12 % for females and males, respectively (Figure 3C). This poor prognosis has not changed in the recent years (Figure 3D).

1.2.1 Types and staging of primary hepatic cancer

Usually, the liver is one of the common sites for metastases in addition to the lymph nodes. In that case, cancer cells migrate from the primary tumor located in another part of the body, such as colon, lung or the breast, through the circulatory or lymphatic system to the liver where they form secondary hepatic cancer, also called metastasis to the liver (Howard, 2011). Primary hepatic cancer is generally caused by cirrhosis or liver inflammation due to alcohol abuse, autoimmune diseases of the liver, hepatitis B or C, or hemochromatosis (Howard, 2011).

The ICD-10-GM-2017 (International classification of diseases, 10th revision, German modification, version 2017) is considered as the official classification for the coding of diagnoses. Malignant neoplasms such as primary hepatic cancer are classified to code C22 (Table 1), secondary hepatic cancer are assigned to code C78.7 and benign neoplasms of the liver are classified to code D13.4 (DIMDI - Deutsches Institut für Medizinische Dokumentation und Information, 2012). Primary hepatic cancer is divided into several types depending on their origin: 1) Hepatocellular carcinoma (C22.0) is the most common type of hepatic cancer and originates in hepatocytes, 2) Cholangiocarcinoma (C22.1) starts in intrahepatic bile ducts, 3) Hepatoblastoma (C22.2.) primarily affects children younger than the age of 4 and risk for developing is assumed to be associated with genetic conditions, 4) Angiosarcoma (C22.3) starts in blood vessels of the liver, 5) other sarcomas of the liver (C22.4), 6) other specified carcinomas of the liver (C22.7) and 7) not specified malignant neoplasm of the liver (C22.9) (Table 1) (DIMDI - Deutsches Institut für Medizinische Dokumentation und Information, 2012).

Table 1: Classification of primary malignant neoplasms in liver.

Indicated are the classifications of primary hepatic cancer based on the diagnosis code according to ICD-10-GM-2017 (International classification of diseases, 10th revision, German modification, version 2017 (DIMDI - Deutsches Institut für Medizinische Dokumentation und Information, 2012)) and the corresponding origin of each primary hepatic cancer type. Listed malignant neoplasms are determined as primary. Excluded are bile ducts and secondary malignant neoplasms of the liver.

Type	ICD	Origin
Hepatocellular carcinoma ¹	C22.0	Hepatocytes
Cholangiocarcinoma ²	C22.1	Intrahepatic bile ducts
Hepatoblastoma ³	C22.2	Genetic conditions
Angiosarcoma of the liver	C22.3	Liver blood vessels
Other sarcomas of the liver	C22.4	
Other specified carcinomas of the liver	C22.7	
Malignant neoplasm of the liver	C22.9	Not specified as primary or secondary

ICD: International classification of diseases

¹Most common type

²Cholangiocarcinoma combined with hepatocellular carcinoma is classified to code C22.0

³This type affects children younger than the age of 4.

Based on physical examinations, imaging procedures (ultrasound (ultrasonography, sonography, US), computed tomography (CT), magnetic resonance imaging (MRI)) and results of operations, staging systems for cancer display how widespread the cancer is at the time of diagnosis (American Cancer Society, 2018). This is used to determine the most appropriate therapy and to estimate a prognosis for the patients. The TNM classification, developed by American Joint Committee on Cancer (AJCC) and adopted by Union for International Cancer Control (UICC), is the most commonly used staging system (AJCC - American Joint Committee on Cancer, 2018) and it is based on three standardized criteria to assess the tumor disease: Tumor (T) – describes the extent of the primary tumor relating to size, number and infiltration depth, whereby increasing severity is indicated by the numbers 0 to 4; Nodes (N) – describes the absence (0) or presence (1) of locoregional lymph node metastases; Metastases (M) – describes spreading of the tumor through the absence (0) or presence (1) of distant metastases in other parts of the body (Brierley *et al.*, 2003). The combination of these three parameters gives indication about the extent of the tumor disease. Hereafter, the TNM classification for staging of hepatocellular carcinoma (HCC) and malignant tumors of the intrahepatic bile ducts, named cholangiocarcinoma (CCA), are displayed according to Brierley *et al.* (2003) (Table 2).

Table 2: TNM classification of hepatocellular carcinoma and cholangiocarcinoma.

Classification of primary hepatic cancer according to anatomical extent by AJCC² developed TNM classification and UICC¹ adopted staging is indicated. Description of each stage to assess the extent of the tumor disease is displayed for hepatocellular carcinoma (HCC) and cholangiocarcinoma (CCA) (Brierley *et al.*, 2003).

Stage ¹	TNM classification ²	Description
IA	T1a, N0, M0	Solitary tumor (HCC < 2 cm, CCA < 5 cm) with or without vascular invasion
IB	T1b, N0, M0	Solitary tumor (HCC > 2 cm, CCA > 5 cm) without vascular invasion
II	T2, N0, M0	HCC: Either a solitary tumor (> 2 cm) with vascular invasion or multiple tumors (< 5 cm) CCA: Either a solitary tumor with intrahepatic vascular invasion or multiple tumors with or without vascular invasion
IIIA	T3a, N0, M0	HCC: Multiple tumors (> 5 cm) CCA: Tumor(s) with perforation of the visceral peritoneum
IIIB	T4, N0, M0	HCC: Tumor(s) with invasion into a branch of major vein of the <i>Vena portae</i> or <i>Vena hepatica</i> with invasion into nearby organs (other than the gallbladder) or perforation of the visceral peritoneum CCA: Tumor(s) with invasion into local extrahepatic structures by direct hepatic invasion
IVA	Any T, N1, M0	The tumor has spread to locoregional lymph nodes but not metastasized to distant parts of the body
IVB	Any T, Any N, M1	The tumor has metastasized to distant parts of the body

¹Staging system adopted by UICC (Union for International Cancer Control)

²Staging system developed by AJCC (American Joint Committee on Cancer)

T: Tumor = Characterization of size, number and growth behavior of primary tumor(s); increasing severity is indicated by numbers 0 to 4

N: *Nodus* = Absence (0) or presence (1) of locoregional lymph node metastases

M: Metastases = Absence (0) or presence (1) of distant metastases

1.2.2 Conventional methods in diagnosis of primary hepatic cancer

In diagnosis of HCC and CCA, serum markers and various imaging modalities play a crucial role. The serum tumor marker alpha-1 fetoprotein (AFP), carcinoembryonic

antigen (CEA) and carbohydrate-antigen 19-9 (CA 19-9), often in combination with US are used to monitor patients at risk to develop primary hepatic cancer or to examine suspected liver diseases. However, to examine the suspicion of HCC and CCA, respectively, more sophisticated imaging procedures such as CT and MRI are required and under circumstances tissue sampling can confirm unclear diagnoses (Bialecki & Di Bisceglie, 2005; Van Beers, 2008).

1.2.2.1 Serum tumor markers in the diagnosis of primary hepatic cancer

In general, blood tests provide information about organ functions. If hepatic cancer is suspected, the blood is checked for various serum markers, especially tumor markers.

AFP is expressed principally by the fetal liver and its synthesis declines subsequently after birth and remains low in adults under physiological conditions (Burtis *et al.*, 2012; Ruoslahti & Seppälä, 1971). On the other hand, previous studies reveal an association between elevated AFP levels and HCC (Abelev *et al.*, 1963; E. Alpert *et al.*, 1971; M.E. Alpert *et al.*, 1968; McIntire *et al.*, 1972; Purves *et al.*, 1968; Ruoslahti & Seppälä, 1971; Smith & Todd, 1968). Due to this, AFP developed to the most widely used tumor marker to detect HCC. However, AFP alone constitutes a poor marker for the recognition of HCC. This limitation is based in the main on the occurrence of increased AFP levels not only in hepatocarcinogenesis (Ding *et al.*, 2005; França *et al.*, 2004; Grizzi *et al.*, 2007; Gupta *et al.*, 2003), but also in gastric (Chen *et al.*, 2003) and lung cancer (Hiroshima *et al.*, 2002), as well as in absence of cancer, particularly under pathological conditions such as chronic liver disease, e.g. liver cirrhosis (Gomaa *et al.*, 2009). Apart from this, normal AFP values are indicated in up to 40 % of patients with early stage of HCC (Malek *et al.*, 2014) and only 60 to 80 % of HCC are positive for AFP. Resulting in varying diagnostic potential (Sensitivity: 40 to 65 %, Specificity: 76 to 96 %) (Cedrone *et al.*, 2000; Collier & Sherman, 1998; Gambarin-Gelwan *et al.*, 2000; Sherman, 2001; Trevisani *et al.*, 2001), as a function of study design, patient population and cut-off values used (Debruyne & Delanghe, 2008; Gebo *et al.*, 2002; Gupta *et al.*, 2003; Trevisani *et al.*, 2001).

The most commonly used markers in the diagnosis of CCA are CA 19-9 and CEA. The glycoprotein CA 19-9 was originally isolated from a human colorectal cancer cell line (Koprowski *et al.*, 1979) and is expressed by normal human pancreatic and biliary ductular cells and by gastric, colon, endometrial and salivary epithelia (Burtis *et al.*, 2012). Although it is the most extensively studied marker for CCA detection, elevated

CA 19-9 values are also associated with HCC or other extrahepatic gastrointestinal cancers, particularly pancreatic cancer (PaCa) (Duffy, 1998; Maestranzi *et al.*, 1998; Nehls *et al.*, 2004; Rhodes, 1999; Torzilli *et al.*, 2002). Additionally, patients with non-malignancies, such as primary sclerosing cholangitis or biliary obstruction indicate also elevated levels of CA 19-9 (Ince *et al.*, 2014; M.S. Lin *et al.*, 2014). Thus, CA 19-9 alone constitutes a poor marker with varying diagnostic potential in sensitivity (50-100 %) and specificity (50-98 %), depending on used cut-off values (Feverly *et al.*, 2007; John *et al.*, 2007; Levy *et al.*, 2005; Nehls *et al.*, 2004; Patel *et al.*, 2000). For instance, detection of CCA with good sensitivity (79 %), high specificity (98 %) and moderate positive predictive value (57 %) in patients with symptomatic primary sclerosing cholangitis is indicated by use of 129 U/mL CA 19-9 serum concentration as cut-off value (Levy *et al.*, 2005).

The glycoprotein CEA is mainly associated with colorectal cancer (CrC) in addition to numerous other cancer entities, such as lung, gastric, breast, pancreatic, ovarian and uterine carcinomas (Burtis *et al.*, 2012). However, CCA is also suggested to be a marker in diagnosis of CCA, with lower diagnostic potential in sensitivity (33-84 %) and specificity (33-100 %), compared to CA 19-9 (Nehls *et al.*, 2004; Siqueira *et al.*, 2002). Thus, serum tumor markers alone are insufficient to detect HCC and CCA, respectively, nor to monitor patients at risk to develop a liver tumor.

1.2.2.2 Imaging modalities to assess primary hepatic cancer

In diagnosis of HCC and CCA, imaging plays a crucial role. However, it also has limitations. Detection of small tumors is difficult, especially in patients with cirrhosis because of an abnormal parenchymal architecture, as well as the differentiation of HCC from benign lesions, which can occur during cirrhosis (Bialecki & Di Bisceglie, 2005). Sonography is one of the first methods for screening focal hepatic lesion and however, sensitivity was shown to be affected by the tumor size. HCC lesions in pre-transplant patients greater than 2 cm revealed in 38 % sensitivity, whereas nodules smaller than 2 cm indicate 30 % sensitivity (C.K. Kim *et al.*, 2001). In addition, 42 % sensitivity was shown for lesions smaller 1 cm by other studies (Bizollon *et al.*, 1998; Dodd *et al.*, 1992; França *et al.*, 2004), in contrast to 95 % sensitivity for larger nodules (Colli *et al.*, 2006). Moreover, detection of HCC and dysplastic nodules in patients with end-stage cirrhosis indicated low sensitivity but high specificity (Saar & Kellner-Weldon, 2008). Thus, the diagnostic potential varies and revealing of HCC by the help of US depends

on size and nature of the tumor. Most small tumors (less than 3 cm) are well defined and homogeneous as opposed to heterogeneous or diffuse as in size growing tumors, which differ in their ultrasonographic characteristic (Gomaa *et al.*, 2009; Saar & Kellner-Weldon, 2008; Yu *et al.*, 2004). Although small tumors can be revealed, in cirrhotic livers with abnormal parenchymal architecture it can be challenging to differ from benign lesions. The diagnostic efficiency in distinguishing malignancies from non-malignancies is improved using contrast-enhanced US due to enhanced visualization of liver tumor vascularity (Albrecht *et al.*, 2004; Claudon *et al.*, 2013; Pompili *et al.*, 2008). CT und MRI imaging examines the suspicion of HCC and both evaluation methods use similar concepts in the assessment of liver lesions. Spiral CT is considered being the imaging modality for the initial assessment of suspected HCC (Lopez Hänninen *et al.*, 1998; Shapiro *et al.*, 1996; Yu *et al.*, 2004), with high diagnostic potential in sensitivity (80 %) and specificity (96 %) (Lim *et al.*, 2000). However, tumor size affects the diagnostic potential as sensitivity for tumors greater than 2 cm is up to 100 %, 93 % for tumors with 1 to 2 cm in size and small-sized tumors less than 1 cm indicated just 60 % sensitivity (Gomaa *et al.*, 2009; T. Kim *et al.*, 1999). Contrast MRI and follow up CT may increase the diagnostic potential in diagnosis of HCC, because, in estimating tumor size MRI was indicated to be more precise (Snowberger *et al.*, 2007), as well as in assessment of tumor architecture, tumoral margins and vascularity of the tumor (Ebara *et al.*, 1986; Gomaa *et al.*, 2009). However, tumor size also influences the diagnostic potential of HCC detection. High sensitivity of about 95 % is given for tumors greater than 2 cm, but this decrease drastically to 30 % for tumors less than 2 cm (Ebara *et al.*, 1986; Gomaa *et al.*, 2009).

In diagnosis of CCA, US alone is also not sufficient. As its difficult to reveal small tumors and to determine the accurately tumor extent (Aljiffry *et al.*, 2009; Ariff *et al.*, 2009; Charatcharoenwitthaya *et al.*, 2008; Khan *et al.*, 2012; Kuszyk *et al.*, 1997). Diagnostic potential of US in patients with primary sclerosing cholangitis and advanced CCA indicate high specificity and negative prediction values (90 %), but low sensitivity and positive prediction value (50 %) (Aljiffry *et al.*, 2009; Charatcharoenwitthaya *et al.*, 2008; Khan *et al.*, 2012; Kuszyk *et al.*, 1997). The sensitivity of contrast CT is up to 80 % in diagnosis of CCA, albeit, the tumor extent is often not well-defined (Aljiffry *et al.*, 2009; Ariff *et al.*, 2009; Charatcharoenwitthaya *et al.*, 2008; Khan *et al.*, 2012; Kuszyk *et al.*, 1997). To delineate hepatobiliary anatomy and tumor extent, contrast MRI is the ideal imaging modality in diagnosis of CCA (Ariff *et al.*, 2009; Khan *et al.*,

2012; Maccioni *et al.*, 2010; Vergel *et al.*, 2006), but is inferior to CT in the detection of distant metastases (Ariff *et al.*, 2009; Khan *et al.*, 2012; Maccioni *et al.*, 2010).

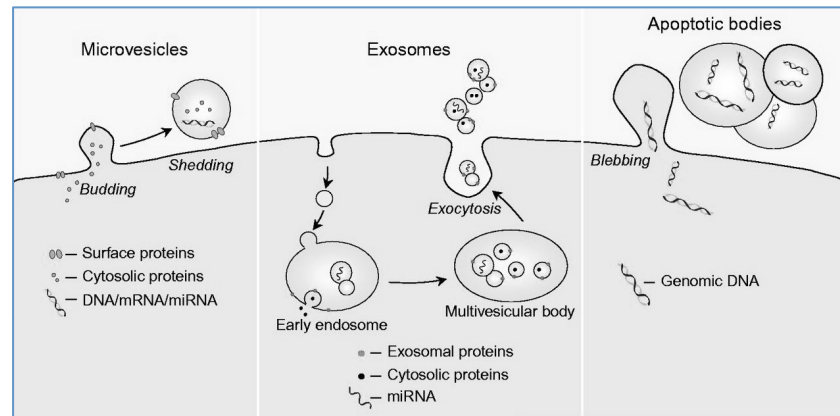


Figure 4: Formation and release of extracellular vesicles.

Extracellular vesicles, including microvesicles/microparticles (MPs), exosomes and apoptotic bodies, differ not only in size but also in formation. Exosomes (50-100 nm) are formed via the endosomal pathway and released by exocytosis through the fusion of multivesicular bodies with the plasma membrane of cells. On the other hand, MPs (100-1,000 nm) shed by budding directly from the plasma membrane and thus probably contain surface markers from the cell of origin. Apoptotic bodies (1-5 μ m) are released during apoptosis through blebbing of the plasma membrane (Lawson *et al.*, 2016)

1.3 Microparticles as a possibly liquid biopsy tool

Liquid biopsies are defined as “A test done on a sample of blood to look for cancer cells from a tumor that are circulating in the blood or for pieces of DNA from tumor cells that are in the blood. A liquid biopsy may be used to help find cancer at an early stage. It may also be used to help plan treatment or to find out how well treatment is working or if cancer has come back.” (National Cancer Institute, 2018).

The importance of liquid biopsies is increasingly becoming the focus of attention. Biomarkers based on liquid biopsies comprise the analysis of circulating tumor cells and circulating tumor DNA (Alix-Panabières & Pantel, 2016; Bardelli & Pantel, 2017; Haber & Velculescu, 2014), as well as microRNAs (Becker *et al.*, 2016) or extracellular vesicles (EVs) (Bach *et al.*, 2017; Becker *et al.*, 2016; Julich *et al.*, 2014; Moore *et al.*, 2017; Siravegna *et al.*, 2017).

1.3.1 Microparticles – a subtype of extracellular vesicles

EVs released from the plasma membrane of various cell types both constitutively and in response to activation or stress (Lynch *et al.*, 2017) appear in different body fluids, including blood (serum/plasma) (Kornek *et al.*, 2011, 2012), bile (Masyuk *et al.*, 2010) and urine (Dimuccio *et al.*, 2014). EVs represent a heterogeneous group, containing exosomes, microparticles (MPs) and apoptotic bodies, differing not only in their size

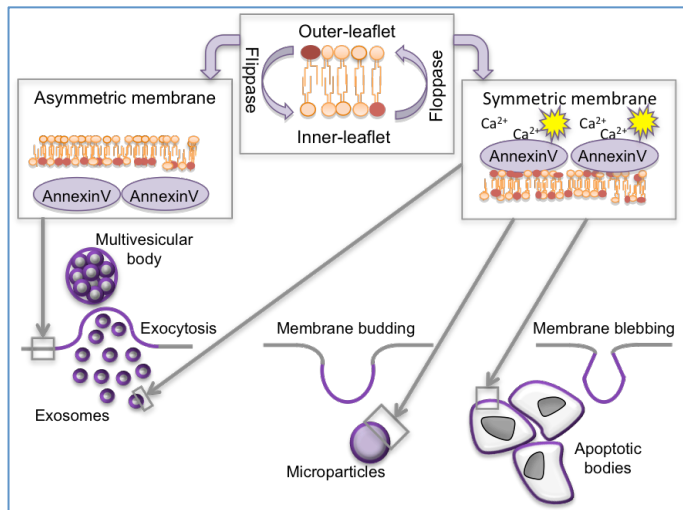


Figure 5: Membrane characteristics of extracellular vesicles.

Extracellular vesicles, including exosomes, microparticles (MPs) and apoptotic bodies exhibit membrane symmetry. Under resting conditions, cell membrane asymmetry with phospholipid phosphatidylserine (red) in the inner leaflet is maintained by the ATP-dependent translocase activity of flippase and floppase. Microparticle release is carried out during cellular activation and early apoptosis by influx of unbound, ionized calcium (Ca^{2+}), which inhibits flippase activity and leads to loss of membrane asymmetry, membrane remodeling, budding of the surface and phosphatidylserine exposure. AnnexinV can bind to phosphatidylserine, which can be used to identify microparticles (Modified according to Kornek & Schuppan, 2012).

terminal steps of programmed cell death (Mause & Weber, 2010). MPs, 100 to 1,000 nm in diameter (Mause & Weber, 2010), are referred to as ectosomes or microvesicles (Cocucci *et al.*, 2009; György *et al.*, 2011; Hess *et al.*, 1999; Holme *et al.*, 1994) and shed by membrane budding directly from the plasma membrane (Mause & Weber, 2010). Thus, MPs contain surface markers, cytosolic proteins and nucleic acids (DNA, mRNA, microRNA) from the cell of origin (Al-Nedawi *et al.*, 2008; Benameur *et al.*, 2010; Diehl *et al.*, 2012; Fritzsche *et al.*, 2002; Rozmyslowicz *et al.*, 2003), whereby MPs seem to resemble their parental cells (Julich *et al.*, 2014).

The process of MP release is associated with the activation of the membrane attack complex of the complement system (C5b-9) and influx of unbound, ionized calcium (Ca^{2+}) (Julich *et al.*, 2014). The phospholipid phosphatidylserine is part of the asymmetric bilayer and were found principally in the inner leaflet (Figure 5) (Seigneuret *et al.*, 1984). This condition is maintained by means of the ATP-dependent aminophospholipid translocase activity, called flippase (Dolis *et al.*, 1997) and floppase (Connor *et al.*, 1992). Cell activation leads to influx of Ca^{2+} , which inhibits flippase activity and activate the ATP-independent but Ca^{2+} -dependent enzyme, named scramblase (Williamson *et al.*, 1995). Thus phospholipids can move randomly between

but also in their formation (Figure 4). Exosomes are the smallest EVs with 50 to 100 nm in diameter (Pan *et al.*, 1985). They originate from the endosomal pathway and are stored in multivesicular bodies, which fuse with the plasma membrane and release their cargo (exosomes) by exocytosis (Harding *et al.*, 1984; Pan *et al.*, 1985). The larger EVs include MPs and apoptotic bodies. Apoptotic bodies, 1 to 5 μm in diameter, are released during

both leaflets, which leads to the loss of bilayer asymmetry (Figure 5) (Simak & Gelderman, 2006). Membrane insertion of C5b-9 proteins or specific resorting of membrane proteins leads to the loss of cytoskeletal attachment to plasma membrane glycoproteins, resulting in budding of the surface (Sims *et al.*, 1988) and phosphatidylserine exposure (Fadok *et al.*, 1992) during cellular activation or early apoptosis (Mause & Weber, 2010). Annexins bind to phospholipids such as phosphatidylserine in a calcium-dependent manner (Römisch & Pâques, 1991), which can be used to identify Microparticles (Biro *et al.*, 2004; Dignat-George *et al.*, 2004; Reutelingsperger, 2001).

The mechanism of MP budding differ from the blebbing of apoptotic buddies, which depends on a myosin adenosine triphosphatase and myosin light chain kinase activity (Mills *et al.*, 1998; Simak & Gelderman, 2006).

1.3.2 Microparticle populations expand injury-specific

Originally considered as inert cell debris (Wolf, 1967), more recent studies suggest that MPs might take part in crosstalk between cells. On the one hand, MPs may be involved in signal transduction between cells by presenting of surface proteins to receptors of target cells. On the other hand, MPs may transfer their cargo to the recipient by transient interaction, membrane assimilation or incorporation of MPs to the target cell, which leads to cell activation, phenotypically modifications or reprogramming of the cell function (Del Conde *et al.*, 2005; Mause *et al.*, 2005; Mause & Weber, 2010; Obregon *et al.*, 2006; Whale *et al.*, 2006). MPs not only mediate signal transduction in close proximity to the parental cell, but also on widely distant target cells, due to their circulating in the vasculature (Mause & Weber, 2010).

The circumstance that MPs carry surface markers of the cell of origin in addition to the ability to circulate possibly enables to use MPs as disease-specific biomarkers in a minimal invasive diagnostic procedure.

Previous studies showed liver disease-specific increases of MP populations, isolated from plasma or serum, derived from the immune cell compartment (Kornek *et al.*, 2011, 2012). This included populations taking part in hepatic inflammation and fibrogenesis (T cells, invariant natural killer T (iNKT) cells, dendritic cells and macrophages) (Hernandez-Gea & Friedman, 2011; Kornek *et al.*, 2012). T cell-derived MPs, particularly CD4⁺ and CD8⁺ MPs, expand in patients with chronic hepatitis C and non-alcoholic fatty liver disease (NAFLD) (Kornek *et al.*, 2011, 2012). Interestingly,

increase of CD14⁺ MPs (monocytes/macrophage/myeloid dendritic cells-derived) and iNKT cells-derived MPs, both markers are associated with adipose tissue inflammation (Day, 2006; Karlmark *et al.*, 2009) are specific for patients with NAFLD (Kornek *et al.*, 2012). Thus, these immune cell-derived MP populations allow distinguishing of two different chronic liver diseases. In addition, increase of MP values correlate with the severity of histological inflammation (Kornek *et al.*, 2012).

Moreover, tumor-associated microparticles (taMPs) carrying one or more surface markers simultaneously detect tumor-bearing patients (Willms *et al.*, 2016). This was enabled by the surface marker combination consisting of EpCAM, upregulated in several epithelial cancers (Momburg *et al.*, 1987) and CD147, associated with tumor cell membranes (Ellis *et al.*, 1989). EpCAM⁺ MPs expand in CrC, PaCa and non-small cell lung cancer (NSCLC) and patients with thyroid nodules and remarkably, EpCAM⁺CD147⁺ MPs only occur increased in tumor-bearing patients (Willms *et al.*, 2016). Furthermore, EpCAM⁺CD147⁺ MPs correlate with the tumor volume in CrC patients and values of EpCAM⁺ MPs drop seven days after surgical R0 resection (no residual tumor after surgical resection) (Willms *et al.*, 2016), suggesting an association between MP value and tumor presence.

1.4 Aim of the current study

The aim of this study was, to examine the diagnostic potential of MPs as novel liquid biopsy tool in diagnosis of hepatic cancer, particularly hepatocellular carcinoma and cholangiocarcinoma.

Primary hepatic cancer is one of the less frequent tumor sites but accompanied by a poor prognosis and low five-year survival rate. Early tumor detection could improve the prognosis.

MPs, a subtype of extracellular vesicles, shed by membrane budding and thus carry surface markers of the cell of origin, have the ability to circulate in the vasculature. Due to this, a specific marker combination should allow to identify the origin of circulating MP populations. Previous studies indicated detection and distinguishing of liver diseases, particularly chronic hepatitis C and NAFLD or the identification of tumor-bearing patients due to different MP population pattern. Therefore it was assumed that liver- and liver tumor-derived MPs carry individual surface marker profiles and thus serve as biomarkers to detect primary hepatic cancer.

For this purpose, the study was divided into several parts. At first, surface marker profiles of human cancer cell lines were investigated. The marker panel, suitable for flow cytometry analysis, included tumor- and hepatic progenitor cells (HPCs)-associated marker to differ human liver cancer cell lines from pancreatic cancer cell lines. The second part comprehends the revising of the murine hepatic progenitor cell compartment (HPCC) to ascertain phenotypically differences between the various subpopulations and examine their involvement in liver injury-specific changes. This was utilized to possibly establish a connection between liver inflammation and liver-derived MPs. The last part of the study evaluated several human MP profiles in healthy individuals and patients bearing cirrhosis, HCC, CCA, CrC, NSCLC and PaCa. The aim was not only the detection of cancer in general, but also to identify patients bearing liver disorders (cirrhosis, HCC, CCA) and further distinction in non-malignancies (cirrhosis) and hepatic cancer patients (HCC, CCA) if not the classification in HCC and CCA.

2 Material & Methods

2.1 Material

2.1.1 Cell culture media and buffer

- **Cell line maintenance media**

Reagents	Stock	Usage	Supplier
RPMI Media			1
Fetal bovine serum (FBS)		10 % (v/v)	1
Penicillin-Streptomycin (P/S)	P: 10,000 U/mL S: 10,000 µg/mL	1 % (v/v)	1

¹Life Technologies™/Gibco by Thermo Fisher Scientific, Waltham, USA

- **Cell line starvation media**

Reagents	Stock	Usage	Supplier
RPMI Media			1
Penicillin-Streptomycin (P/S)	P: 10,000 U/mL S: 10,000 µg/mL	1 % (v/v)	1

¹Life Technologies™/Gibco by Thermo Fisher Scientific, Waltham, USA

- **Cell line conservation media**

Reagents	Stock	Usage	Supplier
RPMI Media			1
Fetal bovine serum (FBS)		10 % (v/v)	1
Penicillin-Streptomycin (P/S)	P: 10,000 U/mL S: 10,000 µg/mL	1 % (v/v)	1
Dimethyl sulfoxide (DMSO)		10 % (v/v)	2

¹Life Technologies™/Gibco by Thermo Fisher Scientific, Waltham, USA

²Sigma-Aldrich®, St. Louis, USA

- **Trypsin-EDTA solution**

Reagents	Stock	Usage	Supplier
Dulbecco's phosphate buffered saline (PBS)			1
Trypsin	0.5 %	0.05 % (v/v)	2
Ethylenediaminetetraacetic acid (EDTA)	0.5 M	4 mM	2

¹Sigma-Aldrich®, St. Louis, USA

²Life Technologies™/Gibco by Thermo Fisher Scientific, Waltham, USA

- **PBS-EDTA solution**

Reagents	Stock	Usage	Supplier
Dulbecco's phosphate buffered saline (PBS)			1
Ethylenediaminetetraacetic acid (EDTA)	0.5 M	4 mM	2

¹Sigma-Aldrich®, St. Louis, USA

²Life Technologies™/Gibco by Thermo Fisher Scientific, Waltham, USA

2.1.2 Buffer for generating liver single-cell suspension

- **Collagenase P**

Reconstitution of collagenase P (Sigma-Aldrich®, St. Louis, USA) in Hanks' balanced salt solution (HBSS, Gibco™/Life Technologies™ by Thermo Fisher Scientific, Waltham, USA) to 100 mg/mL stock concentration and stored at -20 °C.

- **Dispase II**

Reconstitution of dispase II (Gibco™/Life Technologies™ by Thermo Fisher Scientific, Waltham, USA) in Hanks' balanced salt solution (HBSS, Gibco™/Life Technologies™ by Thermo Fisher Scientific, Waltham, USA) to 100 mg/mL stock concentration and stored at -20 °C.

- **DNase-I**

Reconstitution of DNase-I (Sigma-Aldrich®, St. Louis, USA) in DNase-I buffer and stored at -20 °C.

• **DNase-I buffer**

Reagents	Stock	Usage	Supplier
Glycerol	99 %	50 % (v/v)	1
Magnesium chloride	1 M	1 mM	1
Tris-Hydrochloride pH 7.5	1 M	20 mM	1
H ₂ O			

¹Sigma-Aldrich®, St. Louis, USA

• **Digestion buffer for generating liver single-cell suspension**

Reagents	Stock	Usage	Supplier
RPMI Media			1
Fetal bovine serum (FBS)		1 % (v/v)	1
Collagenase P	100 mg/mL	0.2 mg/mL	2
Dispase II	100 mg/mL	0.8 mg/mL	1
DNase-I	50 mg/mL	0.1 mg/mL	2

¹Gibco™/Life Technologies™ by Thermo Fisher Scientific, Waltham, USA

²Sigma-Aldrich®, St. Louis, USA

• **Collection buffer**

Reagents	Stock	Usage	Supplier
RPMI Media			1
Fetal bovine serum (FBS)		1 % (v/v)	1

¹Gibco™/Life Technologies™ by Thermo Fisher Scientific, Waltham, USA

2.1.3 Flow cytometry buffer & reagents used for cell staining

• **Staining buffer**

Reagents	Stock	Usage	Supplier
HBSS			1
Fetal bovine serum (FBS)		1 % (v/v)	1
Sodium azide	1 % (w/v)	0.01 % (v/v)	2

¹Gibco™/Life Technologies™ by Thermo Fisher Scientific, Waltham, USA

²Sigma-Aldrich®, St. Louis, USA

- **1 % (w/v) Sodium azide**

Reagents	Stock	Usage	Supplier
HBSS		50 mL	1
Sodium azide		0.5 g	2

¹Gibco™/Life Technologies™ by Thermo Fisher Scientific, Waltham, USA

²Sigma-Aldrich®, St. Louis, USA

- **1:8 PI for liver single-cell suspension**

Reagents	Stock	Usage	Supplier
HBSS			1
Fetal bovine serum (FBS)		1 % (v/v)	1
Sodium azide	1 % (w/v)	0.01 % (v/v)	2
Propidium iodide (PI)	100 µg/mL	12,5 µg/mL	3

¹Gibco™/Life Technologies™ by Thermo Fisher Scientific, Waltham, USA

²Sigma-Aldrich®, St. Louis, USA

³Miltenyi Biotec GmbH, Bergisch Gladbach, Germany

- **1:10 PI for human cancer cell lines**

Reagents	Stock	Usage	Supplier
HBSS			1
Fetal bovine serum (FBS)		1 % (v/v)	1
Sodium azide	1 % (w/v)	0.01 % (v/v)	2
Propidium iodide (PI)	100 µg/mL	10 µg/mL	3

¹Gibco™/Life Technologies™ by Thermo Fisher Scientific, Waltham, USA

²Sigma-Aldrich®, St. Louis, USA

³Miltenyi Biotec GmbH, Bergisch Gladbach, Germany

2.1.4 Buffer for magnetic MicroBead-based enrichment of progenitor cells

- **HBSS-BSA for magnetic MicroBead-based enrichment of progenitor cells**

Reagents	Stock	Usage	Supplier
HBSS			1
Bovine serum albumin (BSA)	10 %	0.5 %	2

¹Gibco™/Life Technologies™ by Thermo Fisher Scientific, Waltham, USA

²Miltenyi Biotec GmbH, Bergisch Gladbach, Germany

• **Rinsing buffer for automated cell purification of progenitor cells**

Reagents	Stock	Usage	Supplier
autoMACS Rinsing Solution			1
Bovine serum albumin (BSA)	10 %	0.5 %	1

¹Miltenyi Biotec GmbH, Bergisch Gladbach, Germany

2.2 Methods

2.2.1 Tissue culture work of human cancer cell lines

Table 3: Human cancer cell lines used during the current study.

Indicated are each three cancer cell lines for the cancer entities liver cancer and pancreatic cancer, as well as the tissue type, cell type and morphology of each cell line.

	Cell line	Tissue	Morphology	Cell type	Reference
Liver cancer	HuH7 ¹	Liver	Epithelial	Hepatoblastoma (hepatocellular carcinoma)	(Nakabayashi <i>et al.</i> , 1982).
	HepG2 ¹	Liver	Epithelial	Hepatoblastoma (hepatocellular carcinoma)	(Aden <i>et al.</i> , 1979)
	SK-HEP-1 ¹	Liver (ascites)	Epithelial	Adenocarcinoma	(Fogh <i>et al.</i> , 1977)
Pancreatic cancer	Panc-1 ¹	Pancreas (ductal cell origin)		Epithelioid carcinoma	(Lieber <i>et al.</i> , 1975)
	Capan-1 ¹	Pancreas (from metastatic site: liver)	Epithelial	Adenocarcinoma	(Pollack <i>et al.</i> , 1981)
	Capan-2 ¹	Pancreas	Polygonal	Adenocarcinoma	(Dahiya <i>et al.</i> , 1993)

¹CLS Cell Lines Service GmbH, Eppelheim, Germany

All tissue culture work was carried out under sterile conditions in a laminar flow hood. The cell line maintenance media (Section 2.1.1) was used consistently for all tissue culture work and cells were incubated at 37 °C and 5 % CO₂ in a CO₂ incubator.

For characterization of surface antigen profiles of the cancer entities liver cancer (HCC and liver adenocarcinoma) and PaCa, three human cancer cell lines per cancer entity were choose as indicated in Table 3. Sabine Katharina Urban, former master student of the laboratory, performed all tissue culture work of all human cancer cell lines supervised by Henrike Julich-Haertel.

2.2.1.1 Thawing cryopreserved cells

Frozen cells were thawed on ice and immediately transferred to a 15-mL conical centrifugation tube containing 4 mL pre-warmed cell line maintenance media

(Section 2.1.1). To remove the dimethyl sulfoxide (DMSO) containing cell line conservation media (Section 2.1.1), cells were centrifuged at 300 x g for 5 min at room temperature (RT). After discarding the supernatant, the cell pellet was gently resuspended in 3 mL pre-warmed cell line maintenance media and transferred to a T-75 tissue culture flask (Sarstedt AG & Co, Nümbrecht, Germany) containing 12 mL pre-warmed cell line maintenance media. Cells were incubated over night at 37 °C and 5 % CO₂ in a CO₂ incubator. On the next day, the media was removed and the cells once washed with 5 mL dulbecco's phosphate buffered saline (PBS). Afterwards, 12 mL pre-warmed cell line maintenance media was added to the cells and cells subsequently incubated at 37 °C and 5 % CO₂ in a CO₂ incubator until subcultivation.

2.2.1.2 Subcultivation for maintaining adherent cell lines

Cell lines grow *in vitro* either until they occupy the complete growth area or the nutrients contained in the media are exhausted. To keep the cells alive and at an optimal density, the cultured cells have to be split and transferred into fresh media.

All cell lines used in this study were grown in T-75 or T-175 tissue culture flasks (Sarstedt AG & Co, Nümbrecht, Germany) in cell line maintenance media (Section 2.1.1) and incubated at 37 °C and 5 % CO₂ in a CO₂ incubator.

Cells that reached 70 % confluency had to be subcultured. For this purpose, first the media was discarded and the cells once washed with PBS (T-75: 5 mL PBS; T-175: 10 mL PBS). To get the cells into suspension, trypsin-ethylenediaminetetraacetic acid (EDTA) solution (Section 2.1.1) (T-75: 1 mL trypsin-EDTA solution; T-175: 3 mL trypsin-EDTA solution) was added and incubated at 37 °C and 5 % CO₂ in a CO₂ incubator for 5-10 min until the cells were detached and floating. To inactivate the trypsin, 4 mL cell line maintenance media was added and the single-cell suspension transferred to a 15-mL conical centrifugation tube and centrifuged at 300 x g for 5 min at RT. After discarding the supernatant, the cell pellet was gently resuspended in pre-warmed cell line maintenance media and an aliquot transferred to a T-75 or T-175 tissue culture flask containing pre-warmed cell line maintenance media (T-75: 12 mL cell line maintenance media; T-175: 24 mL cell line maintenance media). To gain the optimal cell density, the ratio for subculturing varied from 1:2 to 1:12 depending on the respective cell line. Afterwards, cell lines were incubated at 37 °C and 5 % CO₂ in a CO₂ incubator. To provide enough nutrients for the growing cells, cell line maintenance media was changed every second day by washing the cells with 5 mL PBS and adding

pre-warmed cell line maintenance media (T-75: 12 mL cell line maintenance media; T-175: 24 mL cell line maintenance media) followed by incubation at 37 °C and 5 % CO₂ in a CO₂ incubator. After five days, cell lines were subcultured again.

2.2.1.3 Cryopreservation of cell lines

To minimize genetic changes, risks of cross contamination with other cell lines or morphological changes, cell lines have to be cryopreserved. For this purpose, cell lines get cryopreserved at a low passage number at a confluence of 70 %. Freshly prepared cell line conservation media (Section 2.1.1) containing the cryoprotective agent DMSO was used for all cryopreservations.

For cryopreservation, cells were growing in a T-75 tissue culture flask. The media was discarded and the cells once washed with 5 mL PBS. To get the cells into suspension, 1mL trypsin-EDTA solution (Section 2.1.1) was added and incubated at 37 °C and 5 % CO₂ in a CO₂ incubator for 5-10 min until the cells were detached and floating. To inactivate the trypsin, 4 mL cell line maintenance media was added and the single-cell suspension transferred to a 15-mL conical centrifugation tube and centrifuged at 300 x g for 5 min at RT. After discarding the supernatant, the cell pellet was gently resuspended in 2-12 mL cell line conservation media (Section 2.1.1), depending on the respective cell line. 1 mL cell suspension aliquots were transferred in cryogenic storage vials and stored at -80 °C for one day. On the next day, the cryogenic storage vials were transferred to liquid nitrogen for long-term storage.

2.2.1.4 Harvesting of cell lines to generate cell line single-cell suspension

Adherent cell lines at a confluence of 70 % were first set on starvation by once washing the cells with PBS (T-75: 5 mL PBS; T-175: 10 mL PBS) and adding pre-warmed cell line starvation media (T-75: 12 mL cell line starvation media; T-175: 24 mL cell line starvation media) (Section 2.1.1) for 18 to 24 hours at 37 °C and 5 % CO₂ in a CO₂ incubator.

Afterwards, the cell line starvation media was discarded and the cells once washed with PBS (T-75: 5 mL PBS; T-175: 10 mL PBS). To get gently the cells into suspension, PBS-EDTA solution (Section 2.1.1) (T-75: 10 mL PBS-EDTA solution; T-175: 20 mL PBS-EDTA solution) was added and incubated at 37 °C and 5 % CO₂ in a CO₂ incubator for 15-20 min, depending on the respective cell line, until the cells were detached and floating. The single-cell suspension was transferred to a 50-mL conical

centrifugation tube and centrifuged at 300 x g for 5 min at 4 °C. After discarding the supernatant, the cell pellet was resuspended in 3-5 mL staining buffer (Section 2.1.3) depending on the pellet size, filtered through a 100-µm filter mesh (A. Hartenstein GmbH, Würzburg, Germany) to a 15-mL conical centrifugation tube and placed on ice until surface staining (Section 2.2.3).

2.2.2 Isolation and analysis of murine hepatic progenitor cells

With the approval of the ethics and animal care by the local authorities for animal research (Landesamt für Verbraucherschutz, Saarbrücken, Germany), all experimental procedures with mice were performed. C57BL/6J mice (wild-type inbred strain) were purchased from Charles River (Sulzfeld, Germany) and allowed to rest 24 hours before experiments. Mice were kept in an assigned mouse cabinet (UniProtect Air Flow Cabinet, Bioscape, Castrop-Rauxel, Germany) under specific pathogen free conditions and had *ad libitum* access to food and water. Food and water were checked daily and cages (Innocage[®] mouse cage, Innovive Inc., San Diego, USA) exchanged weekly.

To investigate the hepatic progenitor cell compartment (HPCC) during induced liver injuries, mice were treated with thioacetamide (TAA) or fed with 3,5-diethoxycarbonyl-1,4-dihydrocollidine supplemented diet (DDC-diet) and choline-deficient, ethionine-supplemented diet (CDE-diet), respectively, to induce liver damage. During the treatments, weight of mice was monitored with a precision balance (VWR, Radnor, USA).

Husbandry and experiments took place in the Institute of Internal Medicine II of the Saarland University (Homburg, Germany).

2.2.2.1 Hepatotoxicant thioacetamide to induce acute liver injury

TAA is a well-defined model to induce liver fibrosis in rodents, which was originally established in rats (Dashti *et al.*, 1989; Müller *et al.*, 1988; Munoz Torres *et al.*, 1991).

The centrilobular hepatotoxicant TAA undergoes bioactivation to its S-oxide and S,S-dioxide. The latter is a reactive metabolite, which presumably induce cellular necrosis (Chilakapati *et al.*, 2005; Hajovsky *et al.*, 2012), elevated transaminase activity and liver fibrosis within six weeks (Salguero Palacios *et al.*, 2008).

C57BL/6J mice were administered intraperitoneally (IP) with 200 µg TAA (Sigma-Aldrich®, St. Louis, USA) per g mice weight. Corresponding amount of TAA was dissolved in sterile PBS to get an injection volume of 200 µL. However, first injection

was only half dose (100 µg TAA/g mice weight). Frequent TAA administration took place three times a week for either three or six weeks. Weight of mice was monitored three times a week before IP injection, in order to weigh the exact amount of TAA. Untreated mice served as control for this experiment. Experiment of TAA-induced liver fibrosis was done only once with finally three mice per group. Mice were fed with normal standard chow (cereal based maintenance diet for mice; Altromin Spezialfutter GmbH & Co. KG, Lage, Germany) throughout the experiment.

2.2.2.2 CDE-diet for activation of the hepatic progenitor cell compartment

Choline-deficient diet induces non-alcoholic steatohepatitis (NASH). Feeding with a choline-deficient diet, supplemented with the ethyl analogon methionine leads a stronger NASH development through metabolic changes in hepatocytes, resulting in deposition of lipids and lethal deterioration of hepatocytes. As a consequence oval cells get activated and proliferate (Kroy *et al.*, 2010; Liedtke *et al.*, 2013; Shinozuka *et al.*, 1978; Ueberham *et al.*, 2010).

C57BL/6J mice were fed with CDE-diet (Research Diets, Inc., New Brunswick, USA) or the corresponding control-diet (Research Diets, Inc., New Brunswick, USA). Two time points (7 days and 14 days) were chosen to investigate changes within the HPCC during the progression phase. Weight was monitored daily, due to an accompanied drastic weight loss by this diet.

Experiment to investigate CDE-activated oval cells was done only once with finally three mice per group. However, one mouse died during seven-day treatment. Stephanie Schmid, former master student of the laboratory, performed all mouse care, including feeding and weight monitoring during the CDE-experiment, in addition to the extraction of murine livers at the end of the CDE-treatment supervised by Henrike Julich-Haertel. Preparation of liver single-cell suspension, antibody staining and flow cytometry analysis was performed by Henrike Julich-Haertel.

2.2.2.3 DDC-diet for activation of the hepatic progenitor cell compartment

The porphyrinogenic agent DDC causes formation of Mallory bodies, which are associated with NASH (Denk *et al.*, 2000; Fickert *et al.*, 2002, 2003). In addition, DDC feeding leads to hepatocyte injury, resulting in the inhibition of tissue repair. As a consequence oval cells get activated and proliferate (Jakubowski *et al.*, 2005).

C57BL/6J mice were fed with DDC-diet (0.1 % DDC in maintenance diet for mice; Altromin Spezialfutter GmbH & Co. KG, Lage, Germany) or the normal standard chow (cereal based maintenance diet for mice; Altromin Spezialfutter GmbH & Co. KG, Lage, Germany). Two time points (1 day and 7 days) were chosen to investigate changes within the HPCC during the progression phase. To examine the regression phase, mice were fed one day with DDC-diet and subsequently three days with normal standard chow. Weight was monitored daily, due to an accompanied drastic weight loss by this diet.

Experiment to investigate DDC-activated oval cells was done only once with finally three mice per group. Julia Maiworm, former master student of the laboratory, performed all mouse care, including feeding and weight monitoring during the DDC-treatment, in addition to the extraction of murine livers at the end of the DDC-experiment supervised by Henrike Julich-Haertel. Preparation of liver single-cell suspension, antibody staining and flow cytometry analysis was performed by Henrike Julich-Haertel.

Experiment to investigate gene expression of DDC-activated oval cells during the regression phase was repeated four times with two mice each, combined to one sample. Only Henrike Julich-Haertel performed complete preparation and execution of this experiment to examine gene expression during DDC-regression phase.

2.2.2.4 Preparation of liver single-cell suspension

Preparation of liver single-cell suspension followed the protocol ‘Isolation and Enrichment of Liver Progenitor Subsets Identified by a Novel Surface Marker Combination’ (Julich-Haertel, Tiwari, *et al.*, 2017).

Mice were anesthetized with isoflurane and euthanized by cervical dislocation. Subsequently, mice were placed on a dissection board and the belly fur wetted with 70 % ethanol. The abdomen was opened with a midline incision of the skin from caudal to cranial, followed by a Y-incision towards the limbs by use of scissors and forceps. Then, peritoneum was opened from caudal up to the sternum by use of a scissors and forceps. The intestine was gently displaced using a cotton swab in order to uncover the liver. Every single liver lobe was removed with the help of scissors and forceps and contamination with connective tissue or the gall bladder was avoided.

Liver was weighted with a precision balance (VWR, Radnor, USA) and subsequently placed on ice in a Petri dish containing Hanks’ balanced salt solution (HBSS,

Gibco™/Life Technologies™ by Thermo Fisher Scientific, Waltham, USA). The liver tissue was cut into homogeneous small pieces using a scalpel in a dry Petri dish.

Afterwards liver pieces were transferred into a 15-mL conical centrifuge tube, 2.5 mL pre-warmed Digestion buffer (Section 2.1.2) added and placed in a 37 °C pre-warmed water bath to start the digestion process (Figure 6). If the entire liver was digested, liver pieces were separated into two 15-mL conical centrifuge tubes.

To collect released liver cells, a new 15-mL conical centrifuge tube was placed on ice and prepared with a polyamide 100-µm filter mesh (A. Hartenstein GmbH, Würzburg, Germany) on the top of the tube, which was wet with 800 µL of Collection buffer (Section 2.1.2).

To promote the liver tissue digest, the 15-mL conical centrifuge tube containing the liver pieces in the 37 °C water bath were shaken after 5 and 10 min in order to mix the liver pieces. 15 min after starting the digest, using a 1000-µL pipette with a cut tip to allow liver pieces to pass through carried out gently mixing of the liver tissue. Afterwards, liver pieces were incubated 2 min in the 37 °C water bath, to allow the pieces to settle down. The supernatant containing the disseminated cells (typically 2x 700 µL) was removed after 2 min incubation and transferred through the filter mesh into the prepared 15-mL conical centrifuge tube. The removed supernatant was replaced with Digestion buffer (typically 2x 700 µL) and further incubated in the 37 °C water bath.

The procedure of mixing, incubation, supernatant removal and supernatant replacement was repeated ordinarily at 30, 40, 50, 55, and 60 min until nearly 60-70 min (healthy liver) or 80-90 min (fibrotic liver) since the beginning of the digestion process. At the end of the digest, no liver tissue should be visible anymore in the 15-mL conical centrifuge tube in the 37 °C water bath. From 40 min after start of the digest, the liver pieces should be small enough to pass through an uncut 1,000-µL pipette tip.

At the end, the 15-mL conical centrifuge tube containing the disseminated cells were centrifuged for 8 min at 180 x g and 4 °C (using reduced acceleration (ACC/4) and deceleration (DEC/2)). The supernatant was discarded by pipetting instead of decanting in due to a loose cell pellet. In order to lyse the red blood cells, the pellet was resuspended in 1 mL of ammonium-chloride-potassium lysis buffer (Gibco™/Life Technologies™ by Thermo Fisher Scientific, Waltham, USA) and incubated for 1 min at RT. Reaction was stopped by adding 5 mL Collection buffer and subsequent centrifugation for 8 min at 180 x g and 4 °C (ACC/4 and DEC/2). Supernatant was

discarded by pipetting and finally isolated liver cells resuspended in 4 mL collection buffer and placed on ice until surface staining (Section 2.2.3).

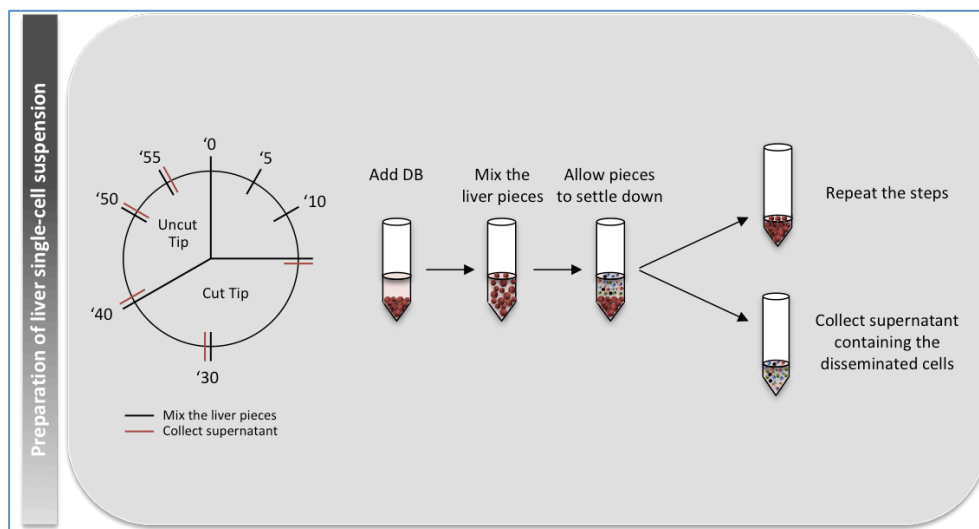


Figure 6: Workflow for preparation of liver single-cell suspension.

Adding pre-warmed Digestion buffer to liver pieces and placing in a 37 °C water bath starts the digestion process. In order to support digestion process, mixing (black) after 5 and 10 min by shaking. At 15 and 30 min after starting the digest, gently mixing with 1000- μ L pipette with a cut tip. From 40 min onwards, the remaining liver pieces should be small enough to pass through an uncut 1,000- μ L pipette tip. 2 min after mixing allow liver pieces to settle down and to collect supernatant containing disseminated liver cells (red). Removed supernatant is replaced by Digestion buffer (DB), in order to repeat the steps until approximately 60-70 min (healthy liver) or 80-90 min (fibrotic liver) have passed since the start of the digestion. At the end, no liver tissue should be visible anymore. (Modified according to Julich-Haertel, Tiwari, *et al.*, 2017).

2.2.3 Surface staining of human cancer cell lines and liver single-cell suspension

Surface protein profiles of several human cancer cell lines derived from different cancer entities (Section 2.2.1) were analyzed using flow cytometry analysis. For this purpose, cell lines were set on starvation for 18-24 hours and subsequently harvested (Section 2.2.1.4) followed by an antibody staining (Section 2.2.3) and further flow cytometry analysis (Section 2.2.6). Sabine Katharina Urban, former master student of the laboratory, performed all tissue culture work, antibody staining and flow cytometry analysis of all human cancer cell lines supervised by Henrike Julich-Haertel (Section 9 – Informed consent by Sabine Katharina Urban). Henrike Julich-Haertel finally analyzed generated data.

To analyze the murine HPCC, liver of healthy or treated mice (Section 2.2.2) were analyzed using flow cytometry analysis. For this purpose, liver single-cell suspension was generated (Section 2.2.2.4) followed by an antibody staining (Section 2.2.3) and further flow cytometry analysis (Section 2.2.6). Determining of the cell count and subsequent staining of the liver single-cell suspension followed the protocol ‘Isolation

and Enrichment of Liver Progenitor Subsets Identifies by a Novel Surface Marker Combination’ (Julich-Haertel, Tiwari, *et al.*, 2017).

2.2.3.1 Determining of the cell count by flow cytometry-based cell quantification

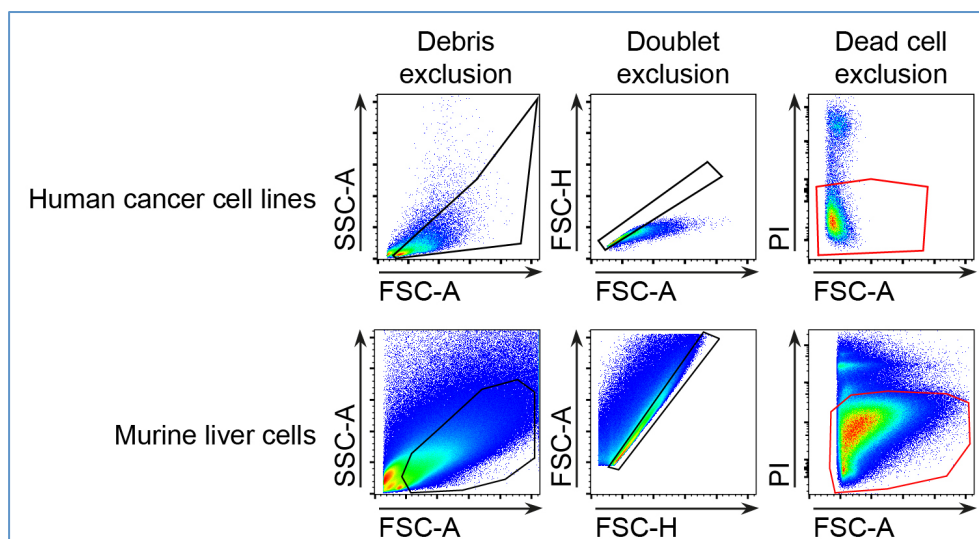


Figure 7: Cell count determination of human cancer cell lines and isolated murine liver cells by flow cytometry analysis.

A single-cell suspension of human cancer cell lines or murine liver was prepared and subsequently stained with propidium iodide (PI) as dead cell dye. Representative dot plot with the gating strategy is depicted. To record living cell events, debris (plotting SSC-A against FSC-A), doublets (plotting FSC-A against FSC-H) and dead cells were excluded (plotting PI against FSC-A) followed by gating on PI negative events (red).

For determination of the amount of living cells per mL using flow cytometry, 20 μL single cell suspension were added to 180 μL staining buffer (Section 2.1.3) containing 2 μL 1:10 propidium iodide (PI, cell lines) or 6 μL 1:8 PI (murine liver cells) (Section 2.1.3) as dead cell dye. Finally, the total volume should be 200 μL in a 1.5-mL reaction tube. Flow cytometry analysis was done by measuring 30 μL of each sample using the MACSQuant® Analyzer 10 (Miltenyi Biotec GmbH, Bergisch Gladbach, Germany). Debris (plotting SSC-A against FSC-A), doublets (plotting FSC-A against FSC-H) and dead cells were excluded (plotting PI against FSC-A) and finally gated on PI negative events (red) as shown in Figure 7. Thus, PI negative events correspond to living cells, which were recorded and cell count calculated using the following algorithm:

$$\text{cell count/mL} = \text{events of living cells/mL} \times 10$$

2.2.3.2 Staining of human cancer cell lines and murine liver cells

1×10^5 PI⁺ human cancer cell lines and 2.5×10^5 PI⁺ murine liver cells were used for each staining. The according amount of single-cell suspension was transferred to a 1.5-mL

reaction tube containing 400 μ L staining buffer and centrifuged at 300 x g for 5 min at 4 °C (human cancer cell lines) or at 300 x g for 3 min at 4 °C (murine liver cells). The supernatant was discarded with a vacuum pump and the cell pellet resuspended in 50 μ L Fc block mix (Table 4) and incubated for 5 min on ice. Further, 50 μ L staining mix (Table 4) were added to reach 100 μ L total staining volume and incubated for 15 min on ice in the dark. Antibodies used during the current study are listed in (Table 5).

To wash the cells, 400 μ L staining buffer was added and cells pelleted at 300 x g for 5 min at 4 °C (human cancer cell lines) or at 300 x g for 3 min at 4 °C (murine liver cells). The supernatant was discarded with a vacuum pump and the cell pellet resuspended in 400 μ L staining buffer containing 4 μ L 1:10 PI (human cancer cell lines) or 200 μ L staining buffer plus 6 μ L 1:8 PI (murine liver cells).

If staining with secondary antibody was necessary, the cell pellet was instead resuspended in 100 μ L secondary mix (Table 4) containing the conjugated secondary antibodies (Table 5) and incubated for 15 min on ice in the dark. Afterwards, 400 μ L staining buffer was added, cells pelleted at 300 x g for 3 min at 4 °C (murine liver cells) and resuspended in 200 μ L staining buffer plus 6 μ L 1:8 PI (murine liver cells). Flow cytometry analysis was done by measuring 150 μ L (human cancer cell lines) or 180 μ L (murine liver cells) of each sample using the MACSQuant® Analyzer 10 (Miltenyi Biotec GmbH, Bergisch Gladbach, Germany).

Table 4: Staining procedure for the analysis of single-cell suspensions.

Cell amount, composition of Fc block mix, staining mix, secondary mix as well as centrifugation steps are displayed for the staining of human cancer cell lines and murine liver cells, respectively.

Workflow	Reagents	Usage	Section	Supplier
Human cancer cell lines				
Single-cell suspension	Staining Buffer	400 µL	Section 2.1.3	-
	Human cancer cells	1×10 ⁵ PI ⁺ cells	-	-
Centrifugation: 300 x g, 5 min, 4 °C				
Fc block mix	Staining Buffer	47,5 µL	Section 2.1.3	-
	Hu FcR Binding Inhibitor	2,5 µL	-	1
Staining mix	Staining Buffer	50 µL	Section 2.1.3	-
	Antibodies	X µL	Table 5	-
Centrifugation: 300 x g, 5 min, 4 °C				
Measurement	Staining Buffer	400 µL	Section 2.1.3	-
	1:10 PI	4 µL	Section 2.1.3	-
Murine liver cells				
Single-cell suspension	Staining Buffer	400 µL	Section 2.1.3	-
	Murine liver cells	2.5×10 ⁵ PI ⁺ cells	-	-
Centrifugation: 300 x g, 3 min, 4 °C				
Fc block mix	Staining Buffer	40 µL	Section 2.1.3	-
	FcR-blocking reagent	10 µL	-	2
	anti-CD64 purified	1 µL	-	3

Staining mix	Staining Buffer	X* µL	Section 2.1.3	-
	Antibodies	X µL	Table 5	-
Centrifugation: 300 x g, 5 min, 4 °C				
Secondary mix**	Staining Buffer	100 µL	Section 2.1.3	-
	Secondary Antibodies	X µL	Table 5	-
Centrifugation: 300 x g, 5 min, 4 °C**				
Measurement	Staining Buffer	400 µL	Section 2.1.3	-
	1:10 PI	4 µL	Section 2.1.3	-

*According to total volume of 50 µL Staining mix

**Not required if secondary antibody not necessary

¹eBioscience™ by Thermo Fisher Scientific, San Diego, USA

²Miltenyi Biotec GmbH, Bergisch Gladbach, Germany

³BioLegend, Inc., San Diego, USA

Table 5: Overview of antibodies and MicroBeads used for the analysis of human cancer cell lines and murine liver cells.
Indicated are the antigen, conjugate, clone, host organism (isotype), stock concentration, final dilution (refer to 100 μ L staining volume) used during the current study, as well as the supplier.

Antigen	Conjugate	Clone	Isotype	Stock [mg/mL]	Dilution*	Supplier
Antibodies - Human cancer cell lines						
ASGPR1	PE	8D7	Mouse IgG1, κ	0.05	1:100	1
CD133/2	APC	293C3	Mouse IgG2b	0.00825	1:20	2
CD326 (EpCAM)	Brilliant Violet 421™	9C4	Mouse IgG2b, κ	0.05	1:800	3
Podoplanin (gp38)	PE-Vio770	REA446	REA Control (S)	0.0055	1:100	2
Isotype	PE	P3.6.2.8.1	Mouse IgG1, κ	0.2	1:400	4
Isotype	APC	eBMG2b	Mouse IgG2b, κ	0.2	1:500	4
Isotype	Brilliant Violet 421™	MPC-11	Mouse IgG2b, κ	0.05	1:800	3
REA Control (S)	PE-Vio770	REA293		0.095	1:1700	2
Antibodies & MicroBeads - Murine liver cells						
ASGPR1	Purified		Polyclonal Goat IgG	0.2	1:100	5
CD16/32	Purified	93	Rat IgG2 α , λ	0.5	1:100	3
CD24	Biotin	M1/69	Rat IgG2 β , κ	0.5	1:100	3
CD31	Alexa Fluor® 488	MEC13.3	Rat IgG2 α , κ	0.5	1:200	3

CD31	Biotin	MEC13.3	Rat IgG2 α , κ	0.5	1:200	3
CD34	Biotin	RAM34	Rat IgG2 α , κ	0.5	1:100	4
CD45	APC/Cy7	30-F11	Rat IgG2 β , κ	0.2	1:200	3
CD54 (ICAM-1)	Biotin	YN1/1.7.4	Rat IgG2 β , κ	0.5	1:100	3
CD64	Purified	X54-5/7.1	Mouse IgG1, κ	0.5	1:100	3
CD90.2	Pacific Blue™	53-2.1	Rat IgG2 α , κ	0.5	1:800	3
CD133	Biotin	315-2C11	Rat IgG2 α , λ	0.5	1:100	3
CD133	PE	MB9-3G8	Rat IgG1	0.03	3 μ L	2
CD326 (EpCAM)	Brilliant Violet 421™	G8.8	Rat IgG2 α , κ	0.2	1:400	3
MICL1C3	Alexa Fluor® 405	MICL1C3	Rat IgG2 α	1.0	1:200	6
Podoplanin	APC	8.1.1	Syrian Hamster IgG	0.2	1:1400**	3
Podoplanin	Biotin	8.1.1	Syrian Hamster IgG	0.5	1:1400**	3
Sca-1	Biotin	D7	Rat IgG2 α , κ	0.03	10 μ L	2
Normal Goat IgG	Purified			1.0		5
Rat IgG1, κ	PE	RTK2071		0.2		3
Rat IgG2α, κ	Alexa Fluor® 488	RTK2758		0.5		3
Rat IgG2α, κ	Biotin	RTK2758		0.5		3

Rat IgG2α, κ	Brilliant Violet 421™	RTK2758	0.2	3
Rat IgG2β, κ	APC/Cy7	RTK4530	0.2	3
Rat IgG2β, κ	Biotin	RTK4530	0.5	3
Syrian Hamster IgG	APC	SHG-1	0.2	3
Syrian Hamster IgG	Biotin	SHG-1	0.5	3
Donkey anti-Goat IgG	Alexa Fluor® 488	Donkey IgG	2.0	1:800
Streptavidin	Alexa Fluor® 405		1.0	1:400
Anti-Biotin	MicroBeads	Mouse IgG1	10 μL***	2
Anti-CD31	MicroBeads	Rat IgG2 α	40 μL	2
Anti-CD45	MicroBeads	Rat IgG2β	30 μL	2
Dead Cell Removal	MicroBeads		100 μL	2

* According to total staining volume of 100 μL

** Use 1 μL of 1:14 pre-dilution

*** CD133-MACS: 10 μL; gp38-MACS: 5 μL

¹BD Biosciences, Heidelberg, USA

²Miltenyi Biotec GmbH, Bergisch Gladbach, Germany

³Biol.Legend, Inc., San Diego, USA

⁴eBioscience™ by Thermo Fisher Scientific, San Diego, USA

⁵R&D Systems a Bio-Techne brand, Minneapolis, USA

⁶Novus Biologicals a Bio-Techne brand, Minneapolis, USA

⁷Life Technologies™ by Thermo Fisher Scientific, Waltham, USA

2.2.4 Gene expression analysis of hepatic progenitor subsets combined from multiple livers

To investigate gene expression within the HPCC, healthy mice or mice fed with DDC-diet (Section 2.2.2.3) to induce liver damage, were examined. Because HPCs represent rare cell populations, they have to be first enriched and purified. At least two livers have to be combined to achieve sufficient cell numbers for gene expression analysis.

Preparation of liver single-cell suspension and furthermore enrichment of HPCs followed the protocol ‘Isolation and Enrichment of Liver Progenitor Subsets Identified by a Novel Surface Marker Combination’ (Julich-Haertel, Tiwari, *et al.*, 2017). Afterwards, expression of several genes was examined by real-time quantitative polymerase chain reaction (qRT-PCR).

2.2.4.1 Magnetic MicroBead-based enrichment and automated cell purification of CD133⁺ progenitor cells

$1.5\text{-}2 \times 10^6$ PI⁺ murine liver cells, according to the cell count determination were transferred into a 15-mL conical centrifuge tube. This typically corresponded to the separation of one healthy C57BL/6J mouse liver into three 15-mL conical centrifuge tubes. Cells were pelleted for 8 min at 180 x g and 4 °C (ACC/4 and DEC/2) and supernatant discarded by pipetting. Afterwards, cells were resuspended in 400 µL HBSS-BSA (Section 2.1.4), 40 µL of anti-CD31 MicroBeads and 30 µL of anti-CD45 MicroBeads (Table 5) added and incubated for 15 min at 4 °C. 5 mL HBSS-BSA were added to the cells and subsequent centrifuged for 8 min at 180 x g and 4 °C (ACC/4 and DEC/2) to wash the cells. The supernatant was discarded by pipetting and the cells resuspended in 100 µL Dead Cell Removal MicroBeads (Table 5) and incubated for 15 min at RT.

During the incubation time, LS Column (Miltenyi Biotec GmbH, Bergisch Gladbach, Germany) with a polyamide 100-µm filter mesh (A. Hartenstein GmbH, Würzburg, Germany) on the top of the LS Column was placed into a MACS Manual Separator (QuadroMACS, Miltenyi Biotec GmbH, Bergisch Gladbach, Germany) and calibrated with 3 mL HBSS-BSA.

900 µL HBSS-BSA were added to the cells and loaded on the LS Column through the 100-µm filter mesh and the flow-through collected. Typically one entire liver was loaded onto one LS Column, if 10^8 total events (including cell debris) according to the

cell count determination were not exceeded. The LS Column was washed three times with 3 mL HBSS-BSA and the flow-through collected. Finally, the flow-through was centrifuged for 8 min at 180 x g and 4 °C (ACC/4 and DEC/2) to pellet the enriched progenitor cells

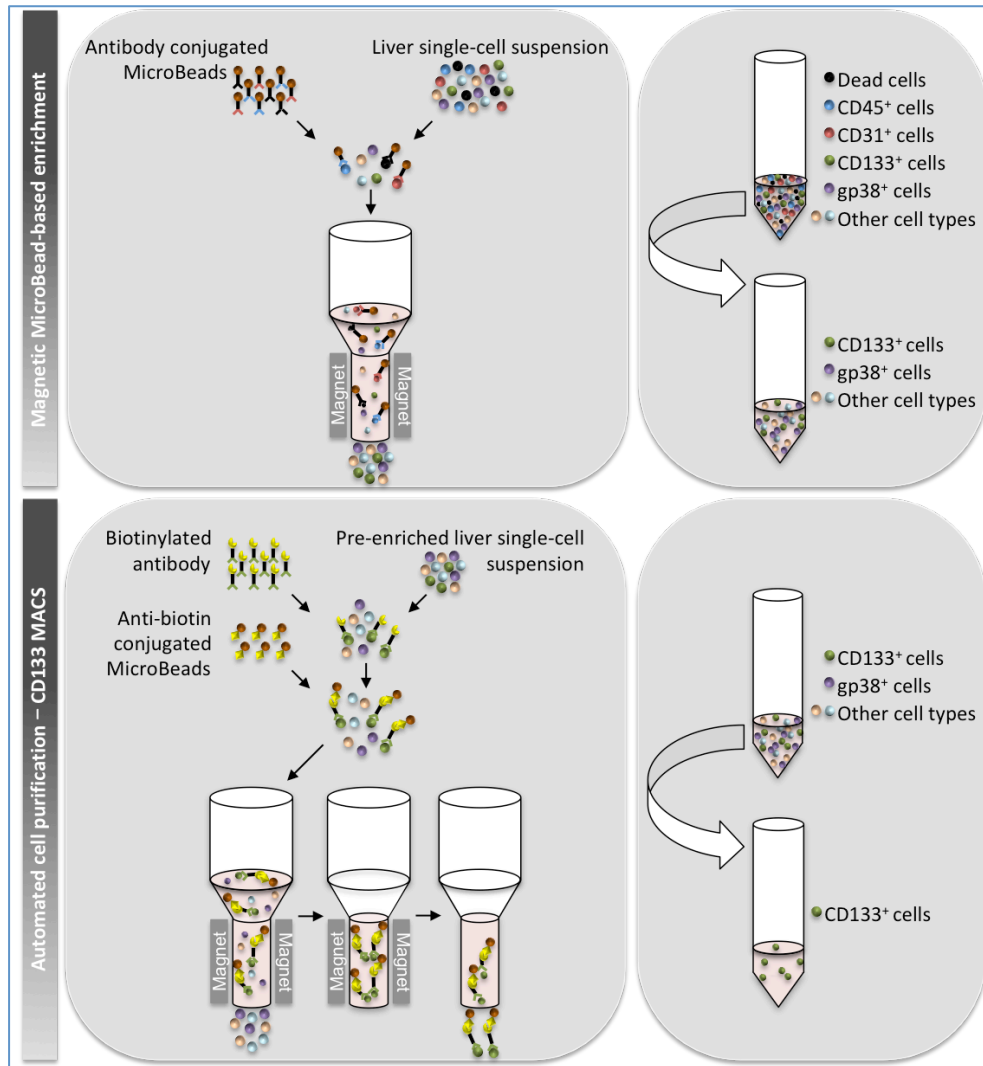


Figure 8: Schematic view of the magnetic MicroBead-based enrichment and automated cell purification of CD133⁺ hepatic progenitor cells.

Staining of murine liver single-cell suspension with antibody conjugated MicroBeads (anti-CD31 MicroBeads, anti-CD45 MicroBeads, Dead Cell Removal MicroBeads) to bind conjugated cells in the magnetic field to remove them from the liver single-cell suspension. Flow-through contains enriched progenitor cells. Subsequent, staining of pre-enriched liver single-cell suspension with biotinylated antibody (anti-CD133) and further with anti-biotin conjugated beads to bind progenitor cells in the magnetic field in order to purify CD133⁺ progenitor cells. Finally, positive fraction contains enriched and purified CD133⁺ oval cells.

The supernatant was discarded by pipetting and the cells of two livers combined by resuspending in total 100 µL rinsing buffer (Section 2.1.4). Afterwards, 1 µL of anti-CD64 (1:100 dilution according to 100 µL staining volume) and 1 µL of anti-CD16/32 (1:100 dilution according to 100 µL staining volume) (Table 5) were added to avoid unspecific antibody binding and incubated on ice for 5 min. Subsequent, 1 µL of anti-

CD133 biotinylated (1:100 dilution according to 100 μ L staining volume) (Table 5) were added for the isolation of CD133⁺ oval cells. Staining was incubated for further 10 min on ice. 5 mL rinsing buffer were added to the cells and centrifuged for 8 min at 180 x g and 4 °C (ACC/4 and DEC/2) to wash the cells. The supernatant was discarded by pipetting and cells were resuspended in 400 μ L rinsing buffer, 10 μ L of anti-Biotin MicroBeads (Table 5) added and incubated for 15 min at 4 °C. 5 mL rinsing buffer were added and cells pelleted for 8 min at 180 x g and 4 °C (ACC/4 and DEC/2) to wash the cells. Afterwards, cells were resuspended in 1 mL rinsing buffer and filtered through a 100- μ m filter mesh (A. Hartenstein GmbH, Würzburg, Germany). Next, 15-mL conical centrifuge tube containing the MicroBeads-labeled cell suspension was placed on a Chill 5 Rack (Miltenyi Biotec GmbH, Bergisch Gladbach, Germany), in addition to two empty 15-mL conical centrifuge tubes to collect the positive and negative fractions. The Chill 5 Rack was placed on the autoMACS Pro Separator (Miltenyi Biotec GmbH, Bergisch Gladbach, Germany) and the positive selection program (Possel_d2) in addition to a washing step (Rinse option) was used for cell purification. Figure 8 indicates a schematic view of the procedure of enrichment and purification of CD133⁺ progenitor cells.

Finally, the positive fraction was pelleted for 8 min at 180 x g and 4 °C (ACC/4 and DEC/2), supernatant discarded by pipetting and oval cells resuspended in 200 μ L RLT Plus Buffer (QIAGEN GmbH, Hilden, Germany) and stored at -20 °C until RNA extraction (Section 2.2.4.2).

2.2.4.2 RNA extraction using RNeasy® Plus Mini Kit

The extraction and purification of RNA from CD133⁺ oval cells (Section 2.2.4.1) was performed according to the user guidelines of the RNeasy® Plus Micro Kit (QIAGEN GmbH, Hilden, Germany).

In general, CD133⁺ progenitor cells in 200 μ L RTL Plus Buffer were thawed on ice and immediately homogenized using a sterile, RNase-free needle (0.4 mm) and syringe. The lysate was transferred to a gDNA Eliminator spin column in order to remove genomic DNA. To achieve optimal binding conditions, 1 volume (200 μ L) 70 % ethanol were added to the flow-through containing RNA and loaded to an RNeasy MinElute spin column. After multiple washes, the RNA was eluted in 14 μ L RNase-free water and synthesis of cDNA was performed immediately (Section 2.2.4.3).

2.2.4.3 Synthesis of cDNA using QuantiNova™ Reverse Transcription Kit

The synthesis of cDNA from CD133⁺ oval cells (Section 2.2.4.1) was performed according to the user guidelines of the QuantiNova™ Reverse Transcription Kit (QIAGEN GmbH, Hilden, Germany).

2 µL gDNA Removal Mix was added to the previous extracted template RNA. After an incubation for 2 min at 45 °C, the mix was immediately placed on ice.

Afterwards, 5 µL Reverse-transcription Master Mix comprising 1 µL Reverse Transcription Enzyme and 4 µL Reverse Transcription Mix was added. Next, incubation was as follows: 1) Annealing step: 3 min, 25 °C; 2) Reverse-transcription step: 10 min, 45 °C; and 3) Inactivation of reaction: 5 min, 85 °C.

The prepared oval cell cDNA was 1:2 diluted by adding 20 µL water to get a total volume of 40 µL cDNA. Until further use by qPCR (Section 2.2.4.4) cDNA was stored at -20 °C.

2.2.4.4 Gene expression analysis of CD133⁺ oval cells using QuantiNova™ SYBR® PCR Kit

The quantification of cDNA from CD133⁺ oval cells (Section 2.2.4.1) was performed according to the user guidelines of the QuantiNova™ SYBR® PCR Kit (QIAGEN GmbH, Hilden, Germany).

At first, QN ROX Reference Dye for normalization of fluorescent signals was diluted 1:100. For this purpose, PCR Master Mix aliquots containing 500 µL 2x SYBR Green PCR Master Mix and 5 µL QN ROX Reference Dye were prepared and stored at -20 °C until utilization. At the day of use, PCR Master Mix, cDNA, Primer and RNase-free water were thawed and a reaction mix prepared containing 5 µL PCR Master Mix, 1 µL QuantiTect Primer Assay (QIAGEN GmbH, Hilden, Germany) and 3 µL RNase-free. 9 µL of the reaction mix was load on a 96-Well PCR Plate (VWR, Radnor, USA) and finally 1 µL template cDNA added to each 96-Well. For the water control, 1 µL RNase-free water was added instead of template cDNA. Composition of the PCR reaction mix, loaded on each well, is indicated in Table 6. For all qRT-PCR analyses, QuantiTect Primer Assays for SYBR® Green-based expression analyses were utilized (Table 7).

The qRT-PCR was carried out in a 7500 Fast Real-Time PCR System with corresponding SDS software (Applied Biosystems® by Thermo Fisher Scientific, San Diego, USA) (Table 8).

Table 6: Composition of the qRT-PCR reaction mix used for gene expression analysis of CD133⁺ oval cells.
Indicated are the components and their corresponding volume according to user guidelines of the QuantiNova™ SYBR® PCR Kit (QIAGEN GmbH, Hilden, Germany).

Component	Volume
PCR Master Mix ¹	5 µL
QuantiTect Primer Assay	1 µL
RNase-free water	3 µL
Template cDNA ²	1 µL

¹Containing 2x SYBR Green PCR Master Mix and 1:100 QN ROX Reference Dye

²Control contains RNase-free water instead of template cDNA

Table 7: Overview of QuantiTect Primer Assays used for the SYBR® Green-based gene expression analysis of CD133⁺ oval cells.

Indicated are the primer, gene symbol, gene name as well as the supplier.

Primer	Gene symbol	Gene name	Supplier
B2m [*]	B2M	Beta-2-microglobulin	1
Ccl2	CCL2	C-C motif chemokine ligand 2	1
Cdh1	CDH1	Cadherin 1	1
Fas	FAS	Fas cell surface death receptor	1
Gp38_1 ^{**}	PDPN	Podoplanin	1
Hnf1a	HNF1A	Hepatocyte nuclear factor 1-alpha	1
Hnf1b	HNF1B	Hepatocyte nuclear factor 1-beta	1
Hnf4a	HNF4A	Hepatic nuclear factor 4-alpha	1
Krt19	KRT19	Keratin 19	1
Onecut1	HNF6	Hepatocyte nuclear factor 6	1
Prom1 ^{**}	PROM1	Prominin 1	1
Yap1	YAP1	Yes-associated Protein 1	1

^{*}Housekeeping gene

^{**}Identification oval cell population

¹ QIAGEN GmbH, Hilden, Germany

Table 8: Conditions of qRT-PCR for gene expression analysis of CD133⁺ oval cells.

The qRT-PCR was carried out in a 7500 Fast Real-Time PCR System (Applied Biosystems® by Thermo Fisher Scientific, San Diego, USA). Indicated are the steps with the corresponding temperature, time and repetitions.

Step	Temperature	Time	Repetition
Initial denaturation	95 °C	2 min	1 cycle
Denaturation	95 °C	5 s	40 cycles
Annealing/Extension	60 °C	30 s	
Denaturation	95 °C	15 s	
Annealing/Extension	60 °C	1 min	
Denaturation	95 °C	15 s	
Annealing/Extension	60 °C	15 s	

2.2.5 Isolation and detection of human cell-derived microparticles

The study was approved by ethic commissions of 1) The state chambers of medicine in Rhineland-Palatinate, Germany (837.151.13 (8836-F)); 2) Saarland, Germany (167/11); 3) San Sebastian, Spain (PI2014187); and 4) Warsaw, Poland (KB/41/A/2016 and AKB/145/2014). All Patients, healthy probands and athletes gave their informed consent.

Human blood samples were collected from 1) Healthy probands, 2) Athletes and patients with 3) Inguinal hernia, 4) Cirrhosis, 5) HCC, 6) CCA, 7) CrC, 8) NSCLC and 9) PaCa.

To avoid data falsification, exclusion of patients, healthy probands and athletes, respectively, with comorbidity (acute inflammation, chronic inflammation, autoimmune diseases or viral infections) during the time of blood sample collection, were done. However, patients with HBV/HCV infection or liver cirrhosis were included in the study.

Additionally, patients who underwent any anti-tumor therapy (chemotherapy, radiotherapy, radiochemotherapy etc.) during the time of blood sample collection were excluded. However, patients who participated in the R0 resection study were included in the study.

2.2.5.1 Isolation of human serum

Table 9: Summary of the various departments involved in collection of human blood samples.

Indicated is the amount (#) of the collected human blood samples of each tumor entity by each department.

Department	Entity	#
Department of Internal Medicine II, Saarland University Medical Center, Homburg/Saar, Germany ¹	Healthy	10
	HCC	11
Department of Molecular and Cellular Sport Medicine, Institute of Cardiovascular Research and Sport Medicine, German Sport University Cologne, Cologne, Germany ²	Athletes	26
	Healthy	22
	Inguinal hernia	26
Department of General, Visceral and Thoracic Surgery, German Armed Forces Central Hospital, Koblenz, Germany ²	CrC	19
	NSCLC	10
	PaCa	6
Laboratory of Metabolic Liver Diseases, Department of General, Transplant and Liver Surgery, Medical University of Warsaw, Warsaw, Poland ³	CCA	38
Department Internal Medicine and Cardiology, Medical University of Warsaw, Warsaw, Poland ³	HCC	75
Department of General, Transplant and Liver Surgery, Medical University of Warsaw, Warsaw, Poland		
Translational Medicine Group, Pomeranian Medical University, Szczecin, Poland ³	Cirrhosis	38
Department of Liver and Gastrointestinal Diseases, Biodonostia Health Research Institute – Donostia University Hospital, University of the Basque Country (UPV/EHU), CIBERehd, Ikerbasque, San Sebastian, Spain ⁴	Cirrhosis	11

HCC: Hepatocellular carcinoma

CCA: Cholangiocarcinoma

CrC: Colorectal cancer

NSCLC: Non-small cell lung cancer

PaCa: Pancreatic cancer

¹Ethics commissions approval number of the state chambers of medicine Saarland, Germany: 167/11

²Ethics commissions approval number of the state chambers of medicine Rhineland-Palatinate, Germany: 837.151.13 (8836-F)

³Ethics commissions approval number of the state chambers of medicine Warsaw, Poland: KB/41/A/2016 and AKB/145/2014

⁴Ethics commissions approval number of the state chambers of medicine San Sebastian, Spain: PI2014187

Blood was collected in S-Monovette® 7.5 mL Z-Gel (Sarstedt AG & Co, Nümbrecht, Germany) blood collection system. This S-Monovette® contains beads coated with a clotting activator (silicate) in addition to a polyacrylic ester gel, which forms a stable separating layer during centrifugation. The blood was rest for 30 to 60 min at RT to enable the blood to clot. Afterwards, the S-Monovette® was centrifuged at 1,500 x g for 20 min at RT. The serum was aliquoted and stored at -80 °C until further usage.

Collection of human blood samples and further isolation of serum was done by various departments. Table 9 summarizes the department and what kind of human blood sample/serum was collected and the amount, respectively.

2.2.5.2 Isolation of cell-derived microparticles from human serum by sequential centrifugation

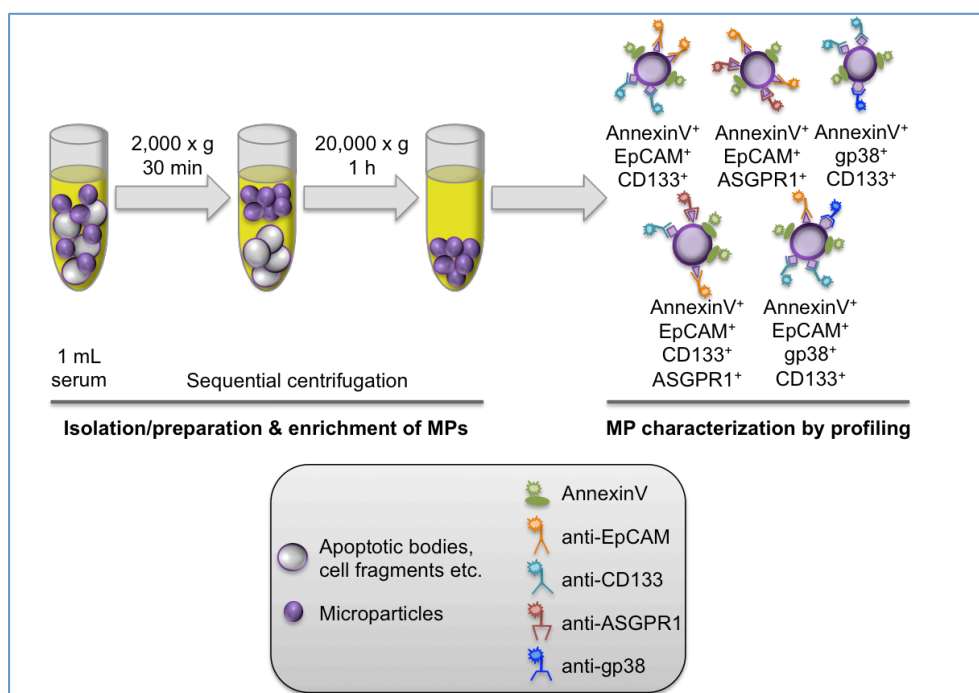


Figure 9: Schematic view of the isolation of cell-derived microparticles from human serum by sequential centrifugation.

Human cell-derived microparticles are isolated and enriched by two centrifugations steps. First, removal of cell debris and apoptotic bodies through centrifugation at 2,000 x g, 4 °C for 30 min. Second, supernatant containing microparticles centrifuged again at 20,000 x g, 4 °C for 1 h to pellet the microparticles. Further staining allows detection of microparticles by the help of flow cytometry analysis.

Serum samples were thawed at RT and 1 mL serum transferred to a 2-mL reaction tube. To remove cell debris and larger vesicles, serum samples were centrifuged at 2,000 x g for 30 min at 4 °C. 950 µL of the supernatant was transferred to a 2-mL reaction tube and centrifuged at 20,000 x g for 60 min at 4 °C to pellet the microparticles (Figure 9). 850 µL of the supernatant was discarded and the remaining liquid, containing the

pelleted microparticles, resuspended in 300 µL filtered PBS. PBS was filtered before using a Steriflip™ vacuum-driven filtration system (Steriflip-GP, pore size: 0.22 µm, media: Express PLUS®; Merck Millipore by Merck KGaA, Darmstadt, Germany). Afterwards, microparticle suspension was filtered through a 100-µm filter mesh (A. Hartenstein GmbH, Würzburg, Germany) placed on a 1.5-mL reaction tube. The microparticles suspension was stored on ice until further usage.

2.2.5.3 Staining of human cell-derived microparticles for flow cytometry analysis

Table 10: Staining procedure to analyze human cell-derived microparticles.

Amount of microparticles, composition of Fc block mix, AnnexinV mix and staining mix are displayed.

	Reagents	Usage	Section	Supplier
Microparticles	Microparticle suspension	50 µL		
	PBS*	11,5 µL		1
Fc block mix	Hu FcR Binding Inhibitor*	2,5 µL		2
	10 % BSA**	1 µL		3
AnnexinV mix	10x Binding Buffer	5 µL		3
	AnnexinV FITC	5 µL		3
Staining mix	PBS*	25 µL		1
	Antibodies	X µL	Table 11	-

*Filtered using a Steriflip™ vacuum-driven filtration system (Steriflip-GP, pore size: 0.22 µm, media: Express PLUS®; Merck Millipore by Merck KGaA, Darmstadt, Germany).

**Centrifuged at 20,000 x g for 60 min at 4 °C

¹Sigma-Aldrich®, St. Louis, USA

²eBioscience™ by Thermo Fisher Scientific, San Diego, USA

³Miltenyi Biotec GmbH, Bergisch Gladbach, Germany

Staining of human cell-derived microparticles followed the protocol ‘Multi-Surface Antigen Staining of Larger Extracellular Vesicles’ (Lukacs-Kornek *et al.*, 2017).

50 µL of microparticle suspension was transferred to a 1.5-mL reaction tube and 15 µL Fc block mix (Table 10) added and incubated for 60 min at 4 °C. The used PBS and Hu FcR Binding Inhibitor (eBioscience™ by Thermo Fisher Scientific, San Diego, USA) were filtered prior using a Steriflip™ vacuum-driven filtration system (Steriflip-GP, pore size: 0.22 µm, media: Express PLUS®; Merck Millipore by Merck KGaA, Darmstadt, Germany), whereby the 10 % bovine serum albumin (BSA; Miltenyi Biotec GmbH, Bergisch Gladbach, Germany) was centrifuged prior at 20,000 x g for 60 min at 4 °C.

Immediately, 10 μ L AnnexinV mix (Table 10) were added and incubated for 30 min at 4 °C in the dark. Afterwards, 25 μ L staining mix (Table 10) were added to reach 100 μ L total staining volume and incubated for 20 min at 4 °C in the dark. The staining mix contained the conjugated antibodies (Table 11) in filtered PBS.

Subsequently, 100 μ L filtered PBS were added and flow cytometry analysis was done by measuring of 150 μ L of each sample using the MACSQuant® Analyzer 10 (Miltenyi Biotec GmbH, Bergisch Gladbach, Germany).

Table 11: Overview of antibodies used for the analysis of human cell-derived microparticles.

Indicated are the antigen, conjugate, clone, host organism (isotype), stock concentration, final dilution (refer to 100 µL staining volume) used during the current study, as well as the supplier.

Antigen	Conjugate	Clone	Isotype	Stock [mg/mL]	Dilution*	Final [µg/mL]	Supplier
AnnexinV	FITC				1:20		2
ASGPR1	PE	8D7	Mouse IgG1, κ	0.05	1:1000	0.05	1
CD133/2	APC	293C3	Mouse IgG2b	0.00825	1:1000	0.00825	2
CD326 (EpCAM)	VioBlue	HEA-125	Mouse IgG1, κ	0.0825	1:1000	0.0825	2
Podoplanin (gp38)	PE-Vio770	REA446	REA Control (S)	0.0055	1:1000	0.0055	2
Isotype	PE	P3.6.2.8.1	Mouse IgG1, κ	0.2	1:4000	0.05	3
Isotype	APC	eBMG2b	Mouse IgG2b, κ	0.2	1:24000	0.00825	3
Isotype	VioBlue	IS5-21F5	Mouse IgG1	0.05	1:660	0.0825	2
REA Control (S)	PE-Vio770	REA293		0.095	1:17300	0.0055	2

* According to total staining volume of 100 µL
¹BD Biosciences, Heidelberg, USA
²Miltenyi Biotec GmbH, Bergisch Gladbach, Germany
³eBioscience™ by Thermo Fisher Scientific, San Diego, USA

2.2.6 Flow cytometry analysis using MACSQuant® Analyzer 10

Table 12: Optical configuration of the MACSQuant® Analyzer 10.

Three lasers and eight incorporated filters allows the analyzer the detection of eight fluorescence channels in addition to the forward-scattered light (FSC, size of cells) and side-scattered light (SSC, internal complexity of cells).

Laser	Channel	Filter (nm)	Dye/Parameter
Violet 405 nm	V1	450/50	VioBlue, Pacific Blue, DAPI
	V2	525/50	VioGreen
Blue 488 nm	B1	525/50	FITC, A488
	B2	585/40	PE
	B3	655-730	PI
	B4	750 LP	PE/Cy7
Red 635 nm	R1	655-730	APC
	R2	750 LP	APC/Cy7
Blue 488 nm	FSC	488/10	Size
	SSC	488/10	Internal complexity

To investigate surface profiles in human cancer cell lines, the HPCC of murine livers or to carry out surface profiling of human cell-derived MPs, flow cytometry was performed with the help of the MACSQuant® Analyzer 10 (Miltenyi Biotec, Bergisch Gladbach, Germany). Optical fluorescence and characteristics of single-cells or particles are measured in a stream of fluid by this laser-based technology. Particles deflect incident laser light, which depends on size (measured through forward-scattered light, FSC) and internal complexity (measured through side-scattered light, SSC). This light scattering is recognized by the detection system. Based thereon, antibody conjugated fluorescent dyes are able to bind specific antigens, which can be recognized also. In due to this, fluorochromes with different emission wavelengths allow distinguishing of cells or microparticles according to various antigen profiles. The MACSQuant® Analyzer 10 is equipped with three lasers and eight incorporated filters. This results in eight fluorescence channels in addition to the FSC and SSC (Table 12).

2.2.7 Data analysis software used within the current study

2.2.7.1 Flow cytometry analysis using FlowJo®

Generated flow cytometry data were analyzed using FlowJo® v10 (FlowJo, LLC, Ashland, USA). Dot plots and histograms were created with the help of the layout

editor. Cell counts, percentages and values of mean fluorescence intensity (MFI) of examined cell subsets and microparticles populations were determined using the table editor.

2.2.7.2 Determining calculations using Excel®

All calculations were performed by the help of Microsoft® Excel® Version 14.7.3 (Microsoft Corporation, Redmond, USA).

All absolute numbers of murine liver cell populations were calculated to 1 g liver tissue and counts of microparticles subpopulations were calculated to 10³ AnnexinV⁺ microparticles.

Determining of mRNA levels in healthy mice (ΔC_t , delta cycle threshold) and changes within the gene expression (fold change) were calculated as follows:

$$\Delta C_t = C_{t_{Gene}} - \text{Mean of } C_{t_{Housekeeping\ Gene}}$$

$$\Delta\Delta C_t = \Delta C_{t_{Treated\ Mice}} - \text{Mean of } \Delta C_{t_{Healthy\ Mice}}$$

$$\text{fold change} = 2^{-\Delta\Delta C_t}$$

In order to assess the diagnostic potential of examined MP subpopulations, positive prediction value (PPV) and negative prediction value (NPV) were determined and calculated as follows (Altman & Bland, 1994):

$$PPV = \frac{\text{Number of true positives}}{\text{Number of true positives} + \text{number of false positives}}$$

$$NPV = \frac{\text{Number of true negatives}}{\text{Number of true negatives} + \text{number of false negatives}}$$

2.2.7.3 Analysis and preparation of scientific data using GraphPad Prism®

All graphs and statistical analyzes were generated with GraphPad Software Prism® 5 (GraphPad Software, Inc., La Jolla, USA) and all data are indicated as mean \pm standard error of the mean (SEM).

- **Determining statistical relevance – Murine hepatic progenitor cell compartment**

In order to determine statistical relevance, either one-way analysis of variance (ANOVA) including Bonferroni post-hoc test or two-tailed unpaired t test was utilized. Data were significant when * $p \leq 0.05$, ** $p \leq 0.01$ or *** $p \leq 0.001$.

• **Determining statistical relevance – Human cell-derived microparticles studies**

Determining of differences between independent cohorts in relation to the examined MP populations was carried out by one-way ANOVA including Dunnett's test as post-hoc test. To define differences between preoperative (pre-OP) and postoperative (post-OP) serum samples of patients who underwent a total R0 tumor resection, a Wilcoxon matched-pairs signed rank test (two-tailed) was utilized. To evaluate diagnostic performance of the examined MP populations, receiver-operating characteristic (ROC) curves, area under curve (AUC) values \pm standard error (SE), p values (p) as well as values of sensitivity [%], specificity [%] were calculated using GraphPad Software Prism[®] 5. Correlation between examined MP populations and age, BMI or serum markers, respectively, were characterized by the help of two-tailed Pearson's correlation (Evans, 1996) including calculation of Pearson's correlation coefficient (r), p value (p) and coefficient of determination (R^2) using GraphPad Software Prism[®] 5. Overall, data were significant when $*p \leq 0.05$, $**p \leq 0.01$ or $***p \leq 0.001$.

2.2.7.4 Statistical power analysis using G*Power

To calculate the approximate number of human sera required, to achieve a particular experimental potency in the human cell-derived MP study, the G*Power program version 3.1.9.3 (Heinrich-Heine-University, Düsseldorf, Germany) was utilized, particularly the priori analysis tool. The human cell-derived MPs studies consist of 8 (tumor-related microparticles) and 6 (HPC-related microparticles) cohorts, respectively. For both studies, different effect sizes f (0.25, 0.45 and 0.65) were tested on the supposition of a α error of 0.1 and test strength of 0.95 (1- β err prob). This results in 56 ($f=0.65$) to 312 ($f=0.25$) or 48 ($f=0.65$) to 276 ($f=0.25$) human sera for the examination of the diagnostic potential of circulating MPs, depending on the desired effect size (Table 13) (Julich-Haertel, Urban, *et al.*, 2017).

Table 13: Statistical power analysis to determine need for sera.

Indicated are the approximate needs for sera according to different effect sizes f (0.25, 0.45 and 0.65) for 8 (tumor-related microparticles) and 6 (HPC-related microparticles) cohorts, respectively. Total sample sizes were calculated according to the supposition of a α error of 0.1 and test strength of 0.95 (1- β err prob). Values were calculated with G*Power program version 3.1.9.3 (Heinrich-Heine-University, Düsseldorf, Germany).

	0.25*	0.45*	0.65*
Needed sera - Tumor-related microparticles	312	104	56
Needed sera - HPC-related microparticles	276	90	48

*Effect size f

3 Results

3.1 Surface marker to distinguish cancer entities and hepatic progenitor cells

The aim of this study was to examine the diagnostic potential of MPs in diagnosis of primary hepatic cancer. On the one hand it was hypothesized if MP subpopulations differ liver tumor patients from patients bearing other cancer entities and further possibly allows classification of hepatic cancer by MP profiling.

For this purpose, a surface marker panel suitable for flow cytometry analysis was chosen to detect liver tumor-derived and HPCs-derived MPs, respectively. Initially, evaluation of surface antigen profiles was carried out on human cancer cell lines, including liver cancer (HCC and liver adenocarcinoma) and PaCa (Section 2.2.1). Each cancer entity was represented by three cell lines, which were cultured (Section 2.2.1.2), harvested (Section 2.2.1.4) and stained (Section 2.2.3) for flow cytometry analysis.

3.1.1 Cancer and hepatic progenitor cells-related surface marker

First, surface marker suitable for flow cytometry analysis had to be chosen. Table 14 summarizes the chosen marker panel, including the function of each surface protein and with which cancer entity they seem related to.

AnnexinV has high affinity to phosphatidylserine (Römisch & Pâques, 1991), which allows identifying MPs in general (Biro *et al.*, 2004; Dignat-George *et al.*, 2004; Reutelingsperger, 2001). Based thereon, AnnexinV was only part of the detection of human cell-derived MPs.

The marker panel was divided into two main points, first, the screening of different cancer entities based on their surface antigen profiles. EpCAM (epithelial cell adhesion molecule; CD326) was chosen to identify epithelial cancers in general (Momburg *et al.*, 1987) and furthermore, CD133 and ASGPR1 (asialoglycoprotein receptor 1) are possibly marker to detect HCC (Ma *et al.*, 2007; Trerè *et al.*, 1999; Yin *et al.*, 2007).

The second part refers to the analysis of human HPC-derived MPs to establish a connection between liver inflammation and liver-derived MPs. Therefore, podoplanin (gp38) and CD133 were included, based on their injury-specific changes within the expression pattern in murine liver (Eckert *et al.*, 2016) and to detect chronic liver inflammation using gp38 (Eckert *et al.*, 2016; Link *et al.*, 2011; Peduto *et al.*, 2009).

Table 14: Assortment of cancer- and hepatic progenitor cells-related surface markers.

Selected surface markers to evaluate microparticle (MP) profiles derived from various cancer entities or hepatic progenitor cell (HPC) populations, respectively. Indicated are the surface markers, the function of each protein and the assumed entity (MPs in general, cancer entity, HPC) to be identified.

Surface marker	Function	Entity
AnnexinV	Actually, annexin was found as vascular protein with anticoagulant properties (Reutelingsperger <i>et al.</i> , 1985). Annexins bind to phospholipids such as phosphatidylserine in a calcium-dependent manner (Römisch & Pâques, 1991). During cellular activation and early apoptosis the cell membrane loses its phospholipid asymmetry (Mause & Weber, 2010; Sims <i>et al.</i> , 1988) and thus exposure of phosphatidylserine occurs (Fadok <i>et al.</i> , 1992) together with the release of microparticles by budding of the cell membrane (Sims <i>et al.</i> , 1988). Based thereon, AnnexinV can be used to identify MPs (Biro <i>et al.</i> , 2004; Dignat-George <i>et al.</i> , 2004; Reutelingsperger, 2001).	MPs
ASGPR1	ASGPR1 is a subunit of the asialoglycoprotein receptor (ASGPR), a glycoprotein uniquely expressed by hepatocytes, which mediates serum glycoprotein homeostasis (Geffen & Spiess, 1992; Morell <i>et al.</i> , 1968). ASGPR1 was shown to be expressed in a large number of human HCCs (Trerè <i>et al.</i> , 1999).	HCC
CD133	CD133 is a transmembrane hematopoietic stem cell antigen (Miraglia <i>et al.</i> , 1997), which has been reported to identify putative cancer stem cells in HCC (Ma <i>et al.</i> , 2007; Yin <i>et al.</i> , 2007). In addition, CD133-expressing liver cells indicate characteristics of liver progenitor cells (Rountree <i>et al.</i> , 2007).	HCC & HPCs
CD326 (EpCAM)	Epithelial cell adhesion molecule (EpCAM), identified as glycoprotein (Göttlinger, Funke, <i>et al.</i> , 1986; Göttlinger, Johnson, <i>et al.</i> , 1986) was first described as CrC-specific antigen (Herlyn <i>et al.</i> , 1979; Koprowski <i>et al.</i> , 1979). Later, expression of EpCAM by most epithelial cell types and further EpCAM upregulation in several epithelial cancers (e.g. CrC, PaCa, liver carcinoma, lung carcinoma) was shown (Momburg <i>et al.</i> , 1987).	Epithelial cancers

gp38 (Podoplanin)

Podoplanin (gp38) is a surface glycoprotein and lymphatic marker based on the specific expression by the lymphatic endothelium (Breiteneder-Geleff *et al.*, 1999; Farr *et al.*, 1992). Podoplanin-expressing cells in nonlymphoid organs, which are similar to those of the secondary lymphoid organs, form parts of tertiary lymphoid structures during chronic inflammation HPCs (Peduto *et al.*, 2009), e.g. in human primary biliary cirrhosis (Link *et al.*, 2011). Subpopulations of CD133-expressing liver cells with characteristics of liver progenitor cells differ in their gp38 expression pattern and indicate injury-specific changes (Eckert *et al.*, 2016).

MPs: Microparticles

HCC: Hepatocellular carcinoma

CrC: Colorectal carcinoma

PaCa: Pancreatic cancer

3.1.2 Surface marker profiles differ liver cancer cell lines from pancreatic cancer cell lines

The aim of this part of the study was the first investigation of the presence of cancer- and HPC-associated surface marker profiles in established human cancer cell lines. This should confirm obtained information from the literature research of section 3.1.1.

A surface marker panel suitable for flow cytometry analysis was used including EpCAM, ASGPR1, CD133 and gp38.

EpCAM should serve as pan-cancer marker, based on the upregulation in several epithelial cancers (Momburg *et al.*, 1987). To specifically identify HCC, CD133 (Ma *et al.*, 2007; Yin *et al.*, 2007) and ASGPR1 (Trerè *et al.*, 1999) should be used, especially in combination with EpCAM. Thus, it was hypothesized to differentiate the liver cancer cell lines from PaCa cell lines based on the surface marker profile.

Additionally, the combination of gp38 and CD133 was assumed to differ liver cancer cell lines from PaCa cell lines. The assumption is based on the gp38 expression pattern in subpopulations of CD133-expressing liver cells which indicate oval cell characteristic and injury-specific changes (Eckert *et al.*, 2016).

Sabine Katharina Urban, former master student of the laboratory, performed all tissue culture work, antibody staining and flow cytometry analysis of all human cancer cell

lines supervised by Henrike Julich-Haertel (Section 9 – Informed consent). Henrike Julich-Haertel finally analyzed generated data.

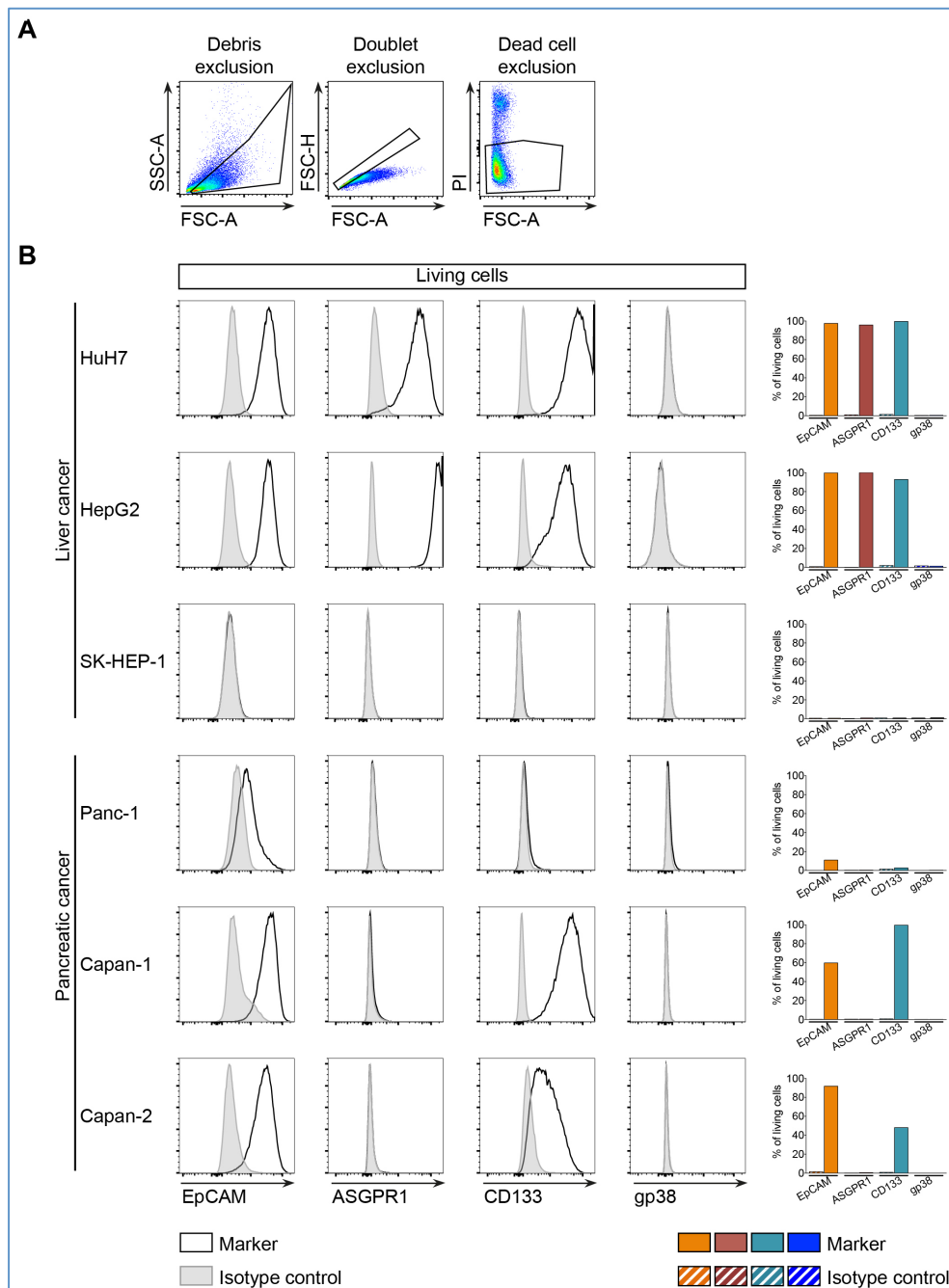


Figure 10: Surface marker profiles in human liver cancer cell lines and pancreatic cancer cell lines.

Human cancer cell lines (liver cancer: HuH7, HepG2, SK-HEP-1; pancreatic cancer: Panc-1, Capan-1, Capan-2) were stained with anti-EpCAM, anti-ASGPR1, anti-CD133 and anti-gp38. To exclude dead cells, propidium iodide (PI) was utilized. A) Representative dot plot with the basic gating strategy is indicated. To investigate expression pattern of living cells, debris (plotting SSC-A against FSC-A), doublets (plotting FSC-A against FSC-H) and dead cells (plotting PI against FSC-A) were excluded by gating on PI negative events. B) Distinguishing marker expression are shown as histograms for the different cell lines compared to the corresponding isotype controls (left) in addition to percentages of marker-positive cells present among the living cells (right). Statistical analyzes were not performed, because experiment was done only once. Sabine Katharina Urban, former master student of the laboratory, performed all tissue culture work, antibody staining and flow cytometry analysis of all human cancer cell lines supervised by Henrike Julich-Haertel (Section 9 – Informed consent). Henrike Julich-Haertel analyzed generated data.

First of all, the different cell lines were examined for their marker expression without specific gating strategy (Figure 10). To investigate expression profiles of all living cells, gating on PI negative cells (plotting PI against FSC-A) by debris (plotting SSC-A against FSC-A), doublet (plotting FSC-A against FSC-H) and dead cell exclusion was carried out (Figure 10A). The histograms indicate distinguishing marker characteristics of the different cell lines compared to the corresponding isotype control (Figure 10B, left). Additionally, percentages of marker-positive cells present among the living cells are depicted (Figure 10B, right). Statistical analyzes were not performed, because experiment was done only once.

The liver cancer cell line SK-HEP-1 and the PaCa cell line Panc-1 show almost no expression of the examined surface markers and will leave out of consideration further on.

Liver cancer and PaCa cell lines indicate high expression of EpCAM and CD133. ASGPR1 expression seems to be specific for liver cancer as indicated by high expression in both, HuH7 and HepG2. In contrast, gp38 expression is not detectable in both liver cancer and PaCa cell lines. Thus, for further analysis of human cancer cell lines, only the combination of EpCAM, CD133 and ASGPR1 will be considered further on.

Cell lines were examined for their CD133 and ASGPR1 expression among the EpCAM⁺ cells (Figure 11). For this purpose, debris, doublets and dead cells were excluded (Figure 11A). Afterwards, plotting EpCAM against FSC-A and gating on EpCAM⁺ events according to the corresponding isotype control (Figure 11B, left). Finally, plotting ASGPR1 against CD133 should carry out an HCC-specific gating strategy (Figure 11B, right) by gating on ASGPR1 single positive (Figure 11B, red), CD133 single positive (Figure 11B, turquoise) and CD133/ASGPR1 double positive events (Figure 11B, purple). Representative dot plots are shown for HuH7 and Capan-2. Additionally, percentages of EpCAM⁺, EpCAM⁺CD133⁺ and EPCAM⁺CD133⁺ASGPR1⁺ cells present among the living cells are depicted (Figure 11C). Statistical analyzes were not performed, because experiment was done only once.

EpCAM expression seems to be higher in liver cancer cell lines compared to PaCa cell lines, which seem to differ in their EpCAM expression. PaCa cell lines show about 50 % EpCAM⁺CD133⁺ cells, whereas almost all cells of the liver cancer cell lines seem to be EpCAM⁺CD133⁺ASGPR1⁺. Thus, the investigated cell lines indicated different

expression profiles and give reason to believe that liver cancer can be differentiated from PaCa by surface marker profiling.

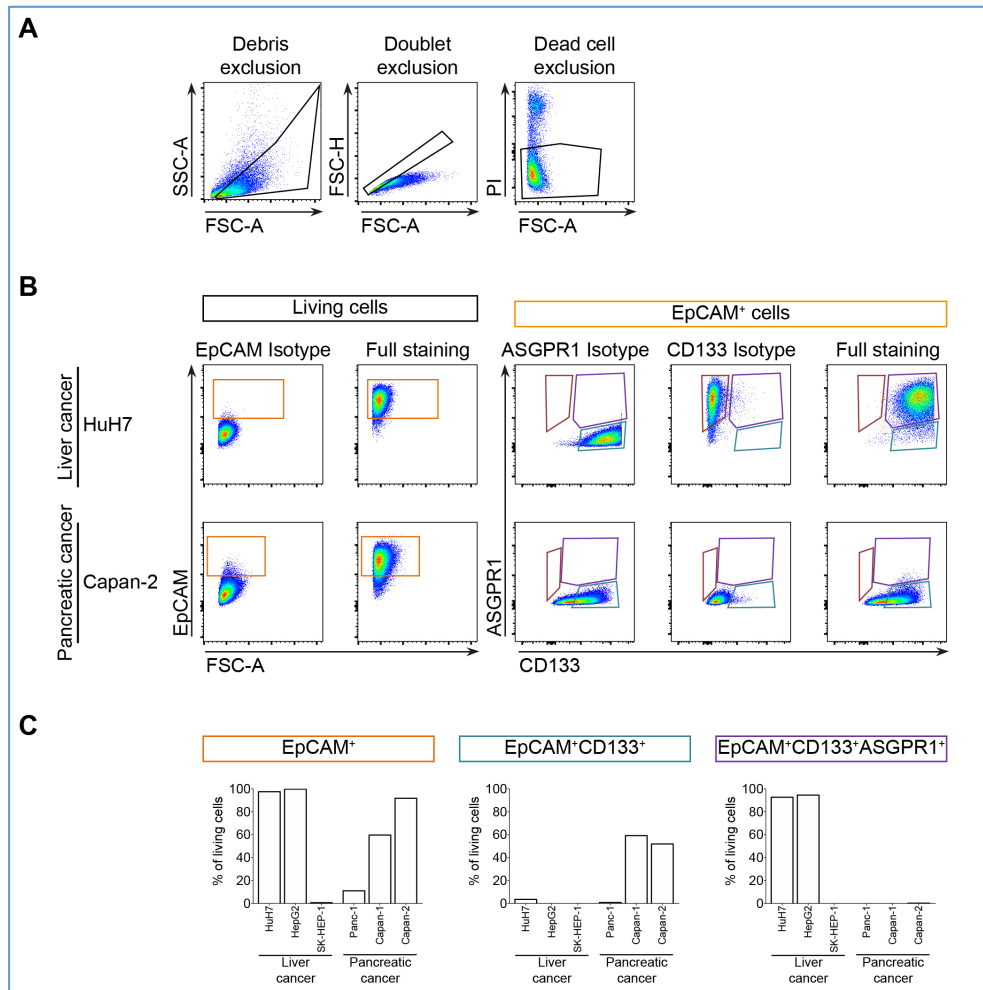


Figure 11: Surface marker profiles differ liver cancer cell lines from pancreatic cancer cell lines.

Human cancer cell lines (liver cancer: HuH7, HepG2, SK-HEP-1; pancreatic cancer: Panc-1, Capan-1, Capan-2) were stained with anti-EpCAM, anti-ASGPR1, anti-CD133 and anti-gp38. Dead cell exclusion was carried out by using propidium iodide (PI). A) Indicated are representative dot plots with the basic gating strategy. To investigate expression pattern of living cells, debris (plotting SSC-A against FSC-A), doublets (plotting FSC-A against FSC-H) and dead cells were excluded (plotting PI against FSC-A) by gating on PI negative events. B) Cell lines were examined for their CD133 and ASGPR1 expression among the EpCAM⁺ cells. First, gating on EpCAM⁺ events by plotting EpCAM against FSC-A (left). Second, plotting ASGPR1 against CD133 and gating on ASGPR1 single positive (red), CD133 single positive (turquoise) and CD133/ASGPR1 double positive events (purple). C) Percentages of marker-positive cells (EpCAM⁺, EpCAM⁺CD133⁺, EpCAM⁺CD133⁺ASGPR1⁺) present among the living cells are displayed. Statistical analyzes were not performed, because experiment was done only once. Sabine Katharina Urban, former master student of the laboratory, performed all tissue culture work, antibody staining and flow cytometry analysis of all human cancer cell lines supervised by Henrike Julich-Haertel (Section 9 – Informed consent). Henrike Julich-Haertel finally analyzed generated data.

3.2 The murine hepatic progenitor cell compartment

The examined liver cancer and PaCa cell lines lacked any detectable gp38 expression (Section 3.1.2). However, it was shown that gp38-expressing cells in nonlymphoid organs form parts of tertiary lymphoid structures during chronic inflammation (Peduto *et al.*, 2009). In addition, gp38 expression pattern differ in subpopulations of CD133-expressing liver cells and indicate injury-specific changes (Eckert *et al.*, 2016). Due to this, the aim of this part of the study was to further ascertain phenotypically differences between the various HPC subpopulations and examine their involvement in liver injury-specific changes. This was utilized to possibly establish a connection between liver inflammation and liver-derived MPs.

Therefore, a detailed protocol for an optimized isolation technique of these rare HPC populations was established (Section 2.2.2.4) (Julich-Haertel, Tiwari, *et al.*, 2017). Furthermore, expression pattern of several surface markers (Section 2.2.3) and gene expression analysis of HPCs (Section 2.2.4) were investigated in healthy livers and various liver injury models (Section 2.2.2): e.g. TAA-induced fibrosis, a model of NASH (CDE-diet) and cholestatic liver injury (DDC-diet).

3.2.1 Classification of the hepatic progenitor cell compartment in healthy liver

In this part of the study, a detailed protocol for an optimized isolation technique of murine HPC populations was established (Section 2.2.2.4) (Julich-Haertel, Tiwari, *et al.*, 2017). With the help of this, further characterization of the murine HPC subsets classified by their gp38 and CD133 expression (Eckert *et al.*, 2016) was possible by analysis of the expression pattern of various surface markers (Figure 12 & Figure 13). Data represent 3 independent experiments with 3 mice per experiment. Values are given as mean \pm SEM.

First, liver single-cell suspension of wild-type untreated mice was stained with a surface marker panel including CD45, CD31, ASGPR1, CD133 and gp38 (Figure 12A). With the help of the established liver-digestion method (Julich-Haertel, Tiwari, *et al.*, 2017), liver single-cell suspensions containing parenchymal and non-parenchymal cells can be examined. The exclusion of debris (gating SSC-A against FSC-A), doublets (gating FSC-A against FSC-H) and dead cells (gating PI against FSC-A, gating on PI⁺ events) was followed by the gating on cells negative for CD45, CD31 and ASGPR1 to exclude immune cells/hematopoietic cells, endothelial cells and hepatocytes, respectively. The

CD45⁻CD31⁻ASGPR1⁻ cell population comprises the entire HPCC. The HPCC can be classified by their CD133 and gp38 expression according to the corresponding isotype controls, resulting in the following subsets: gp38^{high}CD133⁻ (black), gp38^{low}CD133⁻ (blue), gp38^{low}CD133⁺ (yellow) and gp38⁻CD133⁺ (turquoise). The gp38^{low}CD133⁺ and gp38⁻CD133⁺ cells represent the most common cells among the CD45⁻CD31⁻ASGPR1⁻ cells (Figure 12B) in both percentage and count per 1 g liver tissue in wild-type healthy liver.

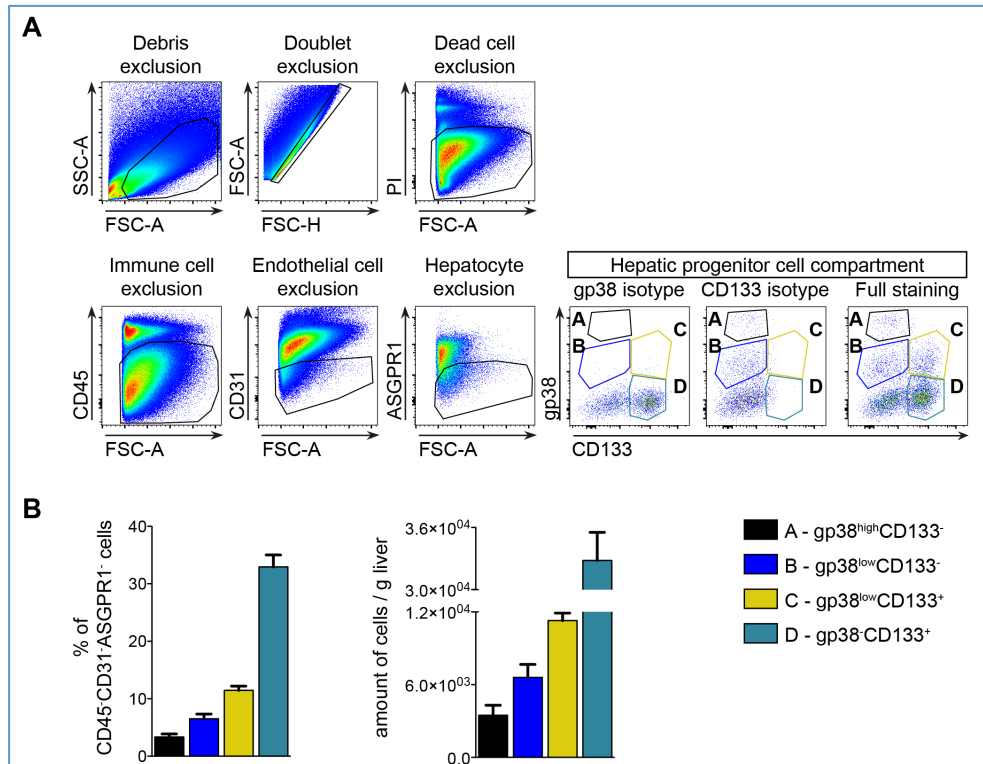


Figure 12: Classification of the murine hepatic progenitor cell compartment in healthy liver.

Liver single-cell suspension of wild-type untreated mice was stained with surface markers suitable for flow cytometry analysis: CD45, CD31, ASGPR1, CD133 and gp38. To exclude dead cells, propidium iodide (PI) was used. A) The basic gating strategy is indicated by representative dot plots. Debris, doublets and dead cell exclusion, followed by gating on cells negative for CD45, CD31 and ASGPR1 allows detections of hepatic progenitor cell subsets, classified by their CD133 and gp38 expression. B) Percentages among the CD45⁻CD31⁻ASGPR1⁻ cells and absolute numbers present per g of liver tissue are shown for the various subsets. Data represent 3 independent experiments with 3 mice per experiment. Values are given as mean ± SEM. (Modified according to Julich-Haertel, Tiwari, *et al.*, 2017)

The subpopulations differ not only in their cell number but also in the expression of several surface markers previously associated with mesenchymal stem and liver progenitor cells (Figure 13). All liver progenitor subtypes among the CD45⁻CD31⁻ASGPR1⁻ cells were examined for the expression of CD24, CD34, CD90.2, EpCAM, intercellular adhesion molecule-1 (ICAM-1, CD54), macrophage inhibitory cytokine-1-1C3 (MIC1-1C3, oval cell marker) and stem cell antigen-1 (Sca-1, Ly-6A/E) to further ascertain phenotypically differences between the progenitor subtypes.

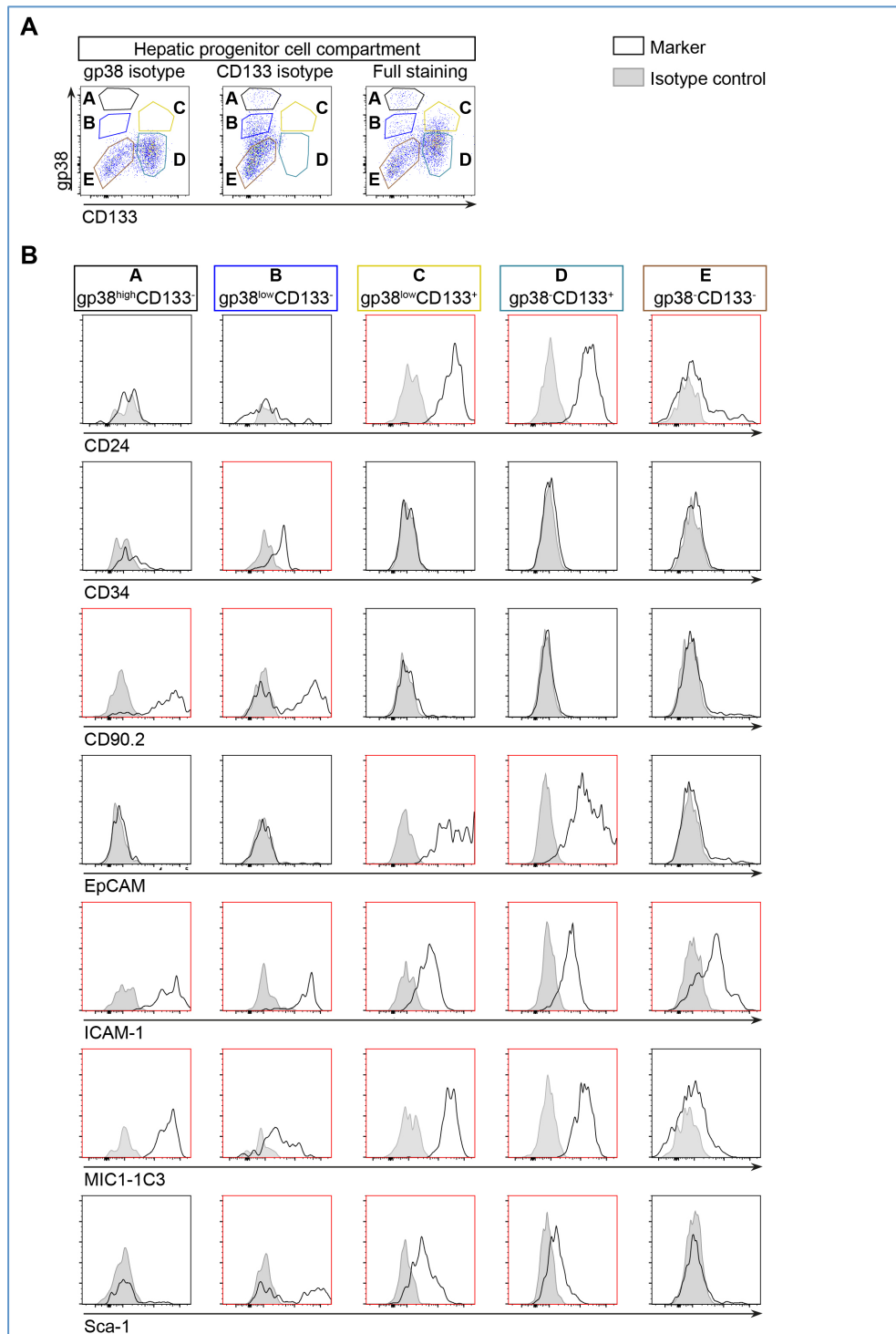


Figure 13: Progenitor cell-associated surface marker expression in murine hepatic progenitor cell (HPC) subsets. Liver single-cell suspension of wild-type untreated mice was stained with various surface markers, including CD45, CD31, ASGPR1, CD133 and gp38 and propidium iodide (PI) was used for dead cell exclusion. A) Representative dot plot with the several HPC subsets, classified by their CD133 and gp38 expression is indicated (gp38^{high}CD133⁻ (black), gp38^{low}CD133⁻ (blue), gp38^{low}CD133⁺ (yellow), gp38⁺CD133⁺ (turquoise) and gp38⁺CD133⁻ (brown)). B) Histograms are indicated for the mesenchymal stem and liver progenitor cells-associated surface markers CD24, CD34, CD90.2, epithelial cell adhesion molecule (EpCAM), intercellular adhesion molecule-1 (ICAM-1), macrophage inhibitory cytokine-1-1C3 (MIC1-1C3, oval cell marker) and stem cell antigen-1 (Sca-1) for each HPC subset compared to the corresponding isotype control. Data represent 3 independent experiments with 3 mice per group.

Expression profiles are indicated as histograms for each surface marker and population compared to the corresponding isotype control (Figure 13B). ICAM-1 expression is

present in all types of subsets among the CD45⁺CD31⁺ASGPR1⁺ cells. Almost all subtypes, except cells lacking both gp38 and CD133 expression, express MIC1-1C3. CD34 expression is specific for gp38^{low}CD133⁺ cells and high CD90.2 expression is present in gp38-expressing cells lacking any CD133 expression (gp38^{high}CD133⁺ and gp38^{low}CD133⁺). The gp38^{high}CD133⁺ cells were identified as mesothelial cells (Eckert *et al.*, 2016) and will not be considered further on.

Sca-1 expression is detectable in low gp38-expressing cells, gp38^{low}CD133⁺ and gp38^{low}CD133⁺, but also in gp38⁺CD133⁺ cells but much less. On the other hand, EpCAM and CD24 expression is present in CD133-expressing cells, gp38^{low}CD133⁺ and gp38⁺CD133⁺. In addition, low CD24 expression is indicated by cells lacking both CD133 and gp38 expression.

HPCs represent rare cell populations, due to this it is difficult to examine them. Hence, a method to enrich and purify CD133⁺ hepatic progenitor cells with high viability, was established during this study (Section 2.2.4.1) (Julich-Haertel, Tiwari, *et al.*, 2017). This method allows further analysis, such as gene expression analysis (Section 2.2.4) of the heterogeneous CD133⁺ oval cell population (Figure 14). Data of magnetic MicroBead-based enrichment and automated cell purification represent 3 independent experiments with 3 mice per group. Results of gene expression analysis represent 2 independent experiments. Values are given as mean \pm SEM and differences were evaluated by two-tailed unpaired t test (* $p \leq 0.05$, ** $p \leq 0.01$, *** $p \leq 0.001$).

Magnetic MicroBead-based enrichment leads to the removal of CD45⁺, CD31⁺ and ASGPR1⁺ cells and enriches the CD45⁺CD31⁺ASGPR1⁺ cell population with over 90 % purity among all living cells (Figure 14A). Magnetic MicroBead-based automated cell purification allows the isolation of CD133-expressing cells, containing gp38⁺ and gp38⁺ cells, respectively, with high viability (Figure 14B). This allows gene expression analysis of this heterogeneous oval cell population (Figure 14C). Several genes using qRT-PCR were considered: 1) PDPN (podoplanin/gp38) and PROM1 (prominin 1/CD133), purity check to identify the cell population, 2) KRT19 (keratin 19) and HNF4A (hepatic nuclear factor 4-alpha) as oval cell-related genes, 3) HNF1A (hepatocyte nuclear factor 1-alpha), HNF1B (hepatocyte nuclear factor 1-beta), HNF4A and HNF6 (hepatocyte nuclear factor 6), as liver specific genes, 4) CDH1 (cadherin 1), as epithelial-mesenchymal transition (EMT)-associated gene, 5) YAP1 (yes-associated protein 1), as main target of the Hippo signaling pathway and 6) FAS (fas cell surface death receptor) and CCL2 (C-C motif chemokine ligand 2), as inflammatory and

apoptosis-associated genes. Expression levels are indicated as ΔCt values according to the housekeeping gene B2M (beta-2-microglobulin).

CD133⁺ progenitor cells, isolated from wild-type healthy liver, indicate low expression of HNF1A, HNF4A, FAS and CCL2, moderate expression of HNF1B, HNF6 and YAP1 and high expression of KRT19 and CDH1.

Based on the surface marker expression in association with the gene expression analysis, the results suggest that murine CD133⁺ liver cells indicate progenitor cell characteristics.

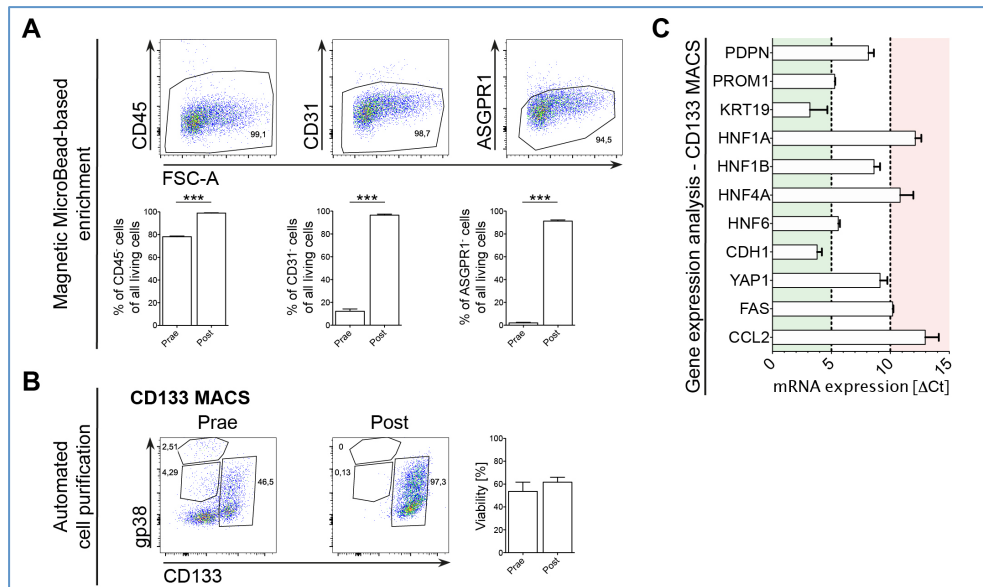


Figure 14: Gene expression analysis of enriched and purified CD133⁺ oval cells in healthy murine liver. Enriched and purified CD133⁺ oval cells of wild-type untreated mice were stained with various surface markers, including CD45, CD31, ASGPR1, CD133 and gp38. Propidium iodide (PI) was used to carry out dead cell exclusion. A) Representative dot plot of magnetic MicroBead-based enriched progenitor cells is indicated. In addition, percentages of CD45⁺, CD31⁺ and ASGPR1⁺ cells among all living cells before and after enrichment are shown. B) Representative dot plot of magnetic MicroBead-based automated cell purification of CD133⁺ oval cells before and after purification is depicted (left). The viability of the purified CD133⁺ progenitor cells before and after purification is indicated as percentage of PI⁺ cells. C) Gene expression of CD133⁺ oval cells is shown as ΔCt values according to the housekeeping gene beta-2-microglobulin. Several genes using qRT-PCR were considered: PDPN (podoplanin/gp38), PROM1 (prominin 1/CD133), KRT19 (keratin 19), HNF1A (hepatocyte nuclear factor 1-alpha), HNF1B (hepatocyte nuclear factor 1-beta), HNF4A (hepatic nuclear factor 4-alpha), HNF6 (hepatocyte nuclear factor 6), CDH1 (cadherin 1), YAP1 (yes-associated protein 1), FAS (fas cell surface death receptor) and CCL2 (C-C motif chemokine ligand 2). Data (A-B) represent 3 independent experiments with 3 mice per group. Data (C) represent 2 independent experiments. Values are given as mean \pm SEM and differences were evaluated by two-tailed unpaired t test (* $p \leq 0.05$, ** $p \leq 0.01$, *** $p \leq 0.001$).

3.2.2 The hepatic progenitor cell compartment during TAA-induced liver fibrosis

To induce liver fibrosis, the well-established TAA model was applied (Section 2.2.2.1). The centrilobular hepatotoxicant TAA undergoes bioactivation to its reactive metabolite, which putative induce cellular necrosis (Chilakapati *et al.*, 2005; Hajovsky *et al.*, 2012) and liver fibrosis within six weeks (Salguero Palacios *et al.*, 2008).

Wild-type mice were frequently administered IP with 200 µg per g mice weight for either three or six weeks. Wild-type untreated mice served as control for this experiment. Data of TAA-induced liver fibrosis represent a single experiment with three mice per group. Values are given as mean ± SEM and differences were assessed by two-tailed unpaired t test (* $p \leq 0.05$, ** $p \leq 0.01$, *** $p \leq 0.001$).

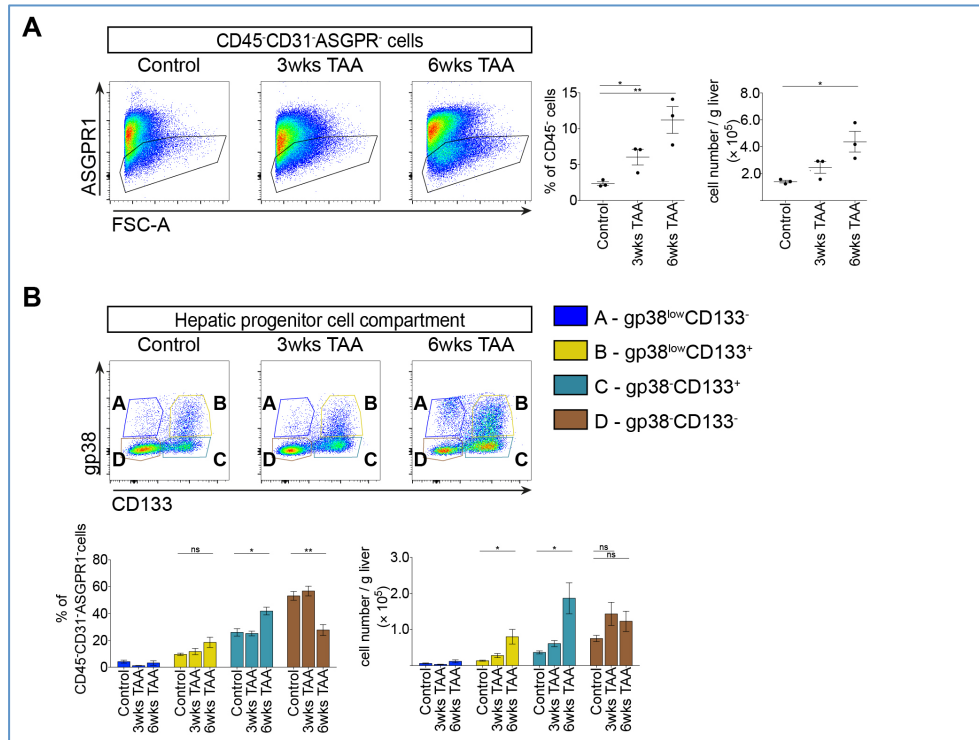


Figure 15: Classification of the murine hepatic progenitor cell compartment (HPCC) in TAA-induced injured liver. Liver single-cell suspension of wild-type untreated and TAA-treated mice (thioacetamide, 3 weeks and 6 weeks) were stained with various surface markers, including CD45, CD31, ASGPR1, CD133 and gp38. Propidium iodide (PI) was used to exclude dead cells. A) Representative dot plots with gating on cells negative for CD45, CD31 and ASGPR1 to identify the entire HPCC in healthy and TAA-treated mice are depicted (left). Percentages among the CD45⁻ cells and absolute numbers present per g of liver tissue for the entire HPCC are shown (right). B) Representative dot plot with the several hepatic progenitor cell subsets, classified by CD133 and gp38 expression (after gating out of gp38^{high}CD133⁻ cells), in healthy and TAA-treated mice are indicated. In addition, percentages among the CD45⁻CD31⁻ASGPR1⁻ cells and absolute numbers present per g of liver tissue of the various subsets are shown. Data represent a single experiment with 3 mice per group. Values are given as mean ± SEM. Differences were evaluated by two-tailed unpaired t test (* $p \leq 0.05$, ** $p \leq 0.01$, *** $p \leq 0.001$).

Liver single-cell suspension was stained with a surface marker panel including CD45, CD31, ASGPR1, CD133 and gp38 (Figure 15). Gating on cells negative for CD45, CD31 and ASGPR1 followed exclusion of debris, doublets and dead cells. The CD45⁻CD31⁻ASGPR1⁻ cell population comprises the entire HPCC (Figure 15A), which increases significant during the TAA-treatment in both percentage among the CD45⁻ cells (3 weeks TAA: 2.5-fold, 6 weeks TAA: 4.8-fold) and count per 1 g liver tissue (3 weeks TAA: 1.8-fold, 6 weeks TAA: 3.1-fold). The HPCC is classified by their CD133 and gp38 expression after gating out of mesothelial cells (gp38^{high}CD133⁻)

resulting in the following subsets: gp38^{low}CD133⁻ (blue), gp38^{low}CD133⁺ (yellow), gp38⁻CD133⁺ (turquoise) and double negative cells (gp38⁻CD133⁻, brown) (Figure 15B).

A little increase of gp38^{low}CD133⁻ cells is indicated in count per g liver tissue after 6 weeks TAA-treatment. CD133-expressing cells increase during TAA-treatment in both percentage among CD45⁻CD31⁻ASGPR1⁻ cells and count per g liver tissue. In detail, frequency of gp38^{low}CD133⁺ cells increase up to 1.9-fold after 6 weeks TAA-treatment and the cell count increases significantly up to 5.9-fold after 6 weeks TAA-treatment. Cells lacking any gp38 expression (gp38⁻CD133⁺) indicate the same tendencies. These results suggest that both CD133-expressing progenitor subsets are activated in the same extent and thus distinguishing them from one another is difficult. Cells lacking any CD133 and gp38 expression (gp38⁻CD133⁻) decrease significant after 6 weeks TAA-treatment in percentage, whereas counts increase after 3 and 6 weeks TAA-treatment.

The TAA-model seems to induce the entire HPCC, but does not seem to trigger different activation processes in the individual progenitor subsets.

3.2.3 CDE-induced activation of the hepatic progenitor cell compartment

Feeding with a choline-deficient diet, supplemented with the ethyl analogon methionine leads to metabolic changes in hepatocytes, resulting in lethal deterioration of them. As a consequence, oval cells get activated and proliferate (Kroy *et al.*, 2010; Liedtke *et al.*, 2013; Shinozuka *et al.*, 1978; Ueberham *et al.*, 2010).

Wild-type mice were fed with CDE-diet or the corresponding control-diet for 7 and 14 days, respectively (Section 2.2.2.2). Stephanie Schmid, former master student of the laboratory, performed all mouse care, in addition to the extraction of murine livers at the end of the CDE-treatment supervised by Henrike Julich-Haertel. Preparation of liver single-cell suspension, antibody staining and flow cytometry analysis was performed by Henrike Julich-Haertel. Data of CDE-activated oval cells represent a single experiment with three mice per group (despite 7 days CDE: 2 mice). Values are given as mean ± SEM and differences were verified by unpaired t test (two-tailed; * $p \leq 0.05$, ** $p \leq 0.01$, *** $p \leq 0.001$).

Liver single-cell suspension was stained with a surface marker panel including CD45, CD31, ASGPR1, CD133 and gp38 (Figure 16). The gating on cells negative for CD45, CD31 and ASGPR1 followed exclusion of debris, doublets and dead cells. The CD45⁻

CD31⁺ASGPR1⁺ cell population comprises the entire HPCC (Figure 16A). After 7 days CDE-feeding CD45⁺CD31⁺ASGPR1⁺ cells increase about 5.0-fold in both percentage among the CD45⁺ cells and cell counts per g liver tissue. After 14 days CDE-feeding, the entire HPCC increases in percentage (7.2-fold) and cell count (10.0-fold) even more.

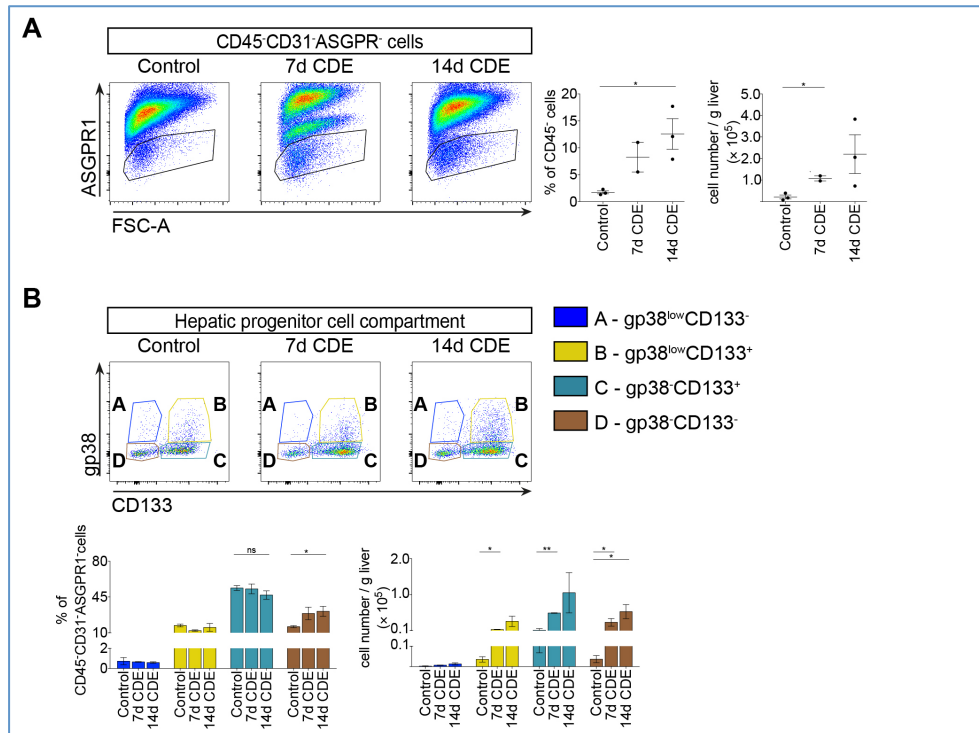


Figure 16: Classification of the murine hepatic progenitor cell compartment (HPCC) in CDE-induced injured liver. Liver single-cell suspension of wild-type untreated and CDE-fed mice (choline-deficient, ethionine-supplemented; 7 days and 14 days) were stained with various surface markers, including CD45, CD31, ASGPR1, CD133 and gp38. Dead cell exclusion was carried out by use of propidium iodide (PI). A) Representative dot plots with gating on cells negative for CD45, CD31 and ASGPR1 to identify the entire HPCC in healthy and CDE-fed mice are depicted (left). Percentages among the CD45⁺ cells and absolute numbers present per g of liver tissue for the entire HPCC are shown (right). B) Representative dot plot with the several hepatic progenitor cell subsets, classified by CD133 and gp38 expression (after gating out of gp38^{high}CD133⁻ cells), in healthy and CDE-fed mice are indicated. In addition, percentages among the CD45⁺CD31⁺ASGPR1⁺ cells and absolute numbers present per g of liver tissue of the various subsets are shown. Data represent a single experiment with 2-3 mice per group. Values are given as mean \pm SEM. Differences were verified by unpaired t test (two-tailed; * $p \leq 0.05$, ** $p \leq 0.01$, *** $p \leq 0.001$).

To investigate changes within the HPCC regarding the individual progenitor subsets, they are classified by their CD133 and gp38 expression after gating out of mesothelial cells (gp38^{high}CD133⁻). This results in the following subsets: gp38^{low}CD133⁻ (blue), gp38^{low}CD133⁺ (yellow), gp38⁻CD133⁺ (turquoise) and the double negative cells (gp38⁻CD133⁻, brown) (Figure 16B). Neither 7 nor 14 days CDE-feeding leads to changes of percentage distribution of the individual subsets within the HPCC. Only gp38⁻CD133⁻ cells increase 2.0-fold after 14 days CDE-feeding, while gp38⁻CD133⁺ cells seem to slightly decrease. Considering cell counts per g liver tissue, almost all subsets of the entire HPCC increase during the CDE-feeding. The cell count of gp38^{low}CD133⁻ cells

are almost unaltered, whereas cells expressing both gp38 and CD133 (gp38^{low}CD133⁺) increase about 3.5 fold after 7 days and 9.8-fold after 14 days CDE-feeding. Cells expressing CD133 and lacking any gp38 expression increase 5.1-fold after 7 days and up to 9.9-fold after 14 days. The same tendency applies to cells lacking both gp38 and CD133 expression. This cell subset increases 8.7-fold after 7 days and up to 16.5-fold after 14 days.

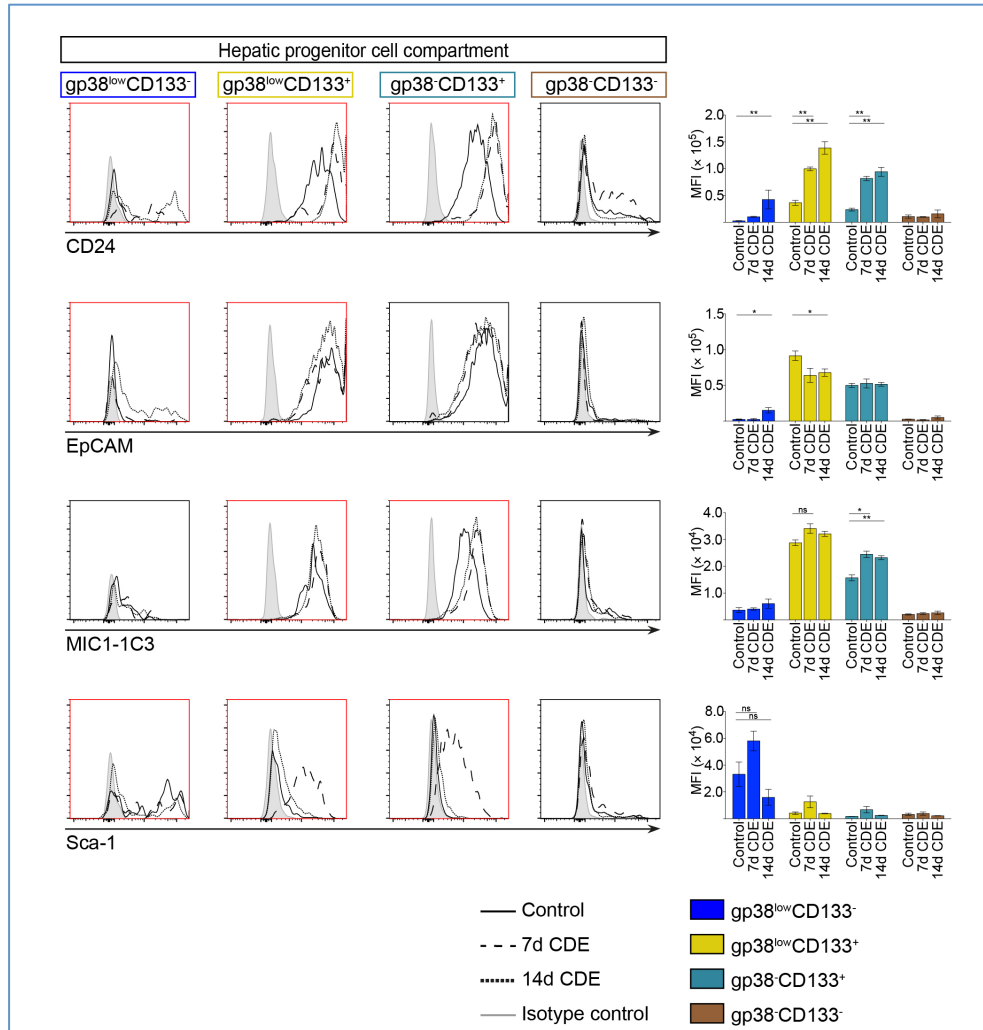


Figure 17: CDE-induced changes within the surface marker expression in progenitor subsets of murine liver. Liver single-cell suspension of wild-type untreated and CDE-fed mice (choline-deficient, ethionine-supplemented; 7 days and 14 days) were stained with various surface markers, including CD45, CD31, ASGPR1, CD133 and gp38. Exclusion of dead cells was carried out by use of propidium iodide (PI). Histograms of the several hepatic progenitor cell subsets, classified by their CD133 and gp38 expression are indicated (gp38^{high}CD133⁻ (black), gp38^{low}CD133⁻ (blue), gp38^{low}CD133⁺ (yellow), gp38⁻CD133⁺ (turquoise) and gp38⁻CD133⁻ (brown)) for the progenitor cells-associated surface markers CD24, epithelial cell adhesion molecule (EpCAM), macrophage inhibitory cytokine-1-1C3 (MIC1-1C3, oval cell marker) and stem cell antigen-1 (Sca-1), compared to the corresponding isotype control. Additionally, bar graphs of the mean fluorescence intensity (MFI) of each surface marker are shown for each progenitor subset and treatment. Data represent a single experiment with 2-3 mice per group. Values are given as mean ± SEM. Differences were verified by unpaired t test (two-tailed; **p* ≤ 0.05, ***p* ≤ 0.01, ****p* ≤ 0.001).

To examine distinctions of the individual progenitor subsets during CDE-treatment, surface markers previously associated with progenitor cells were considered, including

CD24, EpCAM, MIC1-1C3 and Sca-1. Expression profiles are indicated as histograms for each surface marker and population (gp38^{low}CD133⁻ (blue), gp38^{low}CD133⁺ (yellow), gp38⁻CD133⁺ (turquoise), gp38⁻CD133⁻ (brown)) compared to the corresponding isotype control for 7 day and 14 days CDE-feeding and the corresponding control (Figure 17, left). In addition, bar graphs indicating MFI of each surface marker is shown for each progenitor subset and treatment (Figure 17, right).

The MFI of CD24 and MIC1-1C3 increases during CDE-diet in both CD133-expressing subtypes gp38^{low}CD133⁺ and gp38⁻CD133⁺ throughout the period of CDE-treatment. Interestingly, gp38^{low}CD133⁻ cells indicate low expression of CD24 after 14 days CDE-feeding, compared to the healthy control which lacks CD24 expression by this cell type. The same tendency applies to the expression of EpCAM, which seem to be slightly induced in gp38^{low}CD133⁻ cells after 14 days CDE-feeding. In contrast, the EpCAM-expressing cells gp38^{low}CD133⁺ indicate a significant decrease in the MFI during the CDE-treatment, whereas MFI of EPCAM not changes in gp38⁻CD133⁺ cells during the treatment. Sca-1 expression by gp38^{low}CD133⁻ cells is increased after 7 days and decrease after 14 days CDE-diet. Interestingly, also both subtypes of CD133-expressing cells gp38^{low}CD133⁺ and gp38⁻CD133⁺ show a slight increase of Sca-1 expression after 7 days which in turn is lacking after 14 days CDE-feeding.

In summary, CDE-feeding leads to an increase of the HPCC, whereas changes within the percentage distribution are mainly lacking considering the individual subtypes within the HPCC. However, expression pattern of surface markers previously associated with progenitor cells changes due to the CDE-treatment. Thus, CDE-induced HPC activation can be assumed.

3.2.4 DDC-induced activation of the hepatic progenitor cell compartment

To activate the HPCC during cholestatic liver injury, the well-defined DDC-model was applied (Section 2.2.2.3). Feeding with DDC leads to hepatocyte injury, resulting in the inhibition of tissue repair, followed by oval cell activation and proliferation (Jakubowski *et al.*, 2005).

Wild-type mice were fed with DDC-diet (0.1 % DDC in maintenance diet for mice) for 1 or 7 days to investigate the progression phase. To examine the regression phase, mice were fed 1 day with DDC-diet and subsequently 3 days with normal standard chow. Wild-type untreated mice, fed with normal standard chow served as control for this experiment. Julia Maiworm, former master student of the laboratory, performed all

mouse care, in addition to the extraction of murine livers at the end of the DDC-experiment supervised by Henrike Julich-Haertel. Preparation of liver single-cell suspension, antibody staining and flow cytometry analysis was performed by Henrike Julich-Haertel in addition to the preparation and execution of the experiment to examine gene expression during DDC-regression phase. Data of DDC-activated oval cells represent a single experiment with three mice per group and results of gene expression analysis represent 4 independent DDC-treatments (regression phase). Values are given as mean \pm SEM and differences were verified by unpaired t test (two-tailed; * $p \leq 0.05$, ** $p \leq 0.01$, *** $p \leq 0.001$).

Liver single-cell suspension was stained with a surface marker panel including CD45, CD31, ASGPR1, CD133 and gp38 (Figure 18). The gating on cells negative for CD45, CD31 and ASGPR1 followed exclusion of debris, doublets and dead cells. The CD45⁻CD31⁻ASGPR1⁻ cell population comprises the entire HPCC (Figure 18A). Frequency of CD45⁻CD31⁻ASGPR1⁻ cells among the CD45⁻ cells increase slightly during the progression phase (1 day DDC: 1.2-fold, 7 days DDC: 1.4-fold) and decrease in the regression phase to initial state. However, CD45⁻CD31⁻ASGPR1⁻ cells do not change in counts per g liver tissue after 1 day DDC-feeding, but after 7 days DDC-treatment count of CD45⁻CD31⁻ASGPR1⁻ cells decrease 3.3-fold. During the regression phase, the initial state is restored.

To investigate changes within the HPCC regarding the individual progenitor subsets, they are classified by their CD133 and gp38 expression after gating out mesothelial cells (gp38^{high}CD133⁻). This results in the following subsets: gp38^{low}CD133⁻ (blue), gp38^{low}CD133⁺ (yellow), gp38⁻CD133⁺ (turquoise) and double negative cells (gp38⁻CD133⁻, brown) (Figure 18B). During the progression phase, the individual subsets change in their percentage distribution within the HPCC. The gp38⁻CD133⁺ cells decrease significant after 1 day DDC-feeding and nearly disappear after 7 days. This applies to both percentage among CD45⁻CD31⁻ASGPR1⁻ cells and count per g liver tissue. During the regression phase gp38⁻CD133⁺ cells expand again compared to 1 day DDC-treatment, but do not reach the initial state. In contrast, gp38^{low}CD133⁺ cells at first increase in count and percentage (1 day DDC-feeding), but decrease drastic in counts per g liver tissue after 7 days DDC-feeding. During the regression phase, counts of gp38^{low}CD133⁺ cells decrease compared to 1 day DDC-treatment and healthy control. Frequency of gp38^{low}CD133⁻ cells among the CD45⁻CD31⁻ASGPR1⁻ cells increase during the progression phase, albeit only significantly after 7 days DDC-

treatment. This increase is not as drastic relating to the cell counts per g liver tissue. During the regression phase, percentage and count remain increased (compared to healthy control) and indicate comparable values to 1 days DDC-feeding. Cells lacking any gp38 and CD133 expression do decrease significant after 7 days DDC-treatment and reach the initial state during the regression phase.

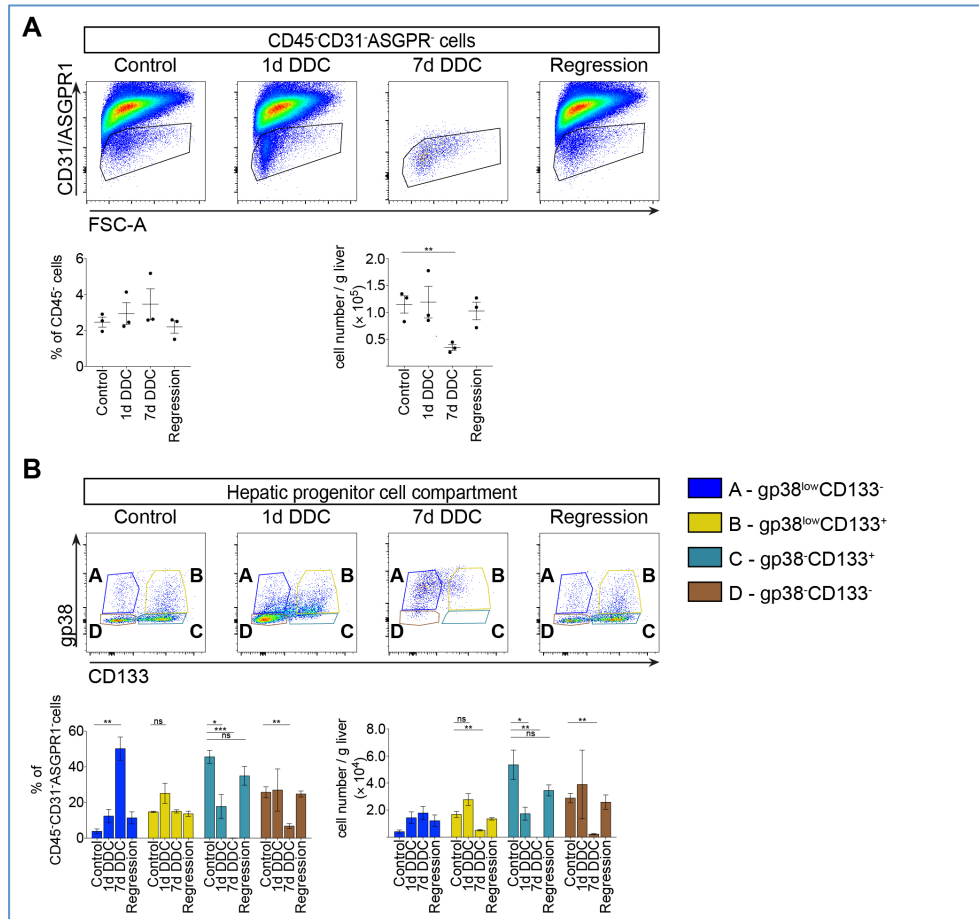


Figure 18: Classification of the murine hepatic progenitor cell compartment (HPCC) in DDC-induced injured liver. Liver single-cell suspension of wild-type untreated and 3,5-diethoxycarbonyl-1,4-dihydrocollidine (DDC)-fed mice were stained with various surface markers, including CD45, CD31, ASGPR1, CD133 and gp38. Exclusion of dead cells was carried out by use of propidium iodide (PI). Hepatic progenitor cell (HPC) activation by DDC-feeding was investigated during the progression phase (1 day and 7 days) and during the regression phase (1 day DDC-feeding and subsequent 3 days control-diet). A) Representative dot plots with gating on cells negative for CD45, CD31 and ASGPR1 to identify the entire HPCC in healthy and DDC-fed mice are depicted. Furthermore, percentages among the CD45⁻ cells and absolute numbers present per g of liver tissue for the entire HPCC are shown. B) Representative dot plot with the several HPC subsets, classified by CD133 and gp38 expression (after gating out of gp38^{high}CD133⁻ cells), in healthy and DDC-fed mice are indicated. In addition, percentages among the CD45⁻CD31⁻ASGPR1⁻ cells and absolute numbers present per g of liver tissue of the various subsets are shown. Data represent a single experiment with 3 mice per group. Values are given as mean \pm SEM. Differences were verified by unpaired t test (two-tailed; * $p \leq 0.05$, ** $p \leq 0.01$, *** $p \leq 0.001$).

Within this model, it seem as if DDC-treatment induces gp38 expression in gp38⁻CD133⁺ cells after 1 day. This would explain the initially increase of gp38^{low}CD133⁺ cells while gp38⁻CD133⁺ cells nearly disappear. After 7 days both type of cells seem to reduce CD133 expression, by what gp38^{low}CD133⁻ cells increase. However, after 7 days

DDC-treatment a massive inflammation was observed, thus this time point was neglect for further considerations.

To examine further distinctions of the individual progenitor subsets, surface markers previously associated with progenitor cells were considered, including CD24, EpCAM, MIC1-1C3 and Sca-1. Expression profiles are indicated as histograms for each surface marker and population (gp38^{low}CD133⁻ (blue), gp38^{low}CD133⁺ (yellow), gp38⁻CD133⁺ (turquoise), gp38⁻CD133⁻ (brown)) compared to the corresponding isotype control for 1 day DDC-feeding and the regression phase (Figure 19A, left). In addition, bar graphs of MFI of each surface marker are shown for each progenitor subset and treatment (Figure 19A, right). After 1 day DDC-feeding, EpCAM expression increase in gp38^{low}CD133⁺ and gp38⁻CD133⁺ cells, whereas expression of CD24 and MIC1-1C3 decreases. During the regression phase, expression levels of CD24, EpCAM and MIC1-1C3 again reach initial state. Sca-1 expression by gp38^{low}CD133⁻ cells decrease after 1 day DDC-treatment and increase during the regression phase.

CD133⁺ cells during the regression phase (4 independent experiments) were enriched and purified for further gene expression analysis (Figure 19B). Several genes using qRT-PCR were considered: 1) PDPN and PROM1, for purity check to identify the cell population, 2) KRT19 and HNF4A as oval cell-related genes, 3) HNF1A, HNF1B, HNF4A and HNF6 as liver specific genes, 4) CDH1 as EMT-associated gene, 5) YAP1 as main target of the Hippo signaling pathway and 6) FAS and CCL2 as inflammatory and apoptosis-associated genes. B2M served as housekeeping gene. Changes in expression levels are compared to wild-type untreated mice and values are indicated as fold change ($2^{-\Delta\Delta C_t}$). CD133⁺ progenitor cells seem to downregulate KRT19 and HNF4A during DDC-regression phase. Upregulation of PROM1, HNF1A, HNF1B, CDH1, YAP1, FAS and CCL2 in CD133⁺ progenitor during the regression phase are indicated. PDPN and HNF6 seem to stay the same.

In summary, DDC-feeding leads to massive changes within the HPCC considering the percentage and count distribution as well as both surface marker expression and gene expression. Thus, DDC-induced HPC activation can be assumed.

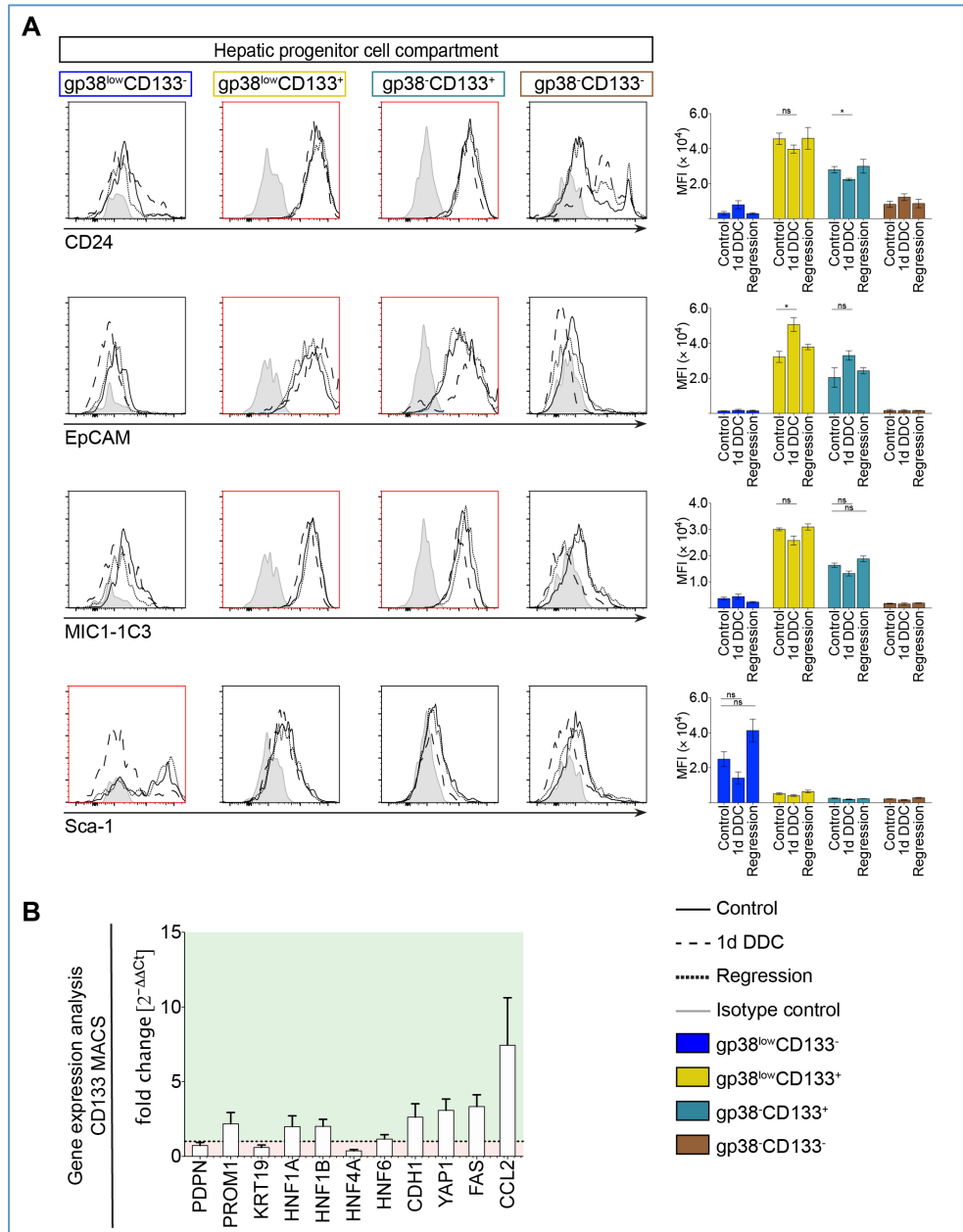


Figure 19: DDC-induced changes within the surface marker and gene expression by progenitor subsets.

Liver single-cell suspension of wild-type untreated and 3,5-diethoxycarbonyl-1,4-dihydrocollidine (DDC)-fed mice were stained with various surface markers, including CD45, CD31, ASGPR1, CD133 and gp38. Exclusion of dead cells was carried out by use of propidium iodide (PI). Hepatic progenitor cell (HPC) activation by DDC-feeding was investigated during the progression phase (1 day) and during the regression phase (1 day DDC-feeding and subsequent 3 days control-diet). A) Histograms of the several HPC subsets, classified by their CD133 and gp38 expression are indicated (gp38^{high}CD133⁻ (black), gp38^{low}CD133⁻ (blue), gp38^{low}CD133⁺ (yellow), gp38^{CD133} (turquoise) and gp38^{CD133} (brown)) for the progenitor cells-associated surface markers CD24, epithelial cell adhesion molecule (EpCAM), macrophage inhibitory cytokine-1-1C3 (MIC1-1C3, oval cell marker) and stem cell antigen-1 (Sca-1) compared to the corresponding isotype control. Additionally, bar graphs of the mean fluorescence intensity (MFI) of each surface marker are shown for each progenitor subset and treatment. B) Changes in gene expression during DDC-regression in CD133⁺ progenitor cells, isolated by magnetic-MicroBead based enrichment and purification, is indicated. Several genes using qRT-PCR were considered: PDPN (podoplanin/gp38), PROM1 (prominin 1/CD133), KRT19 (keratin 19), HNF1A (hepatocyte nuclear factor 1-alpha), HNF1B (hepatocyte nuclear factor 1-beta), HNF4A (hepatic nuclear factor 4-alpha), HNF6 (hepatocyte nuclear factor 6), CDH1 (cadherin 1), YAP1 (yes-associated protein 1), FAS (fas cell surface death receptor) and CCL2 (C-C motif chemokine ligand 2). B2M (beta-2-microglobulin) was utilized as housekeeping gene. Values are indicated as fold change ($2^{-\Delta\Delta Ct}$) according to untreated wild-type mice. Data (A) represent a single experiment with 3 mice per group. Data (B) represent 4 independent experiments. Values are given as mean \pm SEM. Differences were verified by unpaired t test (two-tailed; * $p \leq 0.05$, ** $p \leq 0.01$, *** $p \leq 0.001$).

3.2.5 Summary – The murine hepatic progenitor cell compartment

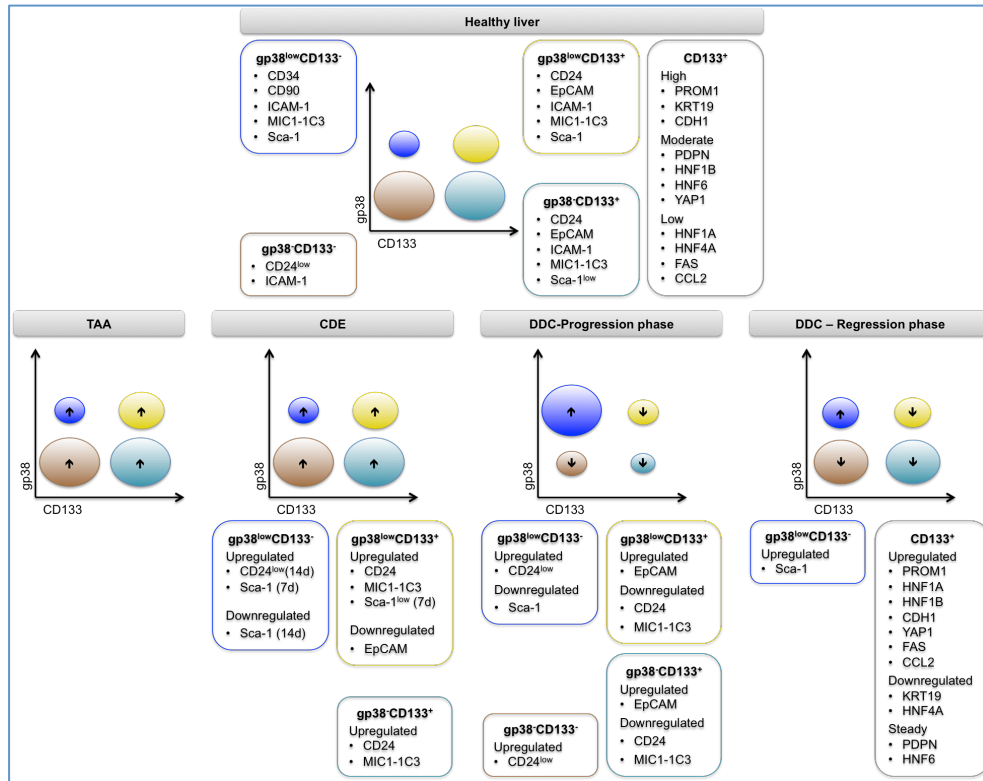


Figure 20: Abstract of the murine hepatic progenitor cell compartment (HPCC) and its expression pattern in healthy and injured liver.

Overview about the HPCC in murine healthy and injured liver is depicted. The HPCC can be classified in several subtypes by their CD133 and gp38 expression: gp38^{low}CD133⁻ (blue), gp38^{low}CD133⁺ (yellow), gp38⁻CD133⁺ (turquoise) and double negative cells (gp38⁻CD133⁻, brown). Additionally, progenitor subtypes differ in expression of various surface markers previously associated with mesenchymal stem and progenitor cells (CD24, CD34, CD90.2, epithelial cell adhesion molecule (EpCAM), intercellular adhesion molecule-1 (ICAM-1), macrophage inhibitory cytokine-1-1C3 (MIC1-1C3, oval cell marker) and stem cell antigen-1 (Sca-1). The heterogeneous CD133⁺ population, isolated and enriched by magnetic MicroBead-based enrichment and purification, indicate expression of genes associated with oval cells (keratin 19 (KRT19), hepatic nuclear factor 4-alpha (HNF4A)), epithelial-mesenchymal transition (cadherin 1 (CDH1)), Hippo signaling pathway (yes-associated protein 1 (YAP1)), apoptosis and inflammation (fas cell surface death receptor (FAS), C-C motif chemokine ligand 2 (CCL2)) or with liver specific genes (hepatocyte nuclear factor 1-alpha (HNF1A), hepatocyte nuclear factor 1-beta (HNF1B), HNF4A, hepatocyte nuclear factor 6 (HNF6)). Three models to induce liver fibrosis to analyze changes within the HPCC were utilized within this study 1) TAA: 3 weeks and 6 weeks treatment, 2) CDE-diet: 7 days and 14 days treatment, 3) DDC-diet: 1 day (progression phase) and 1 day and subsequent 3 days control diet (regression phase).

The HPCC in murine liver comprises CD45⁻CD31⁻ASGPR1⁻ cells classified in several subtypes by their CD133 and gp38 expression: gp38^{high}CD133⁻, gp38^{low}CD133⁻ (blue), gp38^{low}CD133⁺ (yellow), gp38⁻CD133⁺ (turquoise) and double negative cells (gp38⁻CD133⁻, brown) (Figure 20). The gp38^{high}CD133⁻ cells were identified as mesothelial cells (Eckert *et al.*, 2016) and were not be considered within this study.

The individual HPC subtypes differ not only in their CD133 and gp38 expression, but also in relation to various surface markers previously associated with progenitor cells, including CD24, CD34, CD90.2, EpCAM, ICAM-1, MIC1-1C3 and Sca-1 (Figure 20, healthy liver). Furthermore, by means of magnetic MicroBead-based enrichment and

purification of CD133⁺ cells, gene expression analysis by qRT-PCR was utilized. Although this is a heterogeneous cell population, several genes associated with oval cells (KRT19, HNF4A), EMT (CDH1), Hippo signaling pathway (YAP1), apoptosis and inflammation (FAS, CCL2) or liver specific genes (HNF1A, HNF1B, HNF4A, HNF6) could thus be examined. The expression levels of the examined genes differ between low and high expression in CD133⁺ progenitor cells (Figure 20, healthy liver). Within this study three models to induce liver injuries were utilized to investigate changes within the HPCC, including TAA-induced fibrosis, a model of NASH (CDE-diet) and cholestatic liver injury (DDC-diet).

The treatment with TAA and CDE leads to an increase of the entire HPCC, whereas the entire HPCC increase in frequencies and decrease in cell counts during DDC-progression phase, albeit the regression phase is largely unaltered.

Cells expressing only gp38 (gp38^{low}CD133⁻) are not affected by TAA- and CDE-treatment (Figure 20, TAA & CDE), albeit CDE-diet induces Sca-1 expression in gp38^{low}CD133⁻ cells after 7 days treatment which in turn decreases after 14 days CDE-diet. In contrast, gp38^{low}CD133⁻ cells expand during DDC-progression phase (Figure 20, DDC-Progression phase), which is accompanied by decrease of Sca-1 expression by this subtype. Additionally, gp38^{low}CD133⁻ cells stay increased during the regression phase compared to the healthy control (Figure 20, DDC-Regression phase), which is accompanied by increase of Sca-1 expression.

Cells expressing CD133 (gp38^{low}CD133⁺, gp38⁻CD133⁺) expand in count and percentages during TAA-treatment and during CDE-feeding, only the cell count increases but the frequency is largely unaltered (Figure 20, TAA & CDE). In contrast, DDC induces drastic changes considering both CD133-expressing subtypes. On the one hand, gp38^{low}CD133⁺ cells expand in count and frequencies after 1 day DDC and decrease substantially in counts after 7 days. Further, decrease in counts of gp38^{low}CD133⁺ cells compared to the healthy control is indicated during the regression-phase. Frequencies are largely unaltered after 7 days and during regression-phase, compared to the healthy control. On the other hand, the gp38⁻CD133⁺ cell population seems to almost disappear during DDC-treatment in both counts and frequencies and is decreased in the regression phase, compared to the healthy control (Figure 20, DDC-Progression phase & DDC-Regression phase).

Changes within the distribution of the HPCC during CDE- and DDC-treatment are accompanied by changes in the expressions of surface markers in the different subtypes.

EpCAM expression decreases CDE induced in gp38^{low}CD133⁺ cells and in contrast, during DDC-diet EpCAM expression increases in both CD133-expressing subtypes. In addition, CD24 and MIC1-1C3 expression decrease in both CD133-expressing subtypes during DDC-diet and in contrast, expression increases in both CD133-expressing subtypes during CDE-diet. These results suggest, that different injury models induce different activation pattern within the HPCC, which could be important for liver regeneration.

During DDC-regression phase, oval cell-associated genes seem to be downregulated whereas genes associated with EMT, Hippo signaling pathway, apoptosis and inflammation or liver specific genes seem to be upregulated. This suggests that DDC-diet change gene expression in CD133⁺ progenitor cells to regenerate the liver.

3.3 Microparticles detectable in human blood samples

Ethical commission approved the study and healthy probands, athletes and patients gave their informed consent (Section 2.2.5). Human blood samples were collected from 1) Healthy probands, 2) Athletes and patients with 3) Inguinal hernia, 4) Cirrhosis, 5) HCC, 6) CCA, 7) CrC, 8) NSCLC and 9) PaCa.

Human blood samples were collected and serum isolated (Section 2.2.5.1). Isolation of cell-derived microparticles (MPs) was done by sequential centrifugation (Section 0) and further stained using surface antibodies suitable for flow cytometry analysis (Section 2.2.5.3).

3.3.1 Human study cohort - Tumor-related microparticles to identify primary hepatic cancer

Sera of healthy probands and athletes, in addition to sera of patients with cirrhosis, HCC, CCA, CrC, NSCLC and PaCa are incorporated in this part of the study.

The demographics are summarized in Table 15. Indicated are the absolute numbers of patients in each cohort, as well as gender distribution, age [years] and body mass index (BMI). Age and BMI are given as means with standard deviation (mean \pm SD). Additionally, data of patients with cirrhosis, HCC and CCA are combined in the group named 'Liver disorder'.

Males and females are present in each cohort, except the cohort of inguinal hernias, which contains only males. The cohort of patients with liver disorders comprises a double amount of males, which is also noticeable in the separated cohorts of patients with cirrhosis and HCC.

As indicated, the average age (mean \pm SD) of healthy probands (33.9 ± 14.1) and athletes (28.0 ± 5.3) are lower than from all other cohorts. Patients bearing HCC (61.1 ± 12.3), CCA (61.0 ± 9.6), CrC (69.0 ± 8.7) or NSCLC (62.1 ± 10.5) are in the same range of age, whereby patients with cirrhosis are about 10 years younger (51.8 ± 10.5). The age distribution of each cohort participating in this part of the current study is indicated in Figure 21. Data for the age of patients with PaCa were not available, thus they are not incorporated.

The BMI (median \pm SD) of the athletes (23.2 ± 3.6) is less than for patients bearing liver disorders (Liver disorder: 25.4 ± 3.9 , individually: Cirrhosis: 25.1 ± 4.1 ,

HCC: 25.7 ± 3.9 , CCA: 25.2 ± 3.7). For the cohorts of healthy probands, athletes as well as patients bearing CrC, NSCLC or PaCa, BMI values were not available.

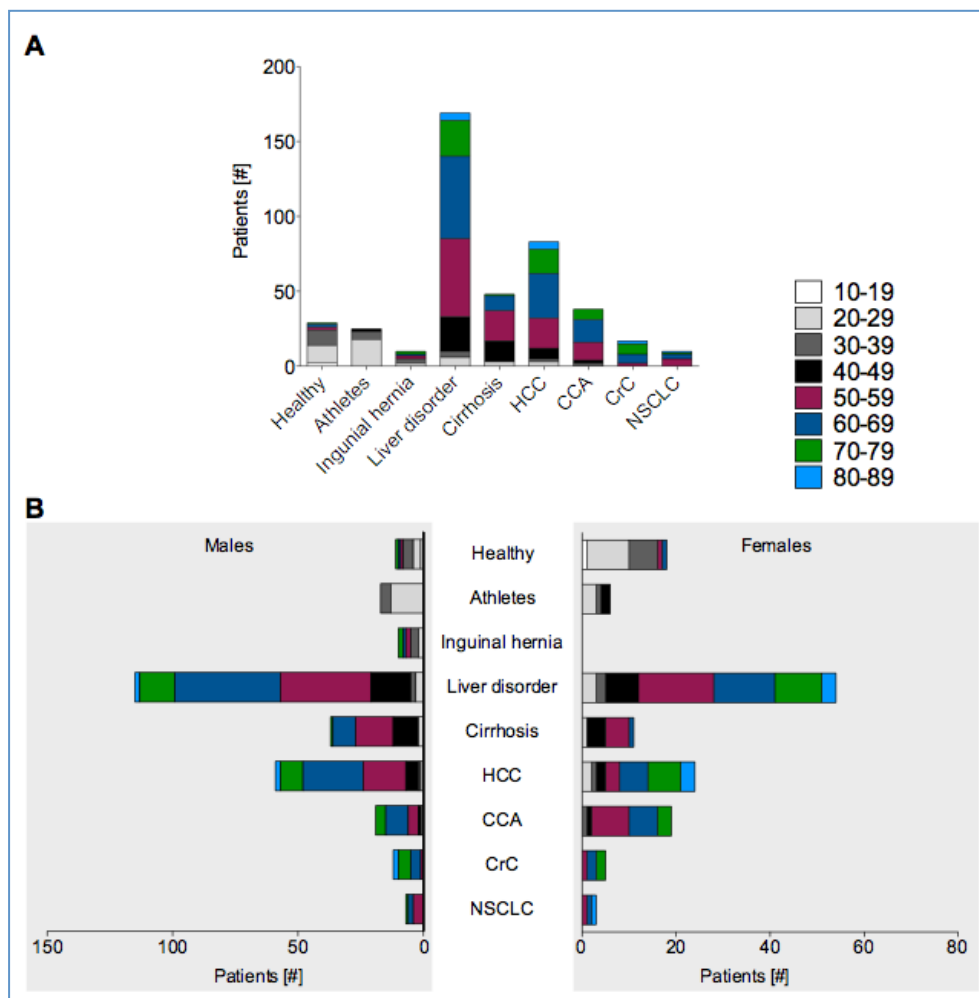


Figure 21: Age distribution of each entity participated in the 'Tumor-related microparticles to identify primary hepatic cancer' study.

Indicated are absolute numbers, separated into groups by increasing age, for probands and patients of each study cohort (A) as well as for both females and males (B).

Table 15: Demographics of each entity participated in the ‘Tumor-related microparticles to identify primary hepatic cancer’ study.

Indicated are the absolute numbers of probands/patients as well as the gender distribution, age and BMI of each study cohort (Modified according to Julich-Haertel, Urban, *et al.*, 2017).

	Healthy	Athletes	Inguinal hernia	Liver disorder	Cirrhosis	HCC	CCA	CrC	NSCLC	PaCa
Patients										
[#]	32	26	26	173	49	86	38	19	10	6
Females										
[#]	19	6	0	56	11	26	19	5	3	2
Males										
[#]	13	18	26	116	37	60	19	14	7	4
Age										
[y]	33.9 ±14.1	28.0 ±5.3	47.0 ±19.6	58.4 ±11.9	51.8 ±10.5	61.1 ±12.3	61.0 ±9.6	69.0 ±8.7	62.1 ±10.5	N/A
BMI										
	N/A	23.2 ±3.6	N/A	25.4 ±3.9	25.1 ±4.1	25.7 ±3.9	25.2 ±3.7	N/A	N/A	N/A

#: Absolute number of probands/patients

y: Age, given in years as mean ± standard deviation (SD)

BMI: Body mass index, given as mean ± SD

N/A: Not available

Liver disorder: Cirrhosis, HCC and CCA combined in one group

HCC: Hepatocellular carcinoma

CCA: Cholangiocarcinoma

CrC: Colorectal cancer

NSCLC: Non-small cell lung cancer

PaCa: Pancreatic cancer

The histological and biochemical parameters of patients with liver disorders as well as for the individually cohorts of cirrhosis, HCC and CCA are summarized in Supplementary Table 1. Incorporated are histological parameters, shown for tumor volume [cm³] and tumor diameter [mm] according to MRI criteria. Data are given as mean ± SD. Furthermore, values of serum tumor markers (mean ± SD) associated with HCC and CCA, such as AFP [ng/mL], CEA [ng/mL] and CA 19-9 [U/mL] together with values for alanine transaminase (ALT [ng/mL]), bilirubin [mg/dL] and creatinine [mg/dL] as additional blood chemistry values (mean ± SD) are indicated.

In addition, MELD-score (model of end-stage liver disease) and Child-Pugh score are shown as absolute numbers for patients with cirrhosis. Both are scoring systems to assess the prognosis of chronic liver disease. MELD-score is based on three laboratory variables (serum creatinine, serum bilirubin and prothrombin time given as international normalized ratio (INR)) and estimates the 3-month mortality (Kamath *et al.*, 2001). It is a scoring system from 9 or less (1.9 % mortality) to 40 (71.3 % mortality). Within this study, MELD-score was scaled in 6-10 (about 1.9 % mortality), 11-15 (about 5 % mortality), 16-20 (about 11 % mortality), 21-24 (about 21 % mortality), 25-28 (about 37 % mortality) (Buscher, 2018). Values above 28 were nonexistent within this study. Child-Pugh is based on the degree of ascites and hepatic encephalopathy as well as INR, and levels of total bilirubin and serum albumin. The range of Child-Pugh is divided into 3 classes and estimates the 1-year survival: A: 5-6 total points, 100 % 1-year survival; B: 7-9 total points, 80 % 1-year survival; C: 10-15 total points, 45 % 1-year survival (Cheung & Cheung, 2013; Pugh *et al.*, 1973).

The total numbers of patients who participated in R0 resection study are shown for patients bearing HCC, CCA and liver disorders, respectively.

3.3.2 Human study cohort - Oval cell-related microparticles to classify primary hepatic cancer

Sera of the control cohort, containing healthy probands and athletes, in addition to patients with cirrhosis, HCC, CCA, NSCLC and PaCa are incorporated in this part of the study. The demographics for all cohorts are summarized in Table 16. Displayed are the absolute numbers of patients in each cohort, as well as gender distribution, age [years] (mean \pm SD) and BMI (mean \pm SD). Additionally, data of patients with cirrhosis, HCC and CCA are combined in the group named ‘Liver disorder’ and data of patients with HCC, NSCLC and PaCa are combined in the group named ‘Non-biliary cancer (CA)’.

Males and females are present in each cohort. The cohort of patients with liver disorders comprises approximately double amount of males, which is mainly due to the gender distribution in cirrhosis (females: n= 4, males: n=21).

As indicated, the average age (mean \pm SD) of the control cohort (32.0 ± 11.8) is lower than from all other cohorts, which indicate average ages of about 60 years (Liver disorder: 59.9 ± 11.7 , individually: Cirrhosis: 55.3 ± 7.9 , HCC: 62.0 ± 14.3 , CCA: 62.0 ± 9.7 ; Non-biliary CA: 61.9 ± 13.7 , individually: NSCLC: 61.0 ± 11.2 ,

PaCa: N/A). The age distribution of each cohort participating in this part of the current study is depicted in Figure 22.

The same tendency goes for the BMI (mean \pm SD). The control cohort has a BMI about 22.9 ± 3.6 , whereas all other cohorts indicate average BMIs of about 26 (Liver disorder: 26.0 ± 4.0 , individually: Cirrhosis: 25.2 ± 3.7 , HCC: 26.6 ± 4.3 , CCA: 25.7 ± 3.6 ; Non-biliary CA: 26.6 ± 4.3 , individually: NSCLC: N/A, PaCa: N/A).

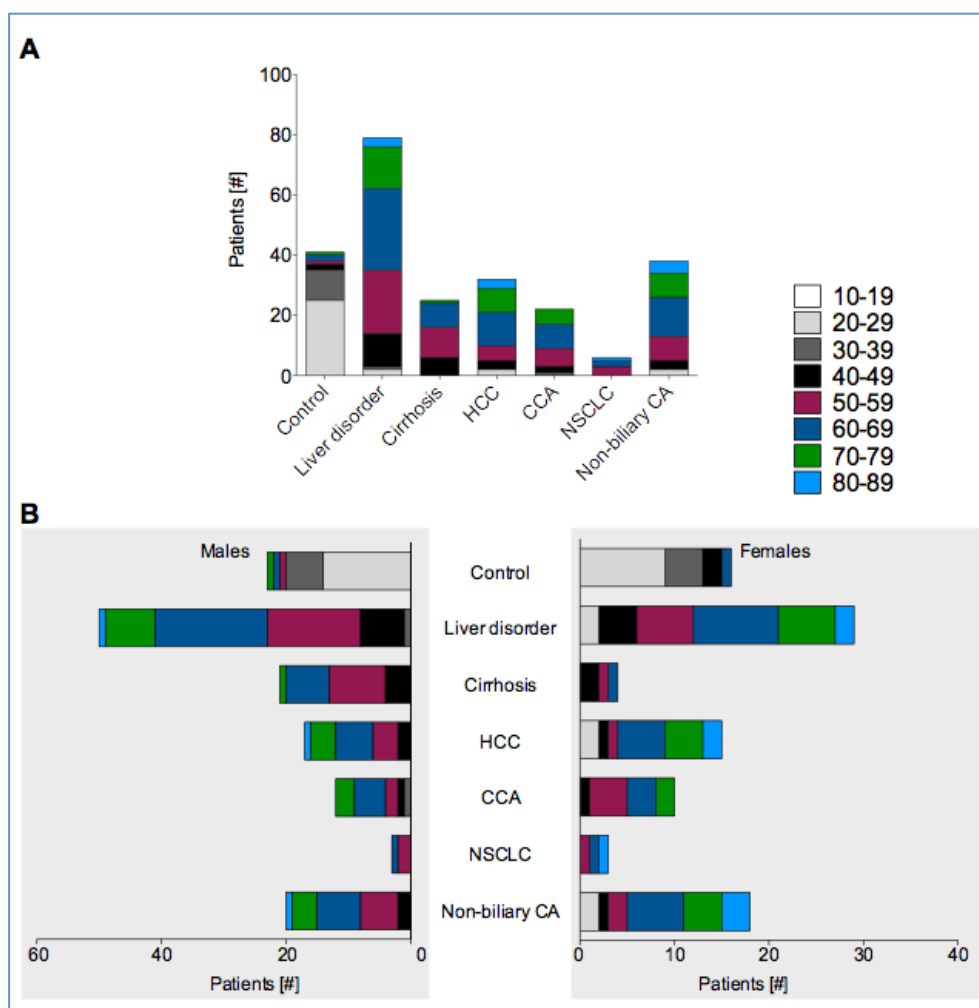


Figure 22: Age distribution of each entity participated in the ‘Oval cell-related microparticles to classify primary hepatic cancer’ study.

Indicated are absolute numbers, separated into groups by increasing age, for probands and patients of each study cohort (A) as well as for both females and males (B).

Table 16: Demographics of each entity participated in the ‘Oval cell-related microparticles to classify primary hepatic cancer’ study.

Indicated are the absolute numbers of probands/patients as well as the gender distribution, age and BMI of each study cohort.

	Control	Liver disorder	Cirrhosis	HCC	CCA	NSCLC	PaCa	Non-biliary CA
Patients #	42	81	26	33	22	6	6	45
Females #	16	29	4	15	10	3	2	20
Males #	20	51	21	18	12	3	4	25
Age [y]	32.0 ±11.8	59.9 ±11.7	55.3 ±7.9	62.0 ±14.3	62.0 ±9.7	61.0 ±11.2	N/A	61.9 ±13.7
BMI	22.9 ±3.6	26.0 ±4.0	25.2 ±3.7	26.6 ±4.3	25.7 ±3.8	N/A	N/A	26.6 ±4.3

#: Absolute number of probands/patients

y: Age, given in years as mean ± standard deviation (SD)

BMI: Body mass index, given as mean ± SD

N/A: Not available

Liver disorder: Cirrhosis, HCC and CCA combined in one group

Non-biliary CA: Non-biliary cancer – HCC, NSCLC and PaCa combined in one group

HCC: Hepatocellular carcinoma

CCA: Cholangiocarcinoma

NSCLC: Non-small cell lung cancer

PaCa: Pancreatic cancer

The histological and biochemical parameters of patients with liver disorders as well as for the individually cohorts of cirrhosis, HCC and CCA are summarized in Supplementary Table 2. Incorporated are histological parameters for tumor volume [cm³] (mean ± SD) and tumor diameter [mm] (mean ± SD), according to MRI criteria. Additionally, tumor markers such as AFP [ng/mL], CEA [ng/mL] and CA 19-9 [U/mL] together with blood chemistry values for ALT [ng/mL], bilirubin [mg/dL] and creatinine [mg/dL] are given as mean ± SD for each cohort participated in this part of the study.

3.3.3 Titration of antibody concentration used for microparticle detection

To analyze cell-derived MPs isolated from human sera, antibody concentrations had to be titrated to reduce background signal and to avoid detection of false positives, as well. AnnexinV was utilized to identify MPs (Biro *et al.*, 2004; Dignat-George *et al.*, 2004; Reutelingsperger, 2001) due to its binding to phosphatidylserine (Römisch & Pâques, 1991), which is exposed during the loss of cell membrane asymmetry by MP release in the course of cellular activation and early apoptosis (Fadok *et al.*, 1992; Mause & Weber, 2010; Sims *et al.*, 1988). MPs were stained with a marker panel including AnnexinV, EpCAM, ASGPR1, CD133 and gp38 to detect human taMPs and human HPC-derived MPs, respectively.

Debris exclusion was carried out by plotting SSC-A against FSC-A followed by doublets exclusion by gating FSC-A against FSC-H. Further, plotting AnnexinV against Marker X and gating on AnnexinV⁺ MPs carried out detection of MPs. Detection of AnnexinV⁺EpCAM⁺, AnnexinV⁺ASGPR1⁺, AnnexinV⁺CD133⁺ and AnnexinV⁺gp38⁺ is based on gating on AnnexinV⁺ MPs, followed by plotting EpCAM, ASGPR1, CD133 or gp38 against FSC-W and gating on the respective positive signals (Figure 23A-B).

1:20 dilution of AnnexinV was used, in addition to the chosen 1:1000 dilution of EpCAM, ASGPR1, CD133 and gp38 (Section 2.2.5.3). In order to identify true positive signals, fluorescence minus one (FMO) control for AnnexinV signals and corresponding isotype controls for EpCAM, ASGPR1, CD133 and gp38 were done and the gating adapted to it (Figure 23A-B). Based thereon, amount of AnnexinV⁺EpCAM⁺, AnnexinV⁺ASGPR1⁺, AnnexinV⁺CD133⁺ and AnnexinV⁺gp38⁺, respectively, were calculated per 10³ AnnexinV⁺ MPs (mean ± SEM) and statistical significance was verified by unpaired t test (two-tailed; * $p \leq 0.05$, ** $p \leq 0.01$, *** $p \leq 0.001$) (Figure 23C).

As indicated, a 1:20 dilution of AnnexinV and 1:1000 dilution of the selected surface markers reduces false negative signals and results in partially significantly differing MP values in comparison of marker to corresponding isotype control (EpCAM: $p \leq 0.01$, ASGPR1: $p \leq 0.01$, CD133: ns, gp38: $p \leq 0.05$).

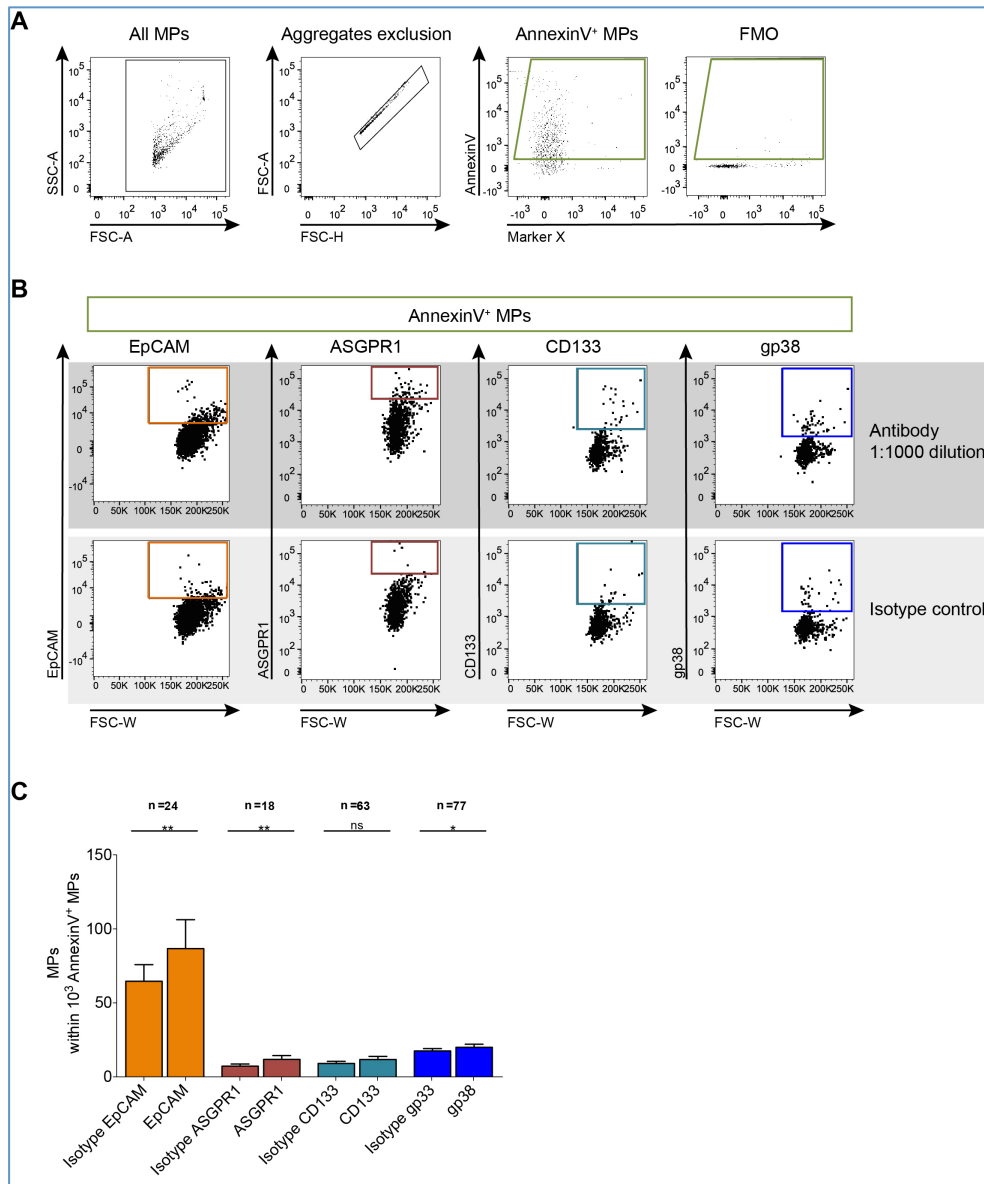


Figure 23: Antibody titration used for microparticle (MP) detection by flow cytometry analysis.

MPs were isolated from sera of control cohorts, including healthy probands, athletes and patients with inguinal hernias, in addition to patients with cirrhosis and cancer patients bearing hepatocellular carcinoma (HCC), cholangiocarcinoma (CCA), colorectal carcinoma (CrC), non-small cell lung cancer (NSCLC) and pancreatic cancer (PaCa). A) Basic gating for detection of AnnexinV⁺ MPs is depicted. Debris exclusion (plotting SSC-A against FSC-A) followed by doublets exclusion (plotting FSC-A against FSC-H) and further plotting AnnexinV against Marker X and gating on AnnexinV⁺ events is displayed. In order to identify true positive signals, fluorescence minus one (FMO) control for AnnexinV is indicated. B) Gating on AnnexinV⁺ MPs is followed by plotting EpCAM, ASGPR1, CD133 or gp38 against FSC-W and gating on the respective positive signals according to the corresponding isotype controls. C) To confirm positive signals, values of AnnexinV⁺EpCAM⁺, AnnexinV⁺ASGPR1⁺, AnnexinV⁺CD133⁺ and AnnexinV⁺gp38⁺ MPs were calculated per 10³ AnnexinV⁺ MPs in comparison to their corresponding isotype controls. Values are given as mean \pm SEM. Statistical significance was verified by unpaired t test (two-tailed; * $p \leq 0.05$, ** $p \leq 0.01$, *** $p \leq 0.001$).

3.3.4 AnnexinV⁺ microparticles detectable in each study cohort

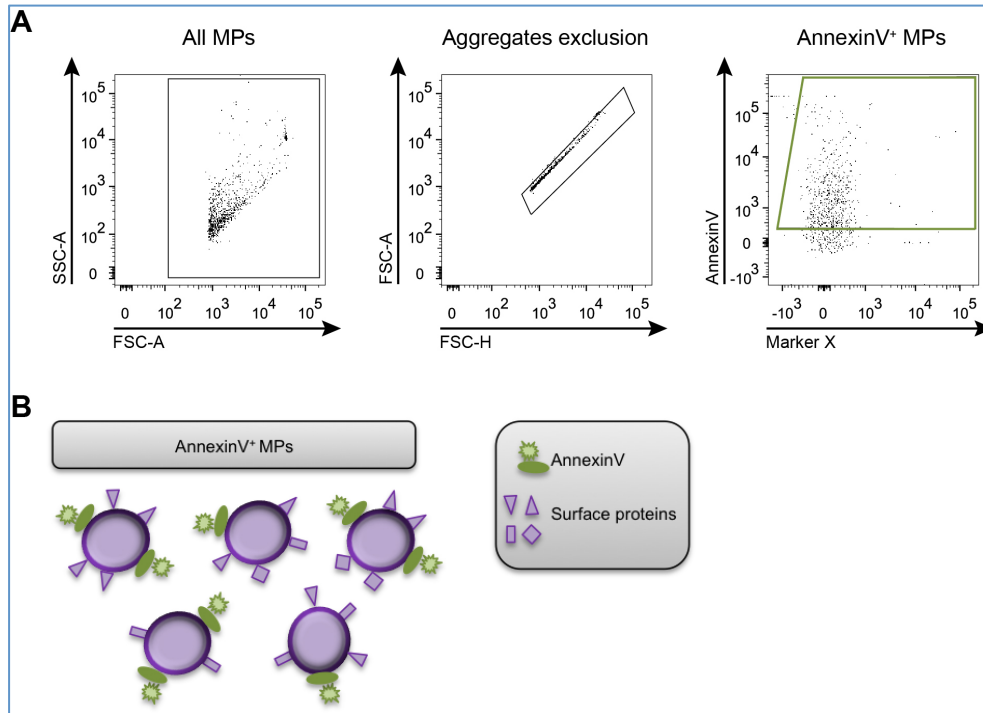


Figure 24: Detection of AnnexinV⁺ microparticles (MPs) using flow cytometry analysis.

A) Representative dot plot with the gating strategy is depicted. Gating on all MPs, followed by aggregates exclusion and detection of AnnexinV⁺ MPs (green) is displayed. MPs were stained with a panel of surface markers: AnnexinV, anti-EpCAM, anti-CD133 and anti-ASGPR1. B) Illustration of AnnexinV⁺ MPs.

Detection of AnnexinV⁺ MPs was achieved by gating on all MPs (SSC-A against FSC-A), followed by debris and background exclusion (FSC-A against FSC-H) and finally, plotting AnnexinV against Marker X and gating on AnnexinV⁺ MPs (Figure 24).

All probands and patients of the human study cohort were examined for correlation between MP values and gender, age [years] and BMI, respectively, to exclude dependencies on the amount of MPs on these parameters (Figure 25A-C). For this purpose, values of AnnexinV⁺ MPs (mean \pm SEM) of all probands and patients participating in the current study were separated in females and males and statistical significance was verified by unpaired t test (two-tailed; * $p \leq 0.05$, ** $p \leq 0.01$, *** $p \leq 0.001$) (Figure 25A). Males (36970 ± 1748) seem to have slightly less AnnexinV⁺ MPs compared to females (45641 ± 2734 , $p \leq 0.01$). Further, determinations of relation between AnnexinV⁺ levels of all cohorts and corresponding age (Figure 25B) and BMI (Figure 25C), respectively, are displayed (Pearson's correlation, two-tailed). Age (Figure 25B) and BMI (Figure 25C) do not correlate with the amount auf AnnexinV⁺ MPs (age: $p = 0.876$, BMI: $p = 0.383$).

AnnexinV⁺ values (mean ± SEM) of each cohort within this study, as well as in dependency of the gender distribution are displayed in Figure 25D-E. Differences were assessed by one-way ANOVA including Dunnett's test (* $p \leq 0.05$, ** $p \leq 0.01$, *** $p \leq 0.001$). Table 17 summarizes the values of AnnexinV⁺ MPs of each cohort as well as for both sexes. Values of AnnexinV⁺ MPs do not differ between healthy probands (53166 ± 5457) and the additional control cohort consisting of athletes (52329 ± 3035). In contrast, levels of AnnexinV⁺ MPs significantly decreases in patients with inguinal hernias (14905 ± 3111 , $p \leq 0.001$) and slightly reduces in tumor-bearing patients (HCC: 39277 ± 2841 , $p \leq 0.05$; CCA: 42629 ± 4205 ; CrC: 40737 ± 2764 ; NSCLC: 43419 ± 5763 ; PaCa: 32633 ± 4871) and patients with liver disorders (39197 ± 1942 , $p \leq 0.05$) or cirrhosis (36396 ± 3418 , $p \leq 0.05$), respectively, compared to the healthy cohort (Figure 25D). Considering the amount of AnnexinV⁺ MPs for females and males, the same trend is evident (Figure 25E). Except the amount of AnnexinV⁺ MPs in athletes, which increases in females and decreases in males.

Table 17: Values of AnnexinV⁺ microparticles (MPs) from human serum of each cohort participated in the human cell-derived MPs study.

Values of AnnexinV⁺ MPs of each cohort as well as for females and males are depicted. Values are given as mean ± SEM.

	Healthy	Athletes	Inguinal hernia	Liver disorder	Cirrhosis	HCC	CCA	CrC	NSCLC	PaCa
Both	53166 ±5457	52329 ±3035	14905 ±3111	39197 ±1942	36396 ±3418	39277 ±2841	42629 ±4205	40737 ±2764	43419 ±5763	32633 ±4871
Females	51830 ±7529	60689 ±5147	-	41895 ±3429	35365 ±7920	42633 ±4566	44667 ±6654	39140 ±6794	60583 ±3424	40410 ±231
Males	55119 ±8034	49130 ±3392	14905 ±3111	37809 ±2374	36360 ±3915	37822 ±3566	40591 ±5286	41307 ±3030	36062 ±6280	28745 ±6647

Liver disorder: Cirrhosis, HCC and CCA combined in one group

HCC: Hepatocellular carcinoma

CCA: Cholangiocarcinoma

CrC: Colorectal cancer

NSCLC: Non-small cell lung cancer

PaCa: Pancreatic cancer

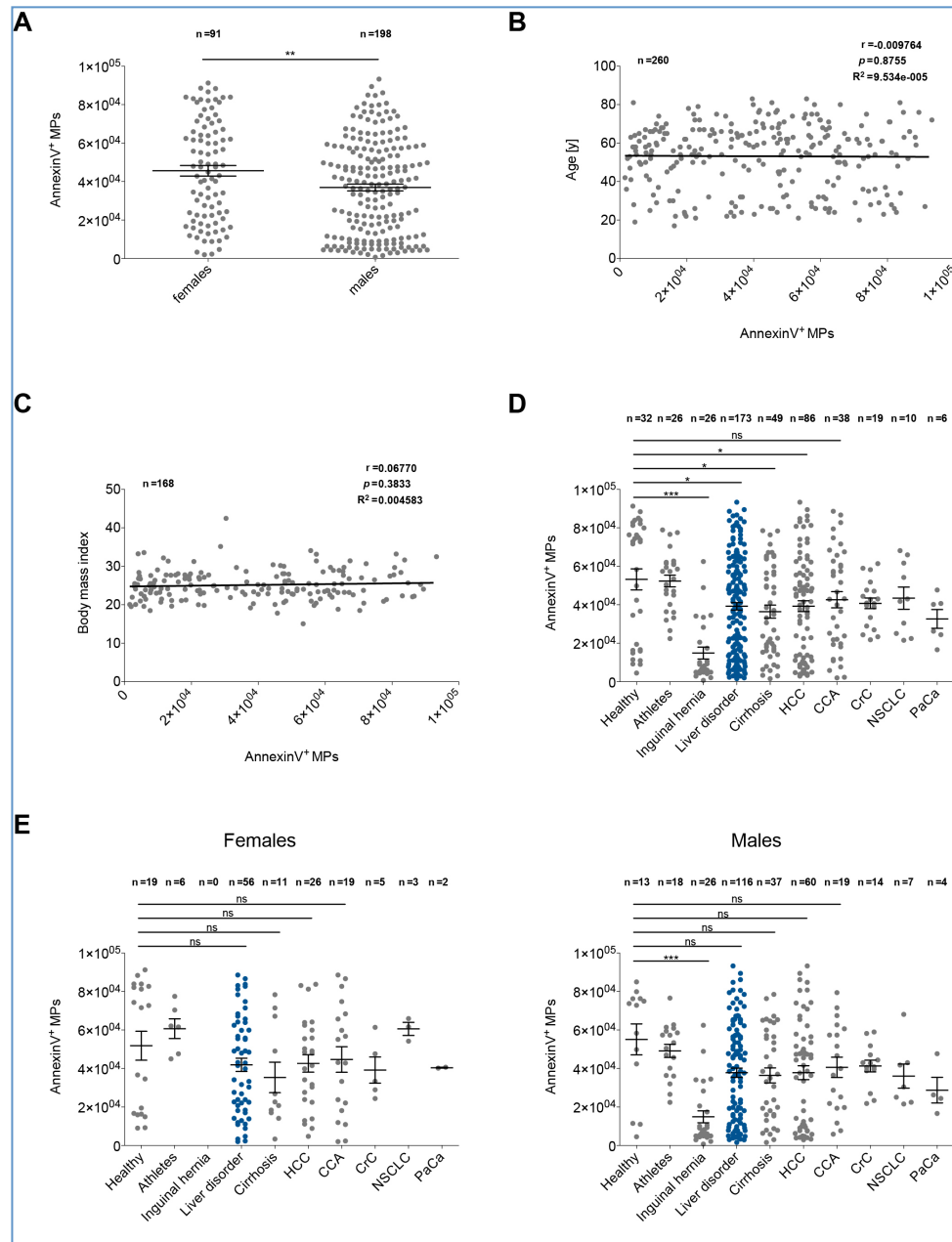


Figure 25: AnnexinV⁺ microparticles (MPs) detected in each cohort of the human cell-derived MPs study. MPs were isolated from sera of control cohorts, including healthy probands, athletes and patients with inguinal hernias. Additionally, MPs were isolated from sera of patients with cirrhosis and cancer patients bearing hepatocellular carcinoma (HCC), cholangiocarcinoma (CCA), colorectal carcinoma (CrC), non-small cell lung cancer (NSCLC) and pancreatic cancer (PaCa). The cohort ‘liver disorder’ (blue) consists of patients with cirrhosis, HCC and CCA. A) Gender distribution of AnnexinV⁺ MPs, including all cohorts of the current study (mean \pm SEM) is displayed. Statistical significance was verified by unpaired t test (two-tailed; * $p \leq 0.05$, ** $p \leq 0.01$, *** $p \leq 0.001$). B-C) Calculated Pearson’s correlation (two-tailed) between AnnexinV⁺ values and age [years] (B) or body mass index (C) is depicted. Indicated are the sample size (n), the corresponding Pearson’s correlation coefficient (r), p value (p) and coefficient of determination (R^2). D-E) AnnexinV⁺ values of each cohort (D) as well as for females and males (E) are indicated. Values are given as mean \pm SEM. Differences were assessed by one-way ANOVA including Dunnett’s test (* $p \leq 0.05$, ** $p \leq 0.01$, *** $p \leq 0.001$).

3.4 Tumor-related microparticles to identify primary hepatic cancer

The aim of this part of the study was to identify liver tumor-derived MPs by usage of a surface marker panel suitable for flow cytometry analysis.

AnnexinV was used to identify MPs (Biro *et al.*, 2004; Dignat-George *et al.*, 2004; Reutelingsperger, 2001). EpCAM was shown to be upregulated in several epithelial cancers (Momburg *et al.*, 1987) and should serve as pan-cancer marker. Further, CD133 has been reported to identify putative cancer stem cells in HCC (Ma *et al.*, 2007; Yin *et al.*, 2007) and ASGPR was shown to be expressed in a large number of human HCCs (Trerè *et al.*, 1999). Based thereon, it was assumed that a combination of surface markers allow distinguishing of hepatic cancer from other cancer entities, particularly by EpCAM in combination with CD133 or ASGPR1, respectively, as well as EPCAM in combination with both CD133 and ASGPR1. This assumption was initially confirmed by the distinction of liver cancer and PaCa cell lines, examined within this study, based on different surface marker profiles (Section 3.1.2). Subsequent extension of the marker panel by AnnexinV leads to the hypothesis that especially liver tumor-derived MPs can be detected. Parts of the results have been published as ‘Cancer-associated circulating large extracellular vesicles in cholangiocarcinoma and hepatocellular carcinoma’ (Julich-Haertel, Urban, *et al.*, 2017).

3.4.1 AnnexinV⁺EpCAM⁺ microparticles indicate moderate diagnostic potential

EpCAM was first described as colorectal carcinoma-specific antigen (Herlyn *et al.*, 1979; Koprowski *et al.*, 1979) and was shown to be upregulated in several epithelial cancers (e.g. CrC, PaCa, liver carcinoma, lung carcinoma) (Momburg *et al.*, 1987). Based thereon, EpCAM in combination with AnnexinV was assumed to identify taMPs. Detection of AnnexinV⁺EpCAM⁺ taMPs is based on gating on AnnexinV⁺ MPs (Section 3.3.4) followed by plotting EpCAM against FSC and gating on EpCAM⁺ taMPs (Figure 26, orange).

First, dependency of taMPs on gender, age [years] and BMI was examined (Figure 27). Values of AnnexinV⁺EpCAM⁺ taMPs of all cohorts of the current study were separated in females and males (Figure 27A) and statistical significance was verified by unpaired t test (two-tailed; * $p \leq 0.05$, ** $p \leq 0.01$, *** $p \leq 0.001$). The values of AnnexinV⁺EpCAM⁺ taMPs per 10³ AnnexinV⁺ MPs (mean \pm SEM) do not differ between females (100.8 \pm 10.8) and males (105.3 \pm 6.5).

Furthermore, Pearson's correlation (two-tailed) between AnnexinV⁺EpCAM⁺ levels and corresponding age (Figure 27B) and BMI (Figure 27C), respectively, are displayed. Correlation between AnnexinV⁺EpCAM⁺ taMPs and age is low ($r=0.116$, $p=0.063$, $R^2=0.013$) and non-existent between BMI and AnnexinV⁺EpCAM⁺ values ($r=0.035$, $p=0.657$, $R^2=0.001$).

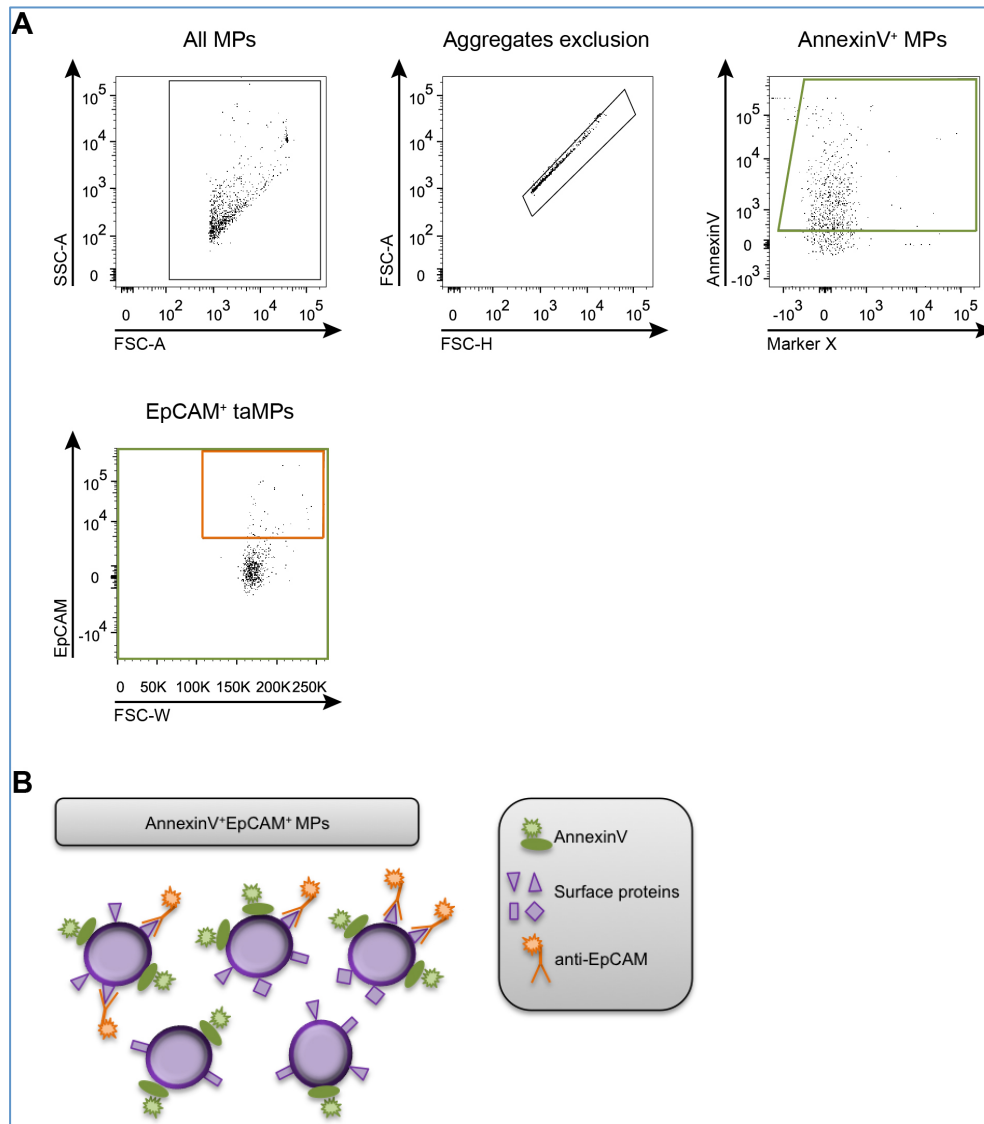


Figure 26: Detection of AnnexinV⁺EpCAM⁺ tumor-associated microparticles (taMPs) using flow cytometry analysis.

A) Representative dot plot with the gating strategy is depicted. Gating on all MPs, followed by aggregates exclusion and gating on AnnexinV⁺ MPs (green) is displayed. Detection of AnnexinV⁺EpCAM⁺ taMPs is carried out by further gating on EpCAM⁺ events (orange). MPs were stained with a panel of surface markers: AnnexinV, anti-EpCAM, anti-CD133 and anti-ASGPR1. B) Illustration of AnnexinV⁺EpCAM⁺ taMPs.

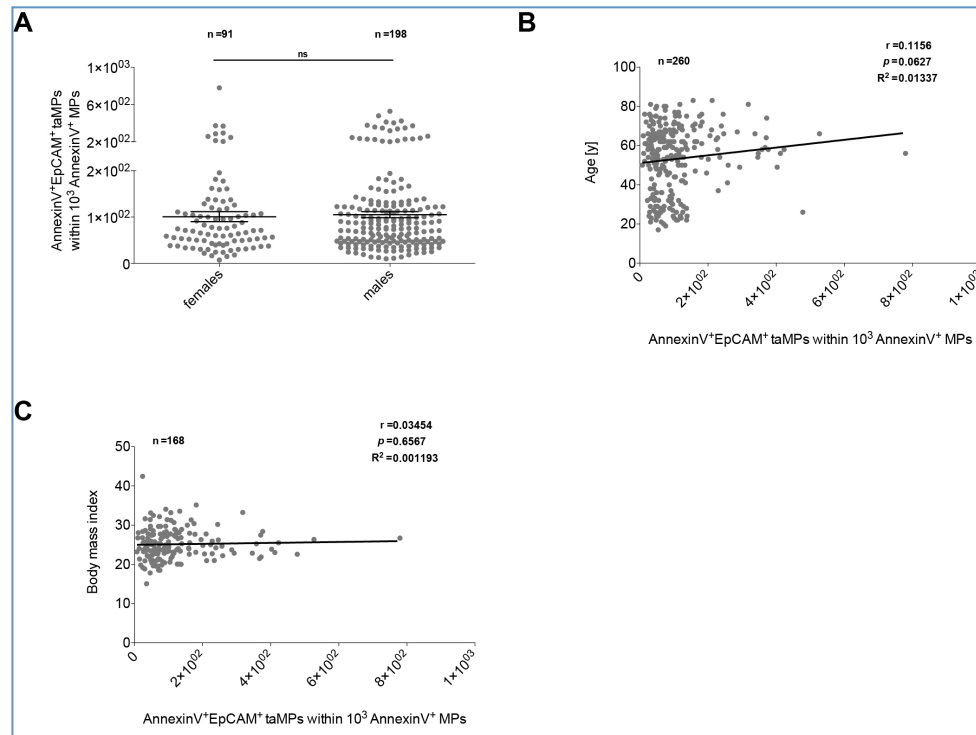


Figure 27: Detection of AnnexinV⁺EpCAM⁺ tumor-associated microparticles (taMPs) in human serum.

MPs were isolated from sera of healthy probands, athletes, patients with inguinal hernias or cirrhosis and cancer patients bearing hepatocellular carcinoma, cholangiocarcinoma, colorectal carcinoma, non-small cell lung cancer and pancreatic cancer. A) Dependency of AnnexinV⁺EpCAM⁺ taMPs (mean \pm SEM) on gender, including all cohorts of the current study, is depicted. Statistical significance was verified by unpaired t test (two-tailed; * $p \leq 0.05$, ** $p \leq 0.01$, *** $p \leq 0.001$). B-C) Calculated Pearson's correlation (two-tailed) between AnnexinV⁺EpCAM⁺ values and age [years] (B) and body mass index (C), respectively, of all cohorts participating in the current study is displayed. Indicated are the sample size (n), the corresponding Pearson's correlation coefficient (r), p value (p) and coefficient of determination (R^2).

3.4.1.1 Tumor-bearing patients indicate elevated levels of AnnexinV⁺EpCAM⁺ tumor-associated microparticles

Figure 28 displays AnnexinV⁺EpCAM⁺ taMPs per 10^3 AnnexinV⁺ MPs (mean \pm SEM) for each cohort (Figure 28A) as well as in dependency of the gender (Figure 28B). Table 18 summarizes these values. Differences were assessed by one-way ANOVA including Dunnett's test (* $p \leq 0.05$, ** $p \leq 0.01$, *** $p \leq 0.001$). Dotted line represents calculated cut-off values (Table 19). To evaluate the diagnostic performance of AnnexinV⁺EpCAM⁺ taMPs, ROC curves were created for each entity of the current study. The calculated cut-off, AUC values \pm SE, p values as well as values of sensitivity [%], specificity [%], PPV [%] NPV [%] are displayed (Table 19). ROC curves, including corresponding AUC and p values are indicated for liver disorders and the individually cohorts of cirrhosis, HCC and CCA in Figure 28C. The angle bisector corresponds to the line of identity, which indicates the lower limit for a diagnostic test.

About 58.8 ± 5.9 AnnexinV⁺EpCAM⁺ taMPs per 10^3 AnnexinV⁺ MPs are determined for healthy probands, whereas females indicate about 10 more AnnexinV⁺EpCAM⁺ taMPs than males (females: 62.8 ± 7.5 , males: 52.4 ± 9.5).

The additional control cohorts consisting of athletes and inguinal hernias show 1.5-fold elevated AnnexinV⁺EpCAM⁺ values compared to the healthy cohort (athletes: 89.1 ± 16.8 , inguinal hernia: 86.8 ± 8.7). However, female athletes show only 1.2-fold increase while the values in males rise about 1.7-fold. However, female athletes sample size is low (n=6) compared to males (n=18). Due to the low increase of taMPs in athletes and inguinal hernias the diagnostic performance is powerless.

Patients carrying other non-liver cancers show increase of AnnexinV⁺EpCAM⁺ taMPs from 1.3-fold to 1.8-fold (CrC: 76.7 ± 8.7 , NSCLC: 106.2 ± 28.7 , PaCa: 87.6 ± 12.4). Also here, male values increases are higher and ranges from 1.6-fold to 2.4-fold, compared to females. The female values hardly change in consideration of these cancer entities. Nevertheless, sample sizes are low for both females (CrC: n=5, NSCLC: n=3, PaCa: n=2) and males (CrC: n=14, NSCLC: n=7, PaCa: n=4). Due to the low increase of taMPs in patients with non-liver tumors the diagnostic performance is powerless.

In liver tumor patients (HCC and CCA) AnnexinV⁺EpCAM⁺ values expand significantly about 2.3-fold (HCC: 134.0 ± 14.2 , $p \leq 0.01$; females: 159.7 ± 31.8 , $p \leq 0.05$; males: 122.8 ± 15.0) and 2.2-fold (CCA: 126.8 ± 15.4 , $p \leq 0.05$; females: 110.6 ± 16.3 ; males: 153.1 ± 25.1 , $p \leq 0.05$), respectively, compared to the healthy cohort. Compared to this, the increase of AnnexinV⁺EpCAM⁺ values is less in cirrhosis (84.8 ± 8.9 , females: 72.9 ± 16.6 , males: 90.1 ± 10.6). Taken together, patients with liver disorders show 2-fold increase of AnnexinV⁺EpCAM⁺ taMPs, regardless of gender (118.5 ± 8.4 , $p \leq 0.05$; females: 122.6 ± 16.6 ; males: 117.4 ± 9.6). The diagnostic performance of AnnexinV⁺EpCAM⁺ taMPs is weak as indicated in 66 % sensitivity and 55 % specificity for liver disorders. In addition, the probability to be correctly recognized as patient with liver disorder is about 89 %, however, the probability to be correctly recognized as healthy is merely about 23 %. Individually, diagnostic performance of AnnexinV⁺EpCAM⁺ taMPs for cirrhosis is moderate also (sensitivity: 57 %, specificity: 55 %, PPV: 67 %, NPV: 45 %). Values for HCC and CCA are slightly increased for sensitivity and unchanged for specificity (HCC: sensitivity: 65 %, specificity: 55 %; CCA: sensitivity: 82 %, specificity: 55 %). The probability to be correctly recognized as liver tumor patients is about 80 % and

69 % for HCC and CCA, respectively. In contrast, the probability to be correctly recognized as healthy is only about 36 % for HCC and about 71 % for CCA.

Table 18: Values of AnnexinV⁺EpCAM⁺ tumor-associated microparticles (taMPs) from human serum of each cohort participated in the human cell-derived MPs study.

Values of AnnexinV⁺EpCAM⁺ taMPs of each cohort as well as for females and males are depicted. Values refer to 10³ AnnexinV⁺ MPs and are given as means ± SEM.

	Healthy	Athletes	Inguinal hernia	Liver disorder	Cirrhosis	HCC	CCA	CrC	NSCLC	PaCa
Both	58.8 ±5.9	89.1 ±16.8	86.8 ±8.7	118.5 ±8.4	84.8 ±8.9	134.0 ±14.2	126.8 ±15.4	76.7 ±8.7	106.2 ±28.7	87.6 ±12.4
Females	62.8 ±7.5	77.8 ±15.0	-	122.6 ±16.6	72.9 ±16.6	159.7 ±31.8	110.6 ±16.3	62.9 ±10.7	61.3 ±12.0	76.6 ±26.9
Males	52.4 ±9.5	95.5 ±23.6	86.8 ±8.7	117.4 ±9.6	90.1 ±10.6	122.8 ±15.0	153.1 ±25.1	81.6 ±11.1	125.4 ±39.2	93.1 ±15.2

Liver disorder: Cirrhosis, HCC and CCA combined in one group

HCC: Hepatocellular carcinoma

CCA: Cholangiocarcinoma

CrC: Colorectal cancer

NSCLC: Non-small cell lung cancer

PaCa: Pancreatic cancer

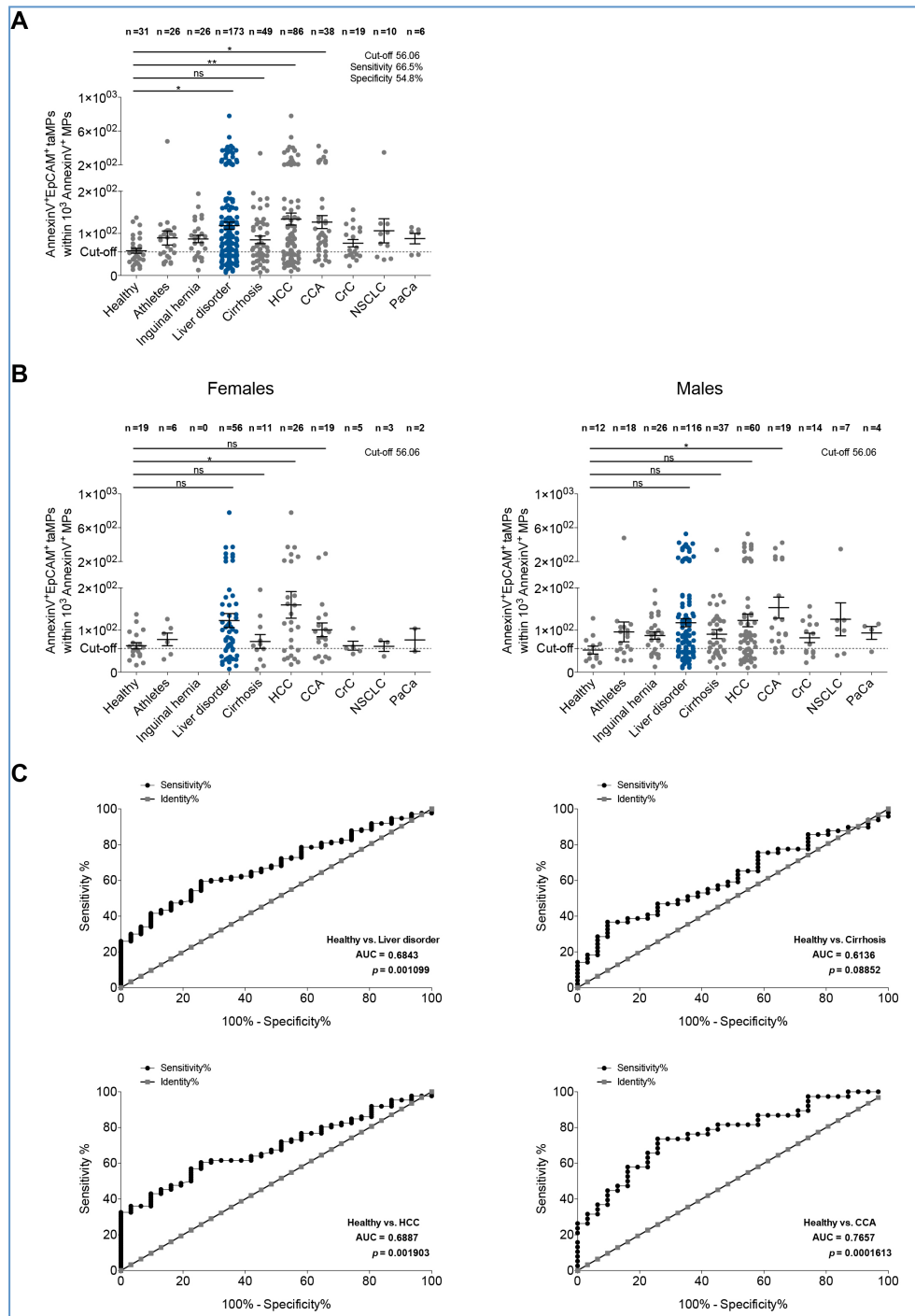


Figure 28: AnnexinV⁺EpCAM⁺ tumor-associated microparticles (taMPs) detect tumor-bearing patients.

MPs were isolated from sera of control cohorts (healthy, athletes, inguinal hernia), patients with cirrhosis and cancer patients bearing hepatocellular carcinoma (HCC), cholangiocarcinoma (CCA), colorectal carcinoma (CrC), non-small cell lung cancer (NSCLC) and pancreatic cancer (PaCa). The cohort ‘liver disorder’ consists of patients with cirrhosis, HCC and CCA. A-B) Levels of AnnexinV⁺EpCAM⁺ taMPs (mean ± SEM) of each cohort (A) as well as in dependency of gender (B) are displayed. Differences were assessed by one-way ANOVA including Dunnett’s test (* $p \leq 0.05$, ** $p \leq 0.01$, *** $p \leq 0.001$). Dotted lines represent calculated cut-off values (Table 19). C) To analyze the diagnostic performance of the AnnexinV⁺EpCAM⁺ taMP population, receiver-operating characteristic (ROC) curves for liver disorders and individually cohorts are depicted. Corresponding values for area under curve (AUC) and p values are indicated. The angle bisector corresponds to the line of identity, which indicates the lower limit for a diagnostic test (Modified according to Julich-Haertel, Urban, *et al.*, 2017).

Table 19: Diagnostic performance of AnnexinV⁺EpCAM⁺ tumor-associated microparticles (taMPs) of each cohort. Indicated are the AnnexinV⁺EpCAM⁺ values (mean ± SEM), and values of calculated cut-off, AUC ± SE of the ROC curves, *p* values as well as values of sensitivity [%], specificity [%], PPV [%] and NPV [%] of each cohort of the current study (Modified according to Julich-Haertel, Urban, *et al.*, 2017).

	Cut-off	Mean ±SEM	AUC ± SE	<i>p</i> Value	Sensitivity [%]	Specificity [%]	PPV [%]	NPV [%]
Healthy		58.8 ±5.9						
Athletes	54.45	89.1 ±16.8	0.6489 ±0.074	0.055	65.38	51.61	53.13	64.00
Inguinal hernia	55.02	86.8 ±8.7	0.6948 ±0.071	0.012	69.23	51.61	54.55	66.67
Liver disorder	56.06	118.5 ±8.4	0.6843 ±0.044	0.001	66.47	54.84	89.15	22.67
Cirrhosis	56.84	84.8 ±8.9	0.6136 ±0.063	0.089	57.14	54.84	66.67	44.74
HCC	56.06	134.0 ±14.2	0.6887 ±0.049	0.002	65.12	54.84	80.00	36.17
CCA	56.08	126.8 ±15.4	0.7657 ±0.057	≤0.001	81.58	54.84	68.89	70.83
CrC	56.30	76.7 ±8.7	0.6401 ±0.080	0.099	57.89	54.84	44.99	68.00
NSCLC	54.72	106.2 ±28.7	0.7194 ±0.039	0.039	70.00	51.61	31.82	84.21
PaCa	54.72	87.6 ±12.4	0.7527 ±0.103	0.053	66.67	51.61	21.05	88.89

SEM: Standard error of the mean

AUC ± SE: Area under curve ± standard error

PPV: Positive prediction value

NPV: Negative prediction value

Liver disorder: Cirrhosis, HCC and CCA combined in one group

HCC: Hepatocellular carcinoma

CCA: Cholangiocarcinoma

CrC: Colorectal cancer

NSCLC: Non-small cell lung cancer

PaCa: Pancreatic cancer

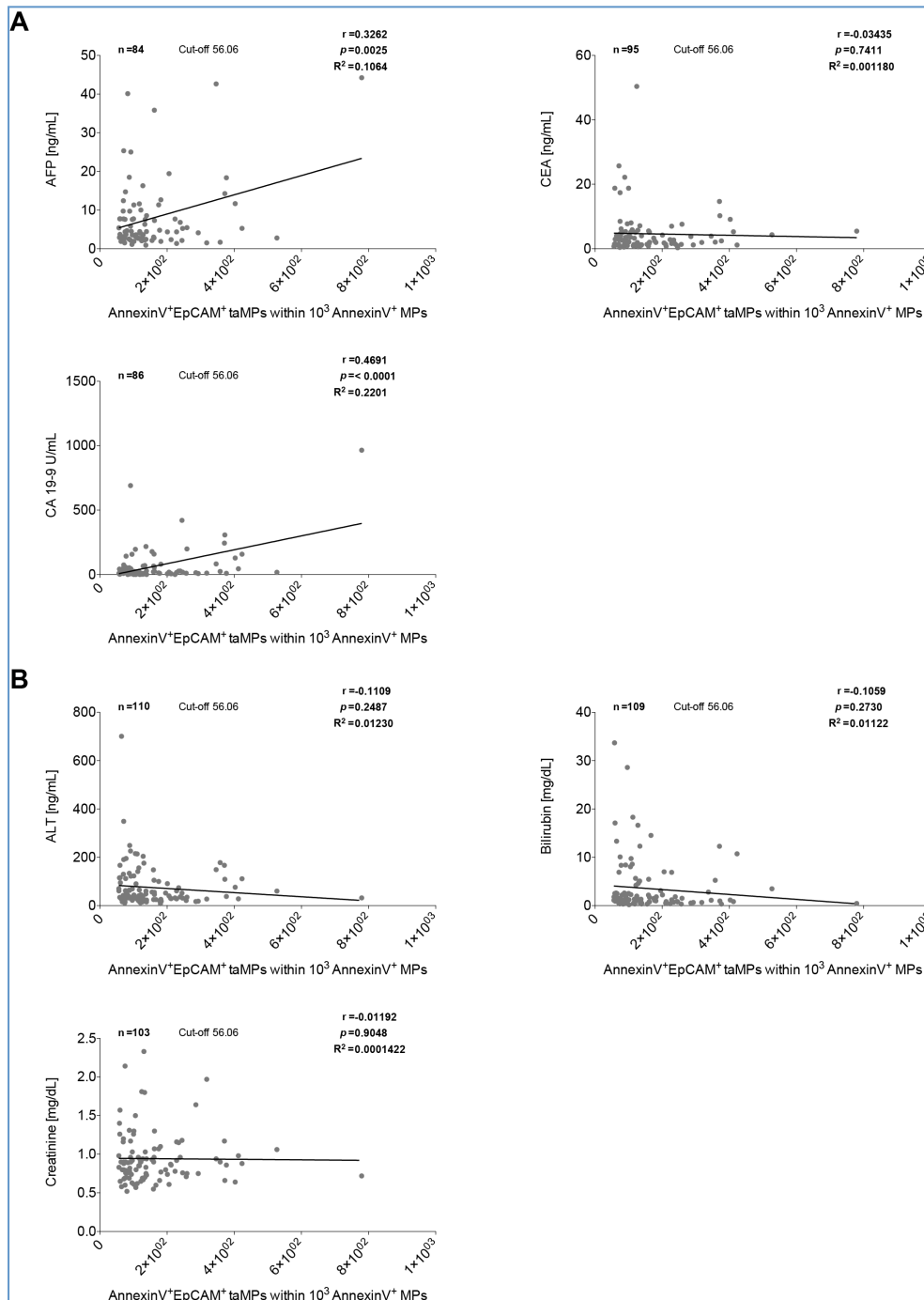


Figure 29: Connection between serum markers and AnnexinV⁺EpCAM⁺ tumor-associated microparticles (taMPs) of patients bearing liver disorders.

MPs were isolated from sera of patients bearing liver disorders (cirrhosis, hepatocellular carcinoma and cholangiocarcinoma). Calculated Pearson's correlation (two-tailed) between AnnexinV⁺EpCAM⁺ values and corresponding serum tumor marker (alpha-1 fetoprotein (AFP [ng/mL]), carcinoembryonic antigen (CEA [ng/mL]) or carbohydrate-antigen 19-9 (CA 19-9 [U/mL]) (A) or blood chemistry values (alanine transaminase (ALT [ng/mL]), bilirubin [mg/dL] or creatinine [mg/dL]) for patients with liver disorders are displayed. Indicated are the sample size (n), the corresponding Pearson's correlation coefficient (r), *p* value (*p*) and coefficient of determination (*R*²). Included AnnexinV⁺EpCAM⁺ levels were restricted to values above the cut-off (Table 19).

Furthermore, correlation between tumor markers (AFP [ng/mL], CEA [ng/mL], CA 19-9 [U/mL]) or blood chemistry values (ALT [ng/mL], bilirubin [mg/dL], creatinine [mg/dL]) and AnnexinV⁺EpCAM⁺ values are analyzed and displayed in Figure 29 as

Pearson's correlation (two-tailed) for patients bearing liver disorders. Included AnnexinV⁺EpCAM⁺ levels were restricted to values above the cut-off (Table 19).

AnnexinV⁺EpCAM⁺ levels do not correlate with the serum tumor marker CEA ($r=-0.034$, $p=0.741$, $R^2=0.001$) (Figure 29A). Nevertheless, serum tumor markers AFP ($r=0.326$, $p=0.003$, $R^2=0.106$) and CA 19-9 ($r=0.469$, $p\leq 0.001$, $R^2=0.220$) correlate moderate with AnnexinV⁺EpCAM⁺ levels (Figure 29A). In addition, AnnexinV⁺EpCAM⁺ values hint a negative correlation between blood chemistry values ALT ($r=-0.111$, $p=0.249$, $R^2=0.012$) and bilirubin ($r=-0.106$, $p=0.273$, $R^2=0.011$) (Figure 29 B). Correlation between AnnexinV⁺EpCAM⁺ taMPs and creatinine seems not to exist ($r=-0.012$, $p=0.905$, $R^2\leq 0.001$).

In summary, AnnexinV⁺EpCAM⁺ taMPs indicate elevated levels in patients with injuries, including inguinal hernias and tumor-bearing patients, compared to the healthy cohort. However, diagnostic potential is restricted for all cohorts participating in the current study. Nevertheless, AnnexinV⁺EpCAM⁺ taMPs assume to especially detect cancer bearing patients.

3.4.1.2 AnnexinV⁺EpCAM⁺ microparticles during cirrhosis

MELD-score (estimates 3-month mortality) and Child-Pugh score (estimates 1-year survival) are scoring systems to assess the prognosis of chronic liver diseases, based on laboratory variables (MELD-score: serum creatinine, serum bilirubin and INR; Child-Pugh: INR, bilirubin, serum albumin, degree of ascites and hepatic encephalopathy) (Kamath *et al.*, 2001; Pugh *et al.*, 1973). Within this study, MELD-score was scaled in 6-10 (about 1.9 % mortality), 11-15 (about 5 % mortality), 16-20 (about 11% mortality), 21-24 (about 21 % mortality), 25-28 (about 37 % mortality) (Buscher, 2018). Values above 28 were nonexistent within this study. The range of Child-Pugh is divided into 3 classes: A: 5-6 total points, 100 % 1-year survival; B: 7-9 total points, 80 % 1-year survival; C: 10-15 total points, 45 % 1-year survival (Cheung & Cheung, 2013; Pugh *et al.*, 1973).

Levels of AnnexinV⁺EpCAM⁺ MPs in dependency of MELD-score (Figure 30A) and Child-Pugh score (Figure 30B) were considered. AnnexinV⁺EpCAM⁺ levels were separated into groups by increasing MELD-score and Child-Pugh, respectively. Values of taMPs refer to 10^3 AnnexinV⁺ MPs and given as mean \pm SEM. Included AnnexinV⁺EpCAM⁺ levels were restricted to values below the cut-off for healthy probands and values above the cut-off for patients with cirrhosis. The dotted line

represents calculated cut-off values (Table 19). Differences were assessed by one-way ANOVA including Dunnett's test ($*p \leq 0.05$, $**p \leq 0.01$, $***p \leq 0.001$).

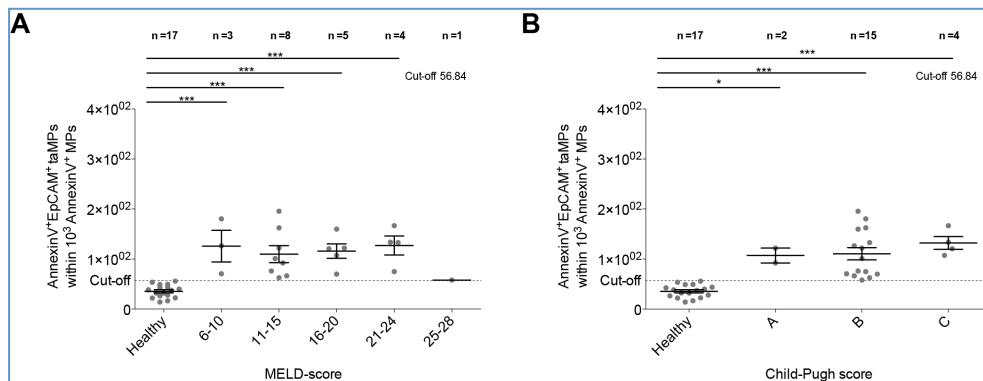


Figure 30: MELD-score and Child-Pugh score to assess the prognosis of chronic liver disease in relation to AnnexinV⁺EpCAM⁺ tumor-associated microparticles (taMPs).

MPs were isolated from sera of healthy probands and patients with cirrhosis. A-B) AnnexinV⁺EpCAM⁺ values (mean \pm SEM) were separated into groups by increasing MELD-score (A) and Child-Pugh score (B), respectively. Differences were assessed by one-way ANOVA including Dunnett's test ($*p \leq 0.05$, $**p \leq 0.01$, $***p \leq 0.001$). Dotted lines represent calculated cut-off value (Table 19). Only values below the cut-off were incorporated for healthy probands and only values above the cut-off were included for patients with cirrhosis.

AnnexinV⁺EpCAM⁺ values are significantly increased at elevated MELD-score (6-10: $p \leq 0.001$, 11-15: $p \leq 0.001$, 16-20: $p \leq 0.001$, 21-24: $p \leq 0.001$) and Child-Pugh (A: $p \leq 0.05$, B: $p \leq 0.001$, C: $p \leq 0.001$). However, AnnexinV⁺EpCAM⁺ values seem not to correlate with the scoring systems, due to the average of AnnexinV⁺EpCAM⁺ taMPs which do not increase with rise of MELD-score and Child-Pugh, respectively.

Relation between tumor markers (AFP [ng/mL]), CEA [ng/mL] or CA 19-9 [U/mL]) (Supplementary Figure 1A) or blood chemistry values (ALT [ng/mL]), bilirubin [mg/dL] or creatinine [mg/dL]) (Supplementary Figure 1B) and AnnexinV⁺EpCAM⁺ values for patients with cirrhosis were examined (Pearson's correlation, two-tailed). Included levels of AnnexinV⁺EpCAM⁺ were restricted to values above the cut-off (Table 19).

A marginal correlation between AnnexinV⁺EpCAM⁺ values and tumor markers AFP ($r = -0.174$, $p = 0.503$, $R^2 = 0.030$) and CA 19-9 ($r = 0.111$, $p = 0.682$, $R^2 = 0.012$) are indicated. However, the correlation between AnnexinV⁺EpCAM⁺ levels and AFP suggest being negative, whereby the correlation between AnnexinV⁺EpCAM⁺ values and CA 19-9 indicate to be positive. In contrast, CEA does not correlate with AnnexinV⁺EpCAM⁺ values as well as creatinine. An implied negative correlation is observable for bilirubin ($r = -0.136$, $p = 0.498$, $R^2 = 0.019$) and furthermore, AnnexinV⁺EpCAM⁺ taMPs and ALT appear to be correlate moderate ($r = -0.368$, $p = 0.059$, $R^2 = 0.135$).

3.4.1.3 Liver tumor load affect levels of AnnexinV⁺EpCAM⁺ microparticles

Levels of AnnexinV⁺EpCAM⁺ MPs in dependency of corresponding tumor volume [cm³] (Figure 31A) or tumor diameter [mm] (Figure 31B) were considered. AnnexinV⁺EpCAM⁺ values refer to 10³ AnnexinV⁺ MPs and are given as mean ± SEM. First, AnnexinV⁺EpCAM⁺ values were separated into groups by increasing tumor volume and tumor diameter, respectively (Figure 31A&B, left). The dotted line represents the calculated cut-off values (Table 19). Differences were assessed by one-way ANOVA including Dunnett's test (* $p \leq 0.05$, ** $p \leq 0.01$, *** $p \leq 0.001$). Additionally, relation between AnnexinV⁺EpCAM⁺ values and corresponding tumor volume or tumor diameter were determined (Pearson's correlation, two-tailed) (Figure 31A&B, right). Included AnnexinV⁺EpCAM⁺ levels were restricted to values below the cut-off for healthy probands and values above the cut-off for patients bearing a liver tumor (HCC and CCA).

Tumor volumes seem to affect levels of AnnexinV⁺EpCAM⁺ taMPs, due to significant increases at tumor volumes up to 10 cm³ ($p \leq 0.01$), 20-50 cm³ ($p \leq 0.001$), or greater than 70 cm³ ($p \leq 0.001$). This dependency is reflected in a moderate correlation between tumor volume and levels of AnnexinV⁺EpCAM⁺ taMPs ($r=0.459$, $p=0.002$, $R^2=0.210$). However, tumor diameter and AnnexinV⁺EpCAM⁺ levels correlate more with each other ($r=0.626$, $p \leq 0.0001$, $R^2=0.392$). AnnexinV⁺EpCAM⁺ values expand significantly in patients bearing a liver tumor with a diameter of 10-30 mm ($p \leq 0.01$), 30-50 mm ($p \leq 0.01$) and >50 mm ($p \leq 0.001$). Interestingly, the smallest tumor detected within this study indicated a tumor diameter of 9.72 mm. Thus, liver tumor load assumes to correlate with AnnexinV⁺EpCAM⁺ values.

Additionally, Pearson's correlation (two-tailed) between serum markers (AFP [ng/mL], CEA [ng/mL], CA 19-9 [U/mL], ALT [ng/mL], bilirubin [mg/dL], creatinine [mg/dL]) (Supplementary Figure 2A&B) and AnnexinV⁺EpCAM⁺ values are displayed. AnnexinV⁺EpCAM⁺ levels were restricted to values above the cut-off for liver tumor patients (Table 19).

Moderate correlations are only indicated for the tumor markers AFP ($r=0.343$, $p=0.003$, $R^2=0.125$) and CA 19-9 ($r=0.457$, $p \leq 0.001$, $R^2=0.209$). All other considered parameters show no correlation to AnnexinV⁺EpCAM⁺ values.

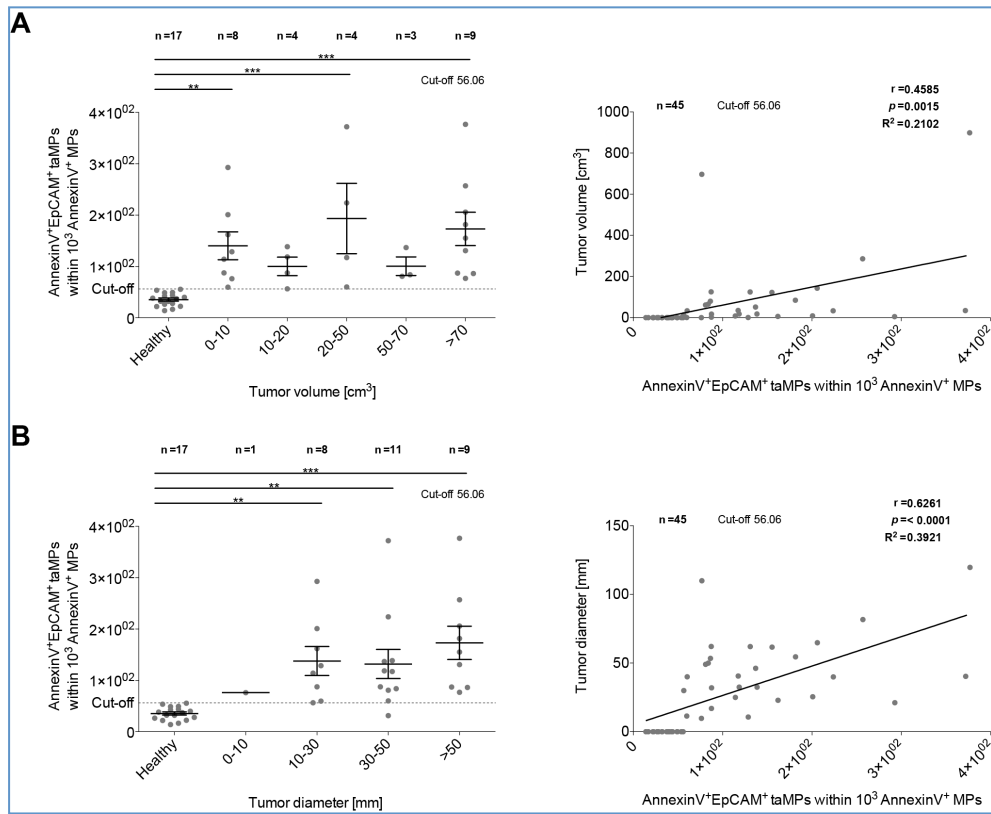


Figure 31: AnnexinV⁺EpCAM⁺ tumor-associated microparticles (taMPs) correlate with liver tumor load.

MPs were isolated from sera of healthy probands and liver tumor patients bearing hepatocellular carcinoma or cholangiocarcinoma. A-B) AnnexinV⁺EpCAM⁺ values in dependency of corresponding tumor volume [cm³] (A) or tumor diameter [mm] (B) are depicted. Left: AnnexinV⁺EpCAM⁺ values (mean ± SEM) were separated into groups by increasing corresponding tumor volume or tumor diameter. Differences were assessed by one-way ANOVA including Dunnett's test (*p≤0.05, **p≤0.01, ***p≤0.001). Dotted lines represent calculated cut-off value (Table 19). Right: Calculated Pearson's correlation (two-tailed) between AnnexinV⁺EpCAM⁺ values and corresponding tumor volume or tumor diameter is displayed. Indicated are the sample size (n), the corresponding Pearson's correlation coefficient (r), p value (p) and coefficient of determination (R²). Only values below the cut-off were incorporated for healthy probands and only values above the cut-off were included for patients bearing liver tumors (Modified according to Julich-Haertel, Urban, *et al.*, 2017).

3.4.2 AnnexinV⁺EpCAM⁺CD133⁺ and AnnexinV⁺EpCAM⁺CD133⁺ASGPR1⁺ microparticles allow detection of liver disorders

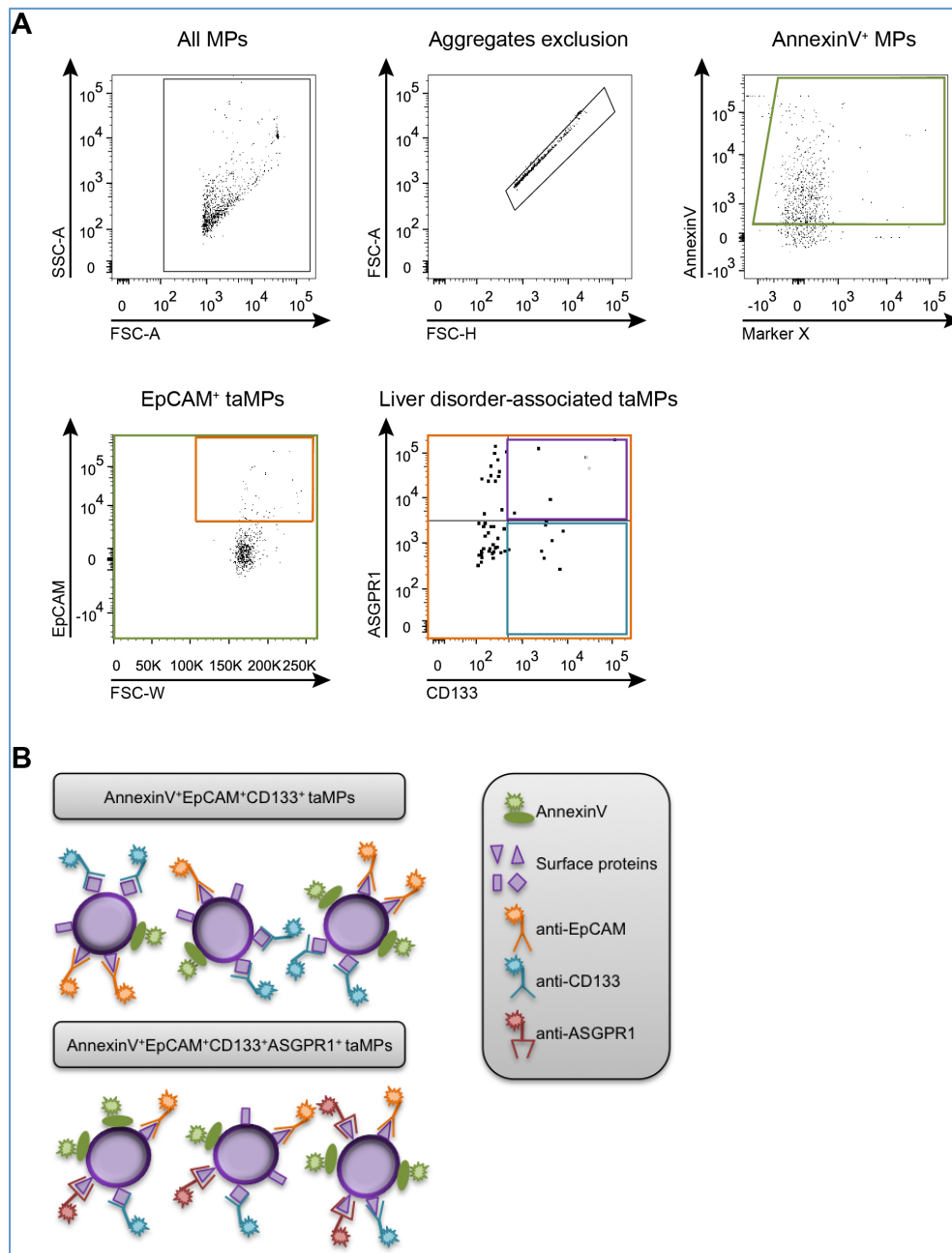


Figure 32: Detection of AnnexinV⁺EpCAM⁺CD133⁺ and AnnexinV⁺EpCAM⁺CD133⁺ASGPR1⁺ liver disorder-associated microparticles (MPs) using flow cytometry analysis.

A) Representative dot plot with the gating strategy is depicted. Gating on all MPs followed by aggregates exclusion and gating on AnnexinV⁺ MPs (green) is displayed. Detection of AnnexinV⁺EpCAM⁺ taMPs is carried out by further gating on EpCAM⁺ events (orange). Next, identification of liver disorder-associated MPs is ensued by gating on CD133 single positive events (blue) and ASGPR1/CD133 double positive events (purple), respectively. MPs were stained with a panel of surface markers: AnnexinV, anti-EpCAM, anti-CD133 and anti-ASGPR1. B) Illustration of AnnexinV⁺EpCAM⁺CD133⁺ and AnnexinV⁺EpCAM⁺CD133⁺ASGPR1⁺ liver disorder-associated MPs.

The aim was, to identify liver tumor-derived MPs. The transmembrane hematopoietic stem cell antigen CD133 (Miraglia *et al.*, 1997) has been reported to identify putative cancer stem cells in HCC (Ma *et al.*, 2007; Yin *et al.*, 2007). In addition, the subunit of

the glycoprotein ASGPR, which is uniquely expressed by hepatocytes (Geffen & Spiess, 1992; Morell *et al.*, 1968), was shown to be expressed in a large number of human HCCs (Trerè *et al.*, 1999). Based thereon, AnnexinV and EpCAM, in combination with CD133 in addition to the combination with both CD133 and ASGPR1 were hypothesized to detect liver tumor-derived taMPs.

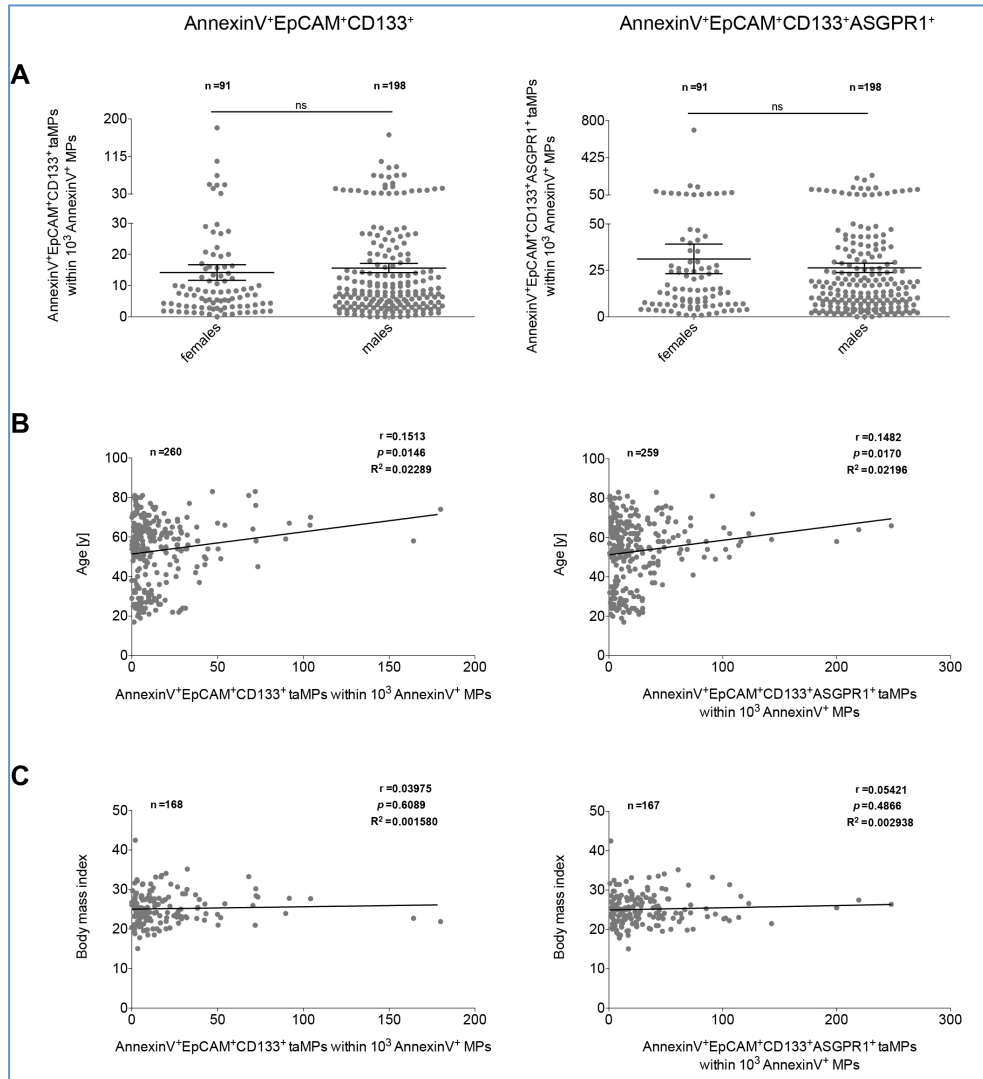


Figure 33: Detection of AnnexinV⁺EpCAM⁺CD133⁺ and AnnexinV⁺EpCAM⁺CD133⁺ASGPR1⁺ tumor-associated microparticles (taMPs) in human serum.

MPs were isolated from sera of healthy probands, athletes, patients with inguinal hernia or cirrhosis and cancer patients bearing hepatocellular carcinoma, cholangiocarcinoma, colorectal carcinoma, non-small cell lung cancer and pancreatic cancer. A) AnnexinV⁺EpCAM⁺CD133⁺ taMPs (left) and AnnexinV⁺EpCAM⁺CD133⁺ASGPR1⁺ taMPs (right) in dependency of gender, including all cohorts of the current study, are indicated. Values are given as mean \pm SEM. Statistical significance was verified by unpaired t test (two-tailed; * $p \leq 0.05$, ** $p \leq 0.01$, *** $p \leq 0.001$). B-C) Calculated Pearson's correlation (two-tailed) between taMP values and age [years] (B) or body mass index (C) of all cohorts of the current study is depicted. Indicated are the sample size (n), the corresponding Pearson's correlation coefficient (r), p value (p) and coefficient of determination (R^2).

AnnexinV⁺EpCAM⁺CD133⁺ and AnnexinV⁺EpCAM⁺CD133⁺ASGPR1⁺ are identified by gating on AnnexinV⁺EpCAM⁺ taMPs (Section 3.4.1) followed by plotting CD133

against ASGPR1 and gating on CD133 single positive (Figure 32, blue) as well as CD133/ASGPR1 double positive (Figure 32, purple) taMPs.

All probands and patients were examined for the correlation between levels of AnnexinV⁺EpCAM⁺CD133⁺ taMPs as well as AnnexinV⁺EpCAM⁺CD133⁺ASGPR1⁺ taMPs and gender, age [years] and BMI (Figure 33), to excluded dependencies on these parameters.

For this purpose, values of AnnexinV⁺EpCAM⁺CD133⁺ taMPs (Figure 33, left) and AnnexinV⁺EpCAM⁺CD133⁺ASGPR1⁺ taMPs (Figure 33, right) of all cohorts of the current study were separated in females and males (Figure 33A). Statistical significance was verified by unpaired t test (two-tailed; * $p \leq 0.05$, ** $p \leq 0.01$, *** $p \leq 0.001$). In addition, relation between values of AnnexinV⁺EpCAM⁺CD133⁺ taMPs and AnnexinV⁺EpCAM⁺CD133⁺ASGPR1⁺ taMPs of all cohorts and corresponding age (Figure 33B) and BMI (Figure 33C) are displayed (Pearson's correlation, two-tailed).

The values of both taMP populations also do not differ between females (AnnexinV⁺EpCAM⁺CD133⁺: 14.2 ± 2.5 , AnnexinV⁺EpCAM⁺CD133⁺ASGPR1⁺: 31.2 ± 8.0) and males (AnnexinV⁺EpCAM⁺CD133⁺: 15.6 ± 1.5 , AnnexinV⁺EpCAM⁺CD133⁺ASGPR1⁺: 26.4 ± 2.5) as observed for AnnexinV⁺EpCAM⁺ taMPs.

Correlations between taMP levels for both populations and age or BMI, respectively, follows the same tendency like for AnnexinV⁺EpCAM⁺ taMPs. Marginally correlation between taMPs values and age is observable (AnnexinV⁺EpCAM⁺CD133⁺: $r=0.151$, $p=0.015$, $R^2=0.023$; AnnexinV⁺EpCAM⁺CD133⁺ASGPR1⁺: $r=0.148$, $p=0.017$, $R^2=0.022$) and non-existent between BMI and both taMP populations.

3.4.2.1 AnnexinV⁺EpCAM⁺CD133⁺ and AnnexinV⁺EpCAM⁺CD133⁺ASGPR1⁺ microparticles expand in patients bearing liver disorders

Values of AnnexinV⁺EpCAM⁺CD133⁺ (Figure 34, left) and AnnexinV⁺EpCAM⁺CD133⁺ASGPR1⁺ taMP populations (Figure 34, right) of each cohort (Figure 34A) as well as separately for females and males (Figure 34B) are displayed and summarized in Table 20. Values of taMP populations refer to 10^3 AnnexinV⁺ MPs (mean \pm SEM). The 'Control' group consists of healthy probands and athletes. Differences were assessed by one-way ANOVA including Dunnett's test (* $p \leq 0.05$, ** $p \leq 0.01$, *** $p \leq 0.001$). Dotted line represents calculated cut-off values (Table 21).

Diagnostic performance of AnnexinV⁺EpCAM⁺CD133⁺ and AnnexinV⁺EpCAM⁺CD133⁺ASGPR1⁺ taMPs were evaluated by creating the corresponding ROC curves and determination of cut-off values, sensitivity [%] and specificity [%] as well as PPV [%] and NPV [%] (Table 21). Created ROC curves for the cohorts liver disorder, cirrhosis, HCC as well as CCA, including corresponding AUC and *p* values are displayed in Figure 34. The angle bisector corresponds to the line of identity, which indicates the lower limit for a diagnostic test.

The control cohort indicates low taMP levels with 7.5 ± 0.9 AnnexinV⁺EpCAM⁺CD133⁺ taMPs per 10^3 AnnexinV⁺ MPs as well as 10.2 ± 1.1 AnnexinV⁺EpCAM⁺CD133⁺ASGPR1⁺ taMPs per 10^3 AnnexinV⁺ MPs. Levels of both do not differ between males and females. Patients with inguinal hernias also indicate low levels of AnnexinV⁺EpCAM⁺CD133⁺ (6.7 ± 1.0) in addition to a marginal increase of AnnexinV⁺EpCAM⁺CD133⁺ASGPR1⁺ taMPs. Thus, diagnostic is nearly powerless, due to low specificity and PPV by what patients with inguinal hernias may serve as additional control cohort.

Compared to the diagnostic performance of taMPs in patients with inguinal hernias, the same is true for both taMPs population for patients bearing non-liver tumors (CrC, NSCLC, PaCa). Based on almost not or low elevated taMP values, diagnostic is nearly powerless, particularly indicated by low PPV values. Patients bearing CrC or NSCLC indicate about 1.2 and 1.4-fold, respectively, increase of AnnexinV⁺EpCAM⁺CD133⁺ levels (CrC: 9.5 ± 2.6 , NSCLC: 10.5 ± 2.6), compared to the control cohort. However, females do not show an increase of AnnexinV⁺EpCAM⁺CD133⁺ values (CrC: 6.1 ± 0.9 , NSCLC: 7.3 ± 1.1), whereas values in males slightly increase (CrC: 10.7 ± 3.5 , NSCLC: 11.9 ± 3.7). However, the female sample size is low (CrC: *n*=5, NSCLC: *n*=3) compared to the males (CrC: *n*=14, NSCLC: *n*=7). In contrast, values of AnnexinV⁺EpCAM⁺CD133⁺ASGPR1⁺ decrease about 2-fold and 1.2-fold in CrC or NSCLC, respectively (CrC: 4.9 ± 0.8 , NSCLC: 8.7 ± 2.0). The same tendency is observable relating to values in females and males. Levels of AnnexinV⁺EpCAM⁺CD133⁺ taMPs increase 2-fold in patients bearing PaCa (15.0 ± 5.6) compared to the control cohort, but only in males (18.9 ± 7.9) and not in females (7.2 ± 2.8). However, the sample size is very low for females (*n*=2) and males (*n*=4). The same tendency is true for values of AnnexinV⁺EpCAM⁺CD133⁺ASGPR1⁺ taMPs in Patients bearing PaCa, compared to the control cohort. Values expand 1.5-fold (15.6 ± 5.0), but only in males (19.2 ± 7.1) and not in females (8.2 ± 0.5).

AnnexinV⁺EpCAM⁺CD133⁺ taMPs and AnnexinV⁺EpCAM⁺CD133⁺ASGPR1⁺ taMPs seem to be associated with liver disorders due to elevated levels in this cohort as well as in the individually cohorts of cirrhosis, HCC and CCA.

Patients bearing liver disorders indicate 2.6-fold increase of AnnexinV⁺EpCAM⁺CD133⁺ values (19.7 ± 2.0 , $p \leq 0.01$) and AnnexinV⁺EpCAM⁺CD133⁺ASGPR1⁺ levels actually expand about 3.4-fold (35.0 ± 3.0 , $p \leq 0.001$). Both values elevate regardless of gender (AnnexinV⁺EpCAM⁺CD133⁺: females: 18.6 ± 3.9 ; males: 20.4 ± 2.3 , $p \leq 0.01$; AnnexinV⁺EpCAM⁺CD133⁺ASGPR1⁺: females: 32.8 ± 4.1 , $p \leq 0.01$; males: 36.3 ± 4.0 , $p \leq 0.01$). This results in a solid diagnostic performance for both liver disorder-associated taMP populations (AnnexinV⁺EpCAM⁺CD133⁺: sensitivity: 73.4 %, specificity: 50.0 %, PPV: 81.4 %, NPV: 38.7 %; AnnexinV⁺EpCAM⁺CD133⁺ASGPR1⁺: sensitivity: 82.6 %, specificity: 50.0 %, PPV: 83.0 %, NPV: 49.2 %).

Patients with cirrhosis, indicate a 2.3-fold increase of AnnexinV⁺EpCAM⁺CD133⁺ values (17.2 ± 2.9). However, levels of AnnexinV⁺EpCAM⁺CD133⁺ taMP expand more in males (19.7 ± 3.6) compared to females (10.2 ± 3.6). Levels of AnnexinV⁺EpCAM⁺CD133⁺ASGPR1⁺ taMPs increase about 2.7-fold in patients with cirrhosis (28.3 ± 3.7 , $p \leq 0.05$) as well as 2.3-fold and 3-fold in females and males, respectively. Further, AnnexinV⁺EpCAM⁺CD133⁺ values expand 2.6-fold in patients bearing HCC (19.2 ± 2.9 , $p \leq 0.05$), whereby values in females increase 3.6-fold and 2-fold in males (females: 26.4 ± 7.8 , males: 16.1 ± 2.4). In addition, AnnexinV⁺EpCAM⁺CD133⁺ASGPR1⁺ taMPs expand about 3.5-fold in patients bearing HCC (35.6 ± 4.8 , $p \leq 0.001$) as well as in females (32.9 ± 7.0 , $p \leq 0.05$) and males (36.7 ± 6.1 , $p \leq 0.01$). Additionally, values of AnnexinV⁺EpCAM⁺CD133⁺ taMPs expand 3.2-fold in patients bearing CCA (24.3 ± 5.2 , $p \leq 0.01$) and here too, differences between females and males are obviously (females: 12.8 ± 2.8 ; males: 35.7 ± 9.4 , $p \leq 0.001$). Compared to this, values of AnnexinV⁺EpCAM⁺CD133⁺ASGPR1⁺ actually increase 4.2-fold in patients bearing CCA (42.4 ± 6.5 , $p \leq 0.001$) and the same is true in females and males (females: 37.3 ± 6.3 , $p \leq 0.05$; males: 47.5 ± 11.5 , $p \leq 0.01$).

In contrast to the diagnostic performance of liver disorder-associated taMPs for patients with inguinal hernias or patients bearing non-liver tumors, elevated diagnostic performance is indicated for patients with cirrhosis, HCC and CCA, whereby AnnexinV⁺EpCAM⁺CD133⁺ASGPR1⁺ display a higher diagnostic potential compared to AnnexinV⁺EpCAM⁺CD133⁺.

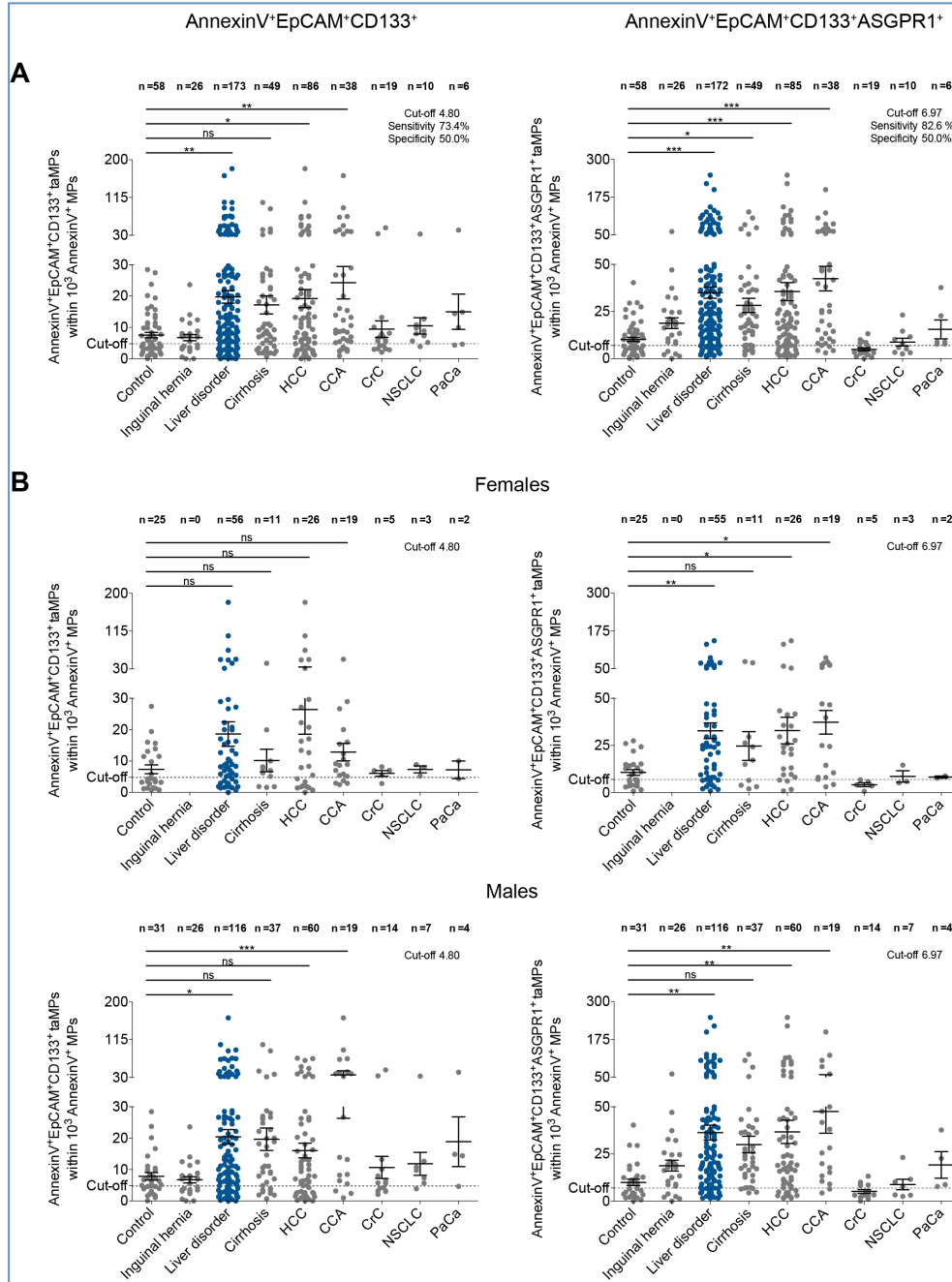


Figure 34: AnnexinV⁺EpCAM⁺CD133⁺ and AnnexinV⁺EpCAM⁺CD133⁺ASGPR1⁺ tumor-associated microparticles (taMPs) detect patients bearing liver disorders.

MPs were isolated from sera of control cohorts (healthy probands and athletes combined in one group) and patients with inguinal hernia as additional control. In addition, MPs were isolated from sera of patients with cirrhosis and cancer patients bearing hepatocellular carcinoma (HCC), cholangiocarcinoma (CCA), colorectal carcinoma (CrC), non-small cell lung cancer (NSCLC) and pancreatic cancer (PaCa). The cohort 'liver disorder' combines patients with cirrhosis, HCC and CCA. A-B) AnnexinV⁺EpCAM⁺CD133⁺ (left) and AnnexinV⁺EpCAM⁺CD133⁺ASGPR1⁺ (right) values for each cohort of the current study (A) as well as in dependency of the gender (B) are displayed. Values are given as mean ± SEM. Differences were assessed by one-way ANOVA including Dunnett's test (* $p \leq 0.05$, ** $p \leq 0.01$, *** $p \leq 0.001$). Dotted lines represent calculated cut-off values (Table 21) (Modified according to Julich-Haertel, Urban, *et al.*, 2017).

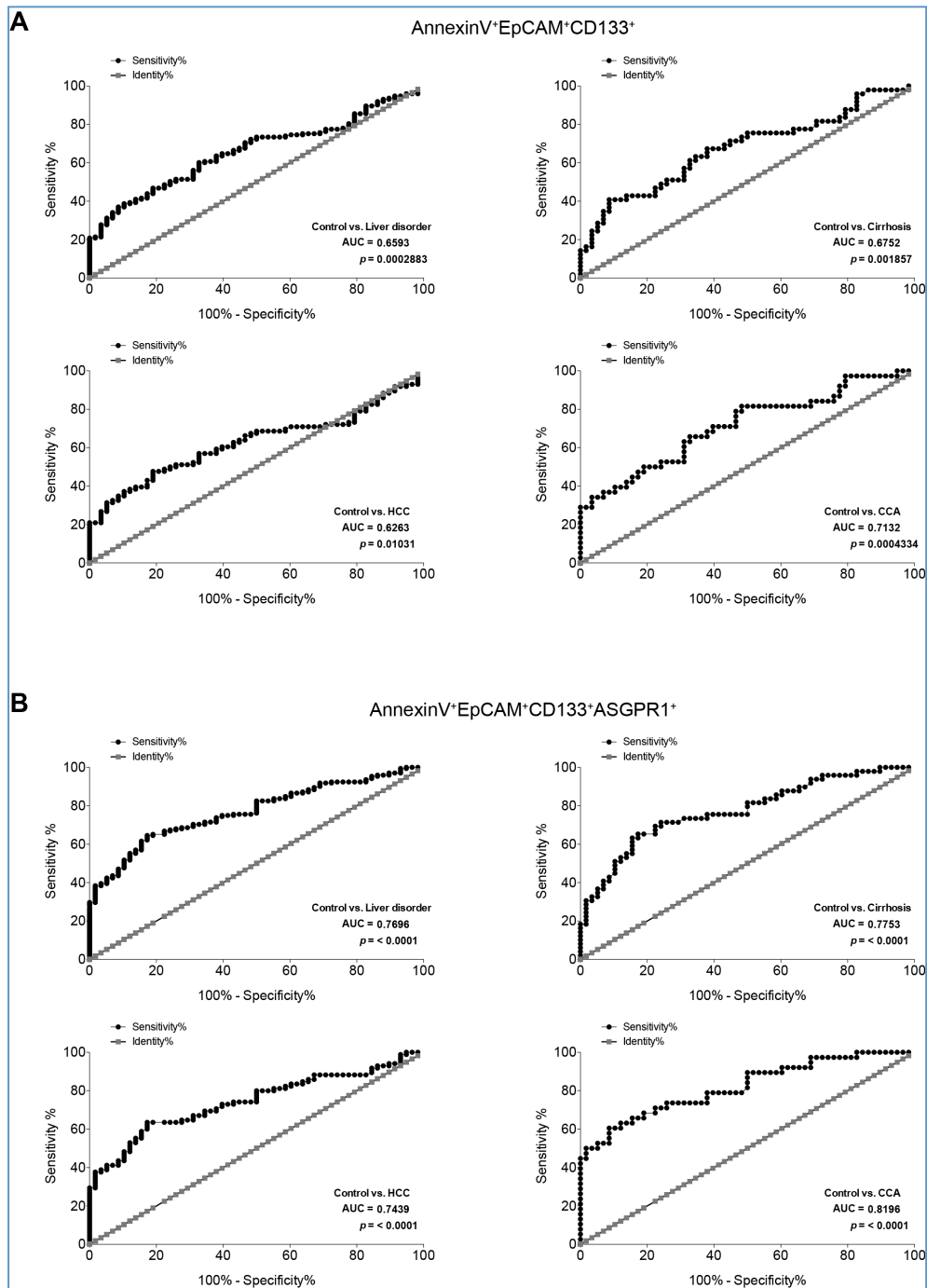


Figure 35: Diagnostic performance of liver disorder-associated AnnexinV⁺EpCAM⁺CD133⁺ and AnnexinV⁺EpCAM⁺CD133⁺ASGPR1⁺ tumor-associated microparticles (taMPs).

MPs were isolated from sera of control cohorts (healthy probands and athletes combined in one group), patients with cirrhosis and cancer patients bearing hepatocellular carcinoma (HCC) and cholangiocarcinoma (CCA). The cohort 'liver disorder' combines patients with cirrhosis, HCC and CCA. A-B) The receiver-operating characteristic (ROC) curves for the cohorts liver disorder, cirrhosis, HCC and CCA, including the corresponding area under curve (AUC) value as well as the p value (p , $*p \leq 0.05$, $**p \leq 0.01$, $***p \leq 0.001$), are indicated for AnnexinV⁺EpCAM⁺CD133⁺ taMPs (A) and AnnexinV⁺EpCAM⁺CD133⁺ASGPR1⁺ taMPs (B). The angle bisector corresponds to the line of identity, which indicates the lower limit for a diagnostic test (Modified according to Julich-Haertel, Urban, *et al.*, 2017)

Table 20: Values of AnnexinV⁺EpCAM⁺CD133⁺ and AnnexinV⁺EpCAM⁺CD133⁺ASGPR1⁺ liver disorder-associated microparticles (MPs) from human serum of each cohort participated in the human cell-derived MPs study. Values of liver disorder-associated MPs for AnnexinV⁺EpCAM⁺CD133⁺ and AnnexinV⁺EpCAM⁺CD133⁺ASGPR1⁺ of each cohort as well as for females and males are depicted. Values refer to 10³ AnnexinV⁺ MPs and are given as mean ± SEM.

	Control	Inguinal hernia	Liver disorder	Cirrhosis	HCC	CCA	CrC	NSCLC	PaCa
AnnexinV⁺EpCAM⁺CD133⁺ liver disorder-associated MPs									
Both	7.5 ±0.9	6.7 ±1.0	19.7 ±2.0	17.2 ±2.9	19.2 ±2.9	24.3 ±5.2	9.5 ±2.6	10.5 ±2.6	15.0 ±5.6
Females	7.4 ±1.4	-	18.6 ±3.9	10.2 ±3.6	26.4 ±7.8	12.8 ±2.8	6.1 ±0.9	7.3 ±1.1	7.2 ±2.8
Males	7.8 ±1.2	6.7 ±1.0	20.4 ±2.3	19.7 ±3.6	16.1 ±2.4	35.7 ±9.4	10.7 ±3.5	11.9 ±3.7	18.9 ±7.9
AnnexinV⁺EpCAM⁺CD133⁺ASGPR1⁺ liver disorder-associated MPs									
Both	10.2 ±1.1	18.8 ±2.9	35.0 ±3.0	28.3 ±3.7	35.6 ±4.8	42.4 ±6.5	4.9 ±0.8	8.7 ±2.0	15.6 ±5.0
Females	10.7 ±1.6	-	32.8 ±4.1	24.7 ±7.6	32.9 ±7.0	37.3 ±6.3	4.2 ±1.1	8.6 ±3.0	8.2 ±0.5
Males	9.9 ±1.7	18.8 ±2.9	36.3 ±4.0	30.0 ±4.4	36.7 ±6.1	47.5 ±11.5	5.2 ±1.1	8.8 ±2.8	19.2 ±7.1

Control: Healthy probands and athletes combined in one group

Liver disorder: Cirrhosis, HCC and CCA combined in one group

HCC: Hepatocellular carcinoma

CCA: Cholangiocarcinoma

CrC: Colorectal cancer

NSCLC: Non-small cell lung cancer

PaCa: Pancreatic cancer

Table 21: Diagnostic performance of AnnexinV⁺EpCAM⁺CD133⁺ and AnnexinV⁺EpCAM⁺CD133⁺ASGPR1⁺ liver disorder-associated microparticles (MPs) of each cohort.

Indicated are the AnnexinV⁺EpCAM⁺CD133⁺ and AnnexinV⁺EpCAM⁺CD133⁺ASGPR1⁺ values (mean ± SEM) and values of calculated cut-off, AUC ± SE of the ROC curves, *p* values as well as values of sensitivity [%], specificity [%], PPV [%] and NPV [%] of each cohort of the current study (Modified according to Julich-Haertel, Urban, *et al.*, 2017).

	Cut-off	Mean ±SEM	AUC ± SE	<i>p</i> Value	Sensitivity [%]	Specificity [%]	PPV [%]	NPV [%]
AnnexinV⁺EpCAM⁺CD133⁺ liver disorder-associated MPs								
Control		7.5 ±0.9						
Inguinal hernia	5.08	6.7 ±1.0	0.5033 ±0.067	0.961	57.69	51.72	34.88	73.17
Liver disorder	4.80	19.7 ±2.0	0.6593 ±0.037	≤0.001	73.41	50.00	81.41	38.67
Cirrhosis	4.82	17.2 ±2.9	0.6752 ±0.053	0.002	75.51	50.00	56.06	70.73
HCC	4.31	19.2 ±2.9	0.6263 ±0.046	0.010	69.77	41.38	63.83	48.00
CCA	5.05	24.3 ±5.2	0.7132 ±0.055	≤0.001	81.58	51.72	52.54	81.08
CrC	5.30	9.5 ±2.6	0.5381 ±0.072	0.620	63.16	53.45	30.77	81.58
NSCLC	5.20	10.5 ±2.6	0.6681 ±0.072	0.091	80.00	51.72	22.22	93.75
PaCa	5.08	15.0 ±5.6	0.7241 ±0.097	0.073	66.67	51.72	12.50	93.75
AnnexinV⁺EpCAM⁺CD133⁺ASGPR1⁺ liver disorder-associated MPs								
Control		10.2 ±1.1						
Inguinal hernia	6.93	18.8 ±2.9	0.6487 ±0.069	0.007	80.77	48.28	41.18	84.85
Liver disorder	6.97	35.0 ±3.0	0.7696 ±0.032	<0.001	82.56	50.00	83.04	49.15

Cirrhosis	6.97	28.3 ±3.7	0.7753 ±0.045	<0.001	81.63	50.00	57.97	76.32
HCC	7.00	35.6 ±4.8	0.7439 ±0.040	<0.001	80.00	50.00	70.10	63.04
CCA	6.98	42.4 ±6.5	0.8196 ±0.045	<0.001	89.47	50.00	53.97	87.88
CrC	6.81	4.9 ±0.8	0.7069 ±0.062	0.007	73.68	55.17	13.51	65.00
NSCLC	6.72	8.7 ±2.0	0.5336 ±0.091	0.736	50.00	56.90	13.16	83.33
PaCa	7.70	15.6 ±5.0	0.6466 ±0.098	0.240	83.33	50.00	14.71	96.67

SEM: Standard error of the mean

AUC ± SE: Area under curve ± standard error

PPV: Positive prediction value

NPV: Negative prediction value

Control: Healthy probands and athletes combined in one group

Liver disorder: Cirrhosis, HCC and CCA combined in one group

HCC: Hepatocellular carcinoma

CCA: Cholangiocarcinoma

CrC: Colorectal cancer

NSCLC: Non-small cell lung cancer

PaCa: Pancreatic cancer

Connection between serum markers (AFP [ng/mL], CEA [ng/mL], CA 19-9 [U/mL], ALT [ng/mL], bilirubin [mg/dL] and creatinine [mg/dL]) (Figure 36) and AnnexinV⁺EpCAM⁺CD133⁺ taMPs (Figure 36, left) as well as AnnexinV⁺EpCAM⁺CD133⁺ASGPR1⁺ taMPs (Figure 36, right) are determined (Pearson's correlation, two-tailed) for patients bearing liver disorders. Included taMPs levels were restricted to values above the cut-off (Table 21).

Almost no correlation between AnnexinV⁺EpCAM⁺CD133⁺ taMPs and AnnexinV⁺EpCAM⁺CD133⁺ASGPR1⁺ taMPs, respectively, and serum markers are observable. However, CA 19-9 indicates low correlation with levels of AnnexinV⁺EpCAM⁺CD133⁺ASGPR1⁺ taMPs ($r=0.153$, $p=0.127$, $R^2=0.023$) and moderate correlation with values of AnnexinV⁺EpCAM⁺CD133⁺ taMPs ($r=0.321$, $p=0.002$, $R^2=0.103$). Further, an indication of a slightly correlation between AnnexinV⁺EpCAM⁺CD133⁺ values and creatinine is given ($r=0.182$, $p=0.060$, $R^2=0.033$). Additionally, a moderate correlation between bilirubin and

AnnexinV⁺EpCAM⁺CD133⁺ASGPR1⁺ taMPs ($r=0.300$, $p\leq 0.001$, $R^2=0.090$) is indicated.

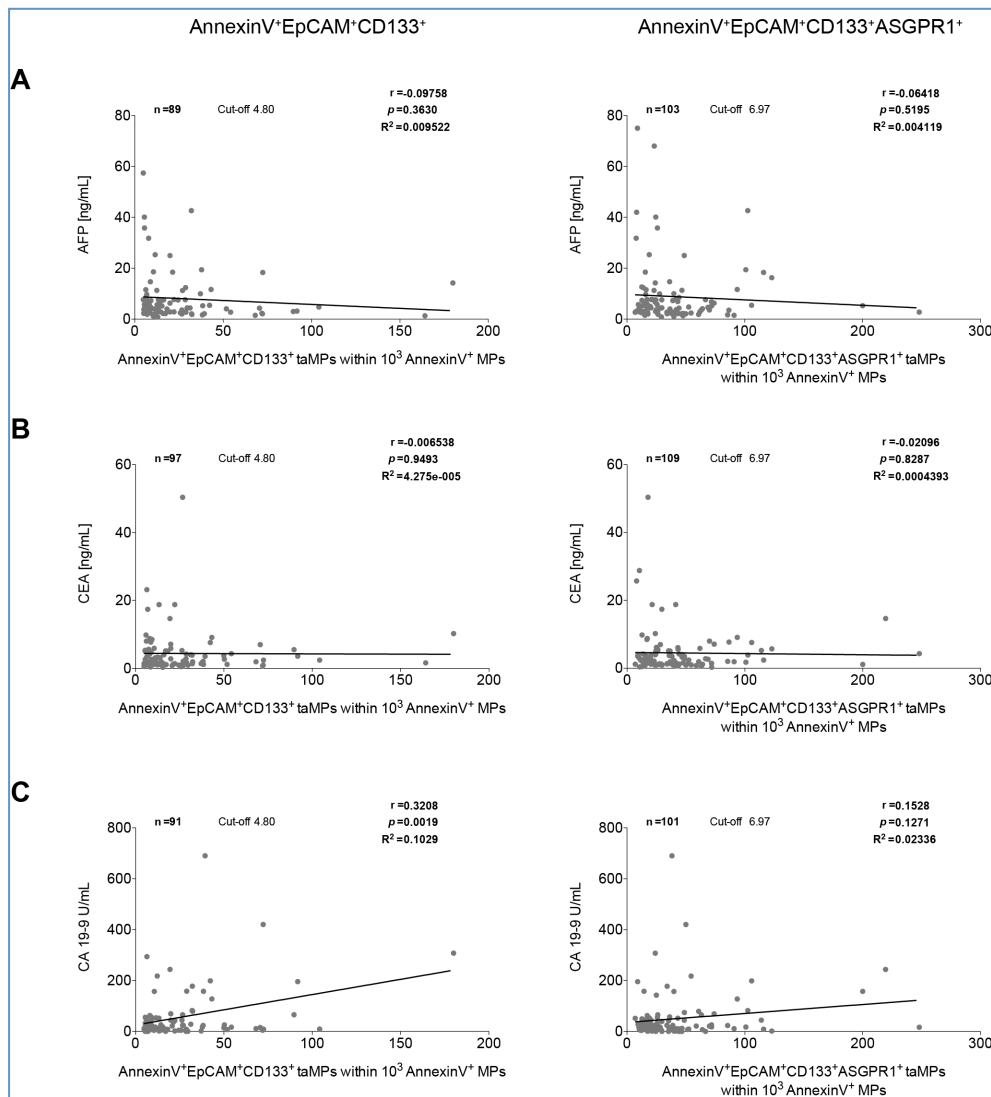


Figure 36: Almost absent association between tumor markers and AnnexinV⁺EpCAM⁺CD133⁺ and AnnexinV⁺EpCAM⁺CD133⁺ASGPR1⁺ tumor-associated microparticles (taMPs) in patients bearing liver disorders. MPs were isolated from sera of patients bearing liver disorders (cirrhosis, hepatocellular carcinoma and cholangiocarcinoma). Calculated Pearson's correlation (two-tailed) between AnnexinV⁺EpCAM⁺CD133⁺ (left) and AnnexinV⁺EpCAM⁺CD133⁺ASGPR1⁺ values (right), respectively, and corresponding serum tumor marker such as: alpha-1 fetoprotein (AFP [ng/mL]) (A), carcinoembryonic antigen (CEA [ng/mL]) (B) or carbohydrate-antigen 19-9 (CA 19-9 [U/mL]) (C) for patients bearing liver disorders are displayed. Indicated are the sample size (n), the corresponding Pearson's correlation coefficient (r), p value (p) and coefficient of determination (R^2). Included taMP levels were restricted to values above the cut-off (Table 21).

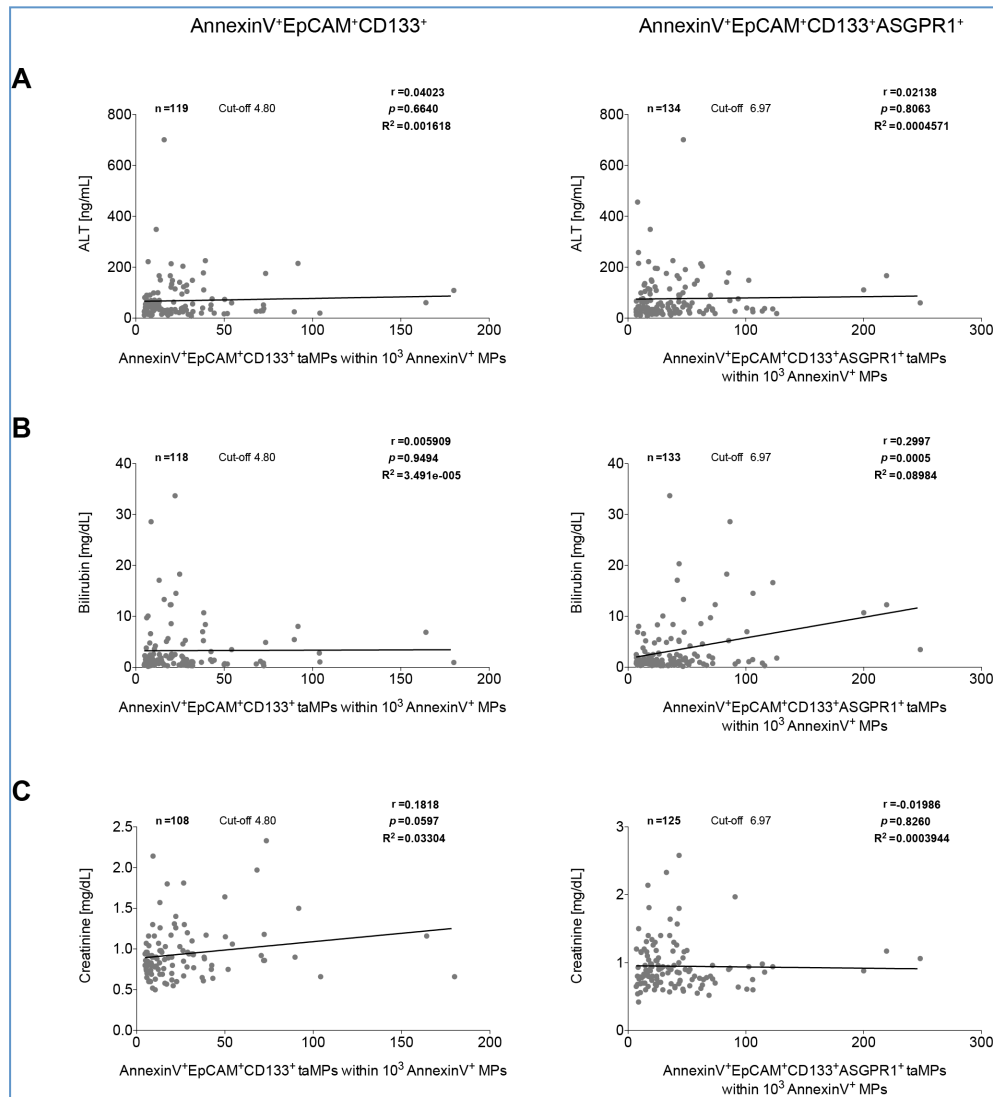


Figure 37: Almost no correlation of blood chemistry with AnnexinV⁺EpCAM⁺CD133⁺ and AnnexinV⁺EpCAM⁺CD133⁺ASGPR1⁺ tumor-associated microparticles (taMPs) in patients bearing liver disorders. MPs were isolated from sera of patients bearing liver disorders (cirrhosis, hepatocellular carcinoma and cholangiocarcinoma). Calculated Pearson's correlation (two-tailed) between AnnexinV⁺EpCAM⁺CD133⁺ (left) and AnnexinV⁺EpCAM⁺CD133⁺ASGPR1⁺ values (right), respectively, and corresponding blood chemistry values such as alanine transaminase (ALT [ng/mL]) (A), bilirubin [mg/dL] (B) or creatinine [mg/dL]) (C) for patients bearing liver disorders are displayed. Indicated are the sample size (n), the corresponding Pearson's correlation coefficient (r), p value (p) and coefficient of determination (R²). Included taMP levels were restricted to values above the cut-off (Table 21).

3.4.2.2 Patients with cirrhosis indicate elevated levels of AnnexinV⁺EpCAM⁺CD133⁺ and AnnexinV⁺EpCAM⁺CD133⁺ASGPR1⁺ microparticles

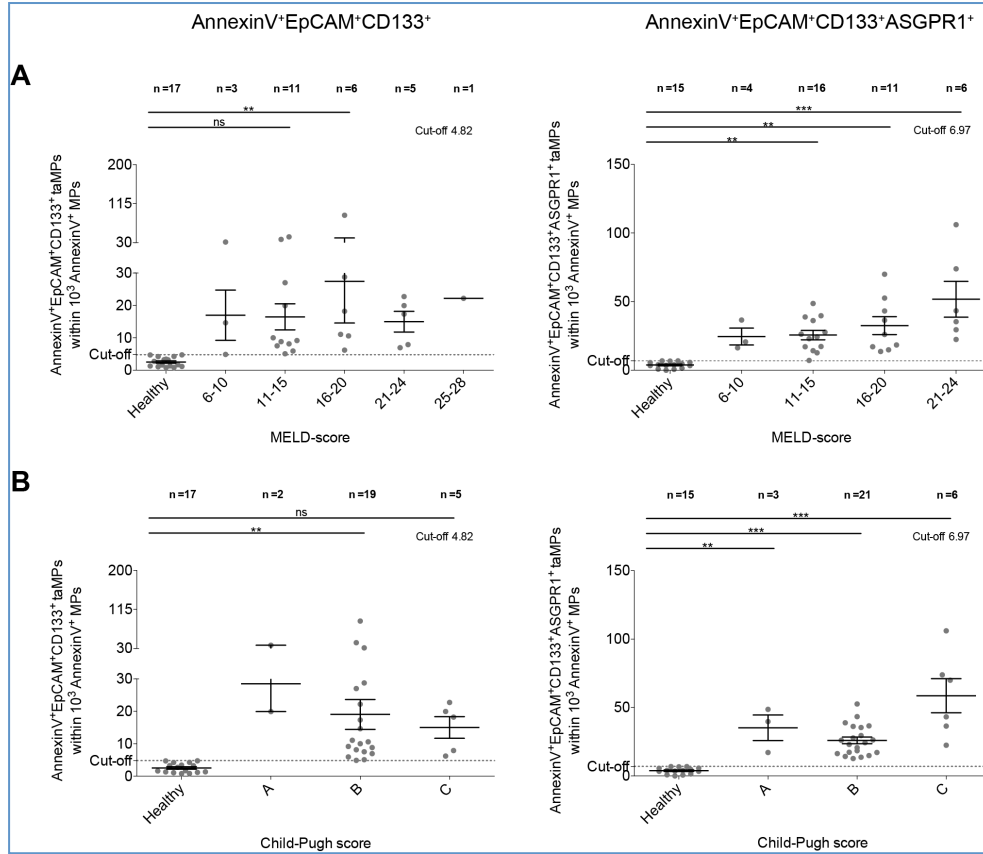


Figure 38: MELD-score and Child-Pugh score to assess the prognosis of cirrhosis in relation to AnnexinV⁺EpCAM⁺CD133⁺ and AnnexinV⁺EpCAM⁺CD133⁺ASGPR1⁺ tumor-associated microparticles (taMPs). MPs were isolated from sera of healthy probands and patients with cirrhosis. A-B) Levels of AnnexinV⁺EpCAM⁺CD133⁺ (left) and AnnexinV⁺EpCAM⁺CD133⁺ASGPR1⁺ taMPs (mean ± SEM) were separated into groups by increasing MELD-score (A) or Child-Pugh score (B). Differences were assessed by one-way ANOVA including Dunnett's test (**p* ≤ 0.05, ***p* ≤ 0.01, ****p* ≤ 0.001). Dotted lines represent calculated cut-off value (Table 21). Only values below the cut-off were incorporated for healthy probands and only values above the cut-off were included for patients with cirrhosis.

To assess the relation between MELD-score as well as Child-Pugh score and AnnexinV⁺EpCAM⁺CD133⁺ taMPs and AnnexinV⁺EpCAM⁺CD133⁺ASGPR1⁺ taMPs for patients with cirrhosis, levels of AnnexinV⁺EpCAM⁺CD133⁺ (Figure 38, left) and AnnexinV⁺EpCAM⁺CD133⁺ASGPR1⁺ taMPs (Figure 38, right) were separated into groups by increasing MELD-score (Figure 38A) or Child-Pugh score (Figure 38B). Only values below the cut-off for healthy probands and only values above the cut-off for patients with cirrhosis were considered. The dotted line represents calculated cut-off value (Table 21). Values of taMP populations refer to 10³ AnnexinV⁺ MPs and given as mean ± SEM. Differences were assessed by one-way ANOVA including Dunnett's test (**p* ≤ 0.05, ***p* ≤ 0.01, ****p* ≤ 0.001).

AnnexinV⁺EpCAM⁺CD133⁺ values are significantly increased at MELD-score about 16-20 ($p \leq 0.001$) and Child-Pugh class B ($p \leq 0.001$). However, AnnexinV⁺EpCAM⁺CD133⁺ taMPs seem not to correlate with the scoring systems, due to the absent increase of average taMP values with rise of MELD-score or Child-Pugh, respectively.

In comparison, levels of AnnexinV⁺EpCAM⁺CD133⁺ASGPR1⁺ taMPs expand significantly with increasing MELD-score (11-15: $p \leq 0.01$, 16-20: $p \leq 0.01$, 21-24: $p \leq 0.001$) and Child-Pugh score as well (A: $p \leq 0.01$, B: $p \leq 0.001$, C: $p \leq 0.001$). In addition, a correlation between these parameters can be assumed due to an increase of the average AnnexinV⁺EpCAM⁺CD133⁺ASGPR1⁺ values with rise of MELD-score and Child-Pugh, respectively.

In addition, association between AnnexinV⁺EpCAM⁺CD133⁺ as well as AnnexinV⁺EpCAM⁺CD133⁺ASGPR1⁺ taMPs and corresponding serum tumor markers (AFP [ng/mL], CEA [ng/mL], CA 19-9 [U/mL]) (Supplementary Figure 3) or blood chemistry values (ALT [ng/mL], bilirubin [mg/dL], creatinine [mg/dL]) was determined (Pearson's correlation, two-tailed) (Supplementary Figure 4). Levels of taMPs were restricted to values above the cut-off (Table 21).

AnnexinV⁺EpCAM⁺CD133⁺ taMPs does not correlate with any of these parameters. Albeit a marginally correlation between AnnexinV⁺EpCAM⁺CD133⁺ASGPR1⁺ taMPs and CA 19-9 ($r=0.190$, $p=0.373$, $R^2=0.036$) and creatinine ($r=-0.162$, $p=0.384$, $R^2=0.026$) is indicated, in addition to a moderate correlation with bilirubin ($r=-0.386$, $p=0.015$, $R^2=0.149$).

3.4.2.3 AnnexinV⁺EpCAM⁺CD133⁺ and AnnexinV⁺EpCAM⁺CD133⁺ASGPR1⁺ microparticles correlate with liver tumor load

Relation between liver tumor load and levels of taMPs were considered for liver tumor patients (HCC and CCA). Values of AnnexinV⁺EpCAM⁺CD133⁺ (Figure 39, left) and AnnexinV⁺EpCAM⁺CD133⁺ASGPR1⁺ taMPs (Figure 39, right) were separated into groups by increasing tumor volume [cm³] (Figure 39A) or tumor diameter [mm] (Figure 39B). Values refer to 10³ AnnexinV⁺ MPs and are given as mean \pm SEM. The dotted line represents calculated cut-off value (Table 21). Differences were assessed by one-way ANOVA including Dunnett's test ($*p \leq 0.05$, $**p \leq 0.01$, $***p \leq 0.001$). In addition, Pearson's correlation (two-tailed) between taMPs and corresponding tumor volume (Figure 39C) or tumor diameter (Figure 39D) was determined. Only taMP

values below the cut-off for healthy probands or above the cut-off for patients bearing a liver tumor were included.

Significant elevated levels of AnnexinV⁺EpCAM⁺CD133⁺ASGPR1⁺ taMPs are indicated for tumor volumes of 0-10 cm³ ($p \leq 0.001$) and greater than 70 cm³ ($p \leq 0.001$), compared to AnnexinV⁺EpCAM⁺CD133⁺ASGPR1⁺ taMP values of healthy probands. In addition, significant elevated levels of AnnexinV⁺EpCAM⁺CD133⁺ taMPs are observable for tumor volumes of 30-50 cm³ ($p \leq 0.01$) and greater than 70 cm³.

Further, AnnexinV⁺EpCAM⁺CD133⁺ expand significantly in patients bearing liver tumors with 30-50 mm ($p \leq 0.05$) or greater than 50 mm ($p \leq 0.05$) in diameter. Furthermore, significant elevated levels of AnnexinV⁺EpCAM⁺CD133⁺ASGPR1⁺ taMPs are indicated in patients with tumors 10-30 mm ($p \leq 0.001$) or greater than 50 mm ($p \leq 0.001$) in diameter. Dependencies of taMP levels and liver tumor load are clarified by the correlation. Levels of both AnnexinV⁺EpCAM⁺CD133⁺ and AnnexinV⁺EpCAM⁺CD133⁺ASGPR1⁺ taMPs seem to expand with increasing tumor volume, due to a moderate correlation between these parameters (AnnexinV⁺EpCAM⁺CD133⁺: $r=0.301$, $p \leq 0.044$, $R^2=0.091$; AnnexinV⁺EpCAM⁺CD133⁺ASGPR1⁺: $r=0.435$, $p \leq 0.002$, $R^2=0.190$). In comparison, correlation between tumor diameter and both liver disorder-associated taMP populations is slightly increased (AnnexinV⁺EpCAM⁺CD133⁺: $r=0.422$, $p \leq 0.004$, $R^2=0.177$; AnnexinV⁺EpCAM⁺CD133⁺ASGPR1⁺: $r=0.480$, $p \leq 0.0006$, $R^2=0.230$). Thus, AnnexinV⁺EpCAM⁺CD133⁺ taMPs and AnnexinV⁺EpCAM⁺CD133⁺ASGPR1⁺ taMPs hypothesized to expand depending on liver tumor load.

Additionally, relation between liver disorder-associated taMPs and corresponding serum tumor markers (AFP [ng/mL], CEA [ng/mL], CA 19-9 [U/mL]) (Supplementary Figure 5) or blood chemistry values (ALT [ng/mL], bilirubin [mg/dL] and creatinine [mg/dL]) (Supplementary Figure 6) was determined (Pearson's correlation, two-tailed). Levels of taMPs were restricted to values above the cut-off (Table 21). Marginally correlations are indicated for AFP ($r=-0.107$, $p=0.385$, $R^2=0.011$) and creatinine ($r=0.180$, $p=0.106$, $R^2=0.032$), respectively, and AnnexinV⁺EpCAM⁺CD133⁺ taMPs. Furthermore, low correlation between AnnexinV⁺EpCAM⁺CD133⁺ASGPR1⁺ taMPs and CA 19-9 ($r=0.131$, $p=0.257$, $R^2=0.0171$) and moderate for bilirubin ($r=0.329$, $p=0.001$, $R^2=0.108$) are depicted.

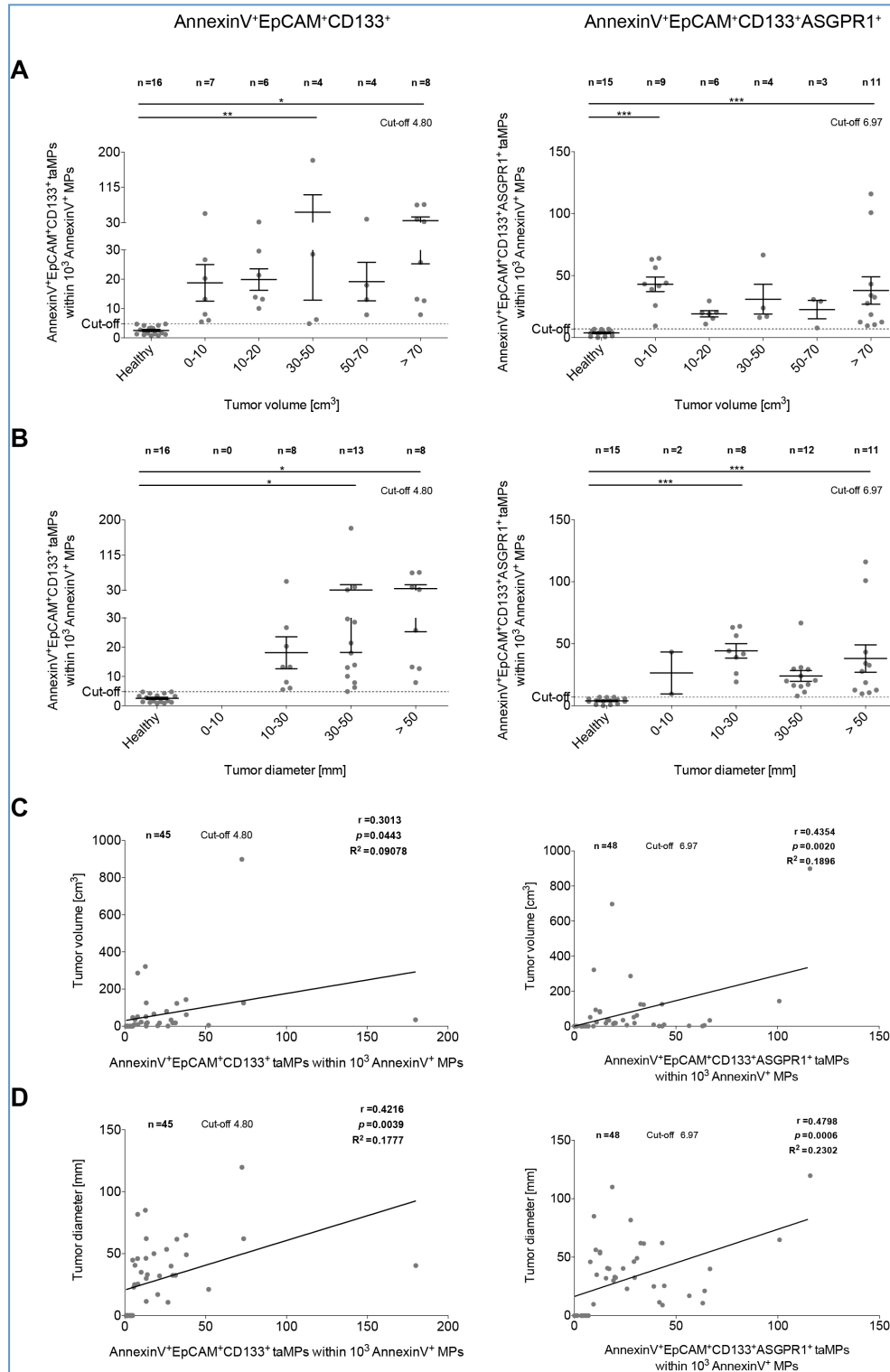


Figure 39: Liver disorder-associated AnnexinV⁺EpCAM⁺CD133⁺ and AnnexinV⁺EpCAM⁺CD133⁺ASGPR1⁺ tumor-associated microparticles (taMPs) correlate with liver tumor load.

MPs were isolated from sera of healthy probands and liver tumor patients bearing hepatocellular carcinoma or cholangiocarcinoma. A-B AnnexinV⁺EpCAM⁺CD133⁺ (left) and AnnexinV⁺EpCAM⁺CD133⁺ASGPR1⁺ (right) values in dependency of corresponding tumor volume [cm³] (A) or tumor diameter [mm] (B) are displayed. Values of taMPs (mean ± SEM) were separated into groups by increasing tumor volume or tumor diameter. Differences were assessed by one-way ANOVA including Dunnett's test (**p* ≤ 0.05, ***p* ≤ 0.01, ****p* ≤ 0.001). Dotted lines represent calculated cut-off value (Table 21). C-D Calculated Pearson's correlation (two-tailed) between taMP values (right) and tumor volume (C) or tumor diameter (D) are displayed. Indicated are the sample size (*n*), the corresponding Pearson's correlation coefficient (*r*), *p* value (*p*) and coefficient of determination (*R*²). Values below the cut-off were incorporated for healthy probands and values above the cut-off were included for patients bearing liver tumors (Modified according to Julich-Haertel, Urban, *et al.*, 2017).

3.4.3 AnnexinV⁺EpCAM⁺ASGPR1⁺ microparticles differ between cirrhosis and liver malignancies

To identify additional liver tumor-derived MPs, ASGPR1 in combination with AnnexinV and EpCAM was utilized.

AnnexinV⁺EpCAM⁺ASGPR1⁺ taMPs are identified by gating on AnnexinV⁺EpCAM⁺ taMPs (Section 3.4.1) followed by plotting CD133 against ASGPR1 and gating on ASGPR1 single positive taMPs (Figure 40).

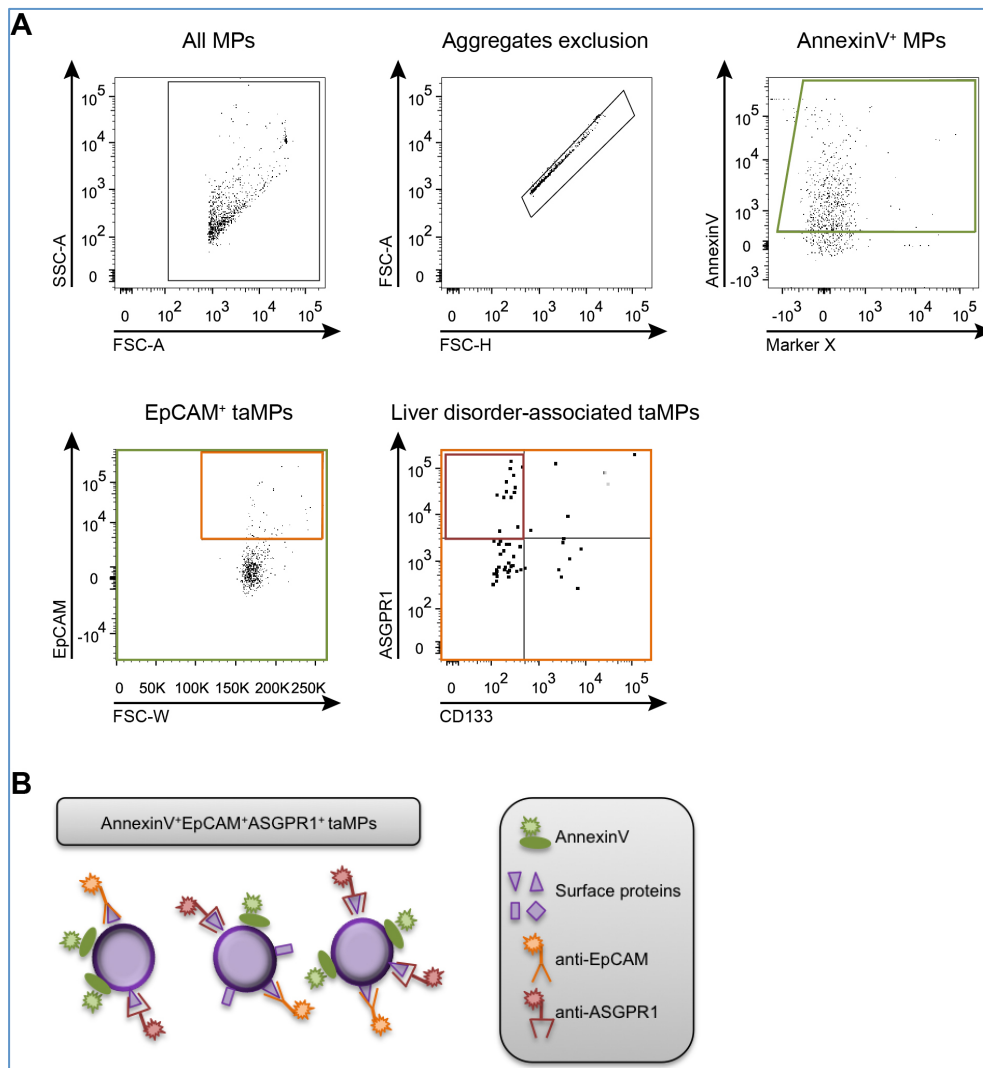


Figure 40: Detection of AnnexinV⁺EpCAM⁺ASGPR1⁺ liver tumor-associated microparticles (taMPs) using flow cytometry analysis.

A) Representative dot plot with the gating strategy is depicted. Gating on all MPs, followed by aggregates exclusion and gating on AnnexinV⁺ MPs (green) is depicted. Detection of AnnexinV⁺EpCAM⁺ taMPs is carried out by further gating on EpCAM⁺ events (orange). Next, identification of liver tumor-associated MPs is ensued by gating on ASGPR1 single positive events (red). MPs were stained with a panel of surface markers: AnnexinV, anti-EpCAM, anti-CD133 and anti-ASGPR1. B) Illustration of AnnexinV⁺EpCAM⁺ASGPR1⁺ taMPs.

Correlation between AnnexinV⁺EpCAM⁺ASGPR1⁺ taMPs and gender, age [years] as well as BMI (Figure 33), was examine to excluded dependencies on these parameters.

For this purpose, values of AnnexinV⁺EpCAM⁺ASGPR1⁺ taMPs of all probands and patients of the current study were separated in females and males (Figure 41A). Values refer to 10³ AnnexinV⁺ MPs and are given as mean ± SEM. Statistical significance was verified by unpaired t test (two-tailed; **p*≤0.05, ***p*≤0.01, ****p*≤0.001). In addition, Pearson's correlation (two-tailed) between values of AnnexinV⁺EpCAM⁺ASGPR1⁺ taMPs of all cohorts and corresponding age (Figure 41B) and BMI (Figure 41C) are displayed.

Levels of AnnexinV⁺EpCAM⁺ASGPR1⁺ taMPs do not differ between females (16.9 ± 2.1) and males (14.0 ± 1.1), as observed for AnnexinV⁺EpCAM⁺, AnnexinV⁺EpCAM⁺CD133⁺ and AnnexinV⁺EpCAM⁺CD133⁺ASGPR1⁺ taMPs. Additionally, neither age nor BMI correlated with AnnexinV⁺EpCAM⁺ASGPR1⁺ taMPs.

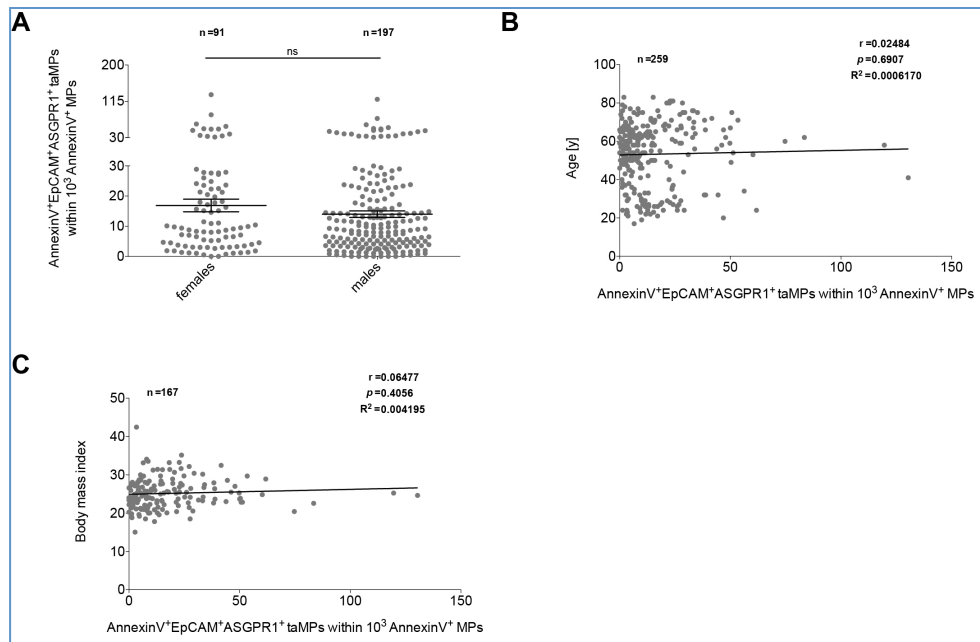


Figure 41: Detection of AnnexinV⁺EpCAM⁺ASGPR1⁺ tumor-associated microparticles (taMPs) in human serum. MPs were isolated from sera of healthy probands, athletes, patients with inguinal hernia or cirrhosis and cancer patients bearing hepatocellular carcinoma, cholangiocarcinoma, colorectal carcinoma, non-small cell lung cancer and pancreatic cancer. A) AnnexinV⁺EpCAM⁺ASGPR1⁺ taMPs (mean ± SEM) in dependency of gender, including all cohorts of the current study, are depicted. Statistical significance was verified by unpaired t test (two-tailed; **p*≤0.05, ***p*≤0.01, ****p*≤0.001). B-C) Pearson's correlation (two-tailed) between AnnexinV⁺EpCAM⁺ASGPR1⁺ and age [years] (B) or body mass index (C) of all cohorts of the current study are displayed. Indicated are the sample size (n), the corresponding Pearson's correlation coefficient (r), *p* value (*p*) and coefficient of determination (*R*²).

3.4.3.1 AnnexinV⁺EpCAM⁺ASGPR1⁺ taMPs differ between patients with cirrhosis and patients bearing liver tumors

Values of AnnexinV⁺EpCAM⁺ASGPR1⁺ taMPs (mean ± SEM) of each cohort (Figure 42A, left) are displayed and summarized in Table 22. Values refer to

10^3 AnnexinV⁺ MPs and differences were assessed by one-way ANOVA including Dunnett's test (* $p \leq 0.05$, ** $p \leq 0.01$, *** $p \leq 0.001$).

The healthy cohort indicates about 13.8 ± 2.1 AnnexinV⁺EpCAM⁺ASGPR1⁺ taMPs per 10^3 AnnexinV⁺ MPs as well as no differences relating to the gender (females: 14.8 ± 3.4 , males: 12.3 ± 1.8). Patients with inguinal hernias, which serve as additional control cohort, indicate slightly less AnnexinV⁺EpCAM⁺ASGPR1⁺ taMPs (9.7 ± 1.5), compared to the healthy cohort. In contrast, 1.5-fold increase of AnnexinV⁺EpCAM⁺ASGPR1⁺ taMPs compared to the healthy probands is observable in the additional control cohort of the athletes.

Table 22: Values of AnnexinV⁺EpCAM⁺ASGPR1⁺ tumor-associated microparticles (taMPs) from human serum of each cohort participated in the human cell-derived MPs study.

Values of AnnexinV⁺EpCAM⁺ASGPR1⁺ of each cohort as well as for females and males are depicted. Values refer to 10^3 AnnexinV⁺ MPs and are given as mean \pm SEM. Patients bearing liver disorders and the individually cohorts of cirrhosis, HCC and CCA are only considered further on (red).

	Healthy	Athletes	Inguinal hernia	Liver disorder	Cirrhosis	HCC	CCA	CrC	NSCLC	PaCa
Both	13.8 ± 2.1	20.9 ± 2.3	9.7 ± 1.5	15.4 ± 1.5	6.3 ± 0.8	19.0 ± 2.2	18.8 ± 4.2	12.4 ± 3.0	12.2 ± 3.6	13.3 ± 3.7
Females	14.8 ± 3.4	22.1 ± 2.7	-	17.4 ± 3.1	5.3 ± 1.1	24.0 ± 5.4	15.4 ± 4.9	12.9 ± 6.1	17.8 ± 7.6	16.3 ± 1.7
Males	12.3 ± 1.8	21.9 ± 3.1	9.7 ± 1.5	14.5 ± 1.6	6.7 ± 1.0	16.9 ± 2.0	22.2 ± 7.0	12.2 ± 3.6	9.8 ± 4.1	11.8 ± 5.6

Liver disorder: Cirrhosis, HCC and CCA combined in one group

HCC: Hepatocellular carcinoma

CCA: Cholangiocarcinoma

CrC: Colorectal cancer

NSCLC: Non-small cell lung cancer

PaCa: Pancreatic cancer

Patients bearing non-liver tumors indicate similar levels of AnnexinV⁺EpCAM⁺ASGPR1⁺ levels (CrC: 12.4 ± 3.0 , NSCLC: 12.2 ± 3.6 , PaCa: 13.3 ± 3.7), compared to the healthy cohort. Females and males show similar levels of AnnexinV⁺EpCAM⁺ASGPR1⁺ taMPs in patients bearing CrC (females: 12.9 ± 6.1 , males: 12.2 ± 3.6). In contrast, slightly elevated values of AnnexinV⁺EpCAM⁺ASGPR1⁺ taMPs are detectable in females bearing NSCLC or

PaCa (NSCLC: 17.8 ± 7.6 , PaCa: 16.3 ± 1.7), whereas males show no increase in taMPs values (NSCLC: 9.8 ± 4.1 , PaCa: 11.8 ± 5.6).

Patients with liver disorders indicate slightly increase of AnnexinV⁺EpCAM⁺ASGPR1⁺ values (15.4 ± 1.5 , females: 17.4 ± 3.1 , males: 14.5 ± 1.6), compared to the healthy cohort. Relating to the individually cohorts of cirrhosis, HCC and CCA, only patients bearing a liver tumor indicate 1.4-fold increase of AnnexinV⁺EpCAM⁺ASGPR1⁺ taMPs (HCC: 19.0 ± 2.2 , CCA: 18.8 ± 4.2), whereas values of patients with cirrhosis decrease 2.2-fold (6.3 ± 0.8). Levels of AnnexinV⁺EpCAM⁺ASGPR1⁺ do not differ between females and males in patients with cirrhosis (females: 5.3 ± 1.1 , males: 6.7 ± 1.0). However, increase of AnnexinV⁺EpCAM⁺ASGPR1⁺ taMPs is indicated in females bearing HCC (24.0 ± 5.4) and males bearing CCA (22.2 ± 7.0), compared to healthy control cohort. Only slightly elevated values are shown for males bearing HCC (16.9 ± 2.0) and females bearing CCA (15.4 ± 4.9).

Compared to the healthy cohort, changes of AnnexinV⁺EpCAM⁺ASGPR1⁺ values are of no significance.

Due to the previous described results of elevated levels of AnnexinV⁺EpCAM⁺ in cancer patients, as well as expand of AnnexinV⁺EpCAM⁺CD133⁺ and AnnexinV⁺EpCAM⁺CD133⁺ASGPR1⁺ taMPs mainly in patients bearing liver disorders, a specific surface marker combination is assumed for patients with liver disorders. As a result of this, only patients bearing a liver disorder are considered further on (Figure 42A, red). Patients with cirrhosis serve as control and the cohort named ‘Liver tumor’ combines patients bearing HCC and CCA. The dotted line represents calculated cut-off values (Table 23).

Diagnostic performance of AnnexinV⁺EpCAM⁺ASGPR1⁺ taMPs was evaluated for the cohorts liver tumor, HCC and CCA by creating the corresponding ROC curves and determination of cut-off values, sensitivity [%] and specificity [%] as well as PPV [%] and NPV [%] (Table 23). Created ROC curves, including corresponding AUC and *p* values for AnnexinV⁺EpCAM⁺ASGPR1⁺ taMPs are displayed (Figure 42C). The angle bisector corresponds to the line of identity, which indicates the lower limit for a diagnostic test.

Compared to taMP levels in patients with cirrhosis, AnnexinV⁺EpCAM⁺ASGPR1⁺ values expand significantly 3-fold in liver tumor patients as well as the individually cohorts of HCC and CCA (HCC: $p \leq 0.01$, CCA: $p \leq 0.05$, Liver tumor: $p \leq 0.001$). This results in a general solid diagnostic performance for liver tumor patients

(sensitivity: 75.0 %, specificity: 46.9 %, PPV: 78.2 %, NPV: 42.6 %) and specific solid diagnostic performance for HCC (sensitivity: 81.4 %, specificity: 46.9 %, PPV: 72.9 %, NPV: 59.0 %) and CCA (sensitivity: 65.8 %, specificity: 46.9 %, PPV: 49.0 %, NPV: 63.9 %).

Table 23: Diagnostic performance of AnnexinV⁺EpCAM⁺ASGPR1⁺ values of patients bearing liver disorders.
Indicated are the AnnexinV⁺EpCAM⁺ASGPR1⁺ values (mean ± SEM) and values of calculated cut-off, AUC ± SE of the ROC curves, *p* values as well as values of sensitivity [%], specificity [%], PPV [%] and NPV [%] for patients with cirrhosis, HCC and CCA (Modified according to Julich-Haertel, Urban, *et al.*, 2017).

	Cut-off	Mean ±SEM	AUC ± SE	<i>p</i> Value	Sensitivity [%]	Specificity [%]	PPV [%]	NPV [%]
Cirrhosis		6.3 ±0.8						
HCC	4.13	19.0 ±2.2	0.7322 ±0.042	≤0.001	81.40	46.94	72.92	58.97
CCA	4.11	18.8 ±4.2	0.6208 ±0.065	0.054	65.79	46.94	49.02	63.89
Liver tumor	4.17	19.0 ±2.0	0.6981 ±0.040	≤0.001	75.00	46.94	78.15	42.59

SEM: Standard error of the mean

AUC ± SE: Area under curve ± standard error

PPV: Positive prediction value

NPV: Negative prediction value

HCC: Hepatocellular carcinoma

CCA: Cholangiocarcinoma

Liver tumor: HCC and CCA combined in one group

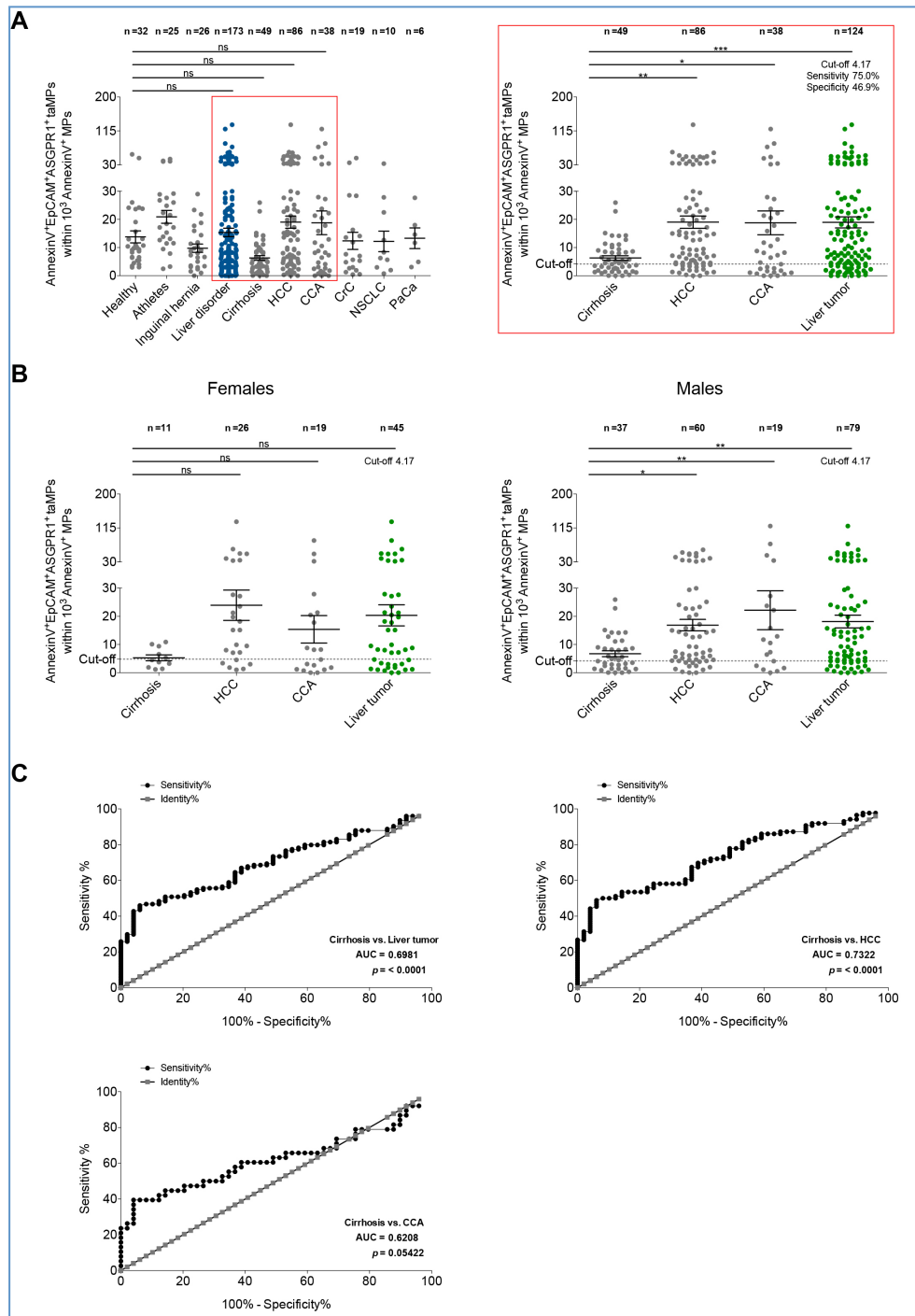


Figure 42: AnnexinV⁺EpCAM⁺ASGPR1⁺ tumor-associated microparticles (taMPs) detect liver tumor-bearing patients.

MPs were isolated from sera of control cohorts (healthy probands, athletes, patients with inguinal hernia), patients with cirrhosis and cancer patients bearing hepatocellular carcinoma (HCC), cholangiocarcinoma (CCA), colorectal carcinoma (CrC), non-small cell lung cancer (NSCLC) and pancreatic cancer (PaCa). The cohort 'Liver disorder' combines patients with cirrhosis, HCC and CCA and the cohort 'Liver tumor' combines patients bearing HCC and CCA. A-B) AnnexinV⁺EpCAM⁺ASGPR1⁺ values (mean ± SEM) for each cohort (A, left), for patients bearing liver disorders (A, right) and for patients bearing liver disorders in dependency of gender (B) are displayed. Differences were assessed by one-way ANOVA including Dunnett's test (* $p \leq 0.05$, ** $p \leq 0.01$, *** $p \leq 0.001$). Dotted lines represent calculated cut-off values (Table 23). C) To analyze the diagnostic performance of the AnnexinV⁺EpCAM⁺ASGPR1⁺ taMP population, receiver-operating characteristic (ROC) curves for the cohorts liver tumor, HCC and CCA, including the corresponding area under curve (AUC) value as well as the p values are indicated. The angle bisector corresponds to the line of identity, which indicates the lower limit for a diagnostic test (Modified according to Julich-Haertel, Urban, *et al.*, 2017).

3.4.3.2 AnnexinV⁺EpCAM⁺ASGPR1⁺ taMPs and liver tumor load

Relation between liver tumor load and levels of AnnexinV⁺EpCAM⁺ASGPR1⁺ taMPs were considered. Values of AnnexinV⁺EpCAM⁺ASGPR1⁺ (mean \pm SEM) were separated into groups by increasing tumor volume [cm³] (Figure 43A, left) or tumor diameter [mm] (Figure 43B, left). The dotted line represents calculated cut-off value (Table 23). Differences were assessed by one-way ANOVA including Dunnett's test (* $p \leq 0.05$, ** $p \leq 0.01$, *** $p \leq 0.001$). Additionally, Pearson's correlation (two-tailed) between AnnexinV⁺EpCAM⁺ASGPR1⁺ taMPs and corresponding tumor volume (Figure 43A, right) or tumor diameter (Figure 43B, right) was determined. Only taMP values below the cut-off for patients with cirrhosis or above the cut-off for patients bearing a liver tumor were incorporated.

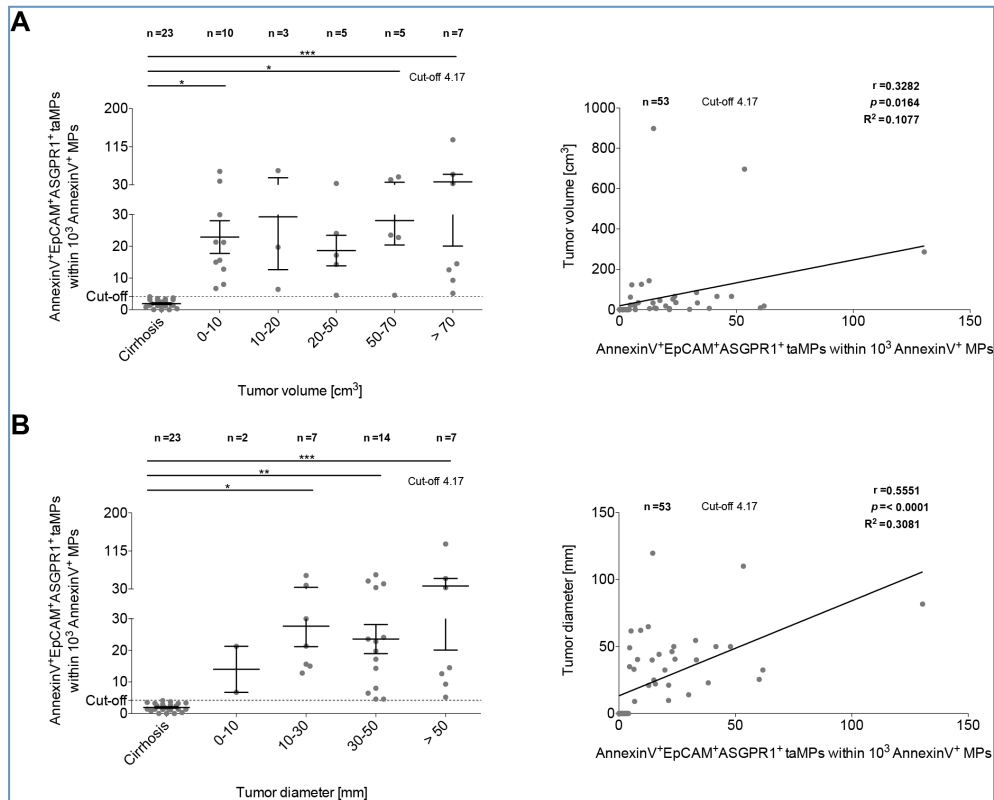


Figure 43: Values of AnnexinV⁺EpCAM⁺ASGPR1⁺ tumor-associated microparticles (taMPs) correlate with liver tumor load.

MPs were isolated from sera of patients with cirrhosis and patients bearing liver tumors (hepatocellular carcinoma and cholangiocarcinoma). A-B) AnnexinV⁺EpCAM⁺ASGPR1⁺ values in dependency of corresponding tumor volume [cm³] (A) or tumor diameter [mm] (B) are displayed. Left: AnnexinV⁺EpCAM⁺ASGPR1⁺ values (mean \pm SEM) were separated into groups by increasing corresponding tumor volume or tumor diameter. Differences were assessed by one-way ANOVA including Dunnett's test (* $p \leq 0.05$, ** $p \leq 0.01$, *** $p \leq 0.001$). Dotted lines represent calculated cut-off value (Table 23). Right: Calculated Pearson's correlation (two-tailed) between AnnexinV⁺EpCAM⁺ASGPR1⁺ values and corresponding tumor volume or tumor diameter are displayed. Indicated are the sample size (n), the corresponding Pearson's correlation coefficient (r), p value (p) and coefficient of determination (R²). Only values below the cut-off were incorporated for patients with cirrhosis and only values above the cut-off were included for patients bearing a liver tumor (Modified according to Julich-Haertel, Urban, *et al.*, 2017).

Significant elevated levels of AnnexinV⁺EpCAM⁺ASGPR1⁺ taMPs are indicated for tumor volumes of 0-10 cm³ ($p \leq 0.05$), 50-70 cm³ ($p \leq 0.05$) and greater than 70 cm³ ($p \leq 0.001$), compared to AnnexinV⁺EpCAM⁺ASGPR1⁺ taMP values in patients with cirrhosis. In addition, AnnexinV⁺EpCAM⁺ASGPR1⁺ values expand significantly in patients bearing a liver tumor of 10-30 mm ($p \leq 0.05$), 30-50 mm ($p \leq 0.01$) and greater than 50 mm ($p \leq 0.001$) in diameter. Dependency of taMP levels and tumor diameter and tumor volume, respectively, are clarified by the correlation. Levels of AnnexinV⁺EpCAM⁺ASGPR1⁺ seem to rise with increasing tumor volume, as indicated by a moderate correlation between these parameters ($r=0.328$, $p=0.016$, $R^2=0.108$). Correlation between tumor diameter and AnnexinV⁺EpCAM⁺ASGPR1⁺ is increased ($r=0.555$, $p \leq 0.0001$, $R^2=0.308$), in comparison to the correlation between tumor volume and values of taMPs.

Pearson's correlation (two-tailed) was determined between AnnexinV⁺EpCAM⁺ASGPR1⁺ taMPs of liver tumor patients and corresponding serum markers (AFP [ng/mL], CEA [ng/mL] and CA 19-9 [U/mL], ALT [ng/mL], bilirubin [mg/dL] and creatinine [mg/dL]) (Supplementary Figure 7A&B). Levels of taMPs were restricted to values above the cut-off (Table 23). However, almost no correlation between AnnexinV⁺EpCAM⁺ASGPR1⁺ taMPs and serum markers of liver tumor patients are observable. Only a slight correlation is implied for ALT ($r=0.126$, $p=0.258$, $R^2=0.016$), in addition to a marginally negative correlation for creatinine ($r=-0.106$, $p=0.342$, $R^2=0.011$).

3.4.4 Surgical resection leads to decrease in liver tumor-specific taMP values

Values of taMP populations were investigated for the association with surgical R0 resection in liver tumor patients (Figure 44). Values of taMPs were examined prior to surgical R0 tumor resection (pre-OP) and at day 2, day 7 and day 10 after tumor resection. Only values above the cut-off were considered. The dotted line represents calculated cut-off values (Table 19, Table 21, Table 23). Values of taMPs refer to 10³ AnnexinV⁺ MPs and are given as mean \pm SEM. Differences were assessed by Wilcoxon matched-pairs signed rank test (two-tailed) between each post-OP day and pre-OP values (* $p \leq 0.05$, ** $p \leq 0.01$, *** $p \leq 0.001$).

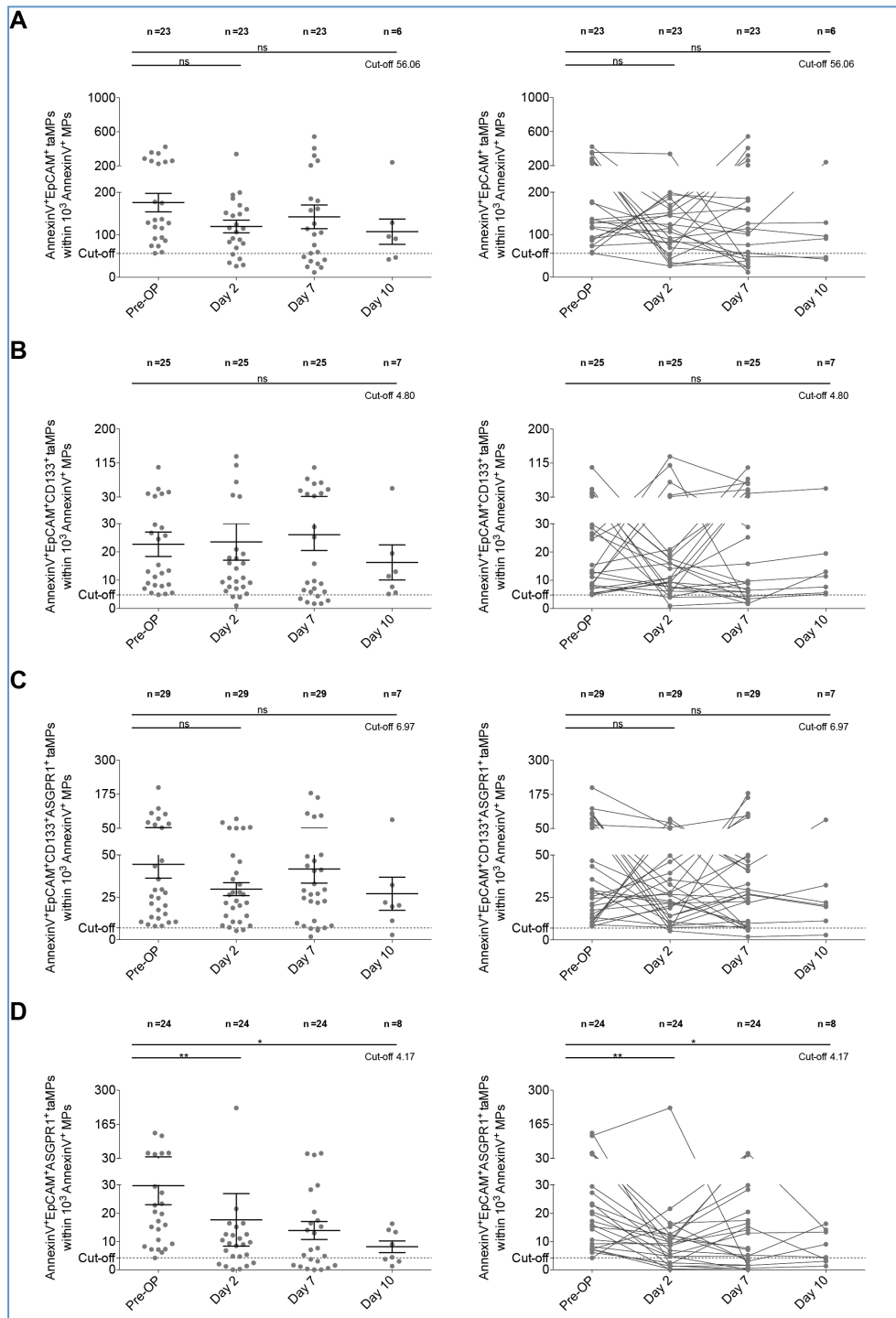


Figure 44: Liver tumor-specific taMPs decrease after surgical R0 resection in liver tumor patients.

MPs were isolated from sera of patients bearing liver tumors (hepatocellular carcinoma and cholangiocarcinoma). A-D) Values of AnnexinV⁺EpCAM⁺ (A), AnnexinV⁺EpCAM⁺CD133⁺ (B), AnnexinV⁺EpCAM⁺CD133⁺ASGPR1⁺ (C) and AnnexinV⁺EpCAM⁺ASGPR1⁺ taMPs (D) prior to tumor resection (pre-OP) and at day 2, day 7 and day 10 after tumor resection are displayed. Left: Mean taMP values \pm SEM are depicted. Right: taMP values individually for each patient participating in the surgical R0 resection study are indicated. Only values above the cut-off were considered. The dotted line represents calculated cut-off values (Table 19, Table 21, Table 23). Differences were verified by Wilcoxon matched-pairs signed rank test (two-tailed; * $p \leq 0.05$, ** $p \leq 0.01$, *** $p \leq 0.001$) (Modified according to Julich-Haertel, Urban, *et al.*, 2017).

The taMP populations AnnexinV⁺EpCAM⁺ and AnnexinV⁺EpCAM⁺CD133⁺ASGPR1⁺ indicate the same tendencies. The mean pre-OP taMP levels (mean \pm SEM) of

176.0 AnnexinV⁺EpCAM⁺ taMPs (Figure 44A, left) and 44.5 AnnexinV⁺EpCAM⁺CD133⁺ASGPR1⁺ taMPs (Figure 44C, left) per 10³ AnnexinV⁺ MPs decrease at day 2 post-OP to 119.8 AnnexinV⁺EpCAM⁺ taMPs and 29.8 AnnexinV⁺EpCAM⁺CD133⁺ASGPR1⁺ taMPs, despite a increase of taMPs levels in some patients. A rebound of mean taMP levels is observable at day 7 post-OP to 142.5 AnnexinV⁺EpCAM⁺ taMPs and 41.7 AnnexinV⁺EpCAM⁺CD133⁺ASGPR1⁺ taMPs, respectively. However, values of taMPs drop again at day 10 post-OP (AnnexinV⁺EpCAM⁺: 107.5, AnnexinV⁺EpCAM⁺CD133⁺ASGPR1⁺: 27.1).

AnnexinV⁺EpCAM⁺CD133⁺ taMPs show no obvious association between levels of taMPs and tumor resection as indicated as stable AnnexinV⁺EpCAM⁺CD133⁺ taMP values at all times examined (pre-OP: 22.7, day 2 post-OP: 23.5, day 7 post-OP: 26.1, day 10 post-OP: 16.3) (Figure 44B, left).

The mean pre-OP values of 29.7 AnnexinV⁺EpCAM⁺ASGPR1⁺ liver tumor-associated taMPs (Figure 44D, left) reduce at day 2 post-OP to 17.6 taMPs. Levels of AnnexinV⁺EpCAM⁺ASGPR1⁺ taMPs remain low at day 7 post-OP at 13.9 AnnexinV⁺EpCAM⁺ASGPR1⁺ taMPs despite a rebound of taMP values in some patients and drop further at day 10 post-OP to 8.1 AnnexinV⁺EpCAM⁺ASGPR1⁺ taMPs.

3.4.5 Summary – Tumor-related microparticles to identify primary hepatic cancer

Increased levels of cancer-related MPs, such as AnnexinV⁺EpCAM⁺ taMPs are detectable in sera of athletes, patients with inguinal hernias, cancer patients (CrC, NSCLC, PaCa, HCC, CCA) and patients bearing liver disorders (Cirrhosis, HCC, CCA). AnnexinV⁺EpCAM⁺ taMPs seem to detect injuries and cancer in general, thus AnnexinV⁺EpCAM⁺ taMPs suggest to be a pan-cancer marker. Cancer detection using AnnexinV⁺EpCAM⁺ taMPs is limited, as indicated by 34 % of patients with liver disorders and 30 % of patients bearing liver tumors, respectively, whose values are below the calculated cut-off (Figure 45B). However, liver tumor load and levels of AnnexinV⁺EpCAM⁺ taMPs correlate moderate with one another. Thus, AnnexinV⁺EpCAM⁺ taMPs suggest to monitor a subpopulation that is closely linked to cancer, as a first step.

The taMP populations AnnexinV⁺EpCAM⁺CD133⁺ and AnnexinV⁺EpCAM⁺CD133⁺ASGPR1⁺ seem to specifically identify patients with liver

disorders due to significant elevated values of these taMP populations in patients bearing HCC, CCA and cirrhosis. 64 % of patients bearing liver disorders were correctly identified using AnnexinV⁺EpCAM⁺ taMPs as first cancer detection-step and additionally AnnexinV⁺EpCAM⁺CD133⁺ and AnnexinV⁺EpCAM⁺CD133⁺ASGPR1⁺ taMPs to confirm the presence of liver disorders (Figure 45A-B, left; Figure 46). Only 2 % of patients with liver disorders indicated values of both AnnexinV⁺EpCAM⁺CD133⁺ and AnnexinV⁺EpCAM⁺CD133⁺ASGPR1⁺ taMPs below the calculated cut-off value. Correlation between MELD-score of patients with cirrhosis and AnnexinV⁺EpCAM⁺CD133⁺ASGPR1⁺ is implied and moreover, AnnexinV⁺EpCAM⁺CD133⁺ and AnnexinV⁺EpCAM⁺CD133⁺ASGPR1⁺ correlate moderate with liver tumor load.

Patients with liver disorders can be distinguished in patients bearing liver malignancies and patients with cirrhosis without malignancies in consequence of expansion of AnnexinV⁺EpCAM⁺ASGPR1⁺ taMPs in patients with primary hepatic cancer in contrast to low levels of AnnexinV⁺EpCAM⁺ASGPR1⁺ taMPs in patients with cirrhosis.

54 % of liver tumor patients were correctly identified using a three-step approach: 1) Cancer detection using AnnexinV⁺EpCAM⁺ taMPs, 2) Confirmation of liver disorders by AnnexinV⁺EpCAM⁺CD133⁺ and AnnexinV⁺EpCAM⁺CD133⁺ASGPR1⁺ taMPs, 3) Detection of liver tumors by elevated levels of AnnexinV⁺EpCAM⁺ASGPR1⁺ taMPs or detection of non-tumor-bearing patients with cirrhosis by low levels of AnnexinV⁺EpCAM⁺ASGPR1⁺ taMPs (Figure 45A-B, right; Figure 46). Only 16 % of patients bearing liver tumors indicated values of AnnexinV⁺EpCAM⁺ASGPR1⁺ taMPs below the calculated cut-off value. This is confirmed by a solid diagnostic performance. In addition, AnnexinV⁺EpCAM⁺ASGPR1⁺ values correlate with tumor load of patients bearing primary hepatic cancer. Moreover, values of AnnexinV⁺EpCAM⁺ASGPR1⁺ taMPs drop at 2 day after surgical R0 tumor resection and remain low at day 10 post-OP.

In relation to patients with elevated levels of AnnexinV⁺EpCAM⁺ taMPs, 39 % of patients with cirrhosis, 61 % of patients bearing CCA and 89 % of patients bearing HCC were correctly identified by the help of liver disorder-associated and liver tumor-associated taMPs (Figure 45C).

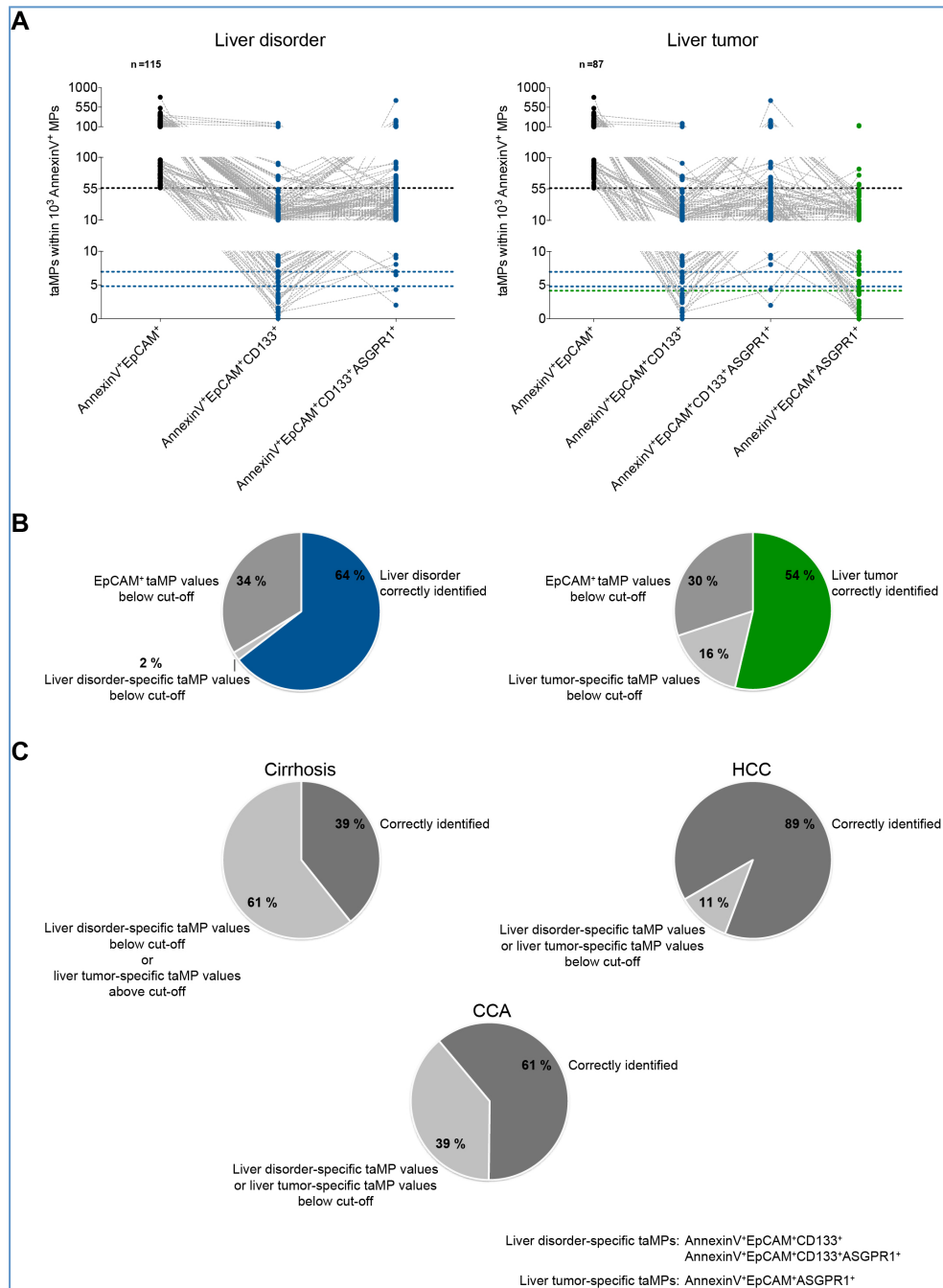


Figure 45: Tumor-associated microparticles (taMPs) and their diagnostic potential.

MPs were isolated from sera of patients with cirrhosis and patients bearing liver tumors (hepatocellular carcinoma (HCC) and cholangiocarcinoma (CCA)). The cohort ‘Liver disorder’ consists of cirrhosis, HCC and CCA and the cohort ‘Liver tumor’ consist of HCC and CCA. A) Values of taMP populations individually for all patients with liver disorders (left) and liver tumor patients (right) are displayed. Dotted line represents calculated cut-off values for AnnexinV⁺EpCAM⁺ (Table 19, black), AnnexinV⁺EpCAM⁺CD133⁺ and AnnexinV⁺EpCAM⁺CD133⁺ASGPR1⁺ (Table 21, blue), as well as AnnexinV⁺EpCAM⁺CD133⁺ASGPR1⁺ taMPs (Table 23, green). B) Percentage distribution of correctly identified patients with liver disorders (left) and primary hepatic cancer (right). C) Percentage distribution of correctly identified patients individually for patients with cirrhosis, HCC and CCA.

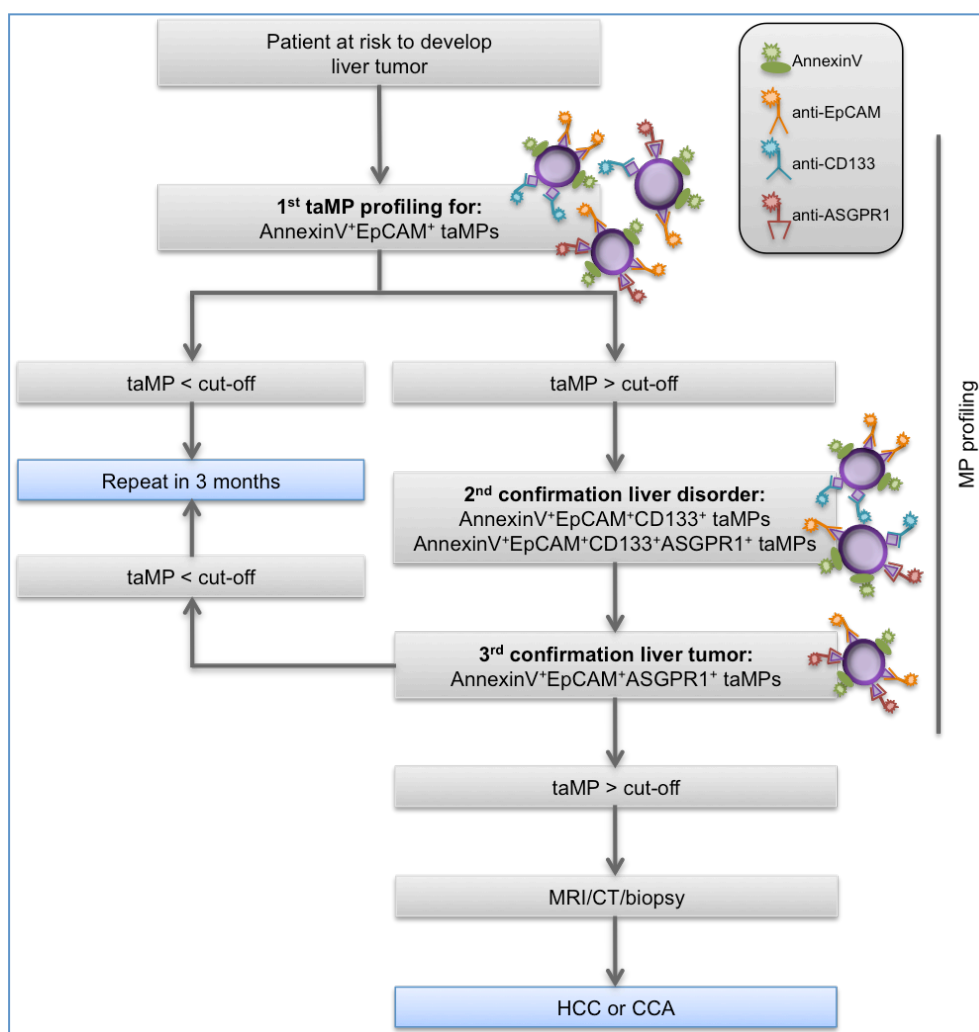


Figure 46: Proposal of a possibly screening method to identify primary hepatic cancer using several tumor-associated microparticle (taMP) populations.

Workflow for a possible application for a minimal invasive diagnostic tool to detect primary hepatic cancer (hepatocellular carcinoma (HCC) and cholangiocarcinoma (CCA)) is depicted. First and foremost is a general screening for elevated levels of AnnexinV⁺EpCAM⁺ tumor-associated microparticles (taMPs), isolated from human sera, for patients at risk to develop liver tumors. Positively identified patients indicated by taMP levels above cut-off value follow two further detection steps. First, examination of the presence of liver disease using liver disorder-associated taMP populations: AnnexinV⁺EpCAM⁺CD133⁺ and AnnexinV⁺EpCAM⁺CD133⁺ASGPR1⁺. Second, discrimination into liver tumor or cirrhosis without malignancies using liver tumor-associated taMPs population: AnnexinV⁺EpCAM⁺ASGPR1⁺. Patients with suspected primary hepatic cancer will undergo tumor assessment with magnetic resonance imaging (MRI), computed tomography (CT) and biopsy (Modified according to Julich-Haertel, Urban, *et al.*, 2017).

3.5 Oval cell-related microparticles to classify primary hepatic cancer

Podoplanin-expressing cells in nonlymphoid organs form parts of tertiary lymphoid structures during chronic inflammation (Peduto *et al.*, 2009). In addition, gp38 expression pattern differ in subpopulations of CD133-expressing liver cells, associated with HPC and indicate injury-specific changes (Eckert *et al.*, 2016), which was also confirmed within this study (Section 3.2). Furthermore, CD133 has been reported to identify putative cancer stem cells in HCC (Ma *et al.*, 2007; Yin *et al.*, 2007). Moreover, CD133 in combination with AnnexinV, EpCAM and ASGPR1 allowed detection of patients with liver disorders and further, distinction of patients with cirrhosis from patients with liver malignancies, due to MP surface profiles (Section 3.4). Based thereon, extension of the marker panel by gp38 in combination with AnnexinV, CD133 and EpCAM leads to the hypothesis to detect HPC-associated MPs, which possibly allow classification in HCC and CCA.

3.5.1 Liver disorders detectable by gp38/CD133 tumor-associated microparticles

AnnexinV⁺EpCAM⁺gp38⁺CD133⁻ and AnnexinV⁺EpCAM⁺gp38⁻CD133⁺ are identified by gating on AnnexinV⁺EpCAM⁺ taMPs (Section 3.4.1) followed by plotting gp38 against CD133 and gating on gp38 single positive taMPs (Figure 47, blue) as well as CD133 single positive taMPs (Figure 47, turquoise).

All probands and patients were examined for the correlation between levels of taMPs and gender, age [years] or BMI (Figure 48), to excluded dependencies on these parameters. For this purpose, values of AnnexinV⁺EpCAM⁺gp38⁺CD133⁻ taMPs (Figure 48, left) and AnnexinV⁺EpCAM⁺gp38⁻CD133⁺ taMPs (Figure 48, right) of all cohorts of the current study were separated in females and males (Figure 33A). Values refer to 10³ AnnexinV⁺ MPs and are given as mean ± SEM. Statistical significance was verified by unpaired t test (two-tailed; **p*≤0.05, ***p*≤0.01, ****p*≤0.001). In addition, relation between values of taMPs subpopulations of all cohorts and corresponding age (Figure 48B) and BMI (Figure 48C) are displayed (Pearson's correlation, two-tailed).

The values of both taMP populations also do not differ between females (AnnexinV⁺EpCAM⁺gp38⁺CD133⁻: 2.2 ± 0.4, AnnexinV⁺EpCAM⁺gp38⁻CD133⁺: 28.5 ± 5.0) and males (AnnexinV⁺EpCAM⁺gp38⁺CD133⁻: 2.0 ± 0.4, AnnexinV⁺EpCAM⁺gp38⁻CD133⁺: 33.6 ± 3.6) as observed for MP populations described in the previous section – ‘Tumor-related microparticles to identify primary

hepatic cancer’. However, just low values of AnnexinV⁺EpCAM⁺gp38⁺CD133⁻ taMPs are detectable in human sera and correlations between AnnexinV⁺EpCAM⁺gp38⁺CD133⁻ taMP level and age or BMI, respectively, are non-existent. AnnexinV⁺EpCAM⁺gp38⁻CD133⁺ values also do not correlate with BMI but with increasing age taMP values expand ($r=0.323$, $p\leq 0.001$, $R^2=0.104$). Both tendencies are also observable for AnnexinV⁺EpCAM⁺CD133⁺ taMPs in the previous section.

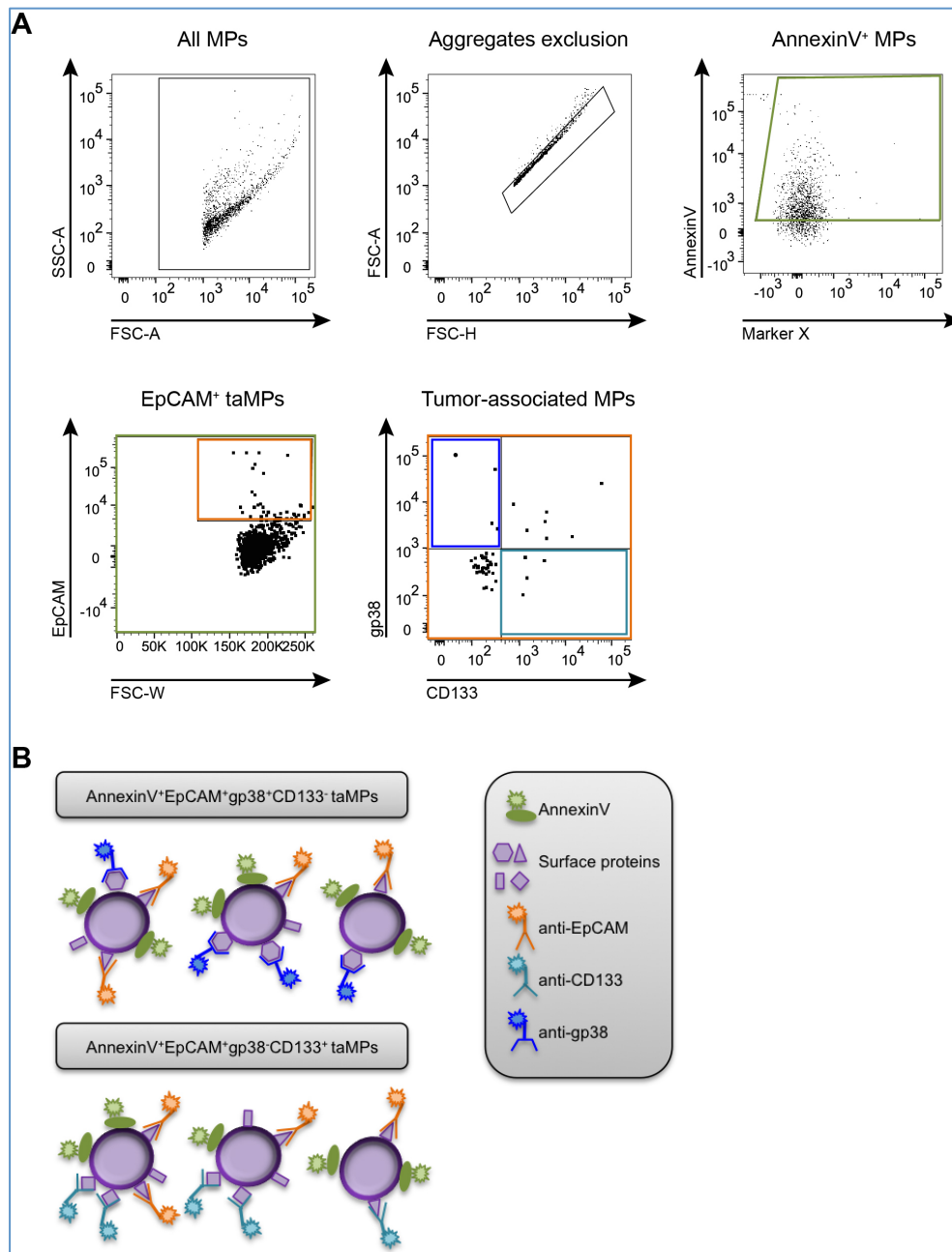


Figure 47: Detection of gp38/CD133 tumor-associated microparticles (taMPs) subpopulations by flow cytometry.
 A) Representative dot plot with corresponding gating strategy is depicted. Gating on all MPs is followed by aggregates exclusion and gating on AnnexinV⁺ MPs (green). Detection of AnnexinV⁺EpCAM⁺ taMPs is carried out by further gating on EpCAM⁺ events (orange). Identification of gp38/CD133 taMP subpopulations is ensued by further plotting gp38 against CD133 and gating on gp38 single positive events (blue) and CD133 single positive events (turquoise), respectively. MPs were stained with a panel of surface markers: AnnexinV, anti-EpCAM, anti-ASGPR1, anti-gp38 and anti-CD133. B) Illustration of gp38/CD133 taMPs subpopulations.

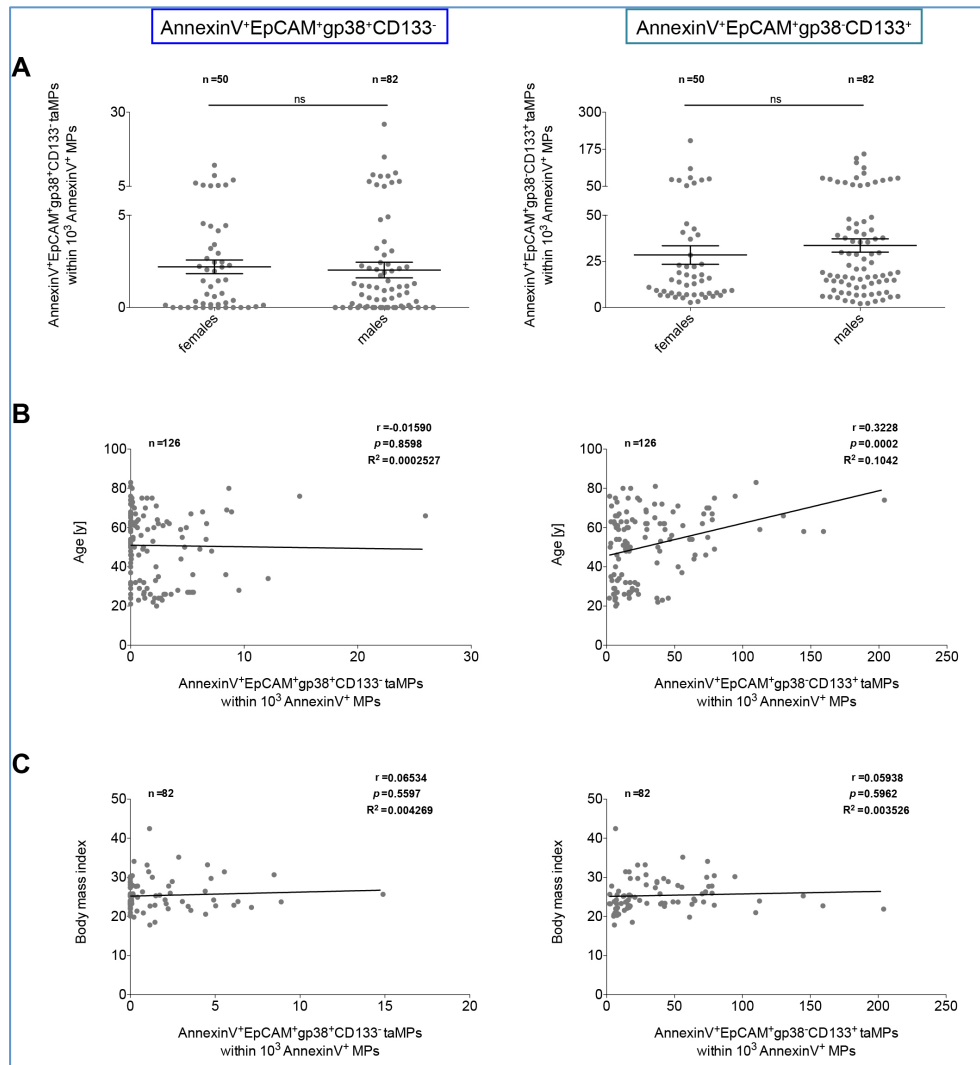


Figure 48: Detection of gp38/CD133 tumor-associated microparticle (taMP) subpopulations in human serum. MPs were isolated from sera of healthy probands, athletes, patients with cirrhosis and cancer patients bearing hepatocellular carcinoma, cholangiocarcinoma, non-small cell lung cancer and pancreatic cancer. A) AnnexinV⁺EpCAM⁺gp38⁺CD133⁻ taMPs (left) and AnnexinV⁺EpCAM⁺gp38⁺CD133⁺ taMPs (right) in dependency of gender, including all cohorts of the current study, are depicted. Values are given as mean ± SEM. Statistical significance was verified by unpaired t test (two-tailed; * $p \leq 0.05$, ** $p \leq 0.01$, *** $p \leq 0.001$). B-C) Calculated Pearson's correlation (two-tailed) between taMPs values and age [years] (B) and body mass index (C), respectively, of all cohorts participating in the current study are displayed. Indicated are the sample size (n), the corresponding Pearson's correlation coefficient (r), p value (p) and coefficient of determination (R²).

Values of taMPs of each cohort (Figure 49A) as well as in dependency of the gender (Figure 49B) are displayed and summarized in Table 24 for AnnexinV⁺EpCAM⁺gp38⁺CD133⁻ (Figure 49, left) and AnnexinV⁺EpCAM⁺gp38⁺CD133⁺ taMPs (Figure 49, right). Values of both taMP populations refer to 10³ AnnexinV⁺ MPs and are given as mean ± SEM. The 'Control' group consists of healthy probands and athletes. Differences were assessed by one-way ANOVA including Dunnett's test (* $p \leq 0.05$, ** $p \leq 0.01$, *** $p \leq 0.001$). Dotted line represents calculated cut-off values (Table 25).

In general, levels of AnnexinV⁺EpCAM⁺gp38⁺CD133⁻ taMPs are very low in all cohorts participating in the current study. The control cohort indicates 2.7 ± 0.4 AnnexinV⁺EpCAM⁺gp38⁺CD133⁻ taMPs per 10^3 AnnexinV⁺ MPs and does not differ between females (3.4 ± 0.7) and males (2.2 ± 0.5). A decrease of AnnexinV⁺EpCAM⁺gp38⁺CD133⁻ taMPs in patients with cirrhosis, HCC and CCA can be assumed (Cirrhosis: 1.6 ± 1.0 , HCC: 1.6 ± 0.6 , CCA: 1.9 ± 0.5). By virtue of low levels of this taMP population, only AnnexinV⁺EpCAM⁺gp38⁻CD133⁺ taMPs are considered further on.

The control cohort indicates 12.0 ± 1.4 AnnexinV⁺EpCAM⁺gp38⁻CD133⁺ taMPs per 10^3 AnnexinV⁺ MPs and do not differ between females (11.1 ± 1.8) and males (12.7 ± 2.0). Patients bearing NSCLC indicate about 1.2-fold increase of AnnexinV⁺EpCAM⁺gp38⁻CD133⁺ taMPs (14.9 ± 3.1) compared to the control cohort. However, females do not show an increase of AnnexinV⁺EpCAM⁺gp38⁻CD133⁺ taMPs (11.7 ± 1.3), whereas males values slightly increase (18.0 ± 6.1). Though, the sample size is low for both sexes (n=3). Levels of AnnexinV⁺EpCAM⁺gp38⁻CD133⁺ taMPs expand 2.7-fold in patients bearing PaCa (32.2 ± 8.9) compared to the control cohort, but only in males (40.1 ± 11.6) and not in females (16.5 ± 5.6). But here too, the sample size is very low (females: n=2, males: n=4). The same tendencies of AnnexinV⁺EpCAM⁺gp38⁻CD133⁺ taMPs are also observable for AnnexinV⁺EpCAM⁺CD133⁺ taMPs as described in the previous section. Due to almost no or low elevated taMP levels, diagnostic performance was not determined.

AnnexinV⁺EpCAM⁺gp38⁻CD133⁺ taMPs seem to be associated with liver disorders as indicated in elevated levels in this cohort as well as in the individually cohorts of cirrhosis, HCC and CCA. This tendency is also noticeable for AnnexinV⁺EpCAM⁺CD133⁺ taMPs as described in the previous section.

Level of AnnexinV⁺EpCAM⁺gp38⁻CD133⁺ taMPs increase significant between 3- and 4-fold in patients bearing liver disorders compared to the control cohort (Liver disorder: 42.3 ± 4.3 , $p \leq 0.001$; individually: Cirrhosis: 38.5 ± 6.3 , $p \leq 0.05$; HCC: 41.1 ± 6.9 , $p \leq 0.01$; CCA: 48.5 ± 9.3 , $p \leq 0.001$). Values are similar in both sexes for patients with liver disorders (females: 40.6 ± 7.9 ; males: 43.9 ± 5.0 , $p \leq 0.01$). Slightly increase of AnnexinV⁺EpCAM⁺gp38⁻CD133⁺ taMPs in females are observable in patients with cirrhosis and CCA (Cirrhosis: 24.3 ± 16.4 ; CCA: 27.6 ± 8.4), compared to significant increase of 3.4- and 5-fold, respectively, in males (Cirrhosis: 42.7 ± 7.0 , $p \leq 0.01$; CCA: 65.8 ± 13.9 , $p \leq 0.001$). In HCC, slightly increase of

AnnexinV⁺EpCAM⁺gp38⁺CD133⁺ taMPs are observable in males (30.7 ± 5.8), compared to significantly increase of 4.8-fold in females (53.7 ± 13.1 , $p \leq 0.05$). All this tendencies are also noticeable for AnnexinV⁺EpCAM⁺CD133⁺ taMPs as described in the previous section.

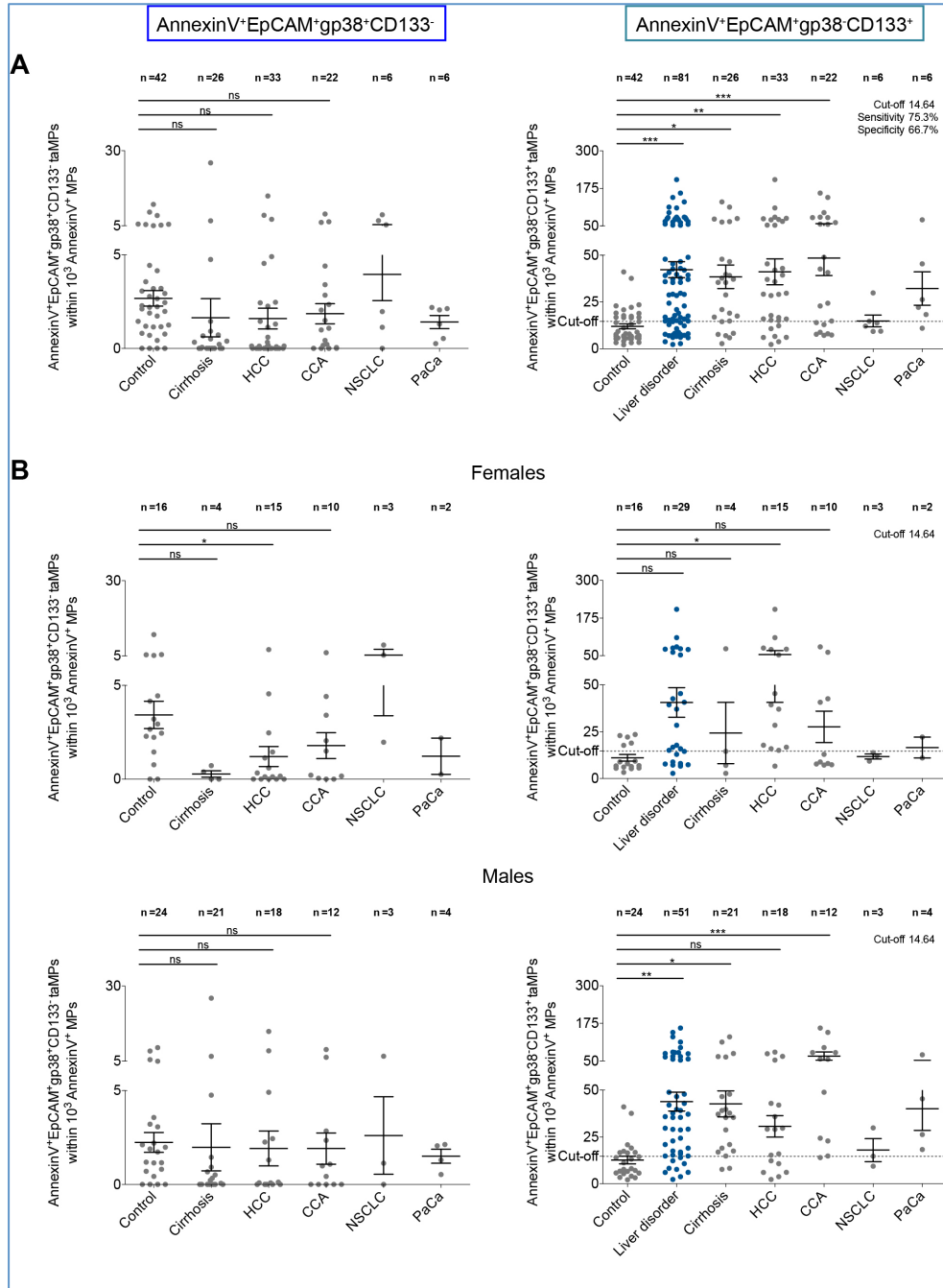


Figure 49: AnnexinV⁺EpCAM⁺gp38⁺CD133⁺ tumor-associated microparticles (taMPs) detect patients bearing liver disorders.

MPs were isolated from sera of control cohorts (healthy probands and athletes combined in one group), patients with cirrhosis and cancer patients bearing hepatocellular carcinoma (HCC), cholangiocarcinoma (CCA), non-small cell lung cancer (NSCLC) and pancreatic cancer (PaCa). The cohort 'liver disorder' combines patients with cirrhosis, HCC and CCA. A-B AnnexinV⁺EpCAM⁺gp38⁺CD133⁺ (left) and AnnexinV⁺EpCAM⁺gp38⁺CD133⁺ (right) values for each cohort of the current study (A) as well as in dependency of the gender (B) are displayed. Values are given as mean \pm SEM. Differences were assessed by one-way ANOVA including Dunnett's test (* $p \leq 0.05$, ** $p \leq 0.01$, *** $p \leq 0.001$). Dotted lines represent calculated cut-off values (Table 25).

Table 24: Values of AnnexinV⁺EpCAM⁺ gp38⁺/CD133⁺ tumor-associated microparticle (taMP) subpopulations from human serum of each cohort participated in the human cell-derived MPs study.
Values of AnnexinV⁺EpCAM⁺gp38⁺CD133⁺ and AnnexinV⁺EpCAM⁺gp38⁺CD133⁺ of each cohort as well as for females and males are depicted. Values refer to 10³ AnnexinV⁺ MPs and are given as mean ± SEM.

	Control	Liver disorder	Cirrhosis	HCC	CCA	NSCLC	PaCa
AnnexinV⁺EpCAM⁺gp38⁺CD133⁺ tumor-associated MPs							
Both	2.7 ±0.4	–	1.6 ±1.0	1.6 ±0.6	1.9 ±0.5	4.0 ±1.4	1.4 ±0.4
Female	3.4 ±0.7	–	0.3 ±0.2	1.2 ±0.5	1.8 ±0.7	5.3 ±1.9	1.2 ±1.0
Male	2.2 ±0.5	–	2.0 ±1.3	1.9 ±0.9	1.9 ±0.8	2.6 ±2.1	1.5 ±0.4
AnnexinV⁺EpCAM⁺gp38⁺CD133⁺ tumor-associated MPs							
Both	12.0 ±1.4	42.3 ±4.3	38.5 ±6.3	41.1 ±6.9	48.5 ±9.3	14.9 ±3.1	32.2 ±8.9
Females	11.1 ±1.8	40.6 ±7.9	24.3 ±16.4	53.7 ±13.1	27.6 ±8.4	11.7 ±1.3	16.5 ±5.6
Males	12.7 ±2.0	43.9 ±5.0	42.7 ±7.0	30.7 ±5.8	65.8 ±13.9	18.0 ±6.1	40.1 ±11.6

Control: Healthy probands and athletes combined in one group

Liver disorder: Cirrhosis, HCC and CCA combined in one group

HCC: Hepatocellular carcinoma

CCA: Cholangiocarcinoma

NSCLC: Non-small cell lung cancer

PaCa: Pancreatic cancer

Diagnostic performance of AnnexinV⁺EpCAM⁺gp38⁺CD133⁺ taMPs was evaluated for patients bearing liver disorders and the individually cohorts of cirrhosis, HCC and CCA by creating the corresponding ROC curves and determination of cut-off values, sensitivity [%] and specificity [%] as well as PPV [%] and NPV [%] (Table 25). Created ROC curves, including corresponding AUC and *p* values for

AnnexinV⁺EpCAM⁺gp38⁺CD133⁺ taMPs are displayed in Figure 50. The angle bisector corresponds to the line of identity, which indicates the lower limit for a diagnostic test. The MP population AnnexinV⁺EpCAM⁺gp38⁺CD133⁺ indicates a solid diagnostic potential to detect patients bearing liver disorders (sensitivity: 75.3 %, specificity: 66.7 %, PPV: 81.3 %, NPV: 58.3 %) and individually cirrhosis, HCC and CCA. What was also observed for AnnexinV⁺EpCAM⁺CD133⁺ taMPs in the previous section.

Table 25: Diagnostic performance of AnnexinV⁺EpCAM⁺gp38⁺CD133⁺ tumor-associated microparticles (taMPs) for patients bearing liver disorders.

Indicated are the AnnexinV⁺EpCAM⁺gp38⁺CD133⁺ values (mean ± SEM) and values of calculated cut-off, AUC ± SE of the ROC curves, *p* values as well as values of sensitivity [%], specificity [%], PPV [%] and NPV [%] for patients bearing liver disorders.

	Cut-off	Mean ±SEM	AUC ± SE	<i>p</i> Value	Sensitivity [%]	Specificity [%]	PPV [%]	NPV [%]
Control		12.0 ±1.4						
Liver disorder	14.64	42.3 ±4.3	0.8048 ±0.038	<0.001	75.31	66.67	81.33	58.33
Cirrhosis	14.45	38.5 ±6.3	0.8086 ±0.058	<0.001	80.77	66.67	60.00	84.85
HCC	14.75	41.1 ±6.9	0.7893 ±0.056	<0.001	78.79	66.67	65.00	80.00
CCA	14.61	48.5 ±9.3	0.8236 ±0.056	<0.001	68.18	66.67	51.72	80.00

SEM: Standard error of the mean

AUC ± SE: Area under curve ± standard error

PPV: Positive prediction value

NPV: Negative prediction value

Control: Healthy probands and athletes combined in one group

Liver disorder: Cirrhosis, HCC and CCA combined in one group

HCC: Hepatocellular carcinoma

CCA: Cholangiocarcinoma

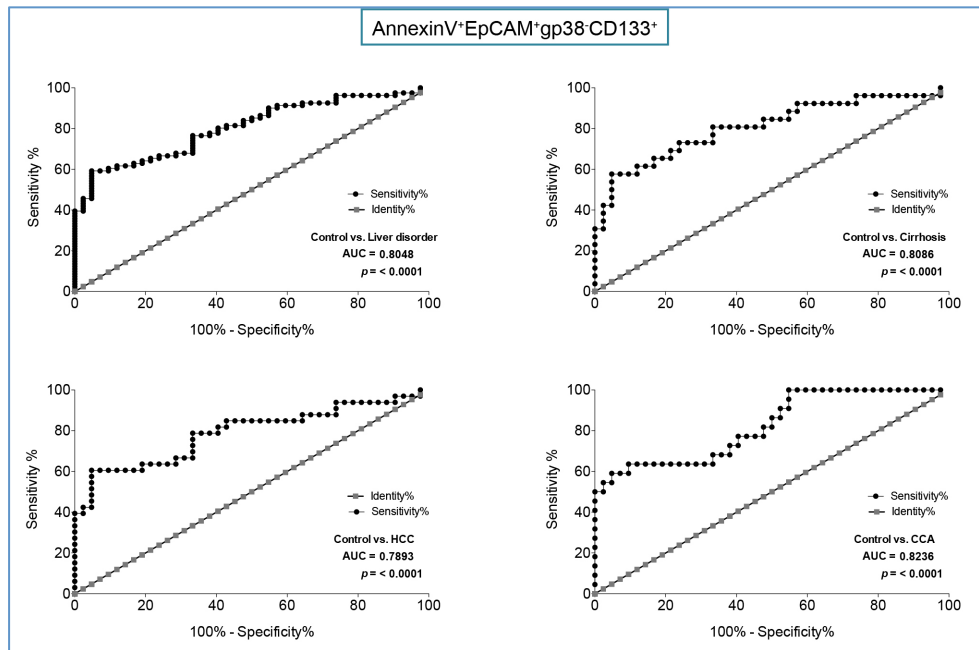


Figure 50: Diagnostic performance of AnnexinV⁺EpCAM⁺gp38⁺CD133⁺ tumor-associated microparticles (taMPs) for patients bearing liver disorders.

MPs were isolated from sera of control cohorts (healthy probands and athletes combined in one group), patients with cirrhosis and cancer patients bearing hepatocellular carcinoma (HCC) and cholangiocarcinoma (CCA). The cohort 'liver disorder' combines patients with cirrhosis, HCC and CCA. The receiver-operating characteristic (ROC) curves for the cohorts liver disorder, liver tumor, cirrhosis, HCC and CCA, including the corresponding area under curve (AUC) value as well as the *p* value (*p*, **p*≤0.05, ***p*≤0.01, ****p*≤0.001), are indicated. The angle bisector corresponds to the line of identity, which indicates the lower limit for a diagnostic test.

3.5.2 AnnexinV⁺ and AnnexinV⁺EpCAM⁺ oval cell-associated microparticle subpopulations differ in hepatocellular carcinoma and cholangiocarcinoma

AnnexinV⁺gp38⁺CD133⁺ oval cell-associated MPs (AnnexinV⁺ ocMPs) are identified by gating on AnnexinV⁺ MPs (Section 3.3.4) followed by plotting gp38 against CD133 and gating on gp38/CD133 double positive events (Figure 51, yellow). AnnexinV⁺EpCAM⁺gp38⁺CD133⁺ (AnnexinV⁺EpCAM⁺ ocMPs) are identified by gating on AnnexinV⁺EpCAM⁺ taMPs (Section 3.4.1) followed by plotting gp38 against CD133 and gating on gp38/CD133 double positive events (Figure 51, pink).

All probands and patients were examined for the correlation between levels of ocMP populations and gender, age [years] and BMI (Figure 52), to excluded dependencies on these parameters. For this purpose, values of AnnexinV⁺ ocMPs (Figure 52, left) and AnnexinV⁺EpCAM⁺ ocMPs (Figure 52, right) of all cohorts of the current study were separated in females and males (Figure 52A). Values refer to 10³ AnnexinV⁺ MPs and are given as mean ± SEM. Statistical significance was verified by unpaired t test (two-tailed; **p*≤0.05, ***p*≤0.01, ****p*≤0.001). Additionally, relation between values of ocMP

populations of all cohorts and corresponding age (Figure 52B) and BMI (Figure 52C) are displayed (Pearson's correlation, two-tailed).

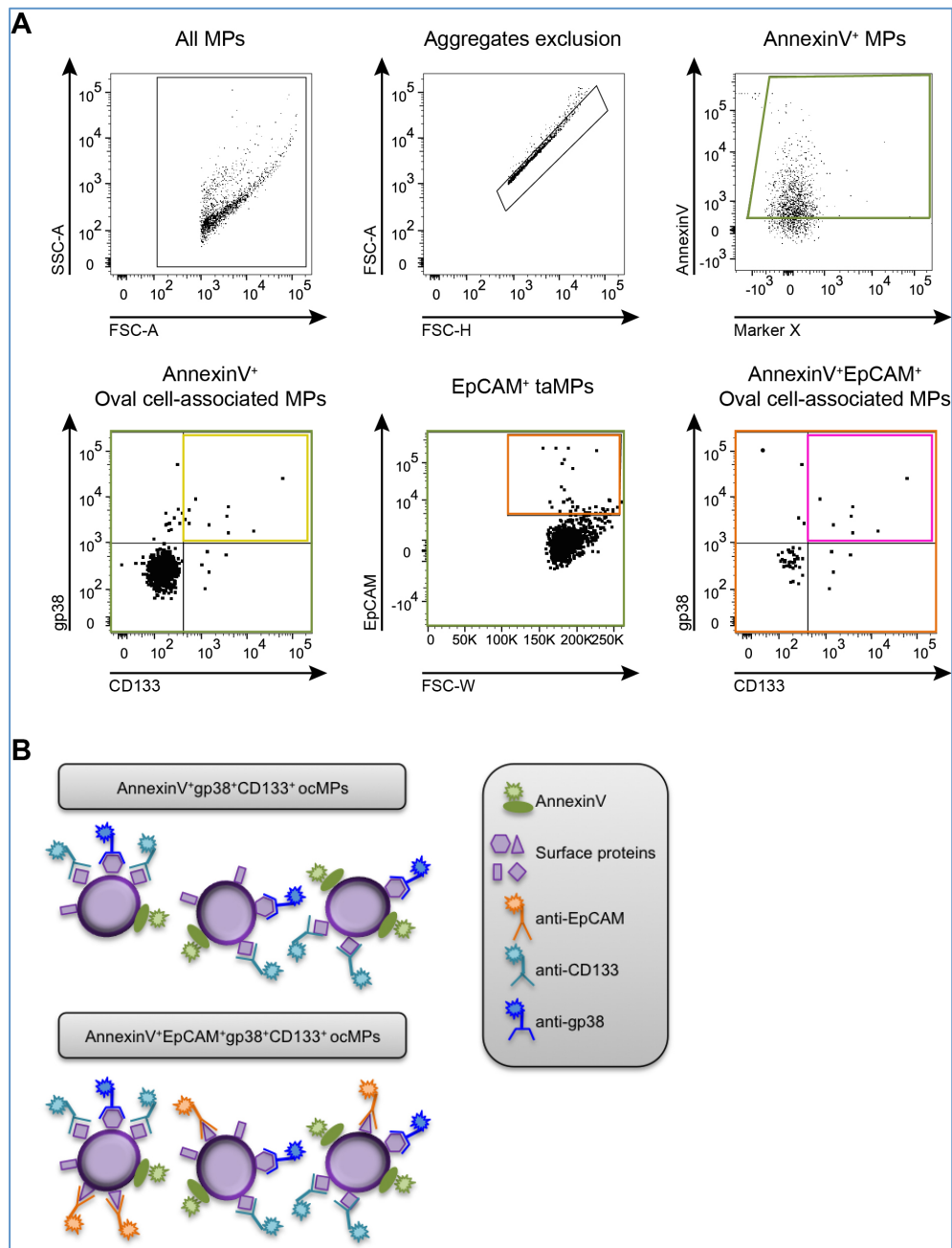


Figure 51: Detection of AnnexinV⁺ and AnnexinV⁺EpCAM⁺ oval cell-associated microparticles (ocMP) using flow cytometry analysis.

A) Representative dot plot with corresponding gating strategy is depicted. Gating on all MPs is followed by aggregates exclusion and gating on AnnexinV⁺ MPs (green). AnnexinV⁺ ocMPs: Identification of AnnexinV⁺gp38⁺CD133⁺ ocMPs by further plotting gp38 against CD133 and gating on gp38/CD133 double positive events (yellow). AnnexinV⁺EpCAM⁺ ocMPs: Detection of AnnexinV⁺EpCAM⁺gp38⁺CD133⁺ ocMPs is carried out by gating on EpCAM⁺ events (orange), followed by plotting gp38 against CD133 and gating on gp38/CD133 double positive events (pink). MPs were stained with a panel of surface markers: AnnexinV, anti-EpCAM, anti-ASGPR1, anti-gp38 and anti-CD133. B) Illustration of ocMPs populations.

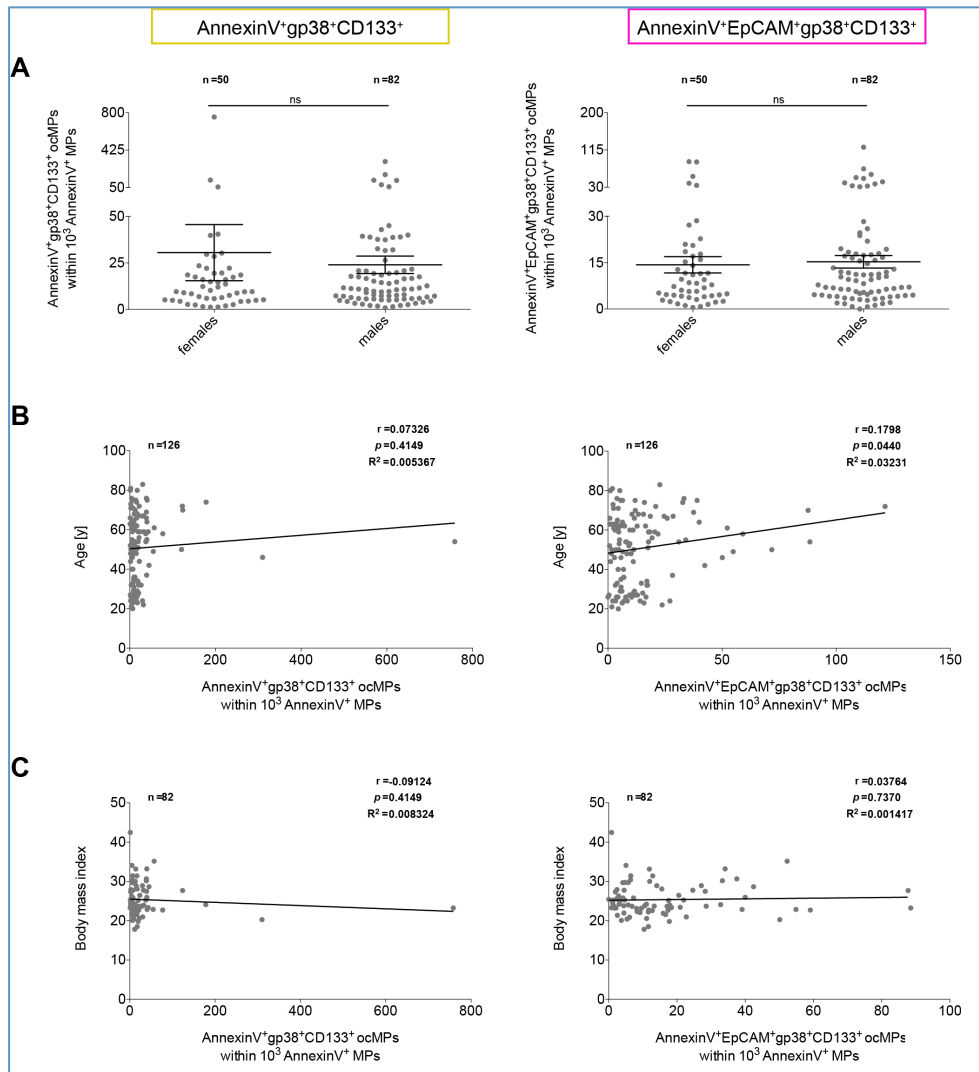


Figure 52: Detection of AnnexinV⁺ and AnnexinV⁺EpCAM⁺ oval cell-associated microparticles (ocMP) in human serum.

MPs were isolated from sera of healthy probands, athletes, patients with cirrhosis and cancer patients bearing hepatocellular carcinoma, cholangiocarcinoma, non-small cell lung cancer and pancreatic cancer. A) AnnexinV⁺gp38⁺CD133⁺ ocMPs (left) and AnnexinV⁺EpCAM⁺gp38⁺CD133⁺ ocMPs (right) in dependency of gender, including all cohorts of the current study, are depicted. Values are given as mean ± SEM. Statistical significance was verified by unpaired t test (two-tailed; * $p \leq 0.05$, ** $p \leq 0.01$, *** $p \leq 0.001$). B-C) Calculated Pearson's correlation (two-tailed) between ocMPs and age [years] (B) and body mass index (C), respectively, of all cohorts participating in the current study are displayed. Indicated are the sample size (n), the corresponding Pearson's correlation coefficient (r), p value (p) and coefficient of determination (R^2).

The values of both ocMP populations do not differ between females (AnnexinV⁺ ocMPs: 30.6 ± 15.1 , AnnexinV⁺EpCAM⁺ ocMPs: 14.3 ± 2.6) and males (AnnexinV⁺ ocMPs: 24.0 ± 4.7 , AnnexinV⁺EpCAM⁺ ocMPs: 15.3 ± 2.0). Correlation between BMI and ocMPs is non-existent, but with increasing age at least AnnexinV⁺EpCAM⁺ ocMPs seem to expand (AnnexinV⁺EpCAM⁺ ocMPs: $r=0.180$, $p=0.044$, $R^2=0.032$).

Values of ocMPs of each cohort (Figure 53A) as well as in dependency of the gender (Figure 53B) are displayed and summarized in Table 26 for AnnexinV⁺ ocMPs (Figure 53, left) and AnnexinV⁺EpCAM⁺ ocMPs (Figure 53, right). Values refer to

10^3 AnnexinV⁺ MPs and are given as mean \pm SEM. The ‘Control’ group consists of healthy probands and athletes. Differences were assessed by one-way ANOVA including Dunnett’s test ($*p \leq 0.05$, $**p \leq 0.01$, $***p \leq 0.001$). Dotted line represents calculated cut-off values (Table 27).

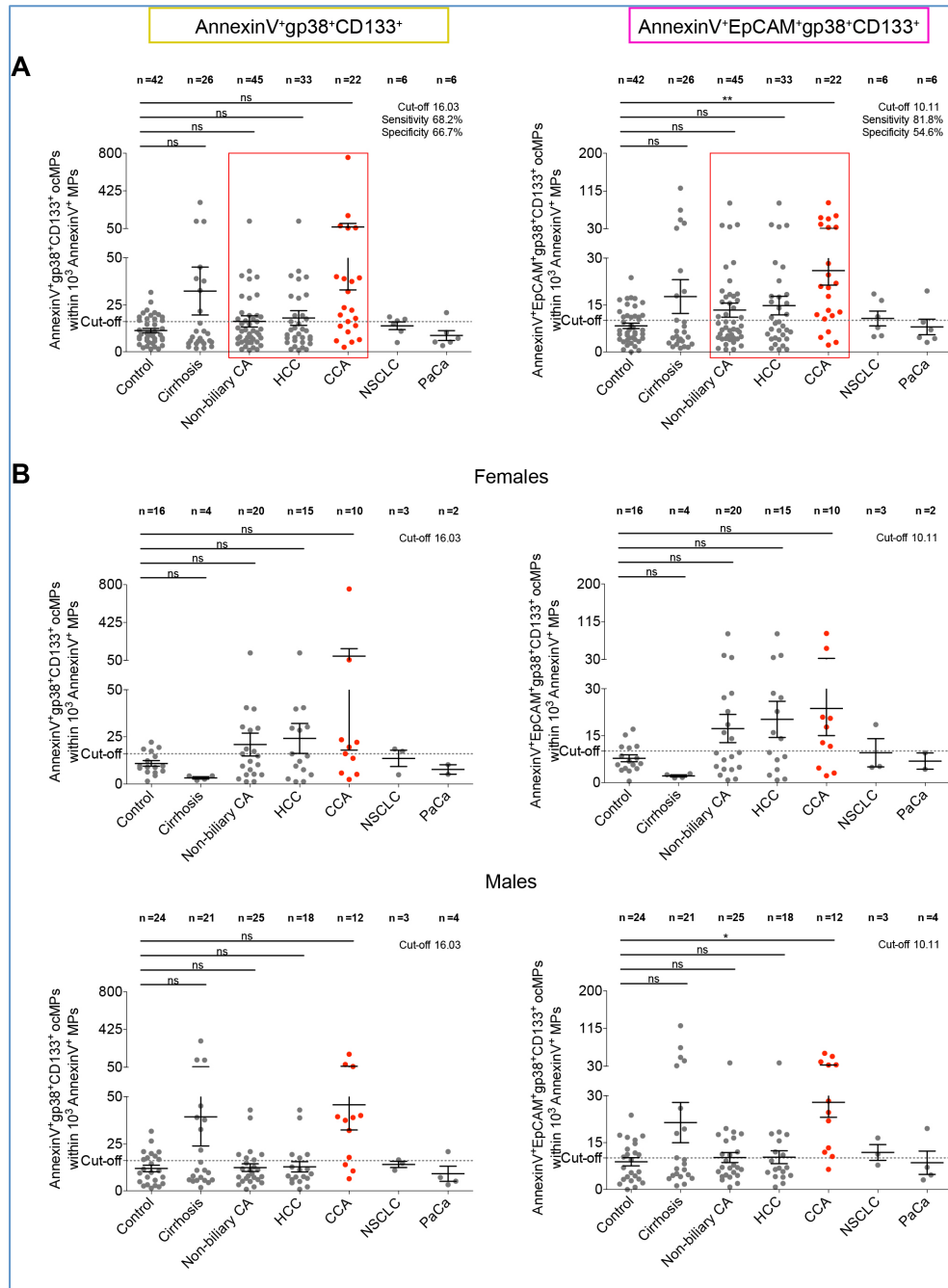


Figure 53: Oval cell-associated microparticles (ocMPs) differ patients bearing cholangiocarcinoma from patients bearing hepatocellular carcinoma.

MPs were isolated from sera of control cohorts (healthy probands and athletes combined in one group), patients with cirrhosis and cancer patients bearing hepatocellular carcinoma (HCC), cholangiocarcinoma (CCA), non-small cell lung cancer (NSCLC) and pancreatic cancer (PaCa). The cohort ‘non-biliary cancer (CA)’ combines cancer patients with HCC, NSCLC and PaCa. A-B) AnnexinV⁺gp38⁺CD133⁺ (left) and AnnexinV⁺EpCAM⁺gp38⁺CD133⁺ (right) values for each cohort of the current study (A) as well as in dependency of the gender (B) are displayed. Values are given as mean \pm SEM. Differences were assessed by one-way ANOVA including Dunnett’s test ($*p \leq 0.05$, $**p \leq 0.01$, $***p \leq 0.001$). Dotted lines represent calculated cut-off values (Table 27).

Table 26: Values of oval cell-associated microparticles (ocMPs) from human serum of each cohort participated in the human cell-derived MPs study.

Values of AnnexinV⁺gp38⁺CD133⁺ and AnnexinV⁺EpCAM⁺gp38⁺CD133⁺ of each cohort as well as for females and males are depicted. Values refer to 10³ AnnexinV⁺ MPs and are given as mean ± SEM.

	Control	Cirrhosis	Non-biliary CA	HCC	CCA	NSCLC	PaCa
AnnexinV⁺gp38⁺CD133⁺ oval cell-associated MPs							
Both	11.3 ±1.1	32.4 ±12.8	16.2 ±3.0	18.0 ±4.0	66.8 ±34.0	13.8 ±2.1	8.6 ±2.6
Females	10.9 ±1.5	3.3 ±0.6	20.9 ±6.1	24.2 ±7.9	92.2 ±74.2	13.6 ±4.4	7.7 ±2.5
Males	11.9 ±1.7	39.3 ±15.5	12.3 ±2.1	12.8 ±2.7	45.7 ±13.4	14.0 ±1.6	9.1 ±4.0
AnnexinV⁺EpCAM⁺gp38⁺CD133⁺ oval cell-associated MPs							
Both	8.4 ±0.9	17.7 ±5.4	13.4 ±2.2	14.8 ±2.9	26.0 ±4.6	10.7 ±2.4	8.0 ±2.5
Females	7.8 ±1.1	2.2 ±0.3	17.3 ±4.5	20.2 ±5.8	23.7 ±8.7	9.6 ±4.5	6.9 ±2.6
Males	8.9 ±1.3	21.4 ±6.4	10.2 ±1.6	10.3 ±2.1	27.9 ±4.8	11.9 ±2.5	8.6 ±3.7

Control: Healthy probands and athletes combined in one group

Non-biliary CA: Non-biliary cancer – HCC, NSCLC and PaCa combined in one group

HCC: Hepatocellular carcinoma

CCA: Cholangiocarcinoma

NSCLC: Non-small cell lung cancer

PaCa: Pancreatic cancer

The control cohort indicates 11.3 ± 1.1 AnnexinV⁺ ocMPs and 8.4 ± 0.9 AnnexinV⁺EpCAM⁺ ocMPs, respectively, per 10³ AnnexinV⁺ MPs and do not differ between females (AnnexinV⁺ ocMPs: 10.9 ± 1.5 , AnnexinV⁺EpCAM⁺ ocMPs: 7.8 ± 1.1) and males (AnnexinV⁺ ocMPs: 11.9 ± 1.7 , AnnexinV⁺EpCAM⁺ ocMPs: 8.9 ± 1.3).

Patients with cirrhosis indicate about 2.8 and 2-fold increase of AnnexinV⁺ ocMPs (32.4 ± 12.8) and AnnexinV⁺EpCAM⁺ ocMPs (17.7 ± 5.4), respectively, compared to the healthy control. Interestingly, only values in male increase (AnnexinV⁺ ocMPs: 39.3 ± 15.5 , AnnexinV⁺EpCAM⁺ ocMPs: 21.4 ± 6.4), whereas values in females decrease (AnnexinV⁺ ocMPs: 3.3 ± 0.6 , AnnexinV⁺EpCAM⁺ ocMPs: 2.2 ± 0.3). The latter, however, has a small sample size (n=4).

AnnexinV⁺ ocMPs and AnnexinV⁺EpCAM⁺ ocMPs indicate a slight increase of about 1.5-fold in patients with non-biliary CA, including HCC, NSCLC and PaCa, compared to the control cohort (AnnexinV⁺ ocMPs: 16.2 ± 3.0 , AnnexinV⁺EpCAM⁺ ocMPs: 13.4 ± 2.2). Obviously, increase is primary observable in females (AnnexinV⁺ ocMPs: 20.9 ± 6.1 , AnnexinV⁺EpCAM⁺ ocMPs: 17.3 ± 4.5) and not in males (AnnexinV⁺ ocMPs: 12.3 ± 2.1 , AnnexinV⁺EpCAM⁺ ocMPs: 10.2 ± 1.6). Values of ocMPs marginally differ from this in the individually cohorts of HCC (AnnexinV⁺ ocMPs: 18.0 ± 4.0 , AnnexinV⁺EpCAM⁺ ocMPs: 14.8 ± 2.9) and NSCLC (AnnexinV⁺ ocMPs: 13.8 ± 2.1 , AnnexinV⁺EpCAM⁺ ocMPs: 10.7 ± 2.4), whereas values in PaCa decrease compared to non-biliary CA (AnnexinV⁺ ocMPs: 8.6 ± 2.6 , AnnexinV⁺EpCAM⁺ ocMPs: 8.0 ± 2.5). Comparable values to non-biliary CA are observable in males of the individually cohorts HCC (AnnexinV⁺ ocMPs: 12.8 ± 2.7 , AnnexinV⁺EpCAM⁺ ocMPs: 10.3 ± 2.1), NSCLC (AnnexinV⁺ ocMPs: 14.0 ± 1.6 , AnnexinV⁺EpCAM⁺ ocMPs: 11.9 ± 2.5) and PaCa (AnnexinV⁺ ocMPs: 9.1 ± 4.0 , AnnexinV⁺EpCAM⁺ ocMPs: 8.6 ± 3.7). In contrast, values of females slightly expand in HCC (AnnexinV⁺ ocMPs: 24.2 ± 7.9 , AnnexinV⁺EpCAM⁺ ocMPs: 20.2 ± 5.8), and decrease in NSCLC (AnnexinV⁺ ocMPs: 13.6 ± 4.4 , AnnexinV⁺EpCAM⁺ ocMPs: 9.6 ± 4.5) and PaCa (AnnexinV⁺ ocMPs: 7.7 ± 2.5 , AnnexinV⁺EpCAM⁺ ocMPs: 6.9 ± 2.6). Though, the sample size for NSCLC and PaCa is low for both sexes. Values of AnnexinV⁺ ocMPs expand about 6-fold in CCA (66.8 ± 34.0) compared to the control cohort, whereas values in females increase more (92.2 ± 74.2) than in males (45.7 ± 13.4). However a greater deviation is observable for the values of this ocMP population. In contrast, AnnexinV⁺EpCAM⁺ ocMPs increase about 3-fold in CCA (26.0 ± 4.6) and do marginally differ in females (23.7 ± 8.7) and males (27.9 ± 4.8).

Under consideration of the screening method to identify liver tumor patients by use of MP profiling, as described in the previous section – ‘Tumor-related microparticles to identify primary hepatic cancer’, only HCC and CCA are considered further on.

In addition to the control cohort, patients with non-biliary CA (HCC, NSCLC and PaCa) serve as additional control (Figure 54A). Values of AnnexinV⁺ ocMPs (Figure 54, left) and AnnexinV⁺EpCAM⁺ ocMPs (Figure 54, right) refer to 10³ AnnexinV⁺ MPs and are given as mean ± SEM. Differences were verified by unpaired t test (two-tailed; * $p \leq 0.05$, ** $p \leq 0.01$, *** $p \leq 0.001$). Dotted line represents calculated cut-off values (Table 27).

Diagnostic performance of AnnexinV⁺ ocMPs and AnnexinV⁺EpCAM⁺ ocMPs were evaluated for patients bearing CCA in comparison to the control cohort, non-biliary CAs and HCC, respectively, by creating the corresponding ROC curves and determination of cut-off values, sensitivity [%] and specificity [%] as well as PPV [%] and NPV [%] (Table 27). Created ROC curves, including corresponding AUC and p values are displayed in Figure 54. The angle bisector corresponds to the line of identity, which indicates the lower limit for a diagnostic test.

Values of AnnexinV⁺ ocMPs and AnnexinV⁺EpCAM⁺ ocMPs expand significantly in CCA compared to the control cohort (AnnexinV⁺ ocMPs: $p \leq 0.05$, AnnexinV⁺EpCAM⁺ ocMPs: $p \leq 0.001$). AnnexinV⁺ ocMPs indicate a lower diagnostic performance (sensitivity: 68.2 %, specificity: 69.1 %, PPV: 53.6 %, NPV: 80.6 %) compared to AnnexinV⁺EpCAM⁺ ocMPs (sensitivity: 81.8 %, specificity: 61.9 %, PPV: 52.9 %, NPV: 86.7 %). The same goes for the comparison between CCA and non-biliary CAs. Differences between both are significant (AnnexinV⁺ ocMPs: $p \leq 0.05$, AnnexinV⁺EpCAM⁺ ocMPs: $p \leq 0.01$) and the diagnostic performance differs between AnnexinV⁺ ocMPs (sensitivity: 68.2 %, specificity: 66.7 %, PPV: 50.0 %, NPV: 81.1 %) and AnnexinV⁺EpCAM⁺ ocMPs (sensitivity: 81.8 %, specificity: 57.8 %, PPV: 48.7 %, NPV: 86.7 %). The same tendencies are observable in the comparison between the primary hepatic tumors CCA and HCC, albeit only AnnexinV⁺EpCAM⁺ ocMPs increase significantly in CCA ($p \leq 0.05$), compared to HCC. However, the diagnostic performance of AnnexinV⁺ ocMPs (sensitivity: 68.2 %, specificity: 66.7 %, PPV: 57.7 %, NPV: 75.9 %) and AnnexinV⁺EpCAM⁺ ocMPs (sensitivity: 81.8 %, specificity: 54.6 %, PPV: 54.6 %, NPV: 81.8 %) are in the same range like the others. Thus, AnnexinV⁺ ocMPs and AnnexinV⁺EpCAM⁺ ocMPs indicate a solid diagnostic performance.

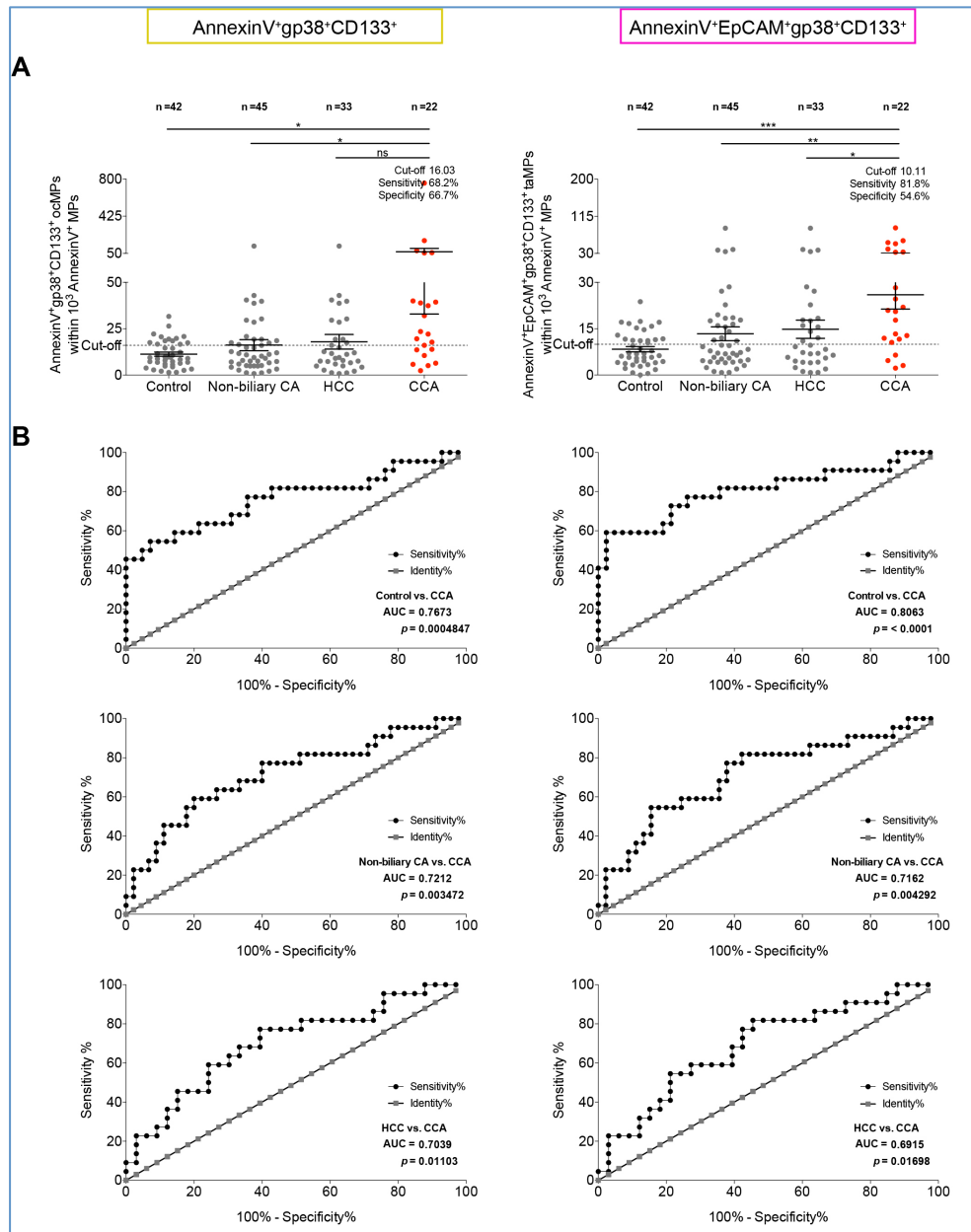


Figure 54: Diagnostic performance of AnnexinV⁺ and AnnexinV⁺EpCAM⁺ oval cell-associated microparticles (ocMPs) for patients bearing cholangiocarcinoma.

MPs were isolated from sera of control cohorts (healthy probands and athletes combined in one group) and patients bearing hepatocellular carcinoma (HCC), cholangiocarcinoma (CCA), non-small cell lung cancer (NSCLC) and pancreatic cancer (PaCa). The cohort 'non-biliary cancer (CA)' combines cancer patients with HCC, NSCLC and PaCa. A) Values of AnnexinV⁺gp38⁺CD133⁺ (left) and AnnexinV⁺EpCAM⁺gp38⁺CD133⁺ (right) are indicated. Values are given as mean \pm SEM. Differences were verified by unpaired t test (two-tailed; * $p \leq 0.05$, ** $p \leq 0.01$, *** $p \leq 0.001$). Dotted lines represent calculated cut-off values (Table 27). B) The receiver-operating characteristic (ROC) curves for the cohort CCA in comparison to the control cohort, non-biliary CA and HCC, respectively, including the corresponding area under curve (AUC) value as well as the p value (p , * $p \leq 0.05$, ** $p \leq 0.01$, *** $p \leq 0.001$) are indicated. The angle bisector corresponds to the line of identity, which indicates the lower limit for a diagnostic test.

Table 27: Diagnostic performance of AnnexinV⁺ and AnnexinV⁺EpCAM⁺ oval cell-associated microparticles (ocMPs) for patients bearing cholangiocarcinoma.

Indicated are the AnnexinV⁺gp38⁺CD133⁺ and AnnexinV⁺EpCAM⁺gp38⁺CD133⁺ values (mean ± SEM) and values of calculated cut-off, AUC ± SE of the ROC curves, *p* values as well as values of sensitivity [%], specificity [%], PPV [%] and NPV [%] for patients bearing cholangiocarcinoma in comparison to the control cohort, non-biliary cancers and hepatocellular carcinoma, respectively.

	Cut-off	AUC ± SE	<i>p</i> Value	Sensitivity [%]	Specificity [%]	PPV [%]	NPV [%]
AnnexinV⁺gp38⁺CD133⁺ oval cell-associated MPs							
Control vs. CCA	15.32	0.7673 ±0.069	<0.001	68.18	69.05	53.57	80.56
Non-biliary CA vs. CCA	16.03	0.7212 ±0.069	0.003	68.18	66.67	50.00	81.08
HCC vs. CCA	16.03	0.7039 ±0.072	0.011	68.18	66.67	57.69	75.86
AnnexinV⁺EpCAM⁺gp38⁺CD133⁺ oval cell-associated MPs							
Control vs. CCA	9.96	0.8063 ±0.064	<0.001	81.82	61.90	52.94	86.67
Non-biliary CA vs. CCA	10.11	0.7162 ±0.069	0.004	81.82	57.78	48.65	86.67
HCC vs. CCA	10.11	0.6915 ±0.073	0.017	81.82	54.55	54.55	81.82

SEM: Standard error of the mean

AUC ± SE: Area under curve ± standard error

PPV: Positive prediction value

NPV: Negative prediction value

Control: Healthy probands and athletes combined in one group

Non-biliary CA: Non-biliary cancer – HCC, non-small cell lung cancer and pancreatic cancer combined in one group

HCC: Hepatocellular carcinoma

CCA: Cholangiocarcinoma

Furthermore, correlation between tumor markers (AFP [ng/mL]), CEA [ng/mL]) or CA 19-9 [U/mL]) (Figure 55) or blood chemistry values (ALT [ng/mL]), bilirubin [mg/dL] or creatinine [mg/dL]) (Figure 56) and AnnexinV⁺ ocMPs (left) as well as AnnexinV⁺EpCAM⁺ ocMPs (right) are analyzed and displayed as Pearson's correlation (two-tailed). Included ocMPs levels were restricted to values above the cut-off for CCA and below the cut off for HCC (Table 27).

In CCA, AnnexinV⁺ ocMPs do not correlate with the tumor marker CEA, whereas AnnexinV⁺EpCAM⁺ ocMPs marginally negative correlate with CEA ($r=-0.164$, $p=0.529$, $R^2=0.027$). A marginally negative correlation is indicated also between CA 19-9 and AnnexinV⁺ ocMPs ($r=-0.231$, $p=0.522$, $R^2=0.053$). However, no correlation is indicated between CA 19-9 and AnnexinV⁺EpCAM⁺ ocMPs and the same goes for AFP and both ocMP populations.

Values of ocMPs in HCC seem to correlate more with tumor markers. CEA correlate marginally with both AnnexinV⁺ ocMPs and AnnexinV⁺EpCAM⁺ ocMPs (AnnexinV⁺ ocMPs: $r=0.106$, $p=0.665$, $R^2=0.011$; AnnexinV⁺EpCAM⁺ ocMPs: $r=-0.159$, $p=0.572$, $R^2=0.025$). In addition, high negative correlation between AFP and both ocMP populations is indicated (AnnexinV⁺ ocMPs: $r=-0.620$, $p=0.011$, $R^2=0.384$; AnnexinV⁺EpCAM⁺ ocMPs: $r=-0.735$, $p=0.004$, $R^2=0.540$). Moreover, CA 19-9 correlates with AnnexinV⁺ ocMPs ($r=0.532$, $p=0.028$, $R^2=0.283$) and not with AnnexinV⁺EpCAM⁺ ocMPs.

In CCA, AnnexinV⁺ ocMPs do not correlate with the serum marker ALT, whereas AnnexinV⁺EpCAM⁺ ocMPs marginally negative correlate with ALT ($r=-0.185$, $p=0.462$, $R^2=0.034$). No correlation between creatinine and both ocMPs populations is indicated. Interestingly, high correlation between bilirubin and both ocMP populations are observable (AnnexinV⁺ ocMPs: $r=0.874$, $p\leq 0.001$, $R^2=0.764$; AnnexinV⁺EpCAM⁺ ocMPs: $r=0.608$, $p=0.007$, $R^2=0.370$).

In contrast, correlation between HCC and serum marker are not existent, for neither AnnexinV⁺ ocMPs nor AnnexinV⁺EpCAM⁺ ocMPs, except a moderate correlation between AnnexinV⁺EpCAM⁺ ocMPs and bilirubin ($r=0.488$, $p=0.077$, $R^2=0.238$).

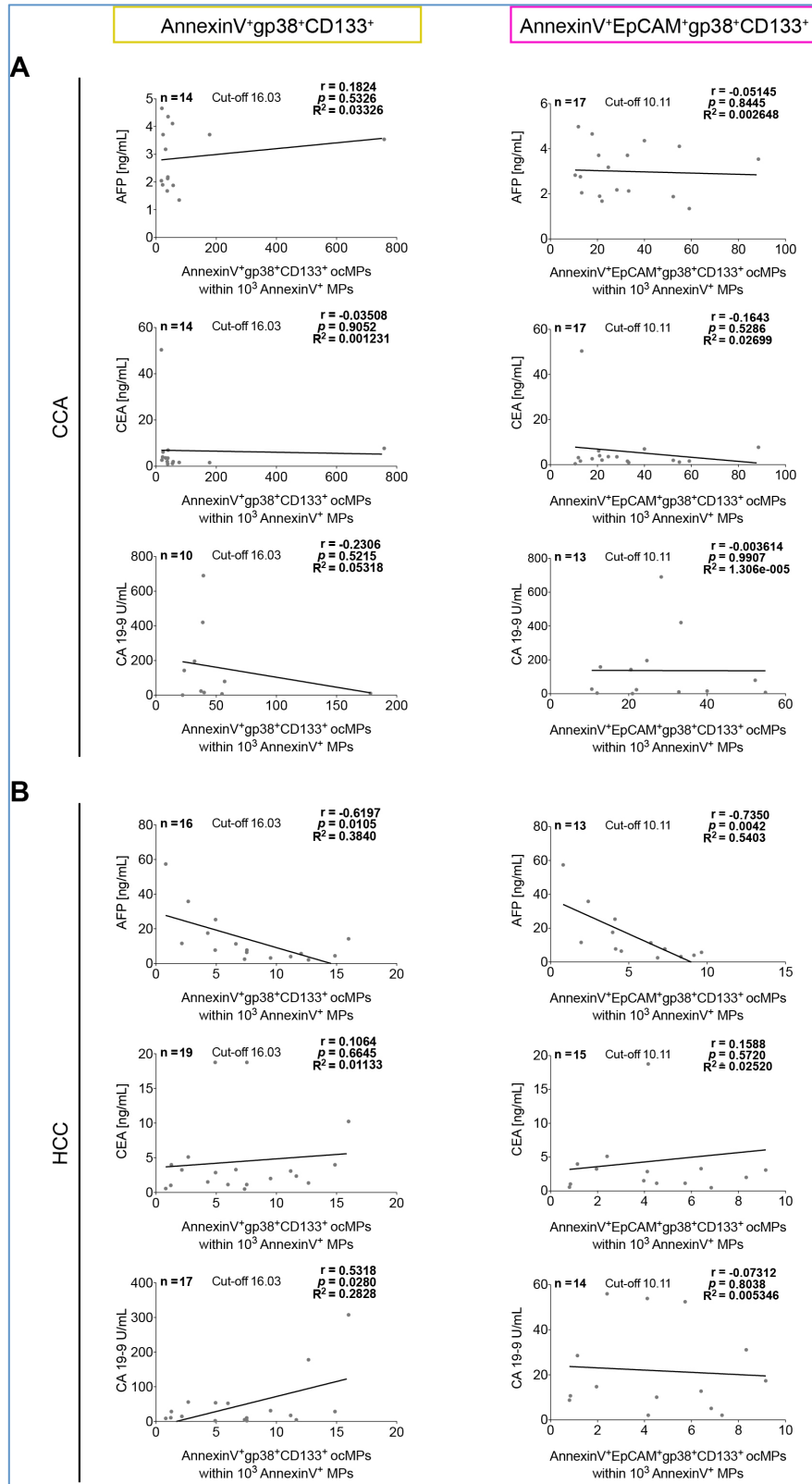


Figure 55: Serum tumor markers correlate moderately with AnnexinV⁺ and AnnexinV⁺EpCAM⁺ oval cell-associated microparticles (ocMPs) of patients bearing primary hepatic cancers.

MPs were isolated from sera of patients bearing cholangiocarcinoma (CCA) (A) and hepatocellular carcinoma (HCC) (B). Calculated Pearson's correlation (two-tailed) between AnnexinV⁺gp38⁺CD133⁺ (left) and AnnexinV⁺EpCAM⁺gp38⁺CD133⁺ values (right), respectively, and corresponding serum tumor marker such as: alpha-1 fetoprotein (AFP [ng/mL]), carcinoembryonic antigen (CEA [ng/mL]) or carbohydrate-antigen 19-9 (CA 19-9 [U/mL]) is displayed. Indicated are the sample size (n), the corresponding Pearson's correlation coefficient (r), p value (p) and coefficient of determination (R²). Included ocMP levels were restricted to values above and below the cut-off for patients bearing CCA and HCC, respectively (Table 27).

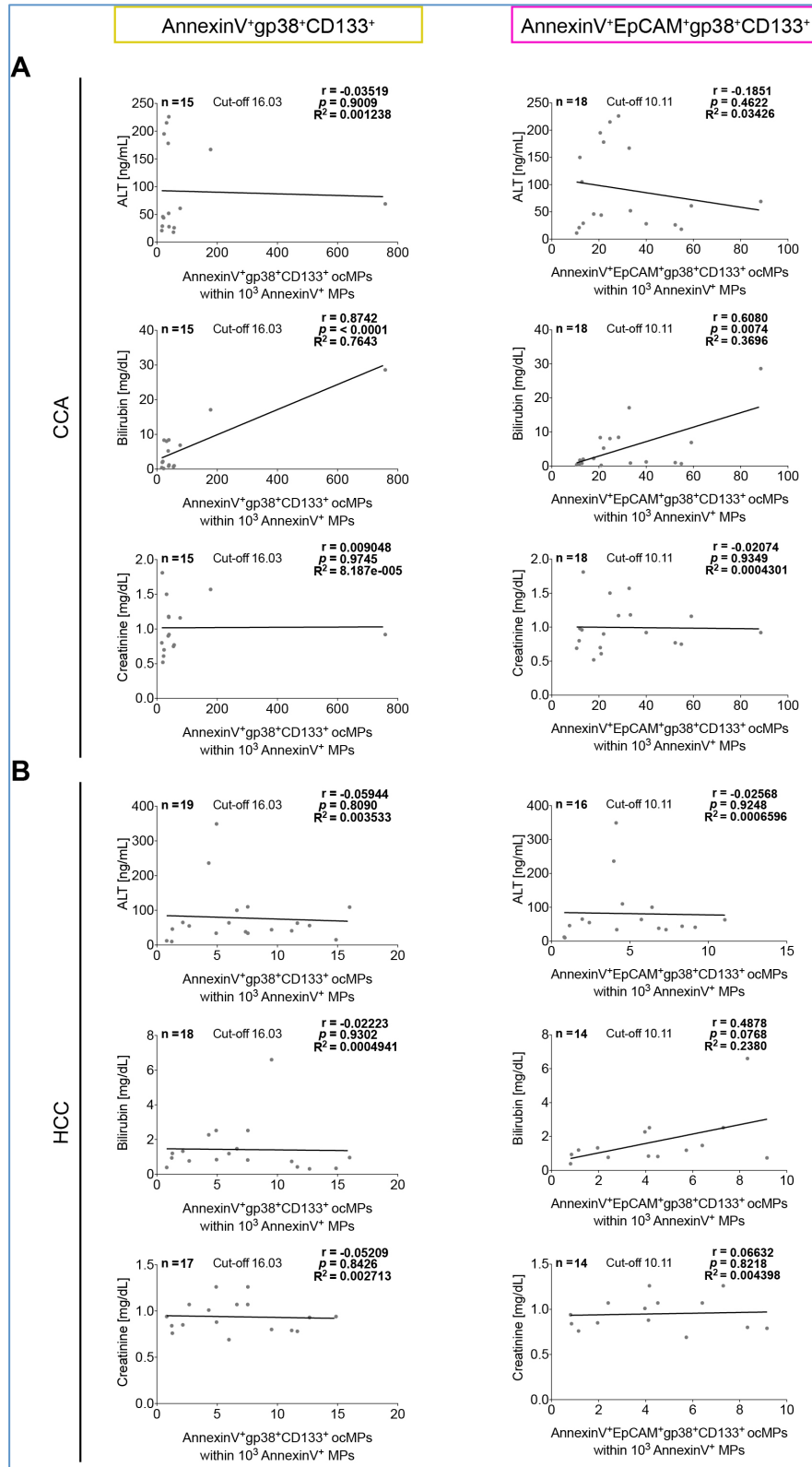


Figure 56: Blood chemistry values correlate almost not with AnnexinV⁺ and AnnexinV⁺EpCAM⁺ oval cell-associated microparticles (ocMPs) of patients bearing primary hepatic cancers.

MPs were isolated from sera of patients bearing cholangiocarcinoma (CCA) (A) and hepatocellular carcinoma (HCC) (B). Calculated Pearson's correlation (two-tailed) between AnnexinV⁺gp38⁺CD133⁺ (left) and AnnexinV⁺EpCAM⁺gp38⁺CD133⁺ values (right), respectively, and corresponding blood chemistry values such as: alanine transaminase (ALT [ng/mL]), bilirubin [mg/dL] or creatinine [mg/dL]) are displayed. Indicated are the sample size (n), the corresponding Pearson's correlation coefficient (r), p value (p) and coefficient of determination (R²). Included ocMP levels were restricted to values above and below the cut-off for patients bearing CCA and HCC, respectively (Table 27).

3.5.3 Summary - Oval cell-related microparticles to classify primary hepatic cancer

The taMP population AnnexinV⁺EpCAM⁺gp38⁺CD133⁻ is almost not detectable in human sera as indicated by low values of this taMP population. In contrast, AnnexinV⁺EpCAM⁺gp38⁻CD133⁺ taMPs seem to specifically identify patients with liver disorders due to significant elevated values of these taMP populations in patients bearing HCC, CCA and cirrhosis, which is confirmed by a solid diagnostic performance. Hence, AnnexinV⁺EpCAM⁺gp38⁻CD133⁺ taMPs may serve as marker to identify patients with liver disorders in addition to AnnexinV⁺EpCAM⁺CD133⁺ and AnnexinV⁺EpCAM⁺CD133⁺ASGPR1⁺ after using the suggested pan-cancer marker AnnexinV⁺EpCAM⁺ taMPs as first cancer detection-step (Section 3.4.1 & Section 3.4.5). Additionally, liver disorders seem to be distinguished in liver malignancies (HCC and CCA) and cirrhosis without malignancies by use of AnnexinV⁺EpCAM⁺ASGPR1⁺ taMPs. Cancer patients indicate an increased level of AnnexinV⁺EpCAM⁺ASGPR1⁺ taMPs in contrast to low levels of AnnexinV⁺EpCAM⁺ASGPR1⁺ taMPs in patients with cirrhosis (Section 3.4.3 & Section 3.4.5).). In consequence of this, 57 % of patients bearing liver tumors were correctly identified as primary hepatic cancer patients (Figure 57A, Figure 58). However, cancer detection by using AnnexinV⁺EpCAM⁺ taMPs as first step is limited, as indicated by 27 % of patients whose values are below the calculated cut-off. Additionally, 16 % of patients bearing primary hepatic cancers indicate values of liver tumor-associated taMPs below the calculated cut-off value.

However, using AnnexinV⁺gp38⁺CD133⁺ and AnnexinV⁺EpCAM⁺gp38⁺CD133⁺ ocMPs allowed a moderate classification of primary hepatic cancers in HCC and CCA. 52 % of patients with HCC and 59 % of patients with CCA were correctly classified by use of a four step approach: 1) Cancer detection using AnnexinV⁺EpCAM⁺ taMPs, 2) Confirmation of liver disorder by AnnexinV⁺EpCAM⁺CD133⁺, AnnexinV⁺EpCAM⁺CD133⁺ASGPR1⁺ and AnnexinV⁺EpCAM⁺gp38⁻CD133⁺ taMPs, 3) Detection of liver tumors by elevated levels of AnnexinV⁺EpCAM⁺ASGPR1⁺ taMPs or detection of non-tumor-bearing patients with cirrhosis by low levels of AnnexinV⁺EpCAM⁺ASGPR1⁺ taMPs, 4) Classification in CCA by elevated levels of AnnexinV⁺gp38⁺CD133⁺ and AnnexinV⁺EpCAM⁺gp38⁺CD133⁺ ocMPs or classification in HCC by low levels of these ocMP populations (Figure 57B-C;

Figure 58). 48 % of HCC patients and 41 % of CCA patients were not recognized. A moderate to solid diagnostic performance confirms this tendency.

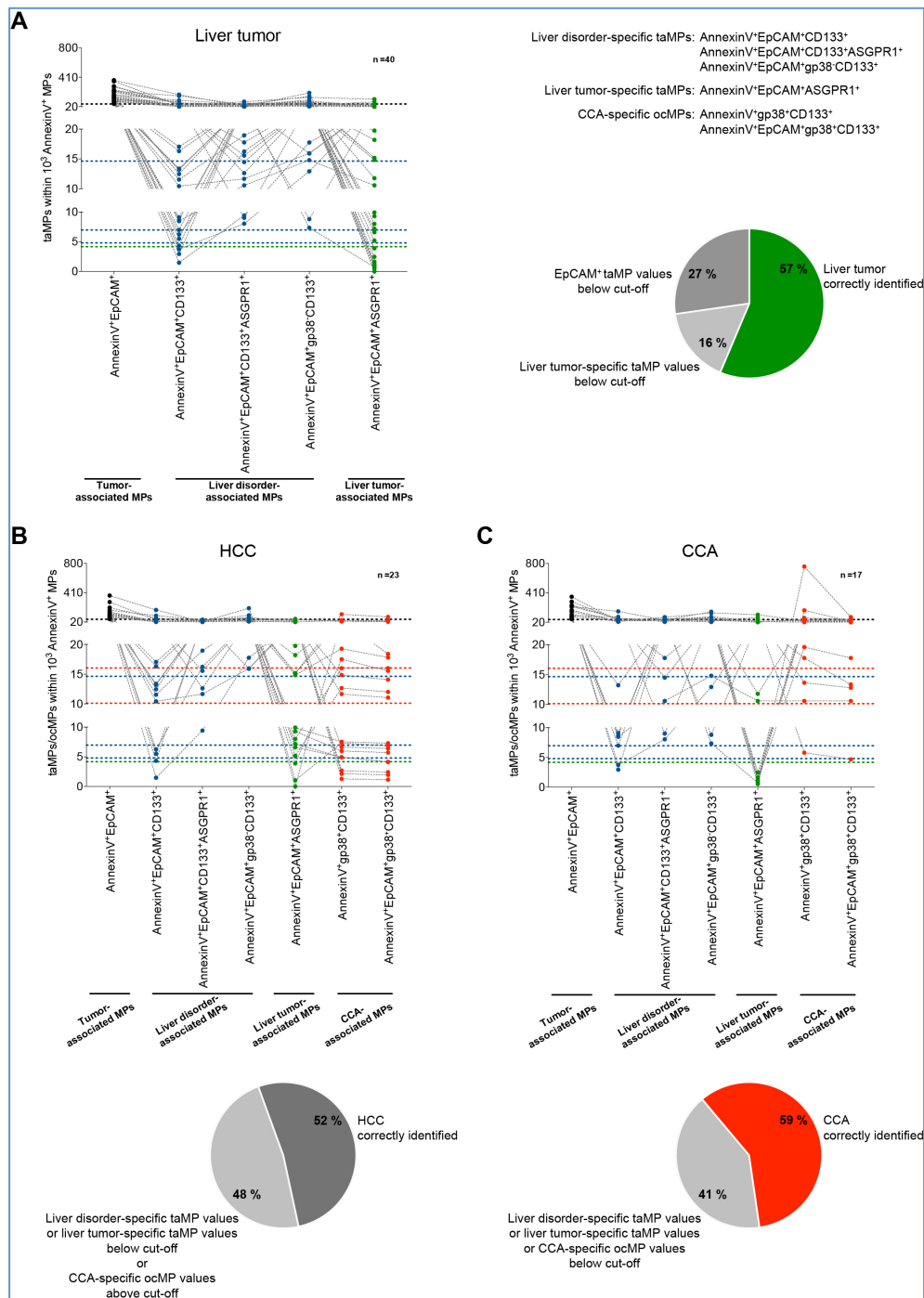


Figure 57: Oval cell-associated microparticles (ocMPs) on their diagnostic potential.

MPs were isolated from sera of patients bearing primary hepatic cancer (hepatocellular carcinoma (HCC) and cholangiocarcinoma (CCA)). A-C) Values of tumor-associated MPs (taMP) and ocMPs, respectively, individually for all patients with liver tumors (A) and separated into HCC (B) and CCA (C) are indicated. Dotted line represents calculated cut-off values for 1) Tumor-associated MPs: AnnexinV⁺EpCAM⁺ (Table 19, black), 2) Liver disorder-associated MPs: AnnexinV⁺EpCAM⁺CD133⁺ (Table 21, blue), AnnexinV⁺EpCAM⁺CD133⁺ASGPR1⁺ (Table 21, blue) and AnnexinV⁺EpCAM⁺gp38⁺CD133⁺ (Table 25, blue), 3) Liver tumor-associated MPs: AnnexinV⁺EpCAM⁺ASGPR1⁺ taMPs (Table 23, green) as well as 4) CCA-associated ocMPs: AnnexinV⁺gp38⁺CD133⁺ (Table 27, red) and AnnexinV⁺EpCAM⁺gp38⁺CD133⁺ (Table 27, red). Furthermore, percentage distributions of correctly identified patients with liver tumors (A, green) and individually for patients with HCC (B, dark grey) and CCA (C, red) are indicated as pie chart.

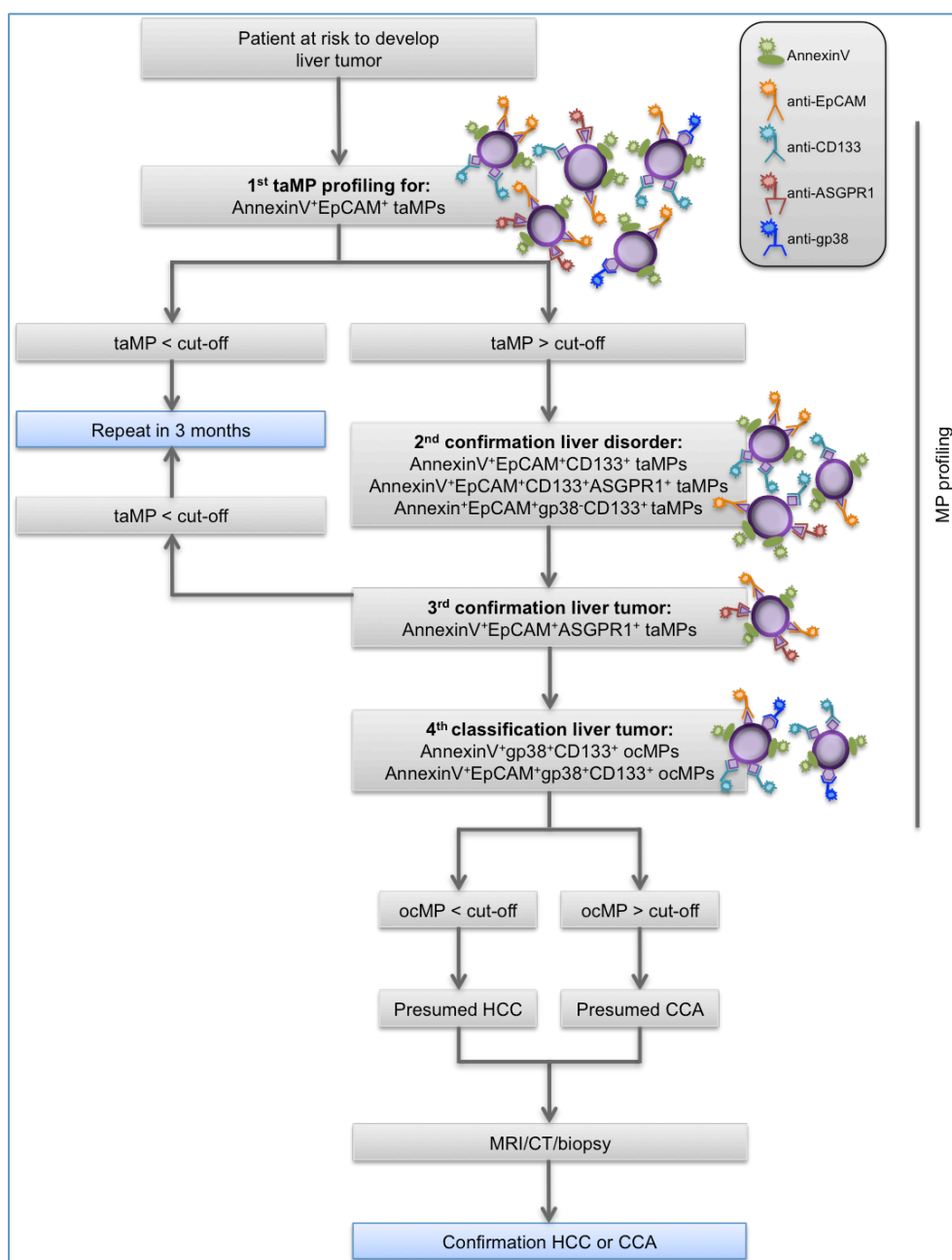


Figure 58: Proposal of a possible screening method to classify primary hepatic cancer in hepatocellular carcinoma and cholangiocarcinoma using several tumor- and oval cell-associated microparticle populations.

Workflow for a possibly application for a minimal invasive diagnostic tool to detect primary hepatic cancers and further classification into hepatocellular carcinoma (HCC) and cholangiocarcinoma (CCA) is depicted. First and foremost is a general screening for elevated levels of AnnexinV⁺EpCAM⁺ tumor-associated microparticles (taMPs), isolated from human sera, for patients at risk to develop liver tumors. Positively identified patients indicated by taMP levels above cut-off value follow three further detection steps. 1) Examination of the presence of a liver disease using liver disorder-associated taMP populations: AnnexinV⁺EpCAM⁺CD133⁺, AnnexinV⁺EpCAM⁺CD133⁺ASGPR1⁺ and AnnexinV⁺EpCAM⁺gp38⁺CD133⁺. 2) Discrimination into liver tumor or cirrhosis without malignancies using liver tumor-associated taMPs population: AnnexinV⁺EpCAM⁺ASGPR1⁺. 3) Classification of primary hepatic cancer into HCC and CCA using CCA-associated oval cell associated MP (ocMP) populations: AnnexinV⁺gp38⁺CD133⁺ and AnnexinV⁺EpCAM⁺gp38⁺CD133⁺. Patients with suspected HCC and CCA, respectively, will undergo tumor assessment with magnetic resonance imaging (MRI), computed tomography (CT) and biopsy (Modified according to Julich-Haertel, Urban, *et al.*, 2017).

4 Discussion

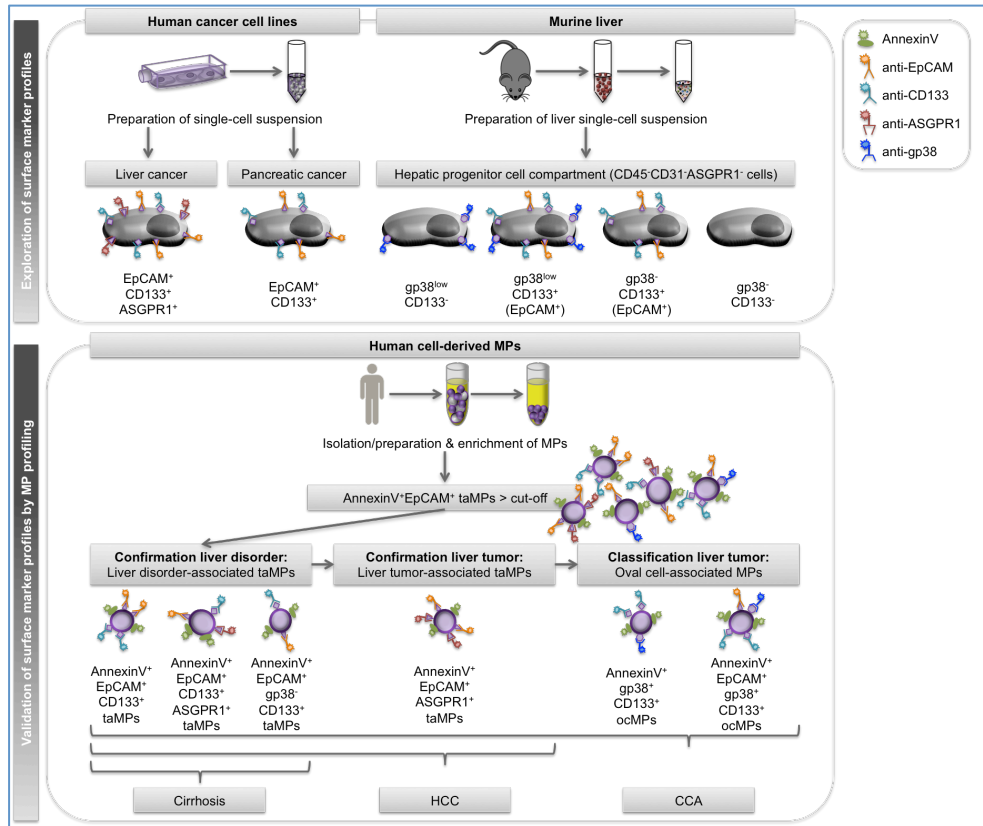


Figure 59: Summary of exploration and validation of surface marker profiles to examine microparticles (MPs) as novel minimal invasive liquid biopsy tool to identify and classify primary hepatic cancer.

First, exploration of surface marker profiles by means of the investigation of human cancer cell lines (top left) and the hepatic progenitor cell compartment (HPCC) of murine liver (top right) using flow cytometry analysis is depicted. Human cancer cell lines: Single-cell suspensions of liver cancer and pancreatic cancer cell lines were stained with a panel of surface markers: EpCAM, CD133, ASGPR1 and gp38. Liver cancer cell lines indicate EpCAM⁺CD133⁺ASGPR1⁺ cells and thus differ from EpCAM⁺CD133⁺ASGPR1⁻ pancreatic cancer cell lines. Murine liver: Liver single-cell suspension were stained with a panel of surface markers: CD45, CD31, ASGPR1, CD133, gp38 and EpCAM. CD45⁺CD31⁺ASGPR1⁺ cells correspond to the entire HPCC classified in four subtypes by their CD133 and gp38 expression: 1) gp38^{low}CD133⁻, 2) gp38^{low}CD133⁺(EpCAM⁺), 3) gp38⁺CD133⁺(EpCAM⁺) and 4) gp38⁺CD133⁻. Second, validation of surface marker profiles by MP profiling of human cell-derived MPs by the help of flow cytometry analysis is shown (bottom). MPs were stained with a panel of surface markers: AnnexinV, EpCAM, CD133, ASGPR1 and gp38. AnnexinV⁺EpCAM⁺ tumor-associated MPs (taMPs) expand (values above the cut-off) in patients bearing liver disorders (cirrhosis, hepatocellular carcinoma (HCC) or cholangiocarcinoma (CCA)). The presence of cirrhosis is confirmed by the presence of liver disorder-associated taMPs (AnnexinV⁺EpCAM⁺CD133⁺, AnnexinV⁺EpCAM⁺CD133⁺ASGPR1⁺, AnnexinV⁺EpCAM⁺gp38⁺CD133⁺). Further, patients bearing HCC indicate elevated values of liver disorder-associated MPs and liver tumor-associated taMPs (AnnexinV⁺EpCAM⁺ASGPR1⁺), whereas CCA patients show additionally elevated levels of oval cell-associated MPs (ocMPs) (AnnexinV⁺gp38⁺CD133⁺ and AnnexinV⁺EpCAM⁺gp38⁺CD133⁺).

4.1 Exploration of surface marker profiles

In order to detect primary hepatic cancer by the help of MP profiling, surface marker profiles of human cancer cell lines and the HPCC of murine liver were examined first and subsequent validated on human cell-derived MPs (Figure 59). For this purpose,

several surface markers suitable for flow cytometry analysis had to be chosen first, to examine them more closely.

The marker panel was divided into two main points. On the one hand surface markers to detect cancer, specifically to differentiate primary hepatic cancer from other cancer entities, were included. For this purpose, EpCAM in combination with CD133 and ASGPR1 were used to allow this. EpCAM was thought to identify epithelial cancers in general (Momburg *et al.*, 1987). ASGPR1 was shown to be expressed in a large number of human HCCs (Trerè *et al.*, 1999) and CD133 has been reported to identify putative cancer stem cells in HCC (Ma *et al.*, 2007; Yin *et al.*, 2007).

On the other hand surface markers to detect HPC-derived MPs were included based on their injury-specific changes within the expression pattern in murine liver (Eckert *et al.*, 2016). For this purpose, CD133 in combination with gp38 were used to identify liver cells with characteristics of liver progenitor cells.

4.1.1 Surface marker profiles differ liver cancer from pancreatic cancer cell lines

Surface marker profiles of established human cancer cell lines were investigated first. The cancer entities liver cancer and PaCa were each represented by three different human cancer cell lines including HuH7, HepG2 and SK-HEP-1 (liver cancer) as well as Panc-1, Capan-1 and Capan-2 (PaCa).

In general, liver cancer and PaCa cell lines indicate high expression of EpCAM and CD133, except the cell lines SK-HEP-1 and Panc-1, respectively.

EpCAM is expressed by most epithelial cell types and shows upregulation in several epithelial cancers (e.g. colorectal carcinoma, pancreas carcinoma, liver carcinoma, lung carcinoma) (Momburg *et al.*, 1987). This is confirmed by almost 100 % EpCAM⁺ cells among all living cells in the liver cancer cell lines HuH7 and HepG2. Compared thereto percentages of EpCAM⁺ cells among all living cells of PaCa cell lines differ between low (Panc-1), moderate (Capan-1) and high (Capan-2). These tendencies are confirmed by antibody bound per cell values by Thege *et al.* (2014), which indicate lower EpCAM counts for Panc-1 in comparison to Capan-1, probably based on a different size distribution.

CD133, a putative marker to identify cancer stem cells in HCC (Ma *et al.*, 2007; Yin *et al.*, 2007), is highly expressed by the liver cancer cell lines HuH7 and HepG2 as indicated by almost 100 % CD133⁺ cells among all living cells. Furthermore, CD133 was shown to be overexpressed in human PaCa tissue, but PaCa cell lines indicate a

wide range of CD133 expression (Moriyama *et al.*, 2010). Within this study, Panc-1 lacks CD133 expression, whereas Capan-2 and Capan-1 indicate moderate to high expression, respectively. Previous studies confirm these results (Lee *et al.*, 2011).

ASGPR1 expression is specific for liver cancer cell lines as indicated by high expression in both, HuH7 and HepG2. This is confirmed by previous studies, which show ASGPR1 expression uniquely by hepatocytes (Morell *et al.*, 1968), in addition to expression in a large number of human HCCs (Trerè *et al.*, 1999) and especially the cell line HepG2 is known to express ASGPR1 in a high level (Park *et al.*, 1998). Based on the lack of ASGPR1 expression by PaCa cell lines, about 50 % among all living cells correspond to EpCAM⁺CD133⁺ cells (except Panc-1) whereas almost all cells of the liver cancer cell lines seem to be EpCAM⁺CD133⁺ASGPR1⁺ (except SK-HEP-1).

The different expression pattern by the individual liver cancer cell lines suggest a classification into two subtypes of hepatocellular carcinoma: hepatic stem cell-like HCC (HuH7) and mature hepatocyte-like HCC (SK-HEP-1) (Yamashita *et al.*, 2009). This classification is mainly based on the expression of EpCAM and AFP. AFP⁺ liver cancer cell lines (HuH7) indicate subpopulations of CD133⁺ and EpCAM⁺ cells, whereas AFP⁻ liver cancer cell lines (SK-HEP-1) lack these expression patterns (Yamashita *et al.*, 2008). Interestingly, lack in gp38 expression is indicated for both, liver cancer and PaCa cell lines. However, expression pattern of surface marker allow discrimination of liver cancer cell lines from PaCa cell lines (Figure 59, top left).

4.1.2 The murine hepatic progenitor cell compartment

The murine HPCC was investigated within this part of the study. With reference to injury-specific changes within the expression pattern among the HPCC in murine liver (Eckert *et al.*, 2016) it was thought that at least the surface marker combination could be applied to human cell-derived MPs. However, the murine HPCC must be first examined and better understood. For this purpose, a novel digestion method for liver was established within this study (Julich-Haertel, Tiwari, *et al.*, 2017) developed based on Eckert *et al.* (2016), which is similar to the one used for lymph node stromal cells (Lukacs-Kornek *et al.*, 2011). Based on previous studies, CD133 in combination with gp38 were used to classify HPC subtypes (Eckert *et al.*, 2016). Referring to the varying expression pattern of CD133 and gp38, five subpopulations are identified among the CD45⁻CD31⁻ASGPR1⁻ cells: gp38^{high}CD133⁻, gp38^{low}CD133⁻, gp38^{low}CD133⁺, gp38⁻CD133⁺ and double negative cells (gp38⁻CD133⁻) (Figure 59, top right). The

gp38^{high}CD133⁻ cells were identified as mesothelial cells (Eckert *et al.*, 2016) and were not be considered within this study. To further determine differences between the cell subtypes under steady state, expression of surface markers and individual genes were examined, followed by the analysis of injury-specific changes within the HPCC.

4.1.2.1 Revising of the hepatic progenitor compartment in murine liver under steady state conditions

In healthy liver, the gp38^{low}CD133⁻ cells represents the rarest cell type, whereas gp38^{low}CD133⁺ and gp38⁻CD133⁺ progenitors represent the most common populations among the CD45⁻CD31⁻ASGPR1⁻ cells apart from cells lacking any gp38 and CD133 expression. These results are consistent with the revising of the HPCC by Eckert *et al.* (2016).

To further ascertain phenotypically differences between the progenitor subtypes, expression of several surface markers associated with mesenchymal stem and HPC under steady state were examined. All progenitor subpopulations among the CD45⁻CD31⁻ASGPR1⁻ cells indicate expression of ICAM-1. In general, ICAM-1 is expressed by various cell types (e.g. activated endothelial cells, T- and B-cells and monocytes) and during inflammation expression of ICAM-1 increases (Dustin *et al.*, 1986). Furthermore, ICAM-1 indicate to mediate the adhesion between lymphocytes and mesenchymal stem cells (Ren *et al.*, 2010). Moreover, all either CD133 or gp38-expressing progenitor subtypes among the CD45⁻CD31⁻ASGPR1⁻ cells, except gp38⁻CD133⁻ cells, indicate expression of Sca-1. However, Sca-1 expression by gp38⁻CD133⁺ is much less compared to both gp38^{low}-expressing subtypes (gp38^{low}CD133⁻ and gp38^{low}CD133⁺). In general, Sca-1 was shown to be a surface protein on hematopoietic and mesenchymal stem cells in the mouse (Baddoo *et al.*, 2003; Morikawa *et al.*, 2009; Spangrude *et al.*, 1988). The expression of ICAM-1 and Sca-1 to a greater or lesser extent by the individual subtypes portend that cells with characteristics of mesenchymal stem cells are present among the progenitor subpopulations.

Otherwise, progenitor subpopulations differ in surface marker expression patterns as indicated by specific expression of CD34 and CD90.2 in gp38^{low}CD133⁻ cells. Actually, CD34 serves as marker for hematopoietic stem cells (Andrews *et al.*, 1989; Civin *et al.*, 1984; Krause *et al.*, 1996) and is also associated to mark bone marrow-mesenchymal stem cells and adipose tissue-derived stem cells (C.S. Lin *et al.*, 2012). In addition,

expression of CD90 is associated with mesenchymal stem cells as well (Hoppe *et al.*, 2004). In summary, among the $gp38^{low}CD133^{-}$ subpopulation occur ICAM-1, Sca-1, CD34 and CD90.2-expressing cells. This suggests that $gp38^{low}CD133^{-}$ cells mainly present cells with characteristics of mesenchymal stem cells. In general, mesenchymal stem cells, originally isolated from bone marrow (Friedenstein *et al.*, 1966; Pittenger *et al.*, 1999), indicate a spindle-shaped morphology (Wagner *et al.*, 2005) and are described as multipotent cells with differentiation potential into mesodermal, ectodermal, endodermal cell lineages (Kopen *et al.*, 1999; Pittenger *et al.*, 1999; Sato *et al.*, 2005). Mesenchymal stem cells have also been isolated from other tissues including the liver (Bieback *et al.*, 2004; da Silva Meirelles *et al.*, 2006; Kuznetsov *et al.*, 2001; Zuk *et al.*, 2001), but differentiation ability, biomarkers and biological functions vary widely among the different origins (Kern *et al.*, 2006; Wagner *et al.*, 2007). However, previous studies showed that mesenchymal stem cells isolated and expanded *in vitro* have the ability to differentiate into hepatocyte-like cells (Banas *et al.*, 2009).

In contrast, either CD133 or gp38-expressing progenitor subtypes among the $CD45^{-}CD31^{-}ASGPR1^{-}$ cells, except $gp38^{-}CD133^{-}$ cells, indicate MIC1-1C3 expression. However, MIC1-1C3 expression by $gp38^{low}CD133^{-}$ cells is much less compared to both CD133-expressing subtypes ($gp38^{low}CD133^{+}$ and $gp38^{-}CD133^{+}$). MIC1-1C3, a duct cell surface marker, is thought to be a marker for cells undergoing an oval cell response (Dorrell *et al.*, 2008, 2011). In addition, CD133-expressing progenitors ($gp38^{low}CD133^{+}$ and $gp38^{-}CD133^{+}$) indicate specific expression of the oval cell associated markers EpCAM and CD24 (Okabe *et al.*, 2009; Qiu *et al.*, 2011; Yovchev *et al.*, 2007). The ovoid cell populations named ‘oval cells’ were first described by Farber (1956). These are unique undifferentiated cells, which arise under pathological conditions (e.g. chronic viral hepatitis, alcoholic liver disease, NAFLD) by the time liver injury limits the self-renewal potential. By the help of flow cytometry-based isolation in combination with surface markers (e.g. EpCAM, CD133 or, MIC1-1C3) an following *in vitro* cultivation could be shown that oval cells indicate clonogenic potential, which can differentiate into cholangiocytes and hepatocytes under certain culture conditions (Miyajima *et al.*, 2014). Gene expression analysis of the heterogeneous $CD133^{+}$ cell population substantiate the association of these cells with oval cells by the expression of genes associated with oval cells (KRT19, HNF4A), EMT (CDH1), Hippo signaling pathway (YAP1), apoptosis and inflammation (FAS, CCL2) or liver specific genes (HNF1A, HNF1B, HNF4A, HNF6). Isolation of the individual CD133-expressing subtypes ($gp38^{low}CD133^{+}$ and

gp38⁺CD133⁺) by fluorescence-activated cell sorting and further characterization by qPCR showed expression of several genes associated with oval cells in both populations: 1) Transcription factors associated with oval cells (FoxJ1 and Sox9), 2) Genes associated with oval cells (albumin, AFP, cytokeratin 7 and 19) and 3) Genes involved in pathways associated with oval cells (Notch, Hedgehog, Wnt and Hippo signaling pathway (Eckert *et al.*, 2016). This confirms the investigations within this study and suggests that both CD133-expressing populations among the CD45⁺CD31⁺ASGPR1⁺ cells represent cells with oval cell-characteristics.

The double negative population, which lacks any gp38 and CD133 expression, indicate low expression of CD24 and ICAM-1. Thus, this suggests being a heterogeneous cell population, which requires further characterization.

4.1.2.2 Populations of the hepatic progenitor cell compartment change liver injury-specific

To further ascertain differences between the individual progenitor subtypes, various models to induce liver injuries were utilized, including TAA-induced fibrosis, a model of NASH (CDE-diet) and cholestatic liver injury (DDC-diet). TAA, a centrilobular hepatotoxicant, undergoes bioactivation to its S-oxide and S,S-dioxide. The latter is a reactive metabolite, which presumably induce cellular necrosis (Chilakapati *et al.*, 2005; Hajovsky *et al.*, 2012), elevated transaminase activity and liver fibrosis within six weeks (Salguero Palacios *et al.*, 2008). In contrast, CDE-diet leads to a strong NASH development through metabolic changes in hepatocytes, resulting in deposition of lipids and lethal deterioration of hepatocytes. As a consequence, oval cells get activated and proliferate (Kroy *et al.*, 2010; Liedtke *et al.*, 2013; Shinozuka *et al.*, 1978; Ueberham *et al.*, 2010). In addition, DDC-feeding was also utilized to activate oval cells. Feeding with DDC leads to hepatocyte injury, resulting in the inhibition of tissue repair, followed by oval cell activation and proliferation (Jakubowski *et al.*, 2005).

The treatment with TAA and CDE, respectively, lead to an increase of the entire HPCC in both percentages and cell counts, whereas DDC-treatment show just a slight increase in frequencies and decrease in cell counts during the DDC-progression phase.

Cells expressing only gp38 (gp38^{low}CD133⁺) are not affected by the treatment with TAA and CDE, respectively, over the entire period, neither in percentages nor in cell counts. The same could be observed in another NASH model (methionine and choline-deficient diet, MCD-diet) and during carbon tetrachloride (CCL₄)-induced fibrosis

(Eckert *et al.*, 2016). However, Sca-1 expression increases in gp38^{low}CD133⁻ cells after seven days and in turn decreases after 14 days CDE-feeding, compared to the healthy control.

In contrast, gp38^{low}CD133⁻ cells expand in frequency and cell count during the progression and regression phase of DDC-treatment, albeit only significantly in frequency of seven day DDC-fed mice. This increase of gp38^{low}CD133⁻ cells was also shown in a model of spontaneously progressive biliary fibrosis (multidrug resistance protein 2-knockout, MDR2-KO) (Eckert *et al.*, 2016). This suggests a contribution of gp38^{low}CD133⁻ cells to the pathogenesis of biliary fibrosis. Changes of the gp38^{low}CD133⁻ cells are accompanied by decreasing Sca-1 expression after one day DDC-feeding and in turn increase in the regression phase. It is postulated that, Sca-1 acts as co-signaling molecule with the ability to generate more functional signaling complexes for example during self-renewal. Thus Sca-1 presence results in the maintenance of tissue homeostasis. Hence, Sca-1 suggests to enable the balance between differentiation and self-renewal during tissue regeneration (Holmes & Stanford, 2007). Surprisingly, CD24 expression seems to be upregulated significantly after 14 days CDE-feeding in the actual CD24⁻ cells.

Furthermore, gp38^{low}CD133⁺ cells increase in percentage and cell count after three and six weeks TAA-treatment albeit only significantly in cell count of six weeks TAA-treated mice. The frequency of gp38^{low}CD133⁺ cells in CDE-fed mice was largely unaltered over the entire period although the cell count significantly increases. The same tendency as for gp38^{low}CD133⁺ cells applies to gp38⁻CD133⁺ cells. During CDE-treatment, expression of MIC1-1C3 increases moderate in both CD133-expressing subtypes. But in general, MIC1-1C3 expression in healthy livers occurs to be higher by gp38^{low}CD133⁺ cells compared to gp38⁻CD133⁺ cells. In contrast, CD24 expression is comparable in both subtypes under steady state but increase more in gp38^{low}CD133⁺ cells during the entire period of CDE-treatment. Furthermore, EpCAM expression in healthy livers occurs to be higher in gp38^{low}CD133⁺ cells compared to gp38⁻CD133⁺ cells. During CDE-treatment, downregulation of EpCAM to a similar level as in gp38⁻CD133⁺ is indicated for gp38^{low}CD133⁺ cells, whereas EpCAM expression by gp38⁻CD133⁺ cells was largely unaltered. In accordance, previous studies showed an increase of gp38^{low}CD133⁺ and gp38⁻CD133⁺ cells during MCD-diet and CCL₄-induced fibrosis accompanied by an increased EpCAM expression in both cell subtypes (Eckert *et al.*, 2016). EpCAM is described to be involved in the regulation of gene transcription and

cell proliferation (Munz *et al.*, 2009). Thus, different expression patterns triggered by different treatments could induce various processes of adhesion, signal transduction or cell proliferation (Eckert *et al.*, 2016).

DDC-treatment leads to drastic changes in both, gp38^{low}CD133⁺ and gp38⁺CD133⁺ cells. After one day DDC-treatment, gp38^{low}CD133⁺ cells expand in cell count and frequency. After seven days and during the regression phase, frequencies were largely unaltered compared to the healthy control. In contrast, cell counts significantly decrease and gp38^{low}CD133⁺ cells seem to almost disappear after seven days and decreased during the regression phase, compared to the healthy control. Furthermore, cell counts and frequencies of gp38⁺CD133⁺ cells decrease significantly during the progression phase until they almost disappear and decrease during the regression phase, in comparison to the healthy control. These changes are accompanied by changes of the expression of various surface markers. MIC-1C3, CD24 and EpCAM are higher expressed in gp38^{low}CD133⁺ cells under steady state conditions compared to gp38⁺CD133⁺ cells. However, changes within the expression pattern of these surface markers follow the same tendencies in both CD133-expressing subtypes. During the progression phase, CD24 and MIC1-1C3 decrease, whereas EpCAM expression increases significantly. During the regression phase, the expression of the surface markers is similar compared to the steady state conditions of the healthy liver.

In general, the results are in line with previous studies, which indicate association of CD133-expressing cells with oval cells (Dollé *et al.*, 2010; Dorrell *et al.*, 2008; Rountree *et al.*, 2007). It also confirms the presence of oval cells in fibrosis and steatohepatitis not only in mouse models but also in humans (Eckert *et al.*, 2016; Gouw *et al.*, 2011).

Gene expression analysis of the heterogeneous CD133⁺ cell population additionally confirms the association of these cells with oval cells. DDC-treatment leads to the downregulation of genes associated with oval cells (KRT19 and HNF4A), in addition to the upregulation of the liver specific genes (HNF1A and HNF1B), genes of EMT (CDH1), Hippo signaling pathway (YAP1) and genes associated with apoptosis and inflammation (FAS, CCL2).

Based on the strong similarities in the gene expression of both CD133-expressing subpopulations (Eckert *et al.*, 2016) in addition to expression of several surface markers, Eckert *et al.* (2016) suggest that these cells present two different

developmental stages of the same cell type. The findings within this study confirm this assumption, which needs further clarification.

Cells lacking any gp38 and CD133 expression (gp38⁻CD133⁻) decrease significantly in frequency after six weeks and in turn increase in cell count in TAA-treated mice. On the contrary, frequency of gp38⁻CD133⁻ cells increase during the CDE-treatment albeit significantly only after 14 days. In cell count, gp38⁻CD133⁻ cells increase significantly at both time points. During DDC-progression phase, gp38⁻CD133⁻ cells almost disappear after seven days and in turn increase during the regression phase, albeit reduced in comparison to the healthy control. Surface marker expression among the gp38⁻CD133⁻ cells was largely unaltered during the entire period of CDE- and DDC-treatment. A detailed importance of these cell population within the HPCC and during liver inflammation remain to be elucidated.

4.2 Validation of surface marker profiles by microparticle profiling

Based on the first part of this study, the exploration of surface marker profiles of human cancer cell lines and the HPCC of murine liver, the validation study was performed on human cell-derived MPs. Parts of the results have been published as ‘Cancer-associated circulating large extracellular vesicles in cholangiocarcinoma and hepatocellular carcinoma’ (Julich-Haertel, Urban, *et al.*, 2017).

Human liver cancer cell lines differ in surface marker expression (EpCAM⁺CD133⁺ASGPR1⁺) from PaCa cell lines (EpCAM⁺CD133⁺). Therefore, human cell-derived MPs were screened for these surface marker combinations to address the hypothesis whether taMP subpopulations identify MPs-derived specifically from hepatic tumors and differ from other cancer entities.

Furthermore, the murine HPCC is classified in several subtypes by their gp38 and CD133 expression. CD133-expressing cells within the HPCC indicate oval cell-association and can be divided into two subtypes: gp38-expressing cells (gp38^{low}CD133⁺) and non-gp38-expressing cells (gp38⁻CD133⁺), which indicate liver injury specific changes. Accordingly, human cell-derived MPs, more specifically liver tumor-derived MPs, were monitored for the presence of both gp38 and CD133 to examine if this allows a distinction in hepatocellular carcinoma and cholangiocarcinoma.

AnnexinV was shown to identify microparticles in general (Biro *et al.*, 2004; Dignat-George *et al.*, 2004; Reutelingsperger, 2001) and AnnexinV⁺ MPs were detectable in

human sera of every study cohort examined within this study. The considered taMP and ocMP populations within this study are regardless of gender, BMI and age. Although the latter shows low correlation in some cases, this is probably due to the fact that the healthy cohort with the lower MP values consists of younger probands compared to the older cancer patients with increased MP values.

4.2.1 Liver disorder-associated microparticles differ in non-malignancies and hepatic cancer

AnnexinV⁺EpCAM⁺ taMPs suggest to be a pan-cancer marker (Figure 59, bottom), due to increased levels in sera of athletes, patients with inguinal hernias, cirrhosis and cancer patients (CrC, NSCLC, PaCa, HCC, CCA), compared to healthy individuals.

Serum tumor markers such as AFP and CA 19-9 correlate moderately with values of AnnexinV⁺EpCAM⁺ taMP in liver disorders and liver tumors, whereas the liver enzyme ALT indicate a negative moderate correlation with AnnexinV⁺EpCAM⁺ taMPs in cirrhosis. Previous studies reveal an association between elevated AFP levels and HCC (Abelev *et al.*, 1963; E. Alpert *et al.*, 1971; M.E. Alpert *et al.*, 1968; McIntire *et al.*, 1972; Purves *et al.*, 1968; Ruoslahti & Seppälä, 1971; Smith & Todd, 1968) as well as expansion of CA 19-9 not only in CCA but also in HCC (Duffy, 1998; Maestranzi *et al.*, 1998; Nehls *et al.*, 2004; Rhodes, 1999; Torzilli *et al.*, 2002) and ALT is commonly used in the differential diagnosis of liver diseases (Rej, 1989). Since the serum markers alone are not sufficient in diagnosis of HCC and CCA, a combination with AnnexinV⁺EpCAM⁺ taMPs could improve this. Nevertheless, the assessment of prognosis in liver cirrhosis by MELD-score and Child-Pugh is independent of AnnexinV⁺EpCAM⁺ taMP values. In contrast, moderate correlation between AnnexinV⁺EpCAM⁺ taMPs and liver tumor load suggest that AnnexinV⁺EpCAM⁺ taMPs are closely linked to cancer. This hypothesis is supported by moderate diagnostic potential with values over 50 % in terms of sensitivity, specificity, PPV and NPV for all cohorts considered within this study. This findings are confirmed by the previous study by Willms *et al.* (2016) due to AnnexinV⁺EpCAM⁺ taMPs which expand in CrC, PaCa, NSCLC and patients with thyroid nodules, resulting in solid diagnostic performance with sensitivity over 90 % and specificity about 50 %. Further, CrC tumor load was shown to be associated with taMP values, in addition to EpCAM⁺ taMPs values, which drop seven days after surgical R0 resection (Willms *et al.*, 2016), this additionally supports the hypothesis that taMPs are closely linked to cancer.

The taMP populations AnnexinV⁺EpCAM⁺CD133⁺ and AnnexinV⁺EpCAM⁺CD133⁺ASGPR1⁺ suggest being specifically associated with liver disorders (Figure 59, bottom). Elevated levels of both populations in patients bearing HCC, CCA and cirrhosis indicate this. These results are underpinned by moderate diagnostic potential with 73 to 83 % sensitivity, 50 % specificity and 81 to 83 % PPV. Values of AnnexinV⁺EpCAM⁺CD133⁺ and AnnexinV⁺EpCAM⁺CD133⁺ASGPR1⁺ correlate slightly to moderately with serum tumor marker CA 19-9 in patients bearing liver disorders. Additionally, AnnexinV⁺EpCAM⁺CD133⁺ASGPR1⁺ values correlate moderate with bilirubin levels in patients bearing liver disorders and the individual cohorts of patients with cirrhosis and hepatic cancer, respectively.

Furthermore, a correlation between AnnexinV⁺EpCAM⁺CD133⁺ASGPR1⁺ values and MELD-score and Child-Pugh is suggested, in addition to a moderate correlation between both liver disorder-associated taMP populations and liver tumor load. These results hypothesize a possible assessment of prognosis by AnnexinV⁺EpCAM⁺CD133⁺ and AnnexinV⁺EpCAM⁺CD133⁺ASGPR1⁺ taMPs in liver cirrhosis and hepatic cancer as well. As a result, patients with liver disorders seem to be identified by a first cancer detection-step (AnnexinV⁺EpCAM⁺ taMPs values above cut-off) followed by the confirmation of bearing a liver disorder by AnnexinV⁺EpCAM⁺CD133⁺ and AnnexinV⁺EpCAM⁺CD133⁺ASGPR1⁺ taMPs (values above cut-off). Thus, this correctly identified 64 % of patients bearing liver disorders within this study. Only 2 % of patients with liver disorders indicated values of both liver disorder-associated taMP populations below the calculated cut-off values. The recognition rate may be increased if the first cancer detection step is improved, because detection of cancer by AnnexinV⁺EpCAM⁺ taMP population is limited. Particularly, 34 % of patients with liver disorders and 30 % of patients bearing liver tumors indicate values below the calculated cut-off. Possibly extension of the surface marker panel by CD147 could improve the first cancer detection step due to EpCAM⁺CD147⁺ taMPs which only occur increased in tumor-bearing patients (CrC, NSCLC, PaCa) (Willms *et al.*, 2016).

By the help of an additional step, discrimination of patients with liver disorders in liver malignancies (hepatic cancer) and non-malignancies (cirrhosis) is suggested. This is achieved by the help of AnnexinV⁺EpCAM⁺ASGPR1⁺ taMPs (Figure 59, bottom), which expand in patients with hepatic cancer compared to low levels in patients with cirrhosis. With 75 % sensitivity and 78 % PPV portend a solid diagnostic potential, which is limited with 47 % specificity and 43 % NPV. Additionally,

AnnexinV⁺EpCAM⁺ASGPR1⁺ taMPs correlate with liver tumor load. Furthermore, values of AnnexinV⁺EpCAM⁺ASGPR1⁺ taMPs drop two days after surgical R0 tumor resection and remain low at day ten post-OP.

In summary, following a three-step approach (Figure 59, bottom) with 1) Cancer detection (AnnexinV⁺EpCAM⁺ taMPs above calculated cut-off), 2) Confirmation of liver disorders (AnnexinV⁺EpCAM⁺CD133⁺ and AnnexinV⁺EpCAM⁺CD133⁺ASGPR1⁺ taMPs above calculated cut-off) and 3) Confirmation of liver tumor (AnnexinV⁺EpCAM⁺ASGPR1⁺ above calculated cut-off) results in 54 % correctly identified liver tumor patients. Of these, 61 % corresponds to patients bearing CCA and 89 % to patients with HCC.

4.2.2 Oval cell-related microparticles allow discrimination in hepatocellular carcinoma and cholangiocarcinoma

Based on data of the murine HPCC and human liver disorder-associated MPs, the hypothesis if oval cell associated surface markers allow detection of liver tumor-derived MPs and particularly classification in HCC and CCA, was verified.

In the healthy murine liver, gp38^{low}CD133⁻ cells represent the rarest cell type. Thus, it is not surprising that tumor-derived MPs with this surface marker combination (AnnexinV⁺EpCAM⁺gp38⁺CD133⁻) are barely detectable in human sera. In contrast, murine gp38⁻CD133⁺ cells are one of the most abundant populations among the HPCC in murine healthy livers, which expand during liver injuries. Thus, the corresponding AnnexinV⁺EpCAM⁺gp38⁻CD133⁺ taMP population is apparently detectable in human sera and seems to be associated with liver disorders due to significant elevated values of these taMP populations in patients bearing HCC, CCA and cirrhosis (Figure 59, bottom). This is confirmed by a solid diagnostic performance with 75 % sensitivity, 67 % specificity, 81 % PPV and 58 % NPV. This corresponds to the AnnexinV⁺EpCAM⁺CD133⁺ taMPs described in the section above.

Furthermore, the second most abundant population among the HPCC in murine healthy livers are gp38^{low}CD133⁺ cells, which expand during liver inflammations and are not only detectable in human sera, but also suggest to allow classification of primary hepatic cancers in HCC and CCA. Based on this ability, the AnnexinV⁺gp38⁺CD133⁺ (AnnexinV⁺ ocMPs) and AnnexinV⁺EpCAM⁺gp38⁺CD133⁺ (AnnexinV⁺EpCAM⁺ ocMPs) populations are named oval cell-associated MPs (ocMPs). Surprisingly, values of AnnexinV⁺ and AnnexinV⁺EpCAM⁺ ocMPs expand in CCA, compared to ocMP

levels in HCC. In contrast, murine gp38^{low}CD133⁺ cells expand during toxin-induced fibrosis and models of NASH whereas gp38^{low}CD133⁻ cells were more likely to be associated with cholestatic liver injury. This can be attributed to distinctions between mice and humans, or varying in functions during the initial pathogenesis, tumor development and during cancer. However, liver tumor classification by ocMPs results in a moderate diagnostic potential (68 to 82 % sensitivity, 55 to 67 % specificity and 55 to 58 % positive prediction value).

Additionally, correlation between serum tumor marker AFP and both ocMP populations as well as CA 19-9 and AnnexinV⁺ ocMPs is indicated in HCC. Furthermore, values of bilirubin and both ocMP populations seem to correlate with each other in both HCC and CCA. A combination of serum markers, such as AFP, CA 19-9 and bilirubin, and ocMPs could improve blood-based diagnosis of HCC and CCA and further, possibly help to assess the prognosis.

By means of these results the three-step approach, described in the previous section, suggest to be extended by an additional step (Figure 59, bottom): 1) Cancer detection (AnnexinV⁺EpCAM⁺ taMPs above calculated cut-off), 2) Confirmation of liver disorders (AnnexinV⁺EpCAM⁺CD133⁺, AnnexinV⁺EpCAM⁺CD133⁺ASGPR1⁺ and AnnexinV⁺EpCAM⁺gp38⁻CD133⁺ taMPs above calculated cut-off), 3) Confirmation of liver tumor (AnnexinV⁺EpCAM⁺ASGPR1⁺ above calculated cut-off) and 4) Classification of liver tumors in CCA (AnnexinV⁺ ocMPs and AnnexinV⁺EpCAM⁺ ocMPs above calculated cut-off) and HCC (AnnexinV⁺ ocMPs and AnnexinV⁺EpCAM⁺ ocMPs below calculated cut-off). Also here, initial cancer detection is limited and results primarily in 57 % correctly identified liver tumor patients. Of these, 59 % corresponds to patients bearing CCA and 52 % to patients with HCC. As mentioned above, possibly surface marker panel extension by CD147 could improve the first cancer detection step due to EpCAM⁺CD147⁺ taMPs which only occur increased in tumor-bearing patients (CrC, NSCLC, PaCa) (Willms *et al.*, 2016).

4.3 Perspectives

To further ascertain phenotypically differences between the individual subtypes of the murine HPCC, additional surface markers must be verified in healthy and injured liver. Additionally, these surface markers should not only be tested individually, but also in combination with others. Furthermore, tamoxifen-inducible Cre/lox-mediated genome modifications can obtain further information about the differences and their function of

the individual subtypes. These must also be verified during liver inflammations, including TAA, CDE and DDC. The investigated models within this study must be repeated and additional time points proven, including long-term treatments which leads to tumor development. This could point out further details about the function of the individual subtypes and a possible involvement in pathogenesis, tumor development and during cancer. At least, isolation of the various subtypes of healthy and injured liver and further cultivations with differentiation, followed by co-culture assays could increase the knowledge about the function of the individual subtypes.

For further investigation of the diagnostic potential of MPs, correlation between ocMPs and tumor load, surgical R0 resection and liver cirrhosis assessment by MELD-score and Child-Pugh has to be proven. Additionally, a link between cancer- and oval cell-related MPs and TNM classification and prognosis must be established, followed by the analysis of MP values of those patients monitored within this study who are still alive. This in turn could provide a correlation between MP values and life expectancy.

As additional studies, MP values could be monitored during tumor therapy and thus validated if tumor treatment is successful. Another experimental approach would be to perform a long-term study. MP values of patients at risk to develop a liver tumor could be regular reviewed until a tumor develops. Accordingly, early tumor detection could be possible and further support the conventional diagnostic methods.

At least, to improve the cancer detection rate, surface marker panel could be extended and supplementary enlarged to other tumor entities.

5 Bibliography

- Abelev, G.I., Perova, S.D., Khramkova, N.I., Postnikova, Z.A. & Irlin, I.S. (1963). Production of embryonal α -globulin by transplantable mouse hepatomas. *Transplantation* 1(2): 174–180.
- Aden, D.P., Fogel, A., Plotkin, S., Damjanov, I. & Knowles, B.B. (1979, December 6). Controlled synthesis of HBsAg in a differentiated human liver carcinoma-derived cell line. *Nature*.
- AJCC - American Joint Committee on Cancer. (2018). Cancer Staging System. *AJCC - American Joint Committee on Cancer*. Retrieved May 27, 2018, from <https://cancerstaging.org/references-tools/Pages/What-is-Cancer-Staging.aspx>
- Al-Nedawi, K., Meehan, B., Micallef, J., Lhotak, V., May, L., Guha, A. & Rak, J. (2008). Intercellular transfer of the oncogenic receptor EGFRvIII by microvesicles derived from tumour cells. *Nature Cell Biology* 10(5): 619–624.
- Albrecht, T., Blomley, M., Bolondi, L., Claudon, M., Correas, J.M., Cosgrove, D., ... Stanford, G. (2004, August 9). Guidelines for the use of contrast agents in ultrasound: January 2004. *Ultraschall in der Medizin*.
- Alix-Panabières, C. & Pantel, K. (2016, May 1). Clinical applications of circulating tumor cells and circulating tumor DNA as liquid biopsy. *Cancer Discovery*.
- Aljiffry, M., Walsh, M.J. & Molinari, M. (2009, September 14). Advances in diagnosis, treatment and palliation of cholangiocarcinoma: 1990-2009. *World Journal of Gastroenterology*. Baishideng Publishing Group Inc.
- Alpert, E., Hershberg, R., Schur, P.H. & Isselbacher, K.J. (1971). -fetoprotein in human hepatoma: improved detection in serum, and quantitative studies using a new sensitive technique. *Gastroenterology* 61(2): 137–143.
- Alpert, M.E., Uriel, J. & de Nechaud, B. (1968). Alpha-1 Fetoglobulin in the Diagnosis of Human Hepatoma. *New England Journal of Medicine* 278(18): 984–986.
- Altman, D.G. & Bland, J.M. (1994, July 9). Diagnostic tests 2: Predictive values. *BMJ (Clinical research ed.)*. BMJ Publishing Group.
- American Cancer Society. (2018). Liver Cancer Stages. *American Cancer Society*. Retrieved May 27, 2018, from <https://www.cancer.org/cancer/liver-cancer/detection-diagnosis-staging/staging.html>
- Andrews, R.G., Singer, J.W. & Bernstein, I.D. (1989). Precursors of colony-forming cells in humans can be distinguished from colony-forming cells by expression of the CD33 and CD34 antigens and light scatter properties. *The Journal of experimental medicine* 169(5): 1721–1731.
- Ariff, B., Lloyd, C.R., Khan, S., Shariff, M., Thillainayagan, A. V., Bansil, D.S., ... Lim, A.K.P. (2009, March 21). Imaging of liver cancer. *World Journal of Gastroenterology*. Baishideng Publishing Group Inc.
- Bach, D.H., Hong, J.Y., Park, H.J. & Lee, S.K. (2017, July 15). The role of exosomes and miRNAs in drug-resistance of cancer cells. *International Journal of Cancer*.
- Baddoo, M., Hill, K., Wilkinson, R., Gaupp, D., Hughes, C., Kopen, G.C. & Phinney, D.G. (2003). Characterization of mesenchymal stem cells isolated from murine bone marrow by negative selection. *Journal of Cellular Biochemistry* 89(6): 1235–1249.

- Banas, A., Teratani, T., Yamamoto, Y., Tokuhara, M., Takeshita, F., Osaki, M., ... Ochiya, T. (2009). Rapid hepatic fate specification of adipose-derived stem cells and their therapeutic potential for liver failure. *Journal of Gastroenterology and Hepatology* 24(1): 70–77.
- Bardelli, A. & Pantel, K. (2017, February). Liquid Biopsies, What We Do Not Know (Yet). *Cancer Cell*.
- Becker, A., Thakur, B.K., Weiss, J.M., Kim, H.S., Peinado, H. & Lyden, D. (2016, December 12). Extracellular Vesicles in Cancer: Cell-to-Cell Mediators of Metastasis. *Cancer Cell*.
- Benameur, T., Soleti, R., Porro, C., Andriantsitohaina, R. & Martínez, M.C. (2010). Microparticles carrying sonic hedgehog favor neovascularization through the activation of nitric oxide pathway in mice. (G.P. Fadini, ed.) *PLoS ONE* 5(9): 1–10.
- Bialecki, E.S. & Di Bisceglie, A.M. (2005). Diagnosis of hepatocellular carcinoma. *HPB* 7(1): 26–34.
- Bieback, K., Kern, S., Klüter, H. & Eichler, H. (2004). Critical Parameters for the Isolation of Mesenchymal Stem Cells from Umbilical Cord Blood. *Stem Cells* 22(4): 625–634.
- Biro, E., Nieuwland, R. & Sturk, A. (2004). Measuring circulating cell-derived microparticles. *Journal of Thrombosis and Haemostasis* 2(10): 1843–1844.
- Bizollon, T., Rode, A., Bancel, B., Gueripel, V., Ducerf, C., Baulieux, J. & Trepo, C. (1998). Diagnostic value and tolerance of lipiodol-computed tomography for the detection of small hepatocellular carcinoma: Correlation with pathologic examination of explanted livers. *Journal of Hepatology* 28(3): 491–496.
- Breiteneder-Geleff, S., Soleiman, A., Horvat, R., Amann, G., Kowalski, H. & Kerjaschki, D. (1999). Podoplanin-a specific marker for lymphatic endothelium expressed in angiosarcoma. *Verh Dtsch Ges Pathol* 83: 270–275.
- Brierley, J.D., Gospodarowicz, M.K. & Wittekind, C. (2003). *TNM Classification of Malignant Tumours. Academic Legal Writing*.
- Burtis, C.A., Ashwood, E.R. & Bruns, D.E. (2012). *Tietz Textbook of Clinical Chemistry and Molecular Diagnostics. Elsevier Saunders. Elsevier Health Sciences*.
- Buscher, H.-P. (2018). MELD-SCORE. *facharztwissen @medicoconsult.de*. Retrieved May 28, 2018, from https://www.medicoconsult.de/MELD_Score/
- Cedrone, A., Covino, M., Caturelli, E., Pompili, M., Lorenzelli, G., Rosaria, M., ... Gasbarrini, G. (2000). Utility of α -fetoprotein (AFP) in the screening of patients with virus-related chronic liver disease: Does different viral etiology influence AFP levels in HCC? A study in 350, western patients. *Hepato-Gastroenterology* 47(36): 1654–1658.
- Charatcharoenwitthaya, P., Enders, F.B., Halling, K.C. & Lindor, K.D. (2008). Utility of serum tumor markers, imaging, and biliary cytology for detecting cholangiocarcinoma in primary sclerosing cholangitis. *Hepatology* 48(4): 1106–1117.
- Chen, J., Röcken, C., Treiber, G., Jentsch-Ulrich, K., Malfertheiner, P. & Ebert, M.P.A. (2003). Clinical Implications of Alpha-Fetoprotein Expression in Gastric Adenocarcinoma. *Digestive Diseases* 21(4): 357–362.
- Cheung, A. & Cheung, A. (2013). The Child-Pugh score: Prognosis in chronic liver disease and cirrhosis [Classics Series]. 2 *Minute Medicine*. Retrieved May 28, 2018, from <https://www.2minutemedicine.com/the-child-pugh-score-prognosis-in-chronic-liver-disease-and-cirrhosis-classics-series/>

- Chilakapati, J., Shankar, K., Korrapati, M.C., Hill, R.A. & Mehendale, H.M. (2005). Saturation toxicokinetics of thioacetamide: Role in initiation of liver injury. *Drug Metabolism and Disposition* 33(12): 1877–1885.
- Civin, C.I., Strauss, L.C., Brovall, C., Fackler, M.J., Schwartz, J.F. & Shaper, J.H. (1984). Antigenic analysis of hematopoiesis. III. A hematopoietic progenitor cell surface antigen defined by a monoclonal antibody raised against KG-1a cells. *The Journal of Immunology* 133(1): 157–165.
- Claudon, M., Dietrich, C.F., Choi, B.I., Cosgrove, D.O., Kudo, M., Nolsøe, C.P., ... Xu, H.X. (2013). Guidelines and Good Clinical Practice Recommendations for Contrast Enhanced Ultrasound (CEUS) in the Liver - Update 2012. A WFUMB-EFSUMB Initiative in Cooperation with Representatives of AFSUMB, AIUM, ASUM, FLAUS and ICUS. *Ultrasound in Medicine and Biology* 39(2): 187–210.
- Cocucci, E., Racchetti, G. & Meldolesi, J. (2009, February). Shedding microvesicles: artefacts no more. *Trends in Cell Biology*.
- Colli, A., Fraquelli, M., Casazza, G., Massironi, S., Colucci, A., Conte, D. & Duca, P. (2006, March). Accuracy of Ultrasonography, Spiral CT, Magnetic Resonance, and Alpha-Fetoprotein in Diagnosing Hepatocellular Carcinoma: A Systematic Review: CME. *American Journal of Gastroenterology*.
- Collier, J. & Sherman, M. (1998). Screening for hepatocellular carcinoma. *Hepatology* 27(1): 273–278.
- Connor, J., Pak, C.H., Zwaal, R.F.A. & Schroit, A.J. (1992). Bidirectional transbilayer movement of phospholipid analogs in human red blood cells. Evidence for an ATP-dependent and protein-mediated process. *Journal of Biological Chemistry* 267(27): 19412–19417.
- da Silva Meirelles, L., Chagastelles, P.C. & Nardi, N.B. (2006). Mesenchymal stem cells reside in virtually all post-natal organs and tissues. *Journal of Cell Science* 119(11): 2204–2213.
- Dahiya, R., Kwak, K.S., Byrd, J.C., Ho, S., Yoon, W.H. & Kim, Y.S. (1993). Mucin synthesis and secretion in various human epithelial cancer cell lines that express the MUC-1 mucin gene. *Cancer research* 53(6): 1437–1443.
- Dashti, H., Jeppsson, B., Hagerstrand, I., Hultberg, B., Srinivas, U., Abdulla, M. & Bengmark, S. (1989). Thioacetamide- and carbon tetrachloride-induced liver cirrhosis. *European Surgical Research* 21(2): 83–91.
- Day, C.P. (2006, January). From fat to inflammation. *Gastroenterology*.
- Debruyne, E.N. & Delanghe, J.R. (2008). Diagnosing and monitoring hepatocellular carcinoma with alpha-fetoprotein: New aspects and applications. *Clinica Chimica Acta*.
- Del Conde, I., Shrimpton, C.N., Thiagarajan, P. & López, J.A. (2005). Tissue-factor-bearing microvesicles arise from lipid rafts and fuse with activated platelets to initiate coagulation. *Blood* 106(5): 1604–1611.
- Denk, H., Stumtner, C. & Zatloukal, K. (2000, April 1). Mallory bodies revisited. *Journal of Hepatology*. Elsevier.
- Diehl, P., Fricke, A., Sander, L., Stamm, J., Bassler, N., Htun, N., ... Peter, K. (2012, March 15). Microparticles: Major transport vehicles for distinct microRNAs in circulation. *Cardiovascular Research*.
- Dignat-George, F., Sabatier, F., Camoin-Jau, L. & Sampol, J. (2004). Measuring circulating cell-derived

- microparticles. *Journal of Thrombosis and Haemostasis* 2(10): 1844–1845.
- DIMDI - Deutsches Institut für Medizinische Dokumentation und Information. (2012). ICD-10-GM. *DIMDI - Deutsches Institut für Medizinische Dokumentation und Information*. DIMDI: Deutsches Institut für Medizinische Dokumentation und Information. Retrieved November 14, 2017, from <http://www.dimdi.de/static/de/klassi/icd-10-gm/index.htm>
- Dimuccio, V., Ranghino, A., Praticò Barbato, L., Fop, F., Biancone, L., Camussi, G. & Bussolati, B. (2014). Urinary CD133+ extracellular vesicles are decreased in kidney transplanted patients with slow graft function and vascular damage. (I. Armando, ed.) *PLoS ONE* 9(8): e104490.
- Ding, X., Yang, L.-Y., Huang, G.-W., Yang, J.-Q., Liu, H.-L., Wang, W., ... Ling, X.-S. (2005). Role of AFP mRNA expression in peripheral blood as a predictor for postsurgical recurrence of hepatocellular carcinoma: A systematic review and meta-analysis. *World Journal of Gastroenterology* 11(17): 2656–2661.
- Dodd, G.D., Miller, W.J., Baron, R.L., Skolnick, M.L. & Campbell, W.L. (1992). Detection of malignant tumors in end-stage cirrhotic livers: Efficacy of sonography as a screening technique. In *American Journal of Roentgenology* (Vol. 159).
- Dolis, D., Moreau, C., Zachowski, A. & Devaux, P.F. (1997). Aminophospholipid translocase and proteins involved in transmembrane phospholipid traffic. In *Biophysical Chemistry* (Vol. 68).
- Dollé, L., Best, J., Mei, J., Al Battah, F., Reynaert, H., van Grunsven, L.A. & Geerts, A. (2010). The quest for liver progenitor cells: A practical point of view. *Journal of Hepatology* 52(1): 117–129.
- Dorrell, C., Erker, L., Lanxon-Cookson, K.M., Abraham, S.L., Victoroff, T., Ro, S., ... Grompe, M. (2008). Surface markers for the murine oval cell response. *Hepatology* 48(4): 1282–1291.
- Dorrell, C., Erker, L., Schug, J., Kopp, J.L., Canaday, P.S., Fox, A.J., ... Grompe, M. (2011). Prospective isolation of a bipotential clonogenic liver progenitor cell in adult mice. *Genes and Development* 25(11): 1193–1203.
- Duffy, M.J. (1998, May 1). CA 19-9 as a marker for gastrointestinal cancers: A review. *Annals of Clinical Biochemistry*.
- Dustin, M., Rothlein, R., Bhan, A., Dinarello, C. & Springer, T. (1986). Induction by IL-1 and interferon- γ : tissue distribution, biochemistry, and function of a natural adherence molecule (ICAM-1). *The Journal of Immunology* 137(1): 245–254.
- Ebara, M., Ohto, M., Watanabe, Y., Kimura, K., Saisho, H., Tsuchiya, Y., ... Ikehira, H. (1986). Diagnosis of small hepatocellular carcinoma: correlation of MR imaging and tumor histologic studies. *Radiology* 159(2): 371–377.
- Eckert, C., Kim, Y.O., Julich, H., Heier, E.-C., Klein, N., Krause, E., ... Lukacs-Kornek, V. (2016). Podoplanin discriminates distinct stromal cell populations and a novel progenitor subset in the liver. *American Journal of Physiology-Gastrointestinal and Liver Physiology* 310(1): G1–G12.
- Ellis, S.M., Nabeshima, K. & Biswas, C. (1989). Monoclonal Antibody Preparation and Purification of a Tumor Cell Collagenase-stimulatory Factor. *Cancer Research* 49(12): 3385–3391.
- Evans, J.D. (1996). *Straightforward Statistics for the Behavioral Sciences*. Pacific Grove: Brooks/Cole Pub. Co.
- Fadok, V.A., Voelker, D.R., Campbell, P.A., Cohen, J.J., Bratton, D.L. & Henson, P.M. (1992). Exposure of phosphatidylserine on the surface of apoptotic lymphocytes triggers specific recognition and

- removal by macrophages. *The Journal of Immunology* 148(7): 2207–16.
- Farber, E. (1956). Similarities in the Sequence of Early Histological Changes Induced in the Liver of the Rat by Ethionine, 2-Acetylaminofluorene, and 3'-Methyl-4-dimethylaminoazobenzene. *Cancer Research* 16(2): 142–148.
- Farr, A.G., Berry, M.L., Kim, A., Nelson, A.J., Welch, M.P. & Aruffo, A. (1992). Characterization and Cloning of a Novel Glycoprotein Expressed by Stromal Cells in T-dependent Areas of Peripheral Lymphoid Tissues. *J Exp Med* 176(5): 1477–82.
- Ferlay, J., Soerjomataram, I., Dikshit, R., Eser, S., Mathers, C., Rebelo, M., ... Bray, F. (2015). Cancer incidence and mortality worldwide: Sources, methods and major patterns in GLOBOCAN 2012. *International Journal of Cancer*. Retrieved January 14, 2018, from <http://globocan.iarc.fr>
- Feverly, J., Verslype, C., Lai, G., Aerts, R. & Van Steenberghe, W. (2007, November 12). Incidence, diagnosis, and therapy of cholangiocarcinoma in patients with primary sclerosing cholangitis. *Digestive Diseases and Sciences*.
- Fickert, P., Trauner, M., Fuchsbichler, A., Stumtner, C., Zatloukal, K. & Denk, H. (2003). Mallory body formation in primary biliary cirrhosis is associated with increased amounts and abnormal phosphorylation and ubiquitination of cytokeratins. *Journal of Hepatology* 38(4): 387–394.
- Fickert, P., Trauner, M., Fuchsbichler, A., Stumtner, C., Zatloukal, K. & Denkt, H. (2002). Bile acid-induced mallory body formation in drug-primed mouse liver. *American Journal of Pathology* 161(6): 2019–2026.
- Fogh, J., Wright, W.C. & Loveless, J.D. (1977). Absence of HeLa cell contamination in 169 cell lines derived from human tumors. *Journal of the National Cancer Institute* 58(2): 209–214.
- França, A.V.C., Elias Junior, J., Lima, B.L.G., Martinelli, A.L.C. & Carrilho, F.J. (2004). Diagnosis, staging and treatment of hepatocellular carcinoma. *Brazilian journal of medical and biological research* 37(11): 1689–1705.
- Friedenstein, A.J., Piatetzky-Shapiro, I.I. & Petrakova, K. V. (1966). Osteogenesis in transplants of bone marrow cells. *Journal of embryology and experimental morphology* 16(3): 381–390.
- Fritzsche, B., Schwer, B., Kartenbeck, J., Pedal, A., Horejsi, V. & Ott, M. (2002). Release and Intercellular Transfer of Cell Surface CD81 Via Microparticles. *The Journal of Immunology* 169(10): 5531–5537.
- Gambaran-Gelwan, M., Wolf, D.C., Shapiro, R., Schwartz, M.E. & Min, A.D. (2000). Sensitivity of commonly available screening tests in detecting hepatocellular carcinoma in cirrhotic patients undergoing liver transplantation. *The American Journal of Gastroenterology* 95(6): 1535–1538.
- Gebo, K.A., Chander, G., Jenckes, M.W., Ghanem, K.G., Herlong, H.F., Torbenson, M.S., ... Bass, E.B. (2002). Screening tests for hepatocellular carcinoma in patients with chronic hepatitis C: A systematic review. *Hepatology* 36(5): S84–S92.
- Geffen, I. & Spiess, M. (1992). Asialoglycoprotein receptor. *Int Rev Cytol* 137B: 181–219.
- Gomaa, A.I., Khan, S.A., Leen, E.L.S., Waked, I. & Taylor-Robinson, S.D. (2009). Diagnosis of hepatocellular carcinoma. *World journal of gastroenterology* 15(11): 1301–1314.
- Göttlinger, H.G., Funke, I., Johnson, J.P., Gokel, J.M. & Riethmüller, G. (1986). The epithelial cell surface antigen 17-1A, a target for antibody-mediated tumor therapy: Its biochemical nature, tissue distribution and recognition by different monoclonal antibodies. *International Journal of Cancer*

- 38(1): 47–53.
- Göttlinger, H.G., Johnson, J.P. & Riethmüller, G. (1986). Biochemical and epitope analysis of the 17-1A membrane antigen. *Hybridoma* 5 Suppl 1(0272–457X SB–M): S29–S37.
- Gouw, A.S.H., Clouston, A.D. & Theise, N.D. (2011, November 1). Ductular reactions in human liver: Diversity at the interface. *Hepatology*. Wiley-Blackwell.
- Grizzi, F., Franceschini, B., Hamrick, C., Frezza, E.E., Cobos, E. & Chiriva-Internati, M. (2007, January 23). Usefulness of cancer-testis antigens as biomarkers for the diagnosis and treatment of hepatocellular carcinoma. *Journal of Translational Medicine*. BioMed Central.
- Gupta, S., Bent, S. & Kohlwes, J. (2003). Test characteristics of alpha-fetoprotein for detecting hepatocellular carcinoma in patients with hepatitis C. A systematic review and critical analysis. *Annals of internal medicine* 139(1): 46–50.
- György, B., Szabó, T.G., Pásztói, M., Pál, Z., Misják, P., Aradi, B., ... Buzás, E.I. (2011, August 11). Membrane vesicles, current state-of-the-art: Emerging role of extracellular vesicles. *Cellular and Molecular Life Sciences*.
- Haber, D.A. & Velculescu, V.E. (2014, June 1). Blood-based analyses of cancer: Circulating tumor cells and circulating tumor DNA. *Cancer Discovery*.
- Hajovsky, H., Hu, G., Koen, Y., Sarma, D., Cui, W., Moore, D.S., ... Hanzlik, R.P. (2012). Metabolism and toxicity of thioacetamide and thioacetamide S-Oxide in rat hepatocytes. *Chemical Research in Toxicology* 25(9): 1955–1963.
- Harding, C., Heuser, J. & Stahl, P. (1984). Endocytosis and intracellular processing of transferrin and colloidal gold-transferrin in rat reticulocytes: demonstration of a pathway for receptor shedding. *European journal of cell biology* 35(2): 256–263.
- Herlyn, M., Steplewski, Z., Herlyn, D. & Koprowski, H. (1979). Colorectal carcinoma-specific antigen: detection by means of monoclonal antibodies. *Proceedings of the National Academy of Sciences of the United States of America* 76(3): 1438–42.
- Hernandez-Gea, V. & Friedman, S.L. (2011). Pathogenesis of Liver Fibrosis. *Annual Review of Pathology: Mechanisms of Disease* 6(1): 425–456.
- Hess, C., Sadallah, S., Hefti, A., Landmann, R. & Schifferli, J.A. (1999). Ectosomes released by human neutrophils are specialized functional units. *The Journal of Immunology* 163(8): 4564–4573.
- Hiroshima, K., Iyoda, A., Toyozaki, T., Haga, Y., Baba, M., Fujisawa, T., ... Ohwada, H. (2002). Alpha-fetoprotein-producing lung carcinoma: Report of three cases. *Pathology International* 52(1): 46–53.
- Holme, P.A., Solum, N.O., Brosstad, F., Roger, M. & Abdelnoor, M. (1994). Demonstration of platelet-derived microvesicles in blood from patients with activated coagulation and fibrinolysis using a filtration technique and Western blotting. *Thrombosis and Haemostasis* 72(5): 666–671.
- Holmes, C. & Stanford, W.L. (2007). Concise Review: Stem Cell Antigen-1: Expression, Function, and Enigma. *Stem Cells* 25(6): 1339–1347.
- Hoppo, T., Fujii, H., Hirose, T., Yasuchika, K., Azuma, H., Baba, S., ... Ikai, I. (2004). Thy1-Positive Mesenchymal Cells Promote the Maturation of CD49f-Positive Hepatic Progenitor Cells in the Mouse Fetal Liver. *Hepatology* 39(5): 1362–1370.
- Howard, A. (2011). Coding for Liver Cancer. *For the Record*. Retrieved November 13, 2017, from <http://www.fortherecordmag.com/archives/060611p27.shtml>

- Ince, A.T., Yildiz, K., Baysal, B., Danalıoğlu, A., Kocaman, O., Tozlu, M., ... Şentürk, H. (2014). Roles of serum and biliary CEA, CA19-9, VEGFR3, and TAC in differentiating between malignant and benign biliary obstructions. *Turkish Journal of Gastroenterology* 25(2): 162–169.
- Jakubowski, A., Ambrose, C., Parr, M., Lincecum, J.M., Wang, M.Z., Zheng, T.S., ... Burkly, L.C. (2005). TWEAK induces liver progenitor cell proliferation. *Journal of Clinical Investigation* 115(9): 2330–2340.
- John, A.R., Haghighi, K.S., Taniere, P., Esmat, M.E., Tan, Y.M. & Bramhall, S.R. (2007). Is a raised CA 19-9 level diagnostic for a cholangiocarcinoma in patients with no history of sclerosing cholangitis? *Digestive Surgery* 23(5–6): 319–324.
- Julich-Haertel, H., Tiwari, M., Mehrfeld, C., Krause, E., Kornek, M. & Lukacs-Kornek, V. (2017). Isolation and Enrichment of Liver Progenitor Subsets Identified by a Novel Surface Marker Combination. *Journal of Visualized Experiments* (120): e55284–e55284.
- Julich-Haertel, H., Urban, S.K., Krawczyk, M., Willms, A., Jankowski, K., Patkowski, W., ... Kornek, M. (2017). Cancer-associated circulating large extracellular vesicles in cholangiocarcinoma and hepatocellular carcinoma. *Journal of Hepatology*.
- Julich, H., Willms, A., Lukacs-Kornek, V. & Kornek, M. (2014). Extracellular vesicle profiling and their use as potential disease specific biomarker. *Frontiers in Immunology*. Frontiers Research Foundation.
- Kamath, P.S., Wiesner, R.H., Malinchoc, M., Kremers, W., Therneau, T.M., Kosberg, C.L., ... Kim, W.R. (2001, February). A model to predict survival in patients with end-stage liver disease. *Hepatology*.
- Karlmak, K.R., Weiskirchen, R., Zimmermann, H.W., Gassler, N., Ginhoux, F., Weber, C., ... Tacke, F. (2009). Hepatic recruitment of the inflammatory Gr1+monocyte subset upon liver injury promotes hepatic fibrosis. *Hepatology* 50(1): 261–274.
- Kern, S., Eichler, H., Stoeve, J., Klüter, H. & Bieback, K. (2006). Comparative Analysis of Mesenchymal Stem Cells from Bone Marrow, Umbilical Cord Blood, or Adipose Tissue. *Stem Cells* 24(5): 1294–1301.
- Khan, S.A., Davidson, B.R., Goldin, R.D., Heaton, N., Karani, J., Pereira, S.P., ... Wasan, H. (2012). Guidelines for the diagnosis and treatment of cholangiocarcinoma: An update. *Gut*.
- Kim, C.K., Lim, J.H. & Lee, W.J. (2001). Detection of hepatocellular carcinomas and dysplastic nodules in cirrhotic liver: accuracy of ultrasonography in transplant patients. *Journal of ultrasound in medicine : official journal of the American Institute of Ultrasound in Medicine* 20(2): 99–104.
- Kim, T., Murakami, T., Takahashi, S., Tsuda, K., Tomoda, K., Narumi, Y., ... Nakamura, H. (1999). Optimal phases of dynamic CT for detecting hepatocellular carcinoma: Evaluation of unenhanced and triple-phase images. *Abdominal Imaging* 24(5): 473–480.
- Kopen, G.C., Prockop, D.J. & Phinney, D.G. (1999). Marrow stromal cells migrate throughout forebrain and cerebellum, and they differentiate into astrocytes after injection into neonatal mouse brains. *Proceedings of the National Academy of Sciences* 96(19): 10711–10716.
- Koprowski, H., Stepkowski, Z., Mitchell, K., Herlyn, M., Herlyn, D. & Fuhrer, P. (1979). Colorectal carcinoma antigens detected by hybridoma antibodies. *Somatic Cell Genetics* 5(6): 957–971.
- Kornek, M., Lynch, M., Mehta, S.H., Lai, M., Exley, M., Afdhal, N.H. & Schuppan, D. (2012).

- Circulating microparticles as disease-specific biomarkers of severity of inflammation in patients with hepatitis C or nonalcoholic steatohepatitis. *Gastroenterology* 143(2): 448–458.
- Kornek, M., Popov, Y., Libermann, T.A., Afdhal, N.H. & Schuppan, D. (2011). Human T cell microparticles circulate in blood of hepatitis patients and induce fibrolytic activation of hepatic stellate cells. *Hepatology* 53(1): 230–242.
- Kornek, M. & Schuppan, D. (2012). Microparticles: Modulators and biomarkers of liver disease. *Journal of Hepatology* 57(5): 1144–1146.
- Krause, D.S., Fackler, M.J., Civin, C.I. & May, W.S. (1996). CD34: Structure, Biology, and Clinical Utility. *Blood* 87(1): 1–13.
- Kroy, D.C., Beraza, N., Tschaharganeh, D.F., Sander, L.E., Erschfeld, S., Giebel, A., ... Streetz, K.L. (2010). Lack of interleukin-6/glycoprotein 130/signal transducers and activators of transcription-3 signaling in hepatocytes predisposes to liver steatosis and injury in mice. *Hepatology* 51(2): 463–473.
- Kuszyk, B.S., Soyer, P., Bluemke, D.A. & Fishman, E.K. (1997). Intrahepatic cholangiocarcinoma: the role of imaging in detection and staging. *Critical reviews in diagnostic imaging*.
- Kuznetsov, S.A., Mankani, M.H., Gronthos, S., Satomura, K., Bianco, P. & Robey, P.G. (2001). Circulating skeletal stem cells. *Journal of Cell Biology* 153(5): 1133–1139.
- Lawson, C., Vicencio, J.M., Yellon, D.M. & Davidson, S.M. (2016, February 1). Microvesicles and exosomes: New players in metabolic and cardiovascular disease. *Journal of Endocrinology*. BioScientifica.
- Lee, H.J., You, D. Do, Choi, D.W., Choi, Y.S., Kim, S.J., Won, Y.S. & Moon, H.J. (2011). Significance of CD133 as a cancer stem cell markers focusing on the tumorigenicity of pancreatic cancer cell lines. *Journal of the Korean Surgical Society* 81(4): 263–270.
- Levy, C., Lymp, J., Angulo, P., Gores, G.J., Larusso, N. & Lindor, K.D. (2005). The value of serum CA 19-9 in predicting cholangiocarcinomas in patients with primary sclerosing cholangitis. *Digestive Diseases and Sciences* 50(9): 1734–1740.
- Lieber, M., Mazzetta, J., Nelson-Rees, W., Kaplan, M. & Todaro, G. (1975). Establishment of a continuous tumor-cell line (PANC-1) from a human carcinoma of the exocrine pancreas. *International Journal of Cancer* 15(5): 741–747.
- Liedtke, C., Luedde, T., Sauerbruch, T., Scholten, D., Streetz, K., Tacke, F., ... Weiskirchen, R. (2013, October 1). Experimental liver fibrosis research: Update on animal models, legal issues and translational aspects. *Fibrogenesis and Tissue Repair*. BioMed Central.
- Lim, J.H., Kim, C.K., Lee, W.J., Park, C.K., Koh, K.C., Paik, S.W. & Joh, J.W. (2000). Detection of hepatocellular carcinomas and dysplastic nodules in cirrhotic livers: Accuracy of helical CT in transplant patients. *American Journal of Roentgenology* 175(3): 693–698.
- Lin, C.S., Ning, H., Lin, G. & Lue, T.F. (2012). Is CD34 truly a negative marker for mesenchymal stromal cells? *Cytotherapy*.
- Lin, M.S., Huang, J.X. & Yu, H. (2014). Elevated serum level of carbohydrate antigen 19-9 in benign biliary stricture diseases can reduce its value as a tumor marker. *International Journal of Clinical and Experimental Medicine* 7(3): 744–750.
- Link, A., Hardie, D.L., Favre, S., Britschgi, M.R., Adams, D.H., Sixt, M., ... Luther, S.A. (2011).

- Association of T-zone reticular networks and conduits with ectopic lymphoid tissues in mice and humans. *American Journal of Pathology* 178(4): 1662–1675.
- Lopez Hänninen, E., Vogl, T.J., Bechstein, W.O., Guckelberger, O., Neuhaus, P., Lobeck, H. & Felix, R. (1998). Biphasic spiral computed tomography for detection of hepatocellular carcinoma before resection or orthotopic liver transplantation. *Investigative radiology* 33(4): 216–221.
- Lukacs-Kornek, V., Julich-Haertel, H., Urban, S.K. & Kornek, M. (2017). Multi-Surface Antigen Staining of Larger Extracellular Vesicles. In *Methods in molecular biology (Clifton, N.J.)* (Vol. 1660). Humana Press, New York, NY.
- Lukacs-Kornek, V., Malhotra, D., Fletcher, A.L., Acton, S.E., Elpek, K.G., Tayalia, P., ... Turley, S.J. (2011). Regulated release of nitric oxide by nonhematopoietic stroma controls expansion of the activated T cell pool in lymph nodes. *Nature immunology* 12(11): 1096–104.
- Lynch, C., Panagopoulou, M. & Gregory, C.D. (2017, September 22). Extracellular vesicles arising from apoptotic cells in tumors: Roles in cancer pathogenesis and potential clinical applications. *Frontiers in Immunology*. Frontiers.
- Ma, S., Chan, K.W., Hu, L., Lee, T.K.W., Wo, J.Y.H., Ng, I.O.L., ... Guan, X.Y. (2007). Identification and Characterization of Tumorigenic Liver Cancer Stem/Progenitor Cells. *Gastroenterology* 132(7): 2542–2556.
- Maccioni, F., Martinelli, M., Al Ansari, N., Kagarmanova, A., De Marco, V., Zippi, M. & Marini, M. (2010). Magnetic resonance cholangiography: past, present and future: a review. *European review for medical and pharmacological sciences* 14(8): 721–725.
- Maestranzi, S., Przemioslo, R., Mitchell, H. & Sherwood, R.A. (1998). The effect of benign and malignant liver disease on the tumour markers CA19-9 and CEA. *Annals of Clinical Biochemistry* 35(1): 99–103.
- Malek, N.P., Schmidt, S., Huber, P., Manns, M.P. & Greten, T.F. (2014). The diagnosis and treatment of hepatocellular carcinoma. *Deutsches Ärzteblatt international* 111(7): 101–6.
- Masyuk, A.I., Huang, B.Q., Ward, C.J., Gradilone, S.A., Banales, J.M., Masyuk, T. V., ... LaRusso, N.F. (2010). Biliary exosomes influence cholangiocyte regulatory mechanisms and proliferation through interaction with primary cilia. *American Journal of Physiology-Gastrointestinal and Liver Physiology* 299(4): G990–G999.
- Mause, S.F., Von Hundelshausen, P., Zerneck, A., Koenen, R.R. & Weber, C. (2005). Platelet microparticles: A transcellular delivery system for RANTES promoting monocyte recruitment on endothelium. *Arteriosclerosis, Thrombosis, and Vascular Biology* 25(7): 1512–1518.
- Mause, S.F. & Weber, C. (2010, October 29). Microparticles: Protagonists of a novel communication network for intercellular information exchange. *Circulation Research*. American Heart Association, Inc.
- McIntire, K.R., Vogel, C.L., Princler, G.L. & Patel, I.R. (1972). Serum alpha-fetoprotein as a biochemical marker for hepatocellular carcinoma. *Cancer research* 32(9): 1941–1946.
- Mills, J.C., Stone, N.L., Erhardt, J. & Pittman, R.N. (1998). Apoptotic membrane blebbing is regulated by myosin light chain phosphorylation. *Journal of Cell Biology* 140(3): 627–636.
- Miraglia, S., Godfrey, W., Yin, A.H., Atkins, K., Warnke, R., Holden, J.T., ... Buck, D.W. (1997). A novel five-transmembrane hematopoietic stem cell antigen: isolation, characterization, and

- molecular cloning. *Blood* 90(12): 5013–21.
- Miyajima, A., Tanaka, M. & Itoh, T. (2014). Stem/progenitor cells in liver development, homeostasis, regeneration, and reprogramming. *Cell Stem Cell*.
- Momburg, F., Moldenhauer, G., Hã, J. & Mã, P. (1987). Immunohistochemical Study of the Expression of a Mr 34 , 000 Human Epithelium-specific Surface Glycoprotein in Normal and Malignant Tissues. *Cancer Research* 47: 2883–2891.
- Moore, C., Kosgodage, U., Lange, S. & Inal, J.M. (2017, August 1). The emerging role of exosome and microvesicle- (EMV-) based cancer therapeutics and immunotherapy. *International Journal of Cancer*.
- Morell, A.G., Irvine, R.A., Sternlieb, I., Scheinberg, I.H. & Ashwell, G. (1968). Physical and chemical studies on ceruloplasmin. V. Metabolic studies on sialic acid-free ceruloplasmin in vivo. *Journal of Biological Chemistry* 243(1): 155–159.
- Morikawa, S., Mabuchi, Y., Niibe, K., Suzuki, S., Nagoshi, N., Sunabori, T., ... Matsuzaki, Y. (2009). Development of mesenchymal stem cells partially originate from the neural crest. *Biochemical and Biophysical Research Communications* 379(4): 1114–1119.
- Moriyama, T., Ohuchida, K., Mizumoto, K., Cui, L., Ikenaga, N., Sato, N. & Tanaka, M. (2010). Enhanced cell migration and invasion of CD133+ pancreatic cancer cells cocultured with pancreatic stromal cells. *Cancer* 116(14): 3357–3368.
- Müller, A., Machnik, F., Zimmermann, T. & Schubert, H. (1988). Thioacetamide-induced cirrhosis-like liver lesions in rats--usefulness and reliability of this animal model. *Experimental pathology* 34(4): 229–36.
- Munoz Torres, E., Paz Bouza, J.I., Lopez Bravo, A., Abad Hernandez, M.M. & Carrascal Marino, E. (1991). Experimental thioacetamide-induced cirrhosis of the liver. *Histology and Histopathology* 6(1): 95–100.
- Munz, M., Baeuerle, P.A. & Gires, O. (2009, July 15). The emerging role of EpCAM in cancer and stem cell signaling. *Cancer Research*. American Association for Cancer Research.
- Nakabayashi, H., Taketa, K., Miyano, K., Yamane, T. & Sato, J. (1982). Growth of human hepatoma cells lines with differentiated functions in chemically defined medium. *Cancer research* 42(9): 3858–3863.
- National Cancer Institute. (2018). NCI Dictionary of Cancer Terms. *National Cancer Institute*. Retrieved May 22, 2018, from <https://www.cancer.gov/publications/dictionaries/cancer-terms>
- Nehls, O., Gregor, M. & Klump, B. (2004, June 11). Serum and bile markers for cholangiocarcinoma. *Seminars in Liver Disease*.
- Obregon, C., Rothen-Rutishauser, B., Gitahi, S.K., Gehr, P. & Nicod, L.P. (2006). Exovesicles from human activated dendritic cells fuse with resting dendritic cells, allowing them to present alloantigens. *American Journal of Pathology* 169(6): 2127–2136.
- Okabe, M., Tsukahara, Y., Tanaka, M., Suzuki, K., Saito, S., Kamiya, Y., ... Miyajima, A. (2009). Potential hepatic stem cells reside in EpCAM+ cells of normal and injured mouse liver. *Development* 136(11): 1951–1960.
- Pan, B.T., Teng, K., Wu, C., Adam, M. & Johnstone, R.M. (1985). Electron microscopic evidence for externalization of the transferrin receptor in vesicular form in sheep reticulocytes. *Journal of Cell*

- Biology* 101(3): 942–948.
- Park, J.-H., Cho, E.-W., Shin, Y., Lee, Y.-J. & Kim, K.L. (1998). Detection of the Asialoglycoprotein Receptor on Cell Lines of Extrahepatic Origin 244: 304–311.
- Patel, A.H., Harnois, D.M., Klee, G.G., Larusso, N.F. & Gores, G.J. (2000). The utility of CA 19-9 in the diagnoses of cholangiocarcinoma in patients without primary sclerosing cholangitis. *American Journal of Gastroenterology* 95(1): 204–207.
- Peduto, L., Dulauroy, S., Lochner, M., Späth, G.F., Morales, M.A., Cumano, A. & Eberl, G. (2009). Inflammation recapitulates the ontogeny of lymphoid stromal cells. *The Journal of Immunology* 182(9): 5789–99.
- Pittenger, M.F., Mackay, A.M., Beck, S.C., Jaiswal, R.K., Douglas, R., Mosca, J.D., ... Marshak, D.R. (1999). Multilineage potential of adult human mesenchymal stem cells. *Science* 284(5411): 143–147.
- Pollack, M.S., Heagney, S.D., Livingston, P.O. & Fogh, J. (1981). HLA-A, B, C and DR alloantigen expression on forty-six cultured human tumor cell lines. *Journal of the National Cancer Institute* 66(6): 1003–1012.
- Pompili, M., Riccardi, L., Semeraro, S., Orefice, R., Elia, F., Barbaro, B., ... Rapaccini, G.L. (2008). Contrast-enhanced ultrasound assessment of arterial vascularization of small nodules arising in the cirrhotic liver. *Digestive and Liver Disease* 40(3): 206–215.
- Pugh, R.N.H., Murray-Lyon, I.M., Dawson, J.L., Pietroni, M.C. & Williams, R. (1973). Transection of the oesophagus for bleeding oesophageal varices. *British Journal of Surgery* 60(8): 646–649.
- Purves, L.R., MacNab, M., Geddes, E.W. & Bersohn, I. (1968). Serum-alpha-foetoprotein and primary hepatic cancer. *Lancet (London, England)* 1(7548): 921–922.
- Qiu, Q., Hernandez, J.C., Dean, A.M., Rao, P.H. & Darlington, G.J. (2011). CD24-Positive Cells from Normal Adult Mouse Liver Are Hepatocyte Progenitor Cells. *Stem Cells and Development* 20(12): 2177–2188.
- Rej, R. (1989). Aminotransferases in disease. *Clinics in laboratory medicine* 9(4): 667–687.
- Ren, G., Zhao, X., Zhang, L., Zhang, J., L 'huillier, A., Ling, W., ... Shi, Y. (2010). Inflammatory Cytokine-Induced Intercellular Adhesion Molecule-1 and Vascular Cell Adhesion Molecule-1 in Mesenchymal Stem Cells Are Critical for Immunosuppression. *J Immunol* 184(5): 2321–2328.
- Reutelingsperger, C.P.M. (2001). Annexins: Key regulators of haemostasis, thrombosis, and apoptosis. *Thrombosis and Haemostasis* 86(1): 413–419.
- Reutelingsperger, C.P.M., Hornstra, G. & HemKER, H.C. (1985). Isolation and partial purification of a novel anticoagulant from arteries of human umbilical cord. *European Journal of Biochemistry* 151(3): 625–629.
- Rhodes, J.M. (1999). Usefulness of novel tumour markers. In *Annals of Oncology* (Vol. 10).
- Robert Koch Institut - Zentrum für Krebsregistrierdaten. (2017). Krebs in Deutschland. *Robert Koch Institut - Zentrum für Krebsregistrierdaten*. Retrieved November 8, 2017, from <https://www.krebsdaten.de>
- Römisch, J. & Pâques, E.P. (1991). Annexins: calcium-binding proteins of multi-functional importance? *Medical microbiology and immunology* 180(3): 109–26.
- Rountree, C.B., Barsky, L., Ge, S., Zhu, J., Senadheera, S. & Crooks, G.M. (2007). A CD133-expressing

- murine liver oval cell population with bilineage potential. *Stem cells* 25(10): 2419–2429.
- Rozmyslowicz, T., Majka, M., Kijowski, J., Murphy, S.L., Conover, D.O., Poncz, M., ... Ratajczak, M.Z. (2003). Platelet- and megakaryocyte-derived microparticles transfer CXCR4 receptor to CXCR4-null cells and make them susceptible to infection by X4-HIV. *AIDS* 17(1): 33–42.
- Ruoslahti, E. & Seppälä, M. (1971). Studies of carcino-fetal proteins. III. Development of a radioimmunoassay for α -fetoprotein. Demonstration of α -fetoprotein in serum of healthy human adults. *International Journal of Cancer* 8(3): 374–383.
- Saar, B. & Kellner-Weldon, F. (2008). Radiological diagnosis of hepatocellular carcinoma. *Liver International* 28(2): 189–199.
- Salguero Palacios, R., Roderfeld, M., Hemmann, S., Rath, T., Atanasova, S., Tschuschner, A., ... Roeb, E. (2008). Activation of hepatic stellate cells is associated with cytokine expression in thioacetamide-induced hepatic fibrosis in mice. *Laboratory investigation; a journal of technical methods and pathology* 88(11): 1192–1203.
- Sato, Y., Araki, H., Kato, J., Nakamura, K., Kawano, Y., Kobune, M., ... Niitsu, Y. (2005). Human mesenchymal stem cells xenografted directly to rat liver are differentiated into human hepatocytes without fusion. *Blood* 106(2): 756–763.
- Seigneuret, M., Zachowski, A., Hermann, A. & Devaux, P.F. (1984). Asymmetric Lipid Fluidity in Human Erythrocyte Membrane: New Spin-Label Evidence. *Biochemistry* 23(19): 4271–4275.
- Shapiro, R.S., Katz, R., Mendelson, D.S., Halton, K.P., Schwartz, M.E. & Miller, C.M. (1996). Detection of hepatocellular carcinoma in cirrhotic patients: sensitivity of CT and ultrasonography. *Journal of ultrasound in medicine : official journal of the American Institute of Ultrasound in Medicine* 15(7): 494–502.
- Sherman, M. (2001, April). Alphafetoprotein: An obituary. *Journal of Hepatology* 34(4): 603–605.
- Shinozuka, H., Lombardi, B., Sell, S. & Lammarino, R.M. (1978). Early Histological and Functional Alterations of Ethionine Liver Carcinogenesis in Rats Fed a Choline-deficient Diet. *Cancer Research* 38(4): 1092–1098.
- Simak, J. & Gelderman, M.P. (2006, January 1). Cell membrane microparticles in blood and blood products: Potentially pathogenic agents and diagnostic markers. *Transfusion Medicine Reviews*. W.B. Saunders.
- Sims, P.J., Faioni, E.M., Wiedmer, T. & Shattil, S.J. (1988). Complement proteins C5b-9 cause release of membrane vesicles from the platelet surface that are enriched in the membrane receptor for coagulation factor Va and express prothrombinase activity. *Journal of Biological Chemistry* 263(34): 18205–18212.
- Siqueira, E., Schoen, R.E., Silverman, W., Martin, J., Rabinovitz, M., Weissfeld, J.L., ... Martini, J. (2002). Detecting cholangiocarcinoma in patients with primary sclerosing cholangitis. *Gastrointestinal endoscopy* 56(1): 40–47.
- Siravegna, G., Marsoni, S., Siena, S. & Bardelli, A. (2017, March 2). Integrating liquid biopsies into the management of cancer. *Nature Reviews Clinical Oncology*.
- Smith, J.B. & Todd, D. (1968). Foetoglobulin and primary liver cancer. *Lancet (London, England)* 2(7572): 833.
- Snowberger, N., Chinnakotla, S., Lepe, R.M., Peattie, J., Goldstein, R., Klintmalm, G.B. & Davis, G.L.

- (2007). Alpha fetoprotein, ultrasound, computerized tomography and magnetic resonance imaging for detection of hepatocellular carcinoma in patients with advanced cirrhosis. *Alimentary Pharmacology and Therapeutics* 26(9): 1187–1194.
- Spangrude, G.J., Heimfeld, S. & Weissman, I.L. (1988). Purification and characterization of mouse hematopoietic stem cells. *Science* 241(4861): 58–62.
- Thege, F.I., Lannin, T.B., Saha, T.N., Tsai, S., Kochman, M.L., Hollingsworth, M.A., ... Kirby, B.J. (2014). Microfluidic immunocapture of circulating pancreatic cells using parallel EpCAM and MUC1 capture: characterization, optimization and downstream analysis. *Lab Chip* 14(10): 1775–1784.
- Torzilli, G., Makuuchi, M., Ferrero, A., Takayama, T., Abe, H., Inoue, K. & Nakahara, K. (2002). Accuracy of the preoperative determination of tumor markers in the differentiation of liver mass lesions in surgical patients. *Hepato-Gastroenterology* 49(45): 740–745.
- Trerè, D., Fiume, L., Giorgi, L.B. De, Stefano, G. Di, Migaldi, M. & Derenzini, M. (1999). The asialoglycoprotein receptor in human hepatocellular carcinomas: its expression on proliferating cells. *British journal of cancer* 81: 404–408.
- Trevisani, F., D’Intino, P.E., Morselli-Labate, A.M., Mazzella, G., Accogli, E., Caraceni, P., ... Bernardi, M. (2001). Serum α -fetoprotein for diagnosis of hepatocellular carcinoma in patients with chronic liver disease: Influence of HBsAg and anti-HCV status. *Journal of Hepatology* 34(4): 570–575.
- Ueberham, E., Böttger, J., Ueberham, U., Grosche, J. & Gebhardt, R. (2010). Response of sinusoidal mouse liver cells to choline-deficient ethionine-supplemented diet. *Comparative Hepatology* 9: 8.
- Van Beers, B.E. (2008). Diagnosis of cholangiocarcinoma. *HPB*. Elsevier.
- Vergel, Y.B., Chilcott, J., Kaltenthaler, E., Walters, S., Blakeborough, A. & Thomas, S. (2006). Economic evaluation of MR cholangiopancreatography compared to diagnostic ERCP for the investigation of biliary tree obstruction. *International Journal of Surgery* 4(1): 12–19.
- Wagner, W., Roderburg, C., Wein, F., Diehlmann, A., Frankhauser, M., Schubert, R., ... Ho, A.D. (2007). Molecular and Secretory Profiles of Human Mesenchymal Stromal Cells and Their Abilities to Maintain Primitive Hematopoietic Progenitors. *Stem Cells* 25(10): 2638–2647.
- Wagner, W., Wein, F., Seckinger, A., Frankhauser, M., Wirkner, U., Krause, U., ... Ho, A.D. (2005). Comparative characteristics of mesenchymal stem cells from human bone marrow, adipose tissue, and umbilical cord blood. *Experimental Hematology* 33(11): 1402–1416.
- Whale, T.A., Wilson, H.L., Tikoo, S.K., Babiuk, L.A. & Griebel, P.J. (2006). Passively acquired membrane proteins alter the functional capacity of bovine polymorphonuclear cells. *Journal of Leukocyte Biology* 80(3): 481–491.
- Williamson, P., Bevers, E.M., Smeets, E.F., Comfurius, P., Schlegel, R.A. & Zwaal, R.F.A. (1995). Continuous Analysis of the Mechanism of Activated Transbilayer Lipid Movement in Platelets. *Biochemistry* 34(33): 10448–10455.
- Willms, A., Müller, C., Julich, H., Klein, N., Schwab, R., Richardsen, I., ... Krawczyk, M. (2016). Tumour-associated circulating microparticles : A novel liquid biopsy tool for screening and therapy monitoring of colorectal carcinoma and other epithelial neoplasia 7(21): 1–9.
- Wolf, P. (1967). The Nature and Significance of Platelet Products in Human Plasma. *British Journal of Haematology* 13(3): 269–288.

- World Health Organisation. (2017). Cancer - Fact sheet. *World Health Organisation*. World Health Organization. Retrieved January 15, 2018, from <http://www.who.int/mediacentre/factsheets/fs297/en/>
- Yamashita, T., Forgues, M., Wang, W., Jin, W.K., Ye, Q., Jia, H., ... Xin, W.W. (2008). EpCAM and α -fetoprotein expression defines novel prognostic subtypes of hepatocellular carcinoma. *Cancer Research* 68(5): 1451–1461.
- Yamashita, T., Ji, J., Budhu, A., Forgues, M., Yang, W., Wang, H.Y., ... Wang, X.W. (2009). EpCAM-Positive Hepatocellular Carcinoma Cells Are Tumor-Initiating Cells With Stem/Progenitor Cell Features. *Gastroenterology* 136(3): 1012–24.
- Yin, S., Li, J., Hu, C., Chen, X., Yao, M., Yan, M., ... Gu, J. (2007). CD133 positive hepatocellular carcinoma cells possess high capacity for tumorigenicity. *International Journal of Cancer* 120(7): 1444–1450.
- Yovchev, M.I., Grozdanov, P.N., Joseph, B., Gupta, S. & Dabeva, M.D. (2007). Novel hepatic progenitor cell surface markers in the adult rat liver. *Hepatology* 45(1): 139–149.
- Yu, S.C.H., Yeung, D.T.K. & So, N.M.C. (2004, February). Imaging features of hepatocellular carcinoma. *Clinical Radiology*.
- Zuk, P.A., Zhu, M., Mizuno, H., Huang, J.I., Futrell, W.J., Katz, A.J., ... Hedrick, M.H. (2001). Multilineage cells from human adipose tissue: implications for cell-based therapies. *Tissue engineering* 7(2): 211–28.

6 Supplementary data

6.1 Supplementary tables

Supplementary Table 1: Histological and biochemical parameters of patients with liver disorders of the study ‘Tumor-related microparticles to identify primary hepatic cancer’.

Indicated are the tumor volume and diameter, as histological parameters for HCC and CCA. Tumor marker such as AFP, CEA and CA 19-9 are shown for each cohort as well as blood chemistry levels of ALT, bilirubin and creatinine. To assess the prognosis of liver disease, MELD-score and Child-Pugh score are shown as absolute numbers of patients with cirrhosis. Absolute numbers of patients who participated in R0 resection study are given for HCC and CCA.

	Liver disorder	Cirrhosis	HCC	CCA
Tumor V [cm³]	104.0 ±199.0	0	114.6 ±209.2	23.7 ±39.6
Tumor Ø [mm]	44.3 ±26.5	0	46.7 ±26.6	26.5 ±18.9
AFP [ng/mL]	1505.0 ±8259.0	7.0 ±5.3	2899.0 ±11332.0	4.9 ±6.5
CEA [ng/mL]	4.6±6.6	4.3±3.7	3.5±3.8	6.6±10.4
CA 19-9 [U/mL]	554.3 ±2612.1	24.8 ±20.6	54.3 ±137.5	1783.4 ±4641.5
ALT [ng/mL]	76.8 ±87.5	57.6 ±55.8	79.0 ±79.7	96.3 ±124.0
Bilirubin [mg/dL]	3.1 ±4.9	4.3 ±5.7	1.7 ±2.8	4.4 ±6.1
Creatinine [mg/dL]	0.9 ±0.3	0.9 ±0.3	1.0 ±0.4	0.9 ±0.3
MELD score	6-10	-	4	N/A

SUPPLEMENTARY DATA
– SUPPLEMENTARY TABLES –

 [#]	11-15	-	16	N/A	N/A
	16-20	-	13	N/A	N/A
	21-24	-	3	N/A	N/A
	25-28	-	1	N/A	N/A
Child-Pugh	A	-	5	N/A	N/A
score	B	-	25	N/A	N/A
 [#]	C	-	6	N/A	N/A
Resected patients [#]		37	0	24	13

Tumor V: Tumor volume given as mean ± standard deviation (SD) according to MRI criteria

Tumor Ø: Tumor diameter given as mean ± SD according to MRI criteria

AFP: Alpha-1 fetoprotein given as mean ± SD

CEA: Carcinoembryonic antigen given as mean ± SD

CA 19-9: Carbohydrate-antigen 19-9 given as mean ± SD

ALT: Alanine transaminase given as mean ± SD

#: Absolute number of patients

N/A: Not available

Liver disorder: Cirrhosis, HCC and CCA combined in one group

HCC: Hepatocellular carcinoma

CCA: Cholangiocarcinoma

Supplementary Table 2: Histological and biochemical parameters of patients with liver disorders of the study ‘Oval cell-related microparticles to classify primary hepatic cancer’.

Indicated are the tumor volume and diameter, as histological parameters for HCC and CCA. Tumor marker such as AFP, CEA and CA 19-9 are shown for each cohort as well as blood chemistry levels of ALT, bilirubin and creatinine.

	Liver disorder	Cirrhosis	HCC	CCA
Tumor V [cm³]	90.4 ±176.3	0	106.8 ±189.7	8.2 ±9.5
Tumor Ø [mm]	42.2 ±25.7	0	46.3 ±26.0	21.9 ±10.8
AFP [ng/mL]	2051.7 ±10637.9	8.9 ±7.5	4098.3 ±14877.2	3.1 ±1.1

SUPPLEMENTARY DATA
– SUPPLEMENTARY TABLES –

CEA [ng/mL]	4.7 ±7.9	3.1 ±2.0	3.5 ±4.6	7.2 ±12.0
CA 19-9 [U/mL]	929.8 ±3661.2	24.8 ±20.6	34.5 ±64.7	2678.3 ±6005.7
ALT [ng/mL]	74.9 ±72.1	74.8 ±68.2	70.6 ±77.3	80.9 ±71.8
Bilirubin [mg/dL]	3.2 ±5.7	4.2 ±7.2	1.2 ±1.2	4.7 ±6.8
Creatinine [mg/dL]	0.9 ±0.3	0.9 ±0.3	0.9 ±0.2	1.0 ±0.3

Tumor V: Tumor volume given as mean ± standard deviation (SD) according to MRI criteria

Tumor Ø: Tumor diameter given as mean ± SD according to MRI criteria

AFP: Alpha-1 fetoprotein given as mean ± SD

CEA: Carcinoembryonic antigen given as mean ± SD

CA 19-9: Carbohydrate-antigen 19-9 given as mean ± SD

ALT: Alanine transaminase given as mean ± SD

#: Absolute number of patients

N/A: Not available

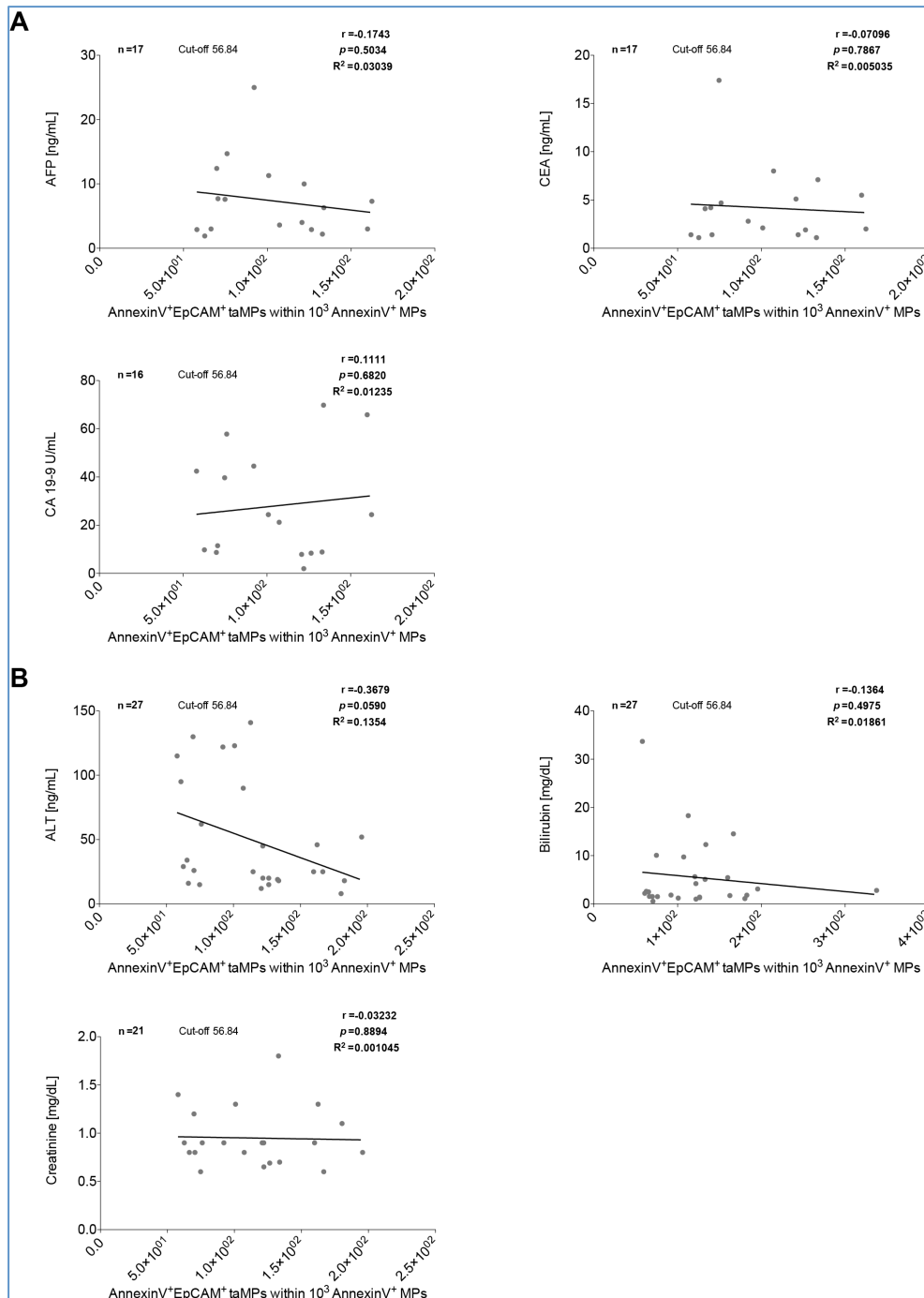
Liver disorder: Cirrhosis, HCC and CCA combined in one group

HCC: Hepatocellular carcinoma

CCA: Cholangiocarcinoma

6.2 Supplementary figures

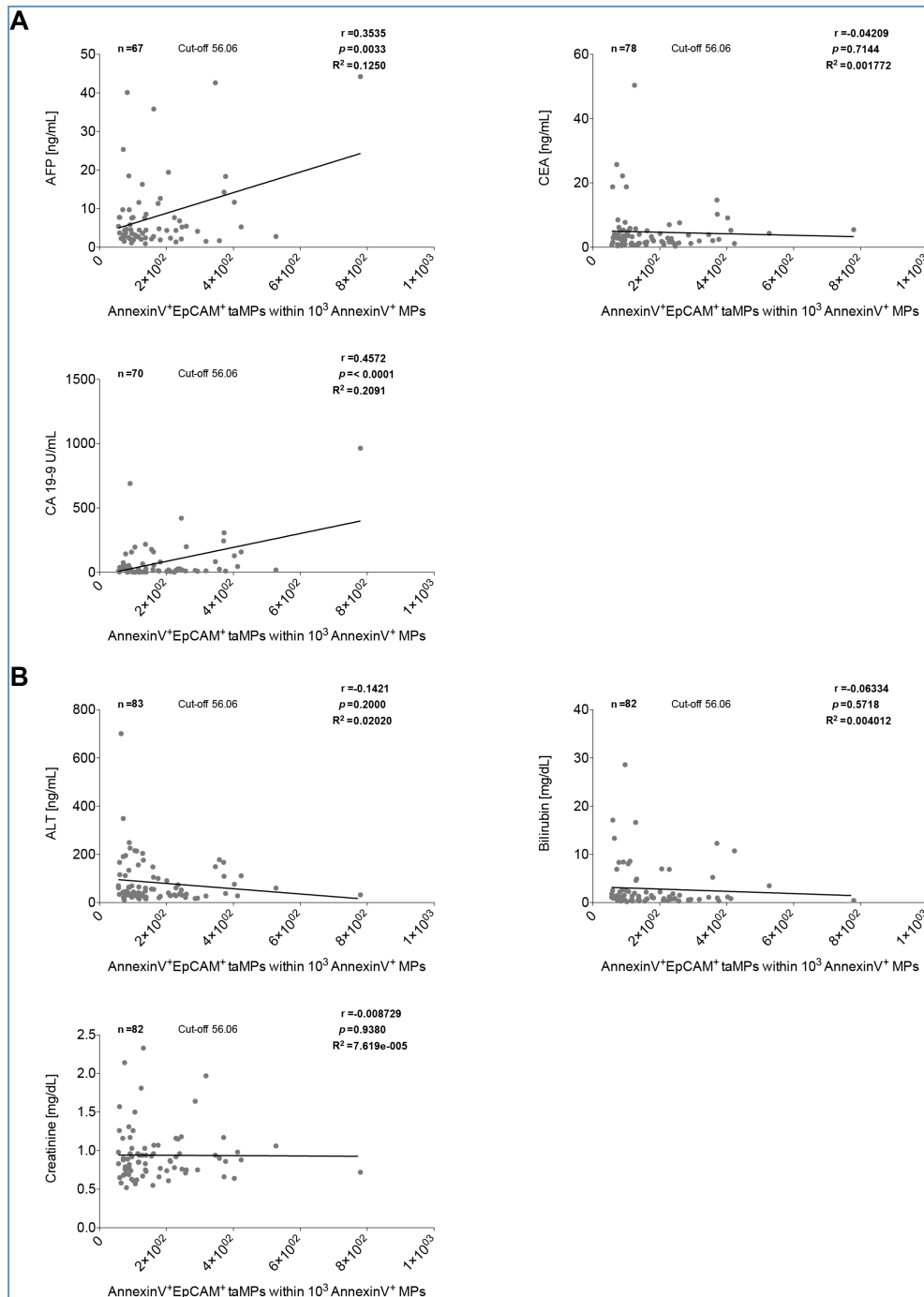
• AnnexinV⁺EpCAM⁺ taMPs and serum markers of patients with cirrhosis



Supplementary Figure 1: Serum tumor marker and blood chemistry correlate moderate with AnnexinV⁺EpCAM⁺ tumor-associated microparticles (taMPs) of patients with cirrhosis.

MPs were isolated from sera of patients with cirrhosis. Calculated Pearson's correlation (two-tailed) between AnnexinV⁺EpCAM⁺ values and corresponding serum tumor marker (alpha-1 fetoprotein (AFP [ng/mL]), carcinoembryonic antigen (CEA [ng/mL]), carbohydrate-antigen 19-9 (CA 19-9 [U/mL])) (A) or blood chemistry values (alanine transaminase (ALT [ng/mL]), bilirubin [mg/dL], creatinine [mg/dL]) are displayed. Indicated are the sample size (n), the corresponding Pearson's correlation coefficient (r), p value (p) and coefficient of determination (R²). Included AnnexinV⁺EpCAM⁺ levels were restricted to values above the cut-off (Table 19).

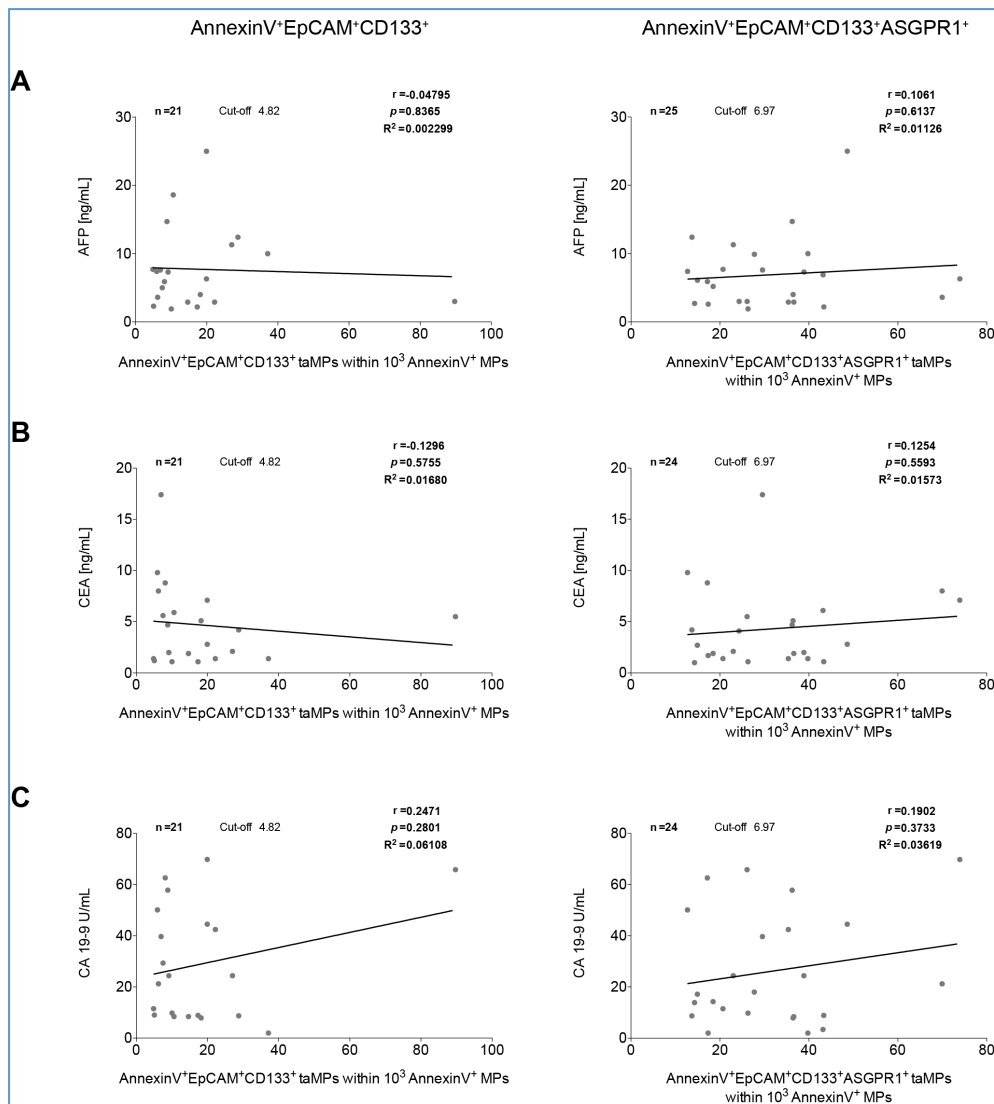
• **AnnexinV⁺EpCAM⁺ taMPs and serum markers of patients bearing liver tumors**



Supplementary Figure 2: Serum tumor marker and blood chemistry values correlate moderate with AnnexinV⁺EpCAM⁺ tumor-associated microparticles (taMPs) of patients bearing liver tumors.

MPs were isolated from sera of patients bearing liver tumors (hepatocellular carcinoma or cholangiocarcinoma). Calculated Pearson's correlation (two-tailed) between AnnexinV⁺EpCAM⁺ values and corresponding serum tumor marker (alpha-1 fetoprotein (AFP [ng/mL]), carcinoembryonic antigen (CEA [ng/mL]), carbohydrate-antigen 19-9 (CA 19-9 [U/mL])) (A) or blood chemistry values (alanine transaminase (ALT [ng/mL]), bilirubin [mg/dL], creatinine [mg/dL])) are displayed. Indicated are the sample size (n), the corresponding Pearson's correlation coefficient (r), p value (p) and coefficient of determination (R²). Included AnnexinV⁺EpCAM⁺ levels were restricted to values above the cut-off (Table 19).

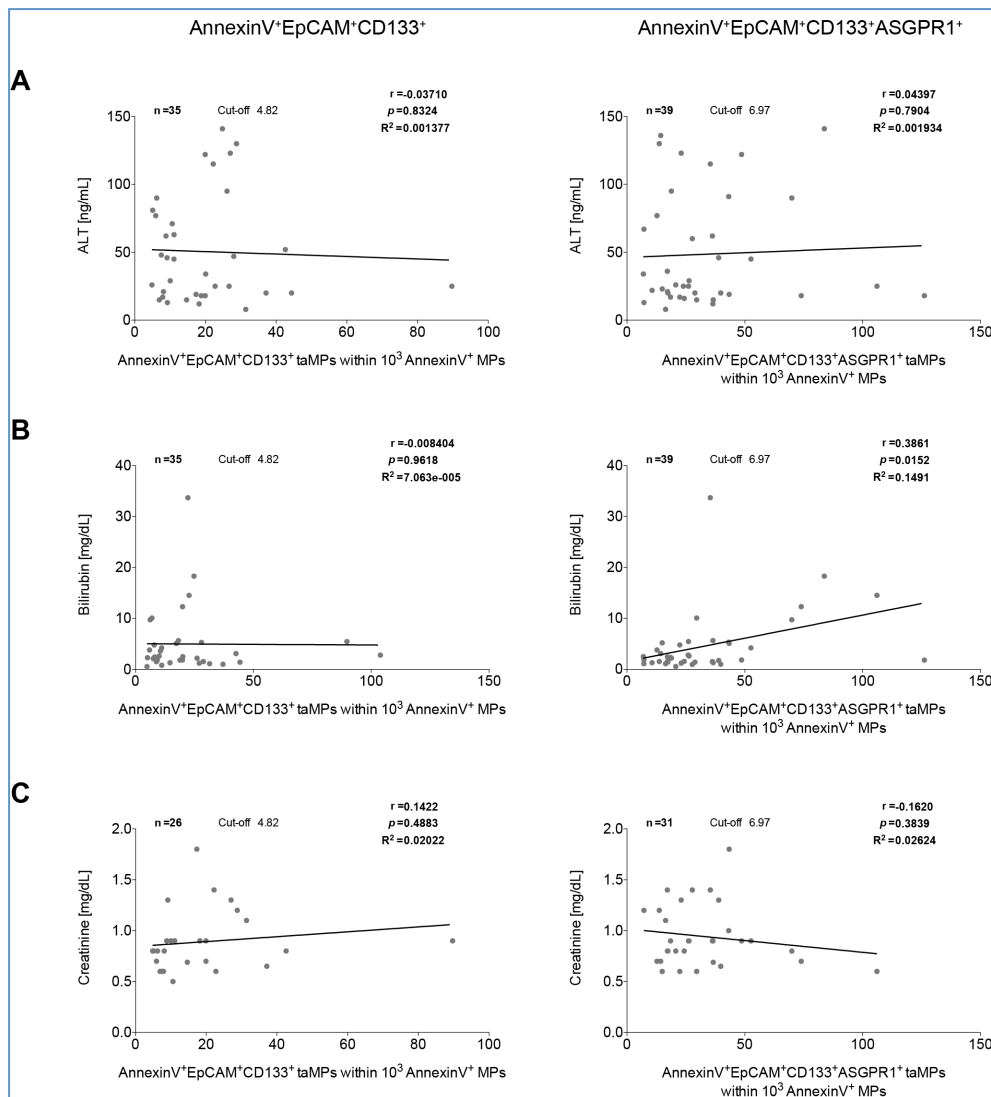
- **AnnexinV⁺EpCAM⁺CD133⁺ taMPs and AnnexinV⁺EpCAM⁺CD133⁺ASGPR1⁺ taMPs, respectively, and serum tumor markers of patients with cirrhosis**



Supplementary Figure 3: Serum tumor marker correlate almost not with AnnexinV⁺EpCAM⁺CD133⁺ and AnnexinV⁺EpCAM⁺CD133⁺ASGPR1⁺ tumor-associated microparticles (taMPs) of patients with cirrhosis.

MPs were isolated from sera of patients with cirrhosis. Calculated Pearson's correlation (two-tailed) between AnnexinV⁺EpCAM⁺CD133⁺ (left) and AnnexinV⁺EpCAM⁺CD133⁺ASGPR1⁺ values (right), respectively, and corresponding serum tumor marker such as: alpha-1 fetoprotein (AFP [ng/mL]) (A), carcinoembryonic antigen (CEA [ng/mL]) (B) or carbohydrate-antigen 19-9 (CA 19-9 [U/mL]) (C) are displayed. Indicated are the sample size (n), the corresponding Pearson's correlation coefficient (r), p value (p) and coefficient of determination (R²). Included taMP levels were restricted to values above the cut-off (Table 21).

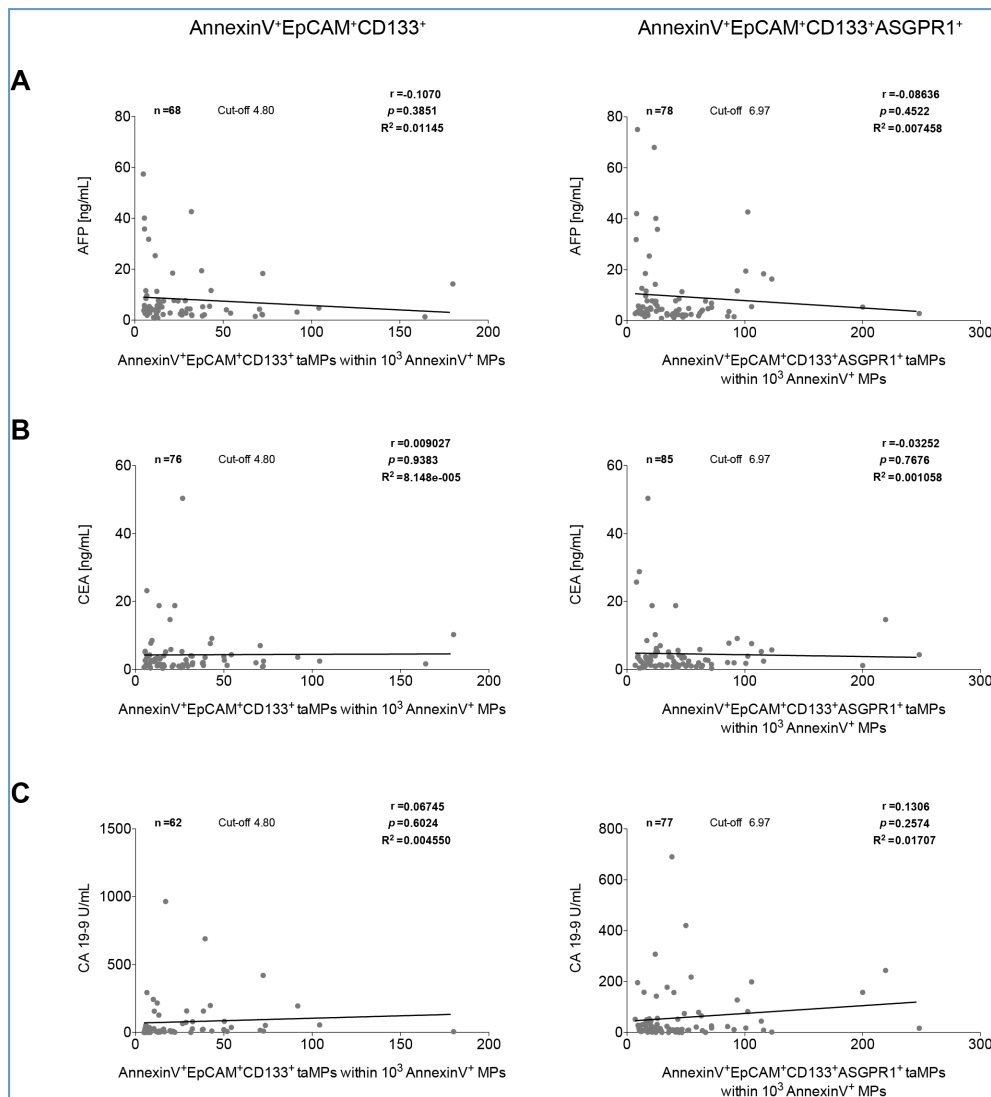
- **AnnexinV⁺EpCAM⁺CD133⁺ taMPs and AnnexinV⁺EpCAM⁺CD133⁺ASGPR1⁺ taMPs, respectively, and blood chemistry values of patients with cirrhosis**



Supplementary Figure 4: Blood chemistry values correlate almost not with AnnexinV⁺EpCAM⁺CD133⁺ and AnnexinV⁺EpCAM⁺CD133⁺ASGPR1⁺ tumor-associated microparticles (taMPs) of patients with cirrhosis.

MPs were isolated from sera of patients with cirrhosis. Calculated Pearson's correlation (two-tailed) between AnnexinV⁺EpCAM⁺CD133⁺ (left) and AnnexinV⁺EpCAM⁺CD133⁺ASGPR1⁺ values (right), respectively, and corresponding blood chemistry values such as: alanine transaminase (ALT [ng/mL]) (A), bilirubin [mg/dL] (B) or creatinine [mg/dL] (C) are displayed. Indicated are the sample size (n), the corresponding Pearson's correlation coefficient (r), p value (p) and coefficient of determination (R²). Included taMP levels were restricted to values above the cut-off (Table 21).

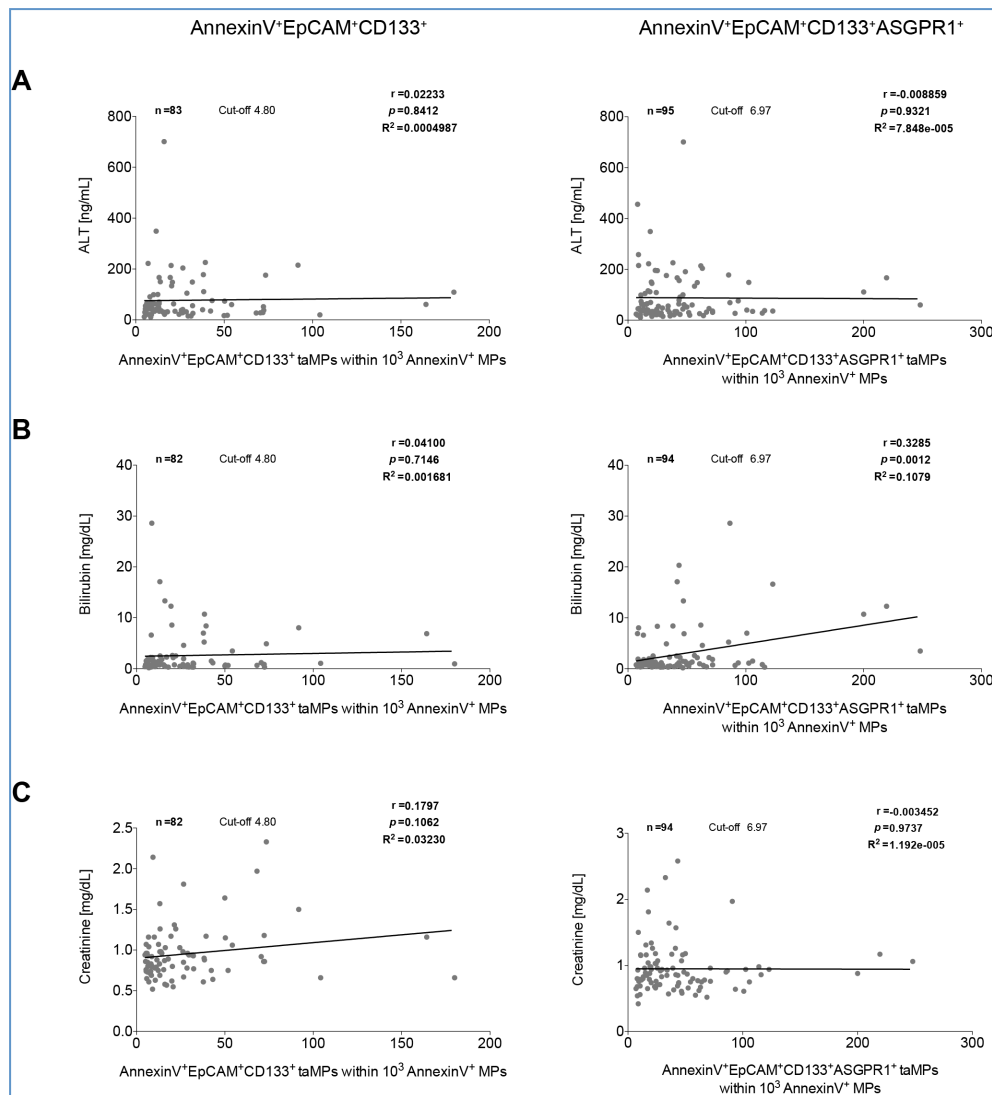
- **AnnexinV⁺EpCAM⁺CD133⁺ taMPs and AnnexinV⁺EpCAM⁺CD133⁺ASGPR1⁺ taMPs, respectively, and serum tumor markers of patients bearing liver tumors**



Supplementary Figure 5: Serum tumor markers do not correlate with AnnexinV⁺EpCAM⁺CD133⁺ and AnnexinV⁺EpCAM⁺CD133⁺ASGPR1⁺ tumor-associated microparticles (taMPs) of patients bearing a liver tumor.

MPs were isolated from sera of patients bearing primary hepatic cancer (hepatocellular carcinoma and cholangiocarcinoma). Calculated Pearson's correlation (two-tailed) between AnnexinV⁺EpCAM⁺CD133⁺ (left) and AnnexinV⁺EpCAM⁺CD133⁺ASGPR1⁺ values (right), respectively, and corresponding serum tumor marker such as: alpha-1 fetoprotein (AFP [ng/mL]) (A), carcinoembryonic antigen (CEA [ng/mL]) (B) or carbohydrate-antigen 19-9 (CA 19-9 [U/mL]) (C) are displayed. Indicated are the sample size (n), the corresponding Pearson's correlation coefficient (r), p value (p) and coefficient of determination (R²). Included taMP levels were restricted to values above the cut-off (Table 21).

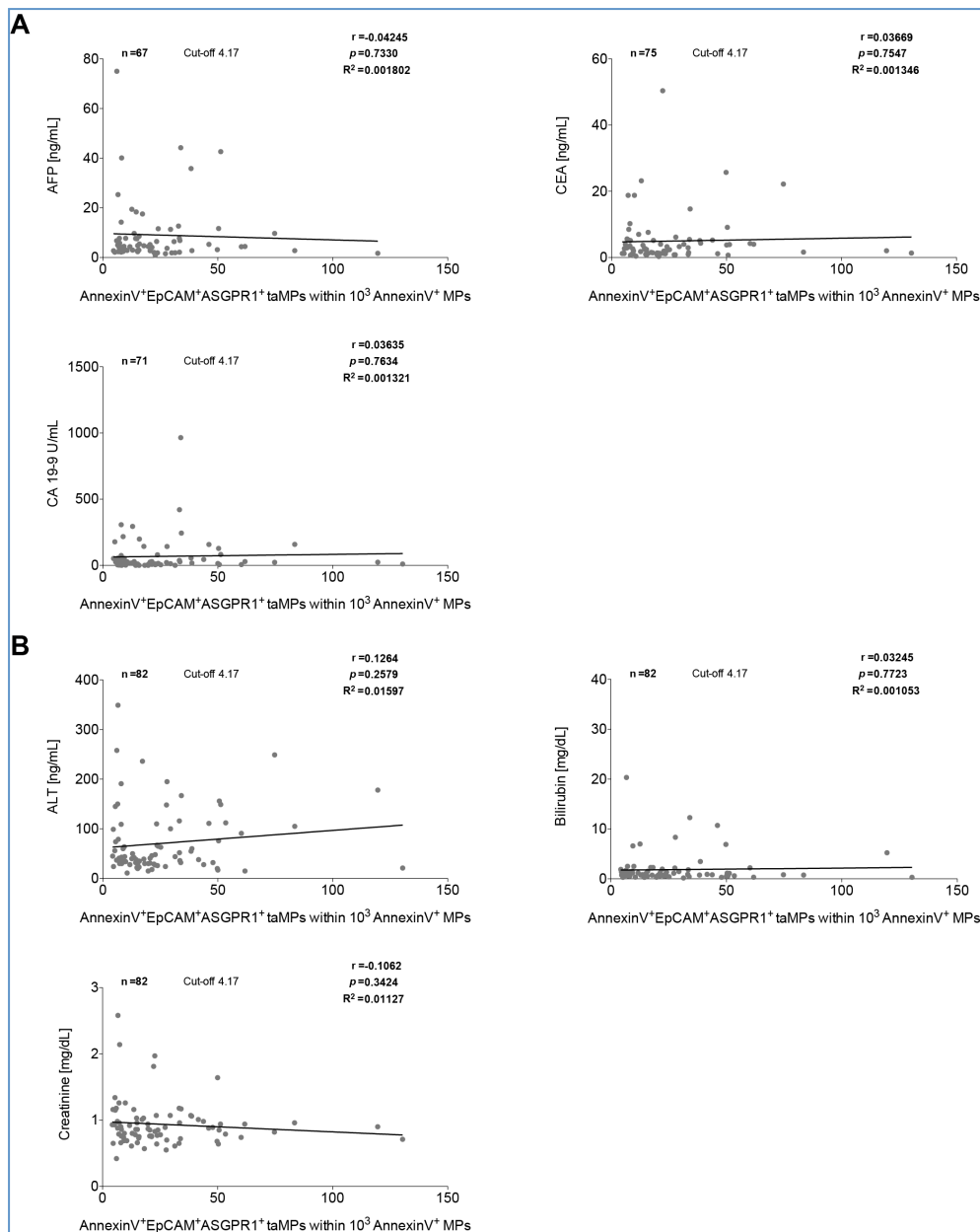
- **AnnexinV⁺EpCAM⁺CD133⁺ taMPs and AnnexinV⁺EpCAM⁺CD133⁺ASGPR1⁺ taMPs, respectively, and blood chemistry values of patients bearing liver tumors**



Supplementary Figure 6: Blood chemistry values do not correlate with AnnexinV⁺EpCAM⁺CD133⁺ and AnnexinV⁺EpCAM⁺CD133⁺ASGPR1⁺ tumor-associated microparticles (taMPs) of patients bearing a liver tumor.

MPs were isolated from sera of patients bearing primary hepatic cancer (hepatocellular carcinoma and cholangiocarcinoma). Calculated Pearson's correlation (two-tailed) between AnnexinV⁺EpCAM⁺CD133⁺ (left) and AnnexinV⁺EpCAM⁺CD133⁺ASGPR1⁺ values (right), respectively, and corresponding blood chemistry values such as: alanine transaminase (ALT [ng/mL]) (A), bilirubin [mg/dL] (B) or creatinine [mg/dL] (C) are displayed. Indicated are the sample size (n), the corresponding Pearson's correlation coefficient (r), *p* value (*p*) and coefficient of determination (*R*²). Included taMP levels were restricted to values above the cut-off (Table 21).

• **AnnexinV⁺EpCAM⁺ASGPR1⁺ taMPs and serum markers of patients bearing liver tumors**



Supplementary Figure 7: Serum tumor marker and blood chemistry values do almost not correlate with AnnexinV⁺EpCAM⁺ASGPR1⁺ tumor-associated microparticles (taMPs) of liver tumor patients.

MPs were isolated from sera of patients bearing primary hepatic cancer (hepatocellular carcinoma or cholangiocarcinoma). Calculated Pearson's correlation (two-tailed) between AnnexinV⁺EpCAM⁺ASGPR1⁺ values and corresponding serum tumor marker (alpha-1 fetoprotein (AFP [ng/mL]), carcinoembryonic antigen (CEA [ng/mL]) or carbohydrate-antigen 19-9 (CA 19-9 [U/mL]) (A) or blood chemistry values (alanine transaminase (ALT [ng/mL]), bilirubin [mg/dL] or creatinine [mg/dL]) (B) are displayed. Indicated are the sample size (n), the corresponding Pearson's correlation coefficient (r), p value (p) and coefficient of determination (R²). Included AnnexinV⁺EpCAM⁺ASGPR1⁺ levels were restricted to values above the cut-off (Table 23).

Background and Aims: Alpha-fetoprotein response (AFP-R) can be used to monitor the response of patients with hepatocellular carcinoma (HCC) to treatment. However, what time-point AFP-R should be evaluated is not clearly defined. Aim of this study was to compare the performances of AFP-R evaluation at 4 and 12 weeks of sorafenib treatment.

TU-060

HEPATOCELLULAR CARCINOMA AND DEFECTION FROM OTHER CANCERS RELATED MICROPAPILLARITIES DETECTED BY IMMUNOFLUORESCENCE

H. Jülich¹, M. Krawczyk^{1,2}, A. Wilms¹, M. Casper¹, M. Giese-Mainland¹, R. Schwab¹, I. Richardson¹, S. Schmitt¹, C. Geis¹, M. Krawczyk¹, F. Lammert¹, V. Lukacs-Kornek¹, D. Schulpan¹, M. Kornak¹, J. Department of Medicine II, Saarland University Medical Center, Homburg/Saar, Germany; ²Department of Internal Medicine, Transplant and Liver Surgery, Medical University of Warsaw, Warsaw, Poland; ³Department of General Internal Medicine and Thoracic Oncology, University of Cologne, Cologne, Germany; ⁴Institute of Pathology, University of Cologne, Cologne, Germany; ⁵Department of Gastroenterology and Hepatology, University of Cologne, Cologne, Germany; ⁶Department of Pediatrics, Saarland University Medical Center, Homburg/Saar, Germany; ⁷Institute of Translational Immunology, Johannes Gutenberg University, Mainz, Germany.

Background and Aims Extracellular vesicles (EVs), exosomes or microparticles (MPs) originating from various cell types including endothelial cells, immune cells and cancer cells, mirror the presence and extent of chronic liver diseases or cancer (Koracevic M et al. Hepatology 2011; Gastroenterology 2012; Mollo MA, Nature 2015). Herein, we identified hepatocellular (HCC) derived MPs (HCC-MPs) or general (epithelial) tumor associated MPs (taMPs) that could aid in diagnosing the presence and extent of HCC, and distinguish between HCC, colorectal carcinoma (CRC), and cholangiocarcinoma (CCA).

vol. 64 | S213-S424

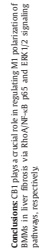
The calculated cut-off values for Amnion/EpCAM, HCC/EpCAM, and HCC/Amnion/EpCAM were 35.1/Amnion/EpCAM, 282/Amnion/EpCAM, and 35.5/Amnion/EpCAM, respectively. The sensitivity and specificity of the HCC-specific MIPs in HCC, the associated cut-off values for HCC-specific MIPs was 4/Amnion/EpCAM in HCC patients (Amnion/EpCAM tAMHs and HCC-MIPs were increased 2.5-fold) and 2.5/Amnion/EpCAM tAMHs and HCC-MIPs were increased 2.5-fold) respectively compared to healthy controls. The sensitivity and specificity of the HCC-specific MIPs in HCC patients were 100% and 100%, respectively.

Conclusions 1. Tumor plasma displays characteristic elevations of EpCAM. 2. Only BACS analysis for HCC-specific MIPs could distinguish HCC from CCA and CCA. 3. HCC-MIPs and Amnion/EpCAM could distinguish HCC from CCA. 4. HCC-MIPs may emerge as a novel tool for HCC cancer screening, surveillance, and therapy monitoring. 4. Whereas differentiation from other cancer entities is important, this distinction will be less relevant for the rapid diagnosis of HCC.

Background and Aims In hepatocellular carcinoma (HCC), aggressive tumors have been associated with increased NFKB1 mRNA expression, increased telomerase activity and longer survival. In this study, we applied the RNAscope technology to analyze the expression of NFKB1 mRNA in formalin-fixed paraffin-embedded (FFPE) HCC specimens and matched non-neoplastic liver tissues to detect the expression of NFKB1 mRNA and searched for relationships between NFKB1 mRNA expression and clinicopathological parameters in HCC, including the expression status of "stemness"-related markers and epithelial-mesenchymal transition (EMT)-related markers.

[illegible]

The CBI-involved M1 polarization was apparently impaired by PTX ($G_{i/o}$ protein inhibitor), Y27632 (ROCK inhibitor) and PD98059 (ERK inhibitor), while SB203580 (p38 inhibitor) and compound C (AMPK inhibitor) had no such effects. We found the mechanism of activated CBI promoting M1 polarization of BMMs was dependent on $G_{i/o}$ (RhoA/NF- κ B/p65 signaling pathway and $G_{i/o}$), ERK1/2



Background and Aims: Abnormal angiotensin is critical for portal hypertension in cirrhosis. Except for etiological treatment, no specific medication or regimen has been explored to treat the early stage of cirrhosis when angiotensin is initiated. In this study, we explored an anti-angiotensin effort through octreotide to treat early stage of cirrhotic portal hypertension in an animal model.

Methods: Peritoneal injection of thiazemide (750 µg) was employed to induce liver cirrhosis every 3 days for 16 weeks. Male Sprague-Dawley rats were randomized into control (TA) and

for fibrinolysis, portal venous pressure, angiogenesis and integration of the fibrinolytic and angiogenic pathways were determined. Methylation of the angiotensin receptor (SSTR2) was determined by using the bisulfite sequencing method and real-time PCR. In vitro, the effect of octreotide on endothelial and pericyte proliferation and on the expression of MMP-2 and MMP-9 was determined. Finally, we investigated the mechanism of SSTR2 up-regulation. Liver fibrosis and portal hypertension were applied to determine levels of SSTR2. SSTR2-5 and SSTR2-6 (CXX-2) in cirrhotic human livers.

Results: Firstly, compared with the TMA group, liver fibrosis and portal hypertension were significantly reduced in the TMA + octreotide group. Portal pressure in the TMA + octreotide group were dramatically reduced. Secondly, the expression of SSTR2 in the TMA + octreotide group was significantly reduced. Secondly, the up-regulation of VEGF, HIF-1 α , c-fos and p-BEK, induced by TMA were significantly inhibited by octreotide in cirrhotic human livers. Octreotide inhibited cell formation and proliferation of endothelial and pericyte. Octreotide inhibited endothelial cell migration via SSTR2-5. RARH-1 (SSTR2) signaling pathway was inhibited by octreotide in endothelial cells. Finally, we observed that the expression of SSTR2-5 and SSTR2-6 were up-regulated in cirrhotic human liver. Levels of CXX-2 were up-regulated in cirrhotic human liver.

Journal of Hepatology 2017 vol. 66 | S333-S542

FRI-060
Novel isolation and high purity enrichment of liver progenitor cell populations
H. Julich-Haertel¹, M. Thwarl², C. Mehrhoff¹, F. Lammerl¹, M. Kornick¹, V. Linkas-Kornick¹, ¹Internal Medicine II, Saarland university, Homburg, Germany
E-mail: henrike.julich-haertel@hotmail.com

Background and Aims: During chronic liver injuries, progenitor cell expansion in a process called ductular reaction, which also entails the appearance of inflammatory cellular infiltrate and epithelial cell activation. The progenitor cell population during such inflammatory reactions has mostly been investigated using single surface markers, either by histological analysis or by flow cytometry-based techniques. However, novel surface marker combination in our laboratory using CD133 and g258 has recently identified various functionally distinct subpopulations within the liver progenitor compartment (Eckert et al. 2016 APB PMID: 265564718). We aimed to isolate and enrich the various subsets of liver progenitor cells with high purity using a novel transmembrane marker.

[illegible]

ENR 061
Syst emic delivery of gene therapy – a proof of concept study in a model of cirrhosis and portal hypertension
 H. Jones¹, A. Habeshion², G. Mehta¹, R. Jalan¹, N.A. Davies¹,
 R.P. Morley-Jones¹, ¹Institute for Liver and Digestive Health, UCL, London
 United Kingdom
 E-mail: helen.jones@ucl.ac.uk

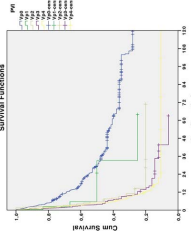
Background and Aims: Chronic liver disease is associated with down-regulation of many genes. Restoration of function by infusion of recombinant proteins has been suggested as therapies for different aspects of chronic liver disease. Drawbacks to this approach include

CIRCULATING TUMOR-ASSOCIATED MICROPARTICLES IN LIVER CANCER: A QUESTION OF TUMOUR DIAMETER AND VOLUME?

URBAN, SK. *ET AL.*, *EASL*, 2017

POSTER PRESENTATIONS

Japan ranging from Vp0-Vp4. Vp0 = PVP = segmental, Vp1 = right anterior or right posterior, parav. vps, Vp2 = right or left portal, Vp3 = right or left main trunk. Median overall survival (OS) was calculated from the date of diagnosis. The corresponding median OS was 105, 105, 105, 105, and 95 days for Vp0-Vp4, respectively. There was no significant difference in OS between the two groups. The corresponding median OS was 105, 105, 105, 105, and 95 days for Vp0-Vp4, respectively. There was no significant difference in OS between the two groups. The corresponding median OS was 105, 105, 105, 105, and 95 days for Vp0-Vp4, respectively. There was no significant difference in OS between the two groups.



Conclusions: PVP in patients with HCC is associated with a dismal prognosis. However, the extent of PVP itself has no significant impact – even minor PVP leads to a very poor prognosis.

SA-001 **Identifying patients at higher risk for hepatocellular carcinoma development: mark from a large scale multicenter study**

Background and Aims: Recently, we showed that subpopulations of patients with chronic liver disease (CLD) are at increased risk for hepatocellular carcinoma (HCC) development. In this study, we aimed to identify patients at higher risk for HCC development. **Methods:** We analyzed data from a large scale multicenter study. **Results:** We identified patients at higher risk for HCC development. **Conclusions:** We identified patients at higher risk for HCC development.

Background and Aims: Patients with chronic liver disease (CLD) and hepatocellular carcinoma (HCC) have a poor prognosis. **Methods:** We analyzed data from a large scale multicenter study. **Results:** We identified patients at higher risk for HCC development. **Conclusions:** We identified patients at higher risk for HCC development.

Here we addressed the potential of soluble Akt (sAkt) as a biomarker of CLD and early HCC.

Methods: Levels of sAkt were measured by enzyme-linked immunosorbent assay (ELISA) in 100 patients with CLD and 100 healthy controls. **Results:** sAkt levels were significantly increased in CLD patients compared to healthy controls. **Conclusions:** sAkt levels were significantly increased in CLD patients compared to healthy controls.

SA-002 **Circulating tumor-associated microparticles in liver cancer: a pilot study**

Background and Aims: Recently, we showed that subpopulations of patients with chronic liver disease (CLD) are at increased risk for hepatocellular carcinoma (HCC) development. In this study, we aimed to identify patients at higher risk for HCC development. **Methods:** We analyzed data from a large scale multicenter study. **Results:** We identified patients at higher risk for HCC development. **Conclusions:** We identified patients at higher risk for HCC development.

Background and Aims: Patients with chronic liver disease (CLD) and hepatocellular carcinoma (HCC) have a poor prognosis. **Methods:** We analyzed data from a large scale multicenter study. **Results:** We identified patients at higher risk for HCC development. **Conclusions:** We identified patients at higher risk for HCC development.

Background and Aims: Patients with chronic liver disease (CLD) and hepatocellular carcinoma (HCC) have a poor prognosis. **Methods:** We analyzed data from a large scale multicenter study. **Results:** We identified patients at higher risk for HCC development. **Conclusions:** We identified patients at higher risk for HCC development.

Background and Aims: Patients with chronic liver disease (CLD) and hepatocellular carcinoma (HCC) have a poor prognosis. **Methods:** We analyzed data from a large scale multicenter study. **Results:** We identified patients at higher risk for HCC development. **Conclusions:** We identified patients at higher risk for HCC development.

POSTER PRESENTATIONS

Background and Aims: Hepatocellular carcinoma (HCC) is the fifth overall cause of deaths globally, and one of the most frequent malignant tumors. **Methods:** We analyzed data from a large scale multicenter study. **Results:** We identified patients at higher risk for HCC development. **Conclusions:** We identified patients at higher risk for HCC development.

Background and Aims: Patients with chronic liver disease (CLD) and hepatocellular carcinoma (HCC) have a poor prognosis. **Methods:** We analyzed data from a large scale multicenter study. **Results:** We identified patients at higher risk for HCC development. **Conclusions:** We identified patients at higher risk for HCC development.

Background and Aims: Patients with chronic liver disease (CLD) and hepatocellular carcinoma (HCC) have a poor prognosis. **Methods:** We analyzed data from a large scale multicenter study. **Results:** We identified patients at higher risk for HCC development. **Conclusions:** We identified patients at higher risk for HCC development.

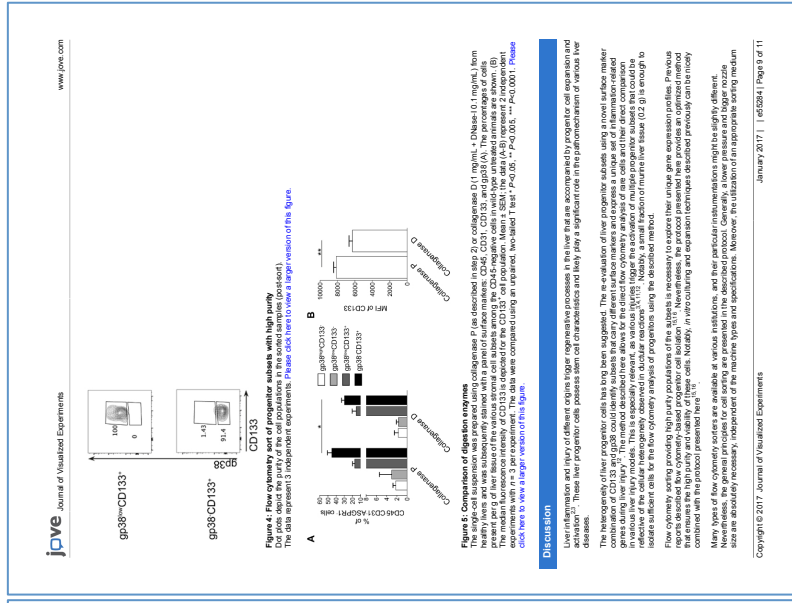
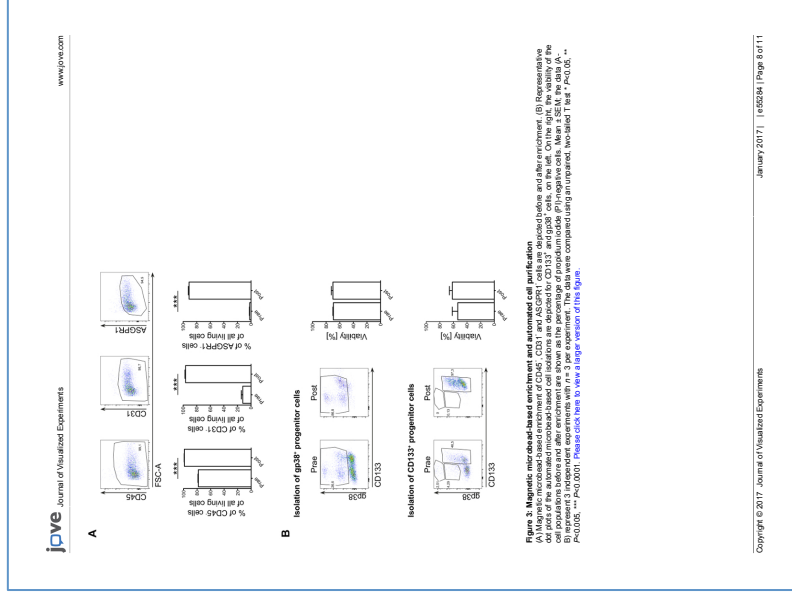
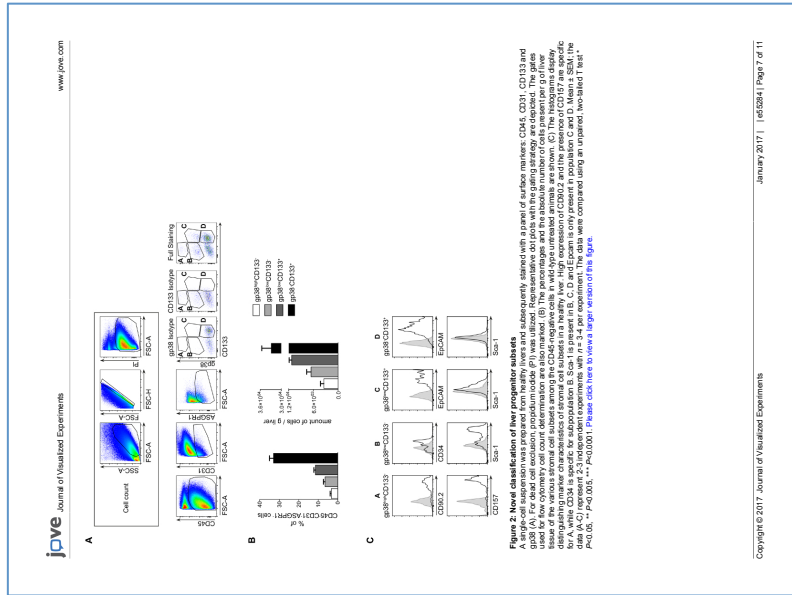
SA-003 **The expression of SAL4 and its clinical significance in hepatocellular carcinoma**

Background and Aims: The gene encoding Sal-like 4 (SAL4) is a zinc-finger transcription factor and a vertebrate ortholog of the Drosophila gene *Sal*. **Methods:** We analyzed data from a large scale multicenter study. **Results:** We identified patients at higher risk for HCC development. **Conclusions:** We identified patients at higher risk for HCC development.

Background and Aims: Patients with chronic liver disease (CLD) and hepatocellular carcinoma (HCC) have a poor prognosis. **Methods:** We analyzed data from a large scale multicenter study. **Results:** We identified patients at higher risk for HCC development. **Conclusions:** We identified patients at higher risk for HCC development.

Background and Aims: Patients with chronic liver disease (CLD) and hepatocellular carcinoma (HCC) have a poor prognosis. **Methods:** We analyzed data from a large scale multicenter study. **Results:** We identified patients at higher risk for HCC development. **Conclusions:** We identified patients at higher risk for HCC development.

JULICH-HAERTEL, H. ET AL., *JVisExp*, 2017



MULTI-SURFACE ANTIGEN STAINING OF LARGER EXTRACELLULAR VESICLES

LUKACS-KORNEK, V. ET AL., METHODS MOL BIOL, 2017

Chapter 16

Multi-Surface Antigen Staining of Larger Extracellular Vesicles

Veronika Lukacs-Kornek, Henrike Julich-Haertel, Sabine Katharina Urban, and Miroslaw Kornek

Abstract

Larger extracellular vesicles, microparticles (MPs) or microvesicles (MVs), especially their acquisition and analysis, are still a challenge for researchers. Several laboratories have shown that MPs/MVs might be suitable for the diagnosis and predicting prognosis in various diseases including cancer. However, FACS staining of larger extracellular vesicles (EVs) can be difficult and results potentially in false positive and inconsistent data interpretation. Despite that FACS equipment is well maintained and the operators have ample experience, a reliable and for larger EVs suitable staining protocol for larger EVs isolated from human serum samples. We describe in detail the needed steps as currently done in our laboratory. Staining is demonstrated exemplarily for multi-antibody mix including CD147, a potential cancer marker if applied in combination with other MP/MV surface markers.

Key words Larger extracellular vesicles, Microparticles, Microvesicles, Surface antigen staining, Antibody, Flow cytometry

1 Introduction

The quantification of larger extracellular vesicles (>100 nm in diameter), known as microparticles (MPs) or microvesicles (MVs), by flow cytometry (FACS), due to its robust statistical power and possibility for measuring various MP/MV subpopulation, has been increasingly used in clinical research, thus raising constantly more and more attention [1, 2]. It became apparent that extracellular vesicles (EVs) are beneficial for disease surveillance especially tumor diagnosis and tumor treatment monitoring as discussed and shown by others and us [3–6]. Recently, we have shown that the so-called tumor-associated microparticles (tAMPs) could most likely aid in detecting cancer neoplasia and that

other MP populations associated with inflammatory events could distinguish between chronic liver diseases [2, 4, 6].

Nowadays, flow cytometers are commonly available at larger medical and research facilities with the aim to screen cancer patients. However, the lack of the necessary know-how to establish a robust, reliable MP/MV multi-antibody staining protocol for the quantitative and qualitative detection of MPs/MVs by FACS, MPs/MVs are shed from the plasma membrane of the parental cell. If the surface antigens for the identification of the parental cell are known, the same markers (antibodies) should be applicable for MPs/MVs originating from the associated parental cell [2, 7].

Since it is known that MPs/MVs have the tendency to take up proteins unspecifically, including IgGs, as some of their parental cells do, it appears almost inevitable that to a certain degree false positive events will occur. In order to avoid this, the use of Fc-Block (BSA is recommended and a careful evaluation of the acquired data is required [2, 4, 6, 8]). To set up a new staining for MPs/MVs, the below-described MP staining protocol for the used singular or multi-antibody mix needs to be established, which should follow certain basic rules to evade false positive events during the quantification of MPs/MVs via flow cytometry.

One of the cornerstones is the right use of isotype controls. Here we describe a comprehensive strategy for the setup of the needed amount or dilution of the used antibodies as part of a multi-antibody mix. As part of good laboratory practice, every antibody should be tested for its specificity. In our case, the use of MP/MV multi-antibody mix, even if a successful dilution for a singular use was found for cells or MPs/MVs previously. However, our strategy guide will allow the interested reader to set up a surface antigen staining of MPs/MVs ensuring both Quality Control (QC) and Quality Assurance (QA) for cross-platform comparison as discussed in a previous chapter (see Chapter 14).

Our methodology will describe how to exemplarily set up CD147 (EMMPRIN) MP/MV surface staining as part of a multi-antibody mix as used currently in our laboratory and partly published [4, 6]. However, each staining protocol is constantly evolving. This protocol represents current knowledge and practice and should be used as a guide. It is not intended to be a protocol for troubleshooting (see associated Notes). The International Society for Extracellular Vesicles (ISEV) has put out general guidelines for proceeding with EV research that we followed regarding the isolations of these larger EVs [9]. With respect to instrumentation, here our MP/MV surface staining guide/protocol and notes are optimized for our flow cytometer but will apply for other FACS instruments too.

202 Veronika Lukacs-Kornek et al.

mlc@lukakornek@web.de

Multi-Surface Antigen Staining of Larger Extracellular Vesicles 203

2 Materials

All solutions except antibody containing solutions as provided by the vendor were centrifuged or filtered prior to their use to remove contaminations such as possible protein aggregates or particles with similar size as larger EVs.

2.1 Solutions

1. PBS, was prior filtered using the Steriflip[®] Vacuum-driven Filtration System (0.22 µm Millipore Express[®] Plus Membrane from Millipore[®], Merck KGaA, Darmstadt, Germany (Cat# SCGP00525).
2. As Fc-Block, Hi FcR Binding Inhibitor, Purified, eBioscience (San Diego, CA, USA) (#14916173) was used. It should be added and filtered before use with Steriflip[®] Vacuum-driven Filtration System (0.22 µm Millipore Express[®] Plus Membrane from Millipore[®], Merck KGaA, Darmstadt, Germany (Cat# SCGP00525).
3. BSA, Miltenyi Biotec GmbH, Bergisch Gladbach, Germany (Order# 130-091-376). BSA stock, before use, is centrifuged at 20,000 × g for 60 min at 4 °C.
4. Annexin V Binding Buffer (20× stock solution), Miltenyi Biotec GmbH, Bergisch Gladbach, Germany (Order# 130-092-820). Annexin V Binding Buffer stock, was filtered before use with Steriflip[®] Vacuum-driven Filtration System (0.22 µm Millipore Express[®] Plus Membrane from Millipore[®], Merck KGaA, Darmstadt, Germany (Cat# SCGP00525).
1. Annexin V-FITC, working dilution is 1:20 for a total staining volume of 100 µL (see Note 1), Miltenyi Biotec GmbH, Bergisch Gladbach, Germany (Order# 130-092-082).
2. CD147-Alexa-488, our recommended working dilution optimized for our multi-antibody mix is 1:2000 for a total staining volume of 100 µL (see Note 2), Miltenyi Biotec GmbH, Bergisch Gladbach, Germany (Order# 130-104-493, REA done REA282).
3. REA Control APC-Vio770, our recommended working dilution fixed to the staining antibody, here CD147-Alexa-488, is 1:1,720 for a total staining volume of 100 µL (see Note 2), Miltenyi Biotec, Bergisch Gladbach, Germany (Order# 130-104-618, REA done REA293).
1. Cytometric data was analyzed with FlowJo X software for MAC OSX, Tree Star, Inc., Ashland, Oregon, USA.
1. The MACSQuant[®] Analyzer 10, Miltenyi Biotec GmbH, Bergisch Gladbach, Germany (Order# 130-096-545).

2.2 Antibodies

2.3 Software

2.4 Hardware

mlc@lukakornek@web.de

mlc@lukakornek@web.de

8 Acknowledgements

Als erstes möchte ich mich bei meiner Doktormutter Jun. Prof. Dr. Dr. Veronika Lukacs-Kornek und meinem Doktorvater Dr. Mirosław Kornek bedanken. Ich danke euch nicht nur für die Möglichkeit, dass ich bei euch arbeiten und von euch lernen durfte, sondern auch für die vielen gemeinsamen Stunden im Labor, die uns auf eine verdrehte Art und Weise zu Freunden machten. Ich wünsche euch von Herzen das Beste und dass ihr niemals die Leidenschaft verliert, die mich so motiviert hat!

Danken möchte ich auch der kompletten Arbeitsgruppe – unabhängig davon wer zu ‚Team Leber‘ oder ‚Team Mikropartikel‘ gehört. In meinen Augen gehörten wir alle zusammen und hatten alle die gleichen Ambitionen! Auch wenn das Büro oft säuisch aussah, so habt ihr mir stets einen schönen Laboralltag beschert. Ein besonderer Dank geht dabei an Sabine, Steffi und Julia, die mich auch experimentell im Rahmen dieser Arbeit unterstützten und diese somit vorangebracht haben.

Ein besonderer Dank geht an Märi, Dine, Fia und Steini die immer ein offenes Ohr haben und mich schon durch mehrere Phasen meines Lebens begleiteten. Ihr seid großartig – ich hab euch lieb!

Ganz besonders danke ich meiner Familie, die mich jederzeit fördert und unterstützt. Dabei möchte ich vor allem meiner Mama und Harry danken – ganz einfach für alles!

Letztendlich möchte ich mich bei meinem Ehemann, besten Freund und Papa der kleinen Schildkröte Oskar bedanken. Lutz, du bist jederzeit für mich da und hast mich oft zum Schreiben und Fertigstellen dieser Arbeit motiviert. Ohne dich wäre vieles nicht möglich. Außerdem schaffst nur du es, graue Tage bunt erscheinen zu lassen und mir ein lächeln ins Gesicht zu zaubern (und wir wissen beide, dass das nicht so leicht ist). Ich liebe dich – bis zum Mond...

9 Informed consent by Sabine Katharina Urban

Einwilligungserklärung

Ich Sabine Katharina Urban willige ein, dass Henrike Julich-Haertel, geb. Julich, (geboren am 28.10.1988 in Erfurt), die von mir erhobenen Daten im Rahmen ihrer Dissertation verwenden und zeigen darf, jedoch müssen diese als die von mir generierten Daten ausgewiesene werde.

Homburg, 5.6.18
Ort, Datum

S. Ul
Unterschrift